Fall 2009

Ortho substitution effects on the acidic and alkaline hydrolyses of formanilides

Salil Dileep Desai
University of Iowa

ORTHO SUBSTITUTION EFFECTS ON THE ACIDIC AND ALKALINE HYDROLYSES OF FORMANILIDES

by

Salil Dileep Desai

An Abstract

Of a thesis submitted in partial fulfillment
of the requirements for the Doctor of
Philosophy degree in Pharmacy
in the Graduate College of
The University of Iowa

December 2009

Thesis Supervisor: Associate Professor Lee E. Kirsch

ABSTRACT

The objectives of this project were to determine the reaction schemes of formanilide and substituted formanilides in acidic and alkaline solutions, to quantiate the kinetics of hydrolysis, to propose reaction mechanisms, and to assess the role of *ortho* substitution in formanilide hydrolysis kinetics.

A set of thirty substituted formanilides were synthesized and characterized. Hydrolysis of the formanilides was carried out under first order conditions in hydrochloric acid (0.01-8 M, 40°C) and in hydroxide solutions (0.01-3 M, 25°C and 40°C). Hydrolysis kinetics were evaluated in terms of temperature (20°C- 60°C), solvent composition(0-50 % dimethyl sulfoxide, dioxane, ethanol and acetone) and ionic strength (0.1-1) effects. The degradation products were separated and identified using RP-HPLC, and the alkaline and acidic reaction schemes were proposed.

For acidic hydrolysis of formanilides, the observed rate constants were proportional to the hydronium concentrations. Modified Hammett plots constructed using the second order rate constants for specific acid catalysis were linear. The *ortho* effect was analyzed using the Fujita-Nishioka method. In alkaline solutions the observed rate constants showed mixed first and second order dependences with respect to hydroxide concentration. A complex degradation scheme was used to estimate individual rate constants and to construct Hammett plots. *Ortho* effects were examined for the first order hydroxide concentration dependent pathway.

Arrhenius plots for substituted formanilides were linear in both acidic and alkaline media. Ionic strength did not show any effect on the acidic and alkaline hydrolysis rates. In both acidic and alkaline media the rate of hydrolysis decreased with increase in organic solvent content.

Formanilide hydrolyzes in acidic solutions by specific acid catalysis and the kinetic study results were consistent with $A_{AC}2$ mechanism. *Ortho* substitution led to

reduction in rates. The *ortho* effect could be split in steric inhibition of resonance, retardation due to steric bulk and through space interactions. In alkaline solutions a complicated kinetic scheme was used to describe the multiple pathways of degradation. The results from the kinetic studies could be explained using a modified $B_{AC}2$ mechanism. The hydrolysis of *meta* and *para* substituted formanilides in alkaline conditions did not show substituent effects however *ortho* substitution led to an decrease in rate constants proportional to the steric bulk of the substituent.

Abstract Approved: _____
Thesis Supervisor

_____
Title and Department

_____
Date

ORTHO SUBSTITUTION EFFECTS ON THE ACIDIC AND ALKALINE HYDROLYSES OF FORMANILIDES

by

Salil Dileep Desai

A thesis submitted in partial fulfillment
of the requirements for the Doctor of
Philosophy degree in Pharmacy
in the Graduate College of
The University of Iowa

December 2009

Thesis Supervisor: Associate Professor Lee E. Kirsch

Graduate College
The University of Iowa
Iowa City, Iowa

CERTIFICATE OF APPROVAL

_____

PH.D. THESIS

_____

This is to certify that the Ph.D. thesis of

Salil Dileep Desai

has been approved by the Examining Committee
for the thesis requirement for the Doctor of Philosophy
degree in Pharmacy at the December 2009 graduation.

Thesis Committee: _____
Lee E. Kirsch, Thesis Supervisor

_____
Douglas R. Flanagan

_____
Maureen D. Donovan

_____
Dale E. Wurster

_____
Daniel M. Quinn

To
My parents, Leena and Dileep Desai

ACKNOWLEDGMENTS

This achievement would not have been possible without the support and encouragement of several people. I would like to express my appreciation and gratitude to all of them.

First and foremost - to Dr. Lee Kirsch, my advisor and mentor, for his support and guidance.

I would like to thank Dr. Wurster, Dr. Quinn, Dr. Flanagan, and Dr. Donovan for serving on my thesis committee. A special thanks to Dr. Matheson for delaying his trip to accommodate my comprehensive exam.

I could not have reached this milestone without the unwavering support of my parents, Leena and Dileep Desai. My brother and his wife, Mihir and Deepali, who checked on me regularly and kept me going through thick and thin. My late grandparents, Indira and Vasudeo Desai, Muktabai and Maharudra Netravali who always guided me to be my best. My extended family, especially my aunts - Sheela, Rekha, and Jyoti who have always nudged me towards research and science.

Special thanks goes out to my former roommates Praveen, Mogili, Subhashish, Ankur, and Bhavik, who have been my family away from home. My years at Iowa could not have been memorable without my friends Vaibhavi, Mowyee, Sushmita, Neeraj, Sriram and Himanshu. I would also like to thank my labmates Bhanu, Lida, Anjali, Lairi, Madhu, Zong, Nui, Fon, and Jiang for all their support and help.

TABLE OF CONTENTS

LIST OF TABLES

LIST OF FIGURES

CHAPTER I

INTRODUCTION

Introduction

Anilides are amides formed by the reaction between carboxylic acids and anilines. They are structural components of drugs such as atorvastatin calcium (Lipitor®, Pfizer), acetaminophen (Tylenol®, McNEIL-PPC), and formoterol (Foradil®, Novartis). The hydrolytic stability of the amide is important to the efficacy of these drug molecules.[1-3] The susceptibility of formanilides to hydrolysis is dependent on the substituents connected to the aromatic nitrogen.[4, 5]

The hydrolytic mechanisms for anilides are different than those associated with the hydrolysis of benzamides and alkyl amides.[6] The hydrolytic reactivities of acetanilides in acidic and alkaline environments have been extensively studied by experimental and computational methods.[4, 5, 7, 8]

In acidic solutions, acetanilide hydrolysis changes mechanisms from acid catalyzed unimolecular (A1) to an acid catalyzed acyl cleavage bimolecular mechanism ($A_{AC}2$). [9, 10] At very high acid concentrations (>70 % w/w sulfuric acid) the reaction follows the A1 mechanism. As depicted in Figure I-1, under strongly acidic conditions the amide exists primarily in the protonated form. The proton on the carboxyl group is transferred to the amine in a fast proton transfer step. The next step involves the slow cleavage of the amide to form the unprotonated amine and the acylium ion. The acylium ion combines with a water molecule to form the corresponding carboxylic acid through a fast proton transfer step.

In dilute acids (< 64% w/w sulfuric acid) acetanilide degrades via the acid catalyzed acyl cleavage bimolecular mechanism ($A_{AC}2$).[4, 6] The $A_{AC}2$ mechanism, as shown in Figure I-2, involves the protonation of the amide at the carbonyl oxygen. The carbonyl carbon is then attacked by water to form the tetrahedral intermediate (THI). The

THI can degrade to products through a series of fast proton transfers or revert to the initial substrate.

At neutral pH, acetanilides are extremely stable unless activated by strongly electron withdrawing groups. Studies done on trifluoroacetanilide hydrolysis at neutral pH indicated a complicated multistep mechanism.[11]

Amide hydrolysis in alkaline solutions is catalyzed by the hydroxide ion. In basic solutions, the hydrolysis of amides occurs by the pathways shown in Figure I- 3.[4] The first step involves the formation of the tetrahedral intermediate (THI) which can then revert to reactants or break down to products by reactions catalyzed by water, another hydroxide ion, and/or buffer species.[12] First and second-order dependences on hydroxide ion concentration are observed for alkaline hydrolysis of acetanilides, formanilides, and trifluoroacetanilides.[13-16] Structure-reactivity relationships of phenyl ring substituted trifluoroacetanilides indicate a complex mechanism where the reaction mechanism is affected by changes in amine basicity of the leaving group.[17] Structure-reactivity studies carried out on the substitution of the acyl group of acetanilides have shown a complicated dependence on steric and electronic properties of the substituent.[18]

Formoterol, a potent β_2-agonist used in the treatment of asthma, is unstable in aqueous solutions.[19] In buffered systems at alkaline pH formoterol degrades to des-formoterol with the formation of a formate molecule as shown in Figure I- 4. This reaction was faster than expected and it was hypothesized that this is due to intramolecular catalysis by the neighboring ortho-hydroxyl group.[20] A survey of the literature showed that all the studies on anilide hydrolysis have been performed on *para* and *meta* substituted anilides, and have not accounted for ortho effects. In spite of the importance of *ortho* substitution on pharmaceutically important compounds such as

formoterol and antimycin-A_1, no systematic studies on the *ortho* substitution of anilides have been conducted to elucidate the effect of *ortho* substituents on reaction rates.

Project Objectives

The main objectives of this work were to conduct hydrolytic kinetic studies on substituted formanilides, propose a mechanism, and then evaluate the effect of ortho substitution on the rate of hydrolysis. The central hypothesis for this work is that steric effects which occur only in ortho substituents are significant factors which control the rate of anilide hydrolysis. The rationale for these studies is that the successful development of linear free energy relationships will help evaluate the factors controlling stability of pharmaceutically relevant anilides. The goal was to develop linear free relationships between ortho substitution on the anilide ring and its stability. These relationships could then quantitatively predict the effect of the electronic and steric factors on the hydrolysis rates.

To test the hypothesis, kinetic studies were carried out using selected formanilides as model compounds. Substituents on the phenyl ring of formanilide were chosen based on unique steric and electronic properties. A library of compounds with selected substituents was compiled either by procuring the compounds commercially or by synthesizing them from the appropriate starting anilines. The structure and identity of the compounds were determined using nuclear magnetic resonance (NMR) spectroscopy and melting points. The purity of the compounds was estimated using differential scanning calorimetry (DSC). If the compounds had ionizable groups, the pK_a values of the ionizable groups were determined.

The substituted formanilides were degraded in alkaline and acidic solutions under pseudo-first-order conditions. The reaction solutions were quenched and analyzed by high performance liquid chromatography (HPLC) to identify the reaction products. HPLC peaks were identified by comparison with authentic samples of formanilide and

Figure I- 1:A1 mechanism for the acidic hydrolysis of acetanilide.[10]

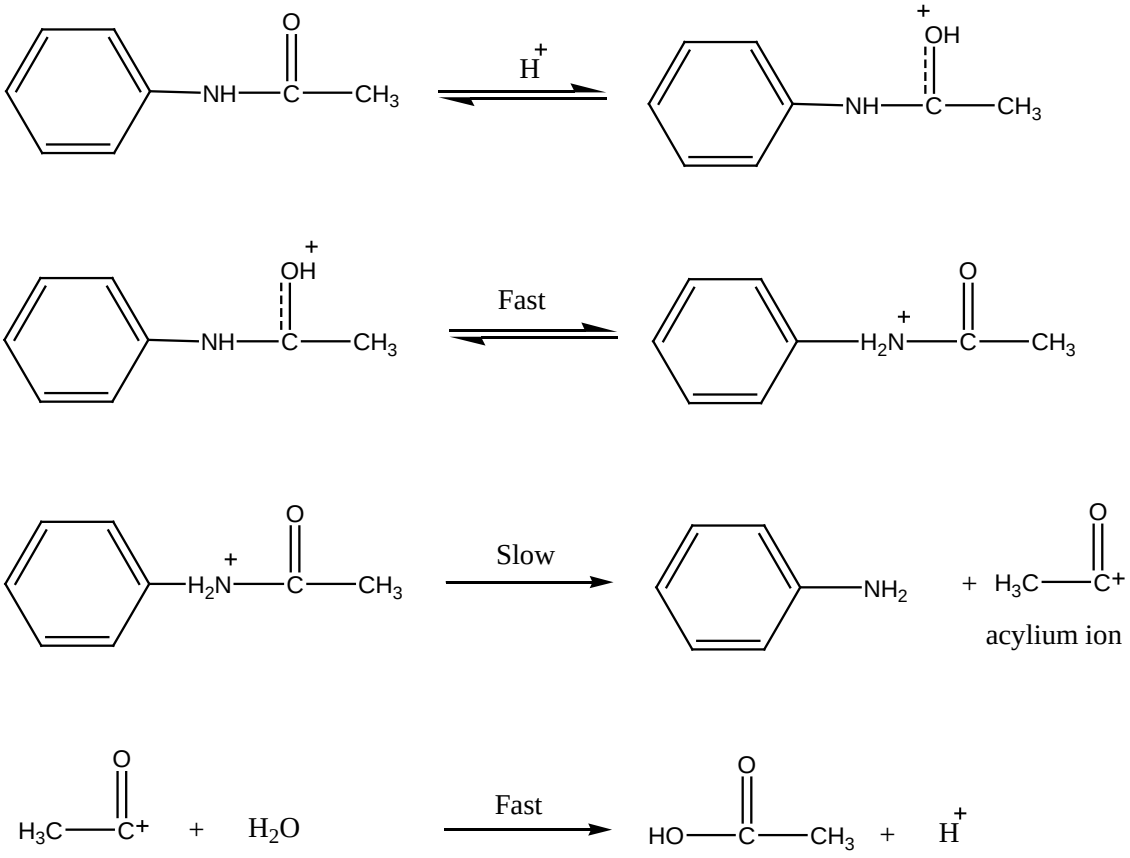

Figure I- 2: Acid catalyzed acyl cleavage bimolecular ($A_{AC}2$) mechanism for acidic hydrolysis of amides.[4]

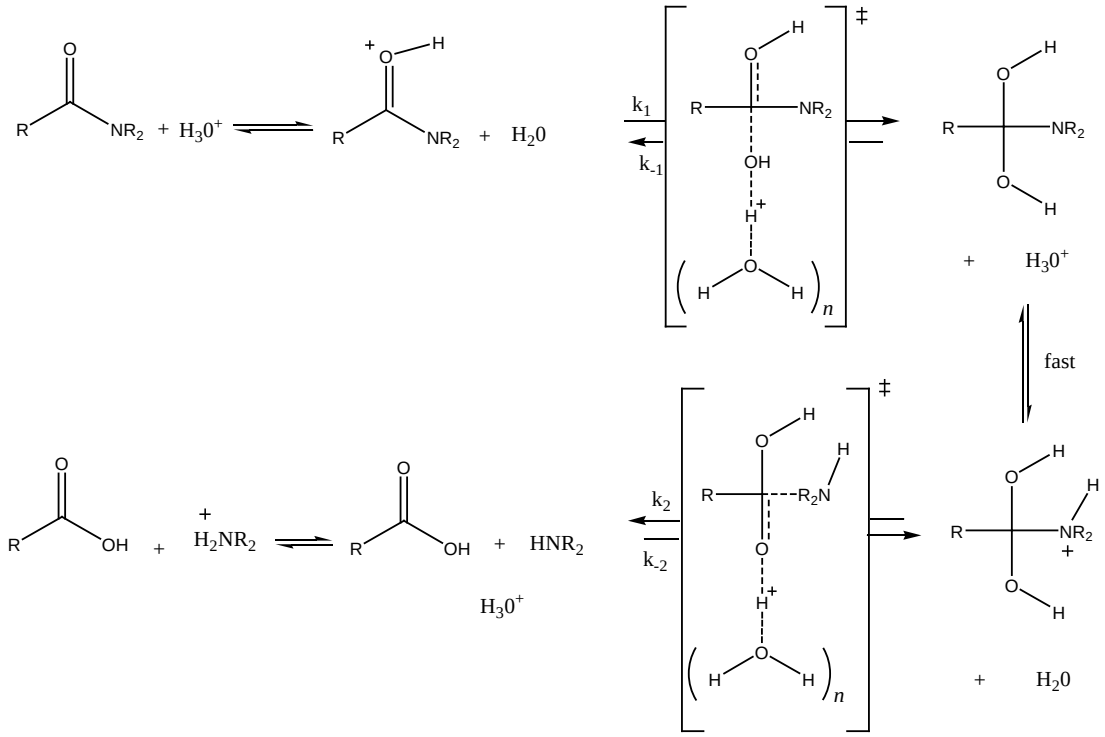

Figure I- 3: Pathways for amide hydrolysis in alkaline solutions. [4]

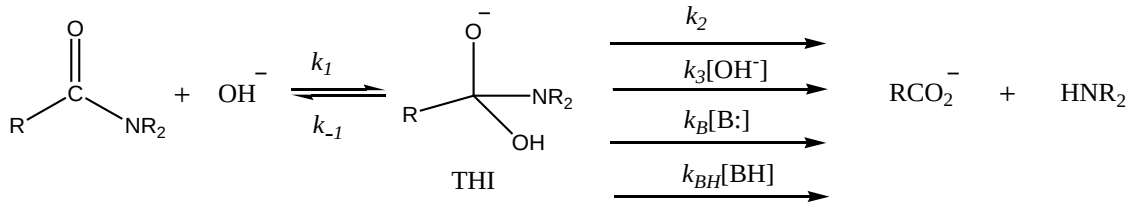

Figure I- 4: Scheme for alkaline hydrolysis of formoterol.

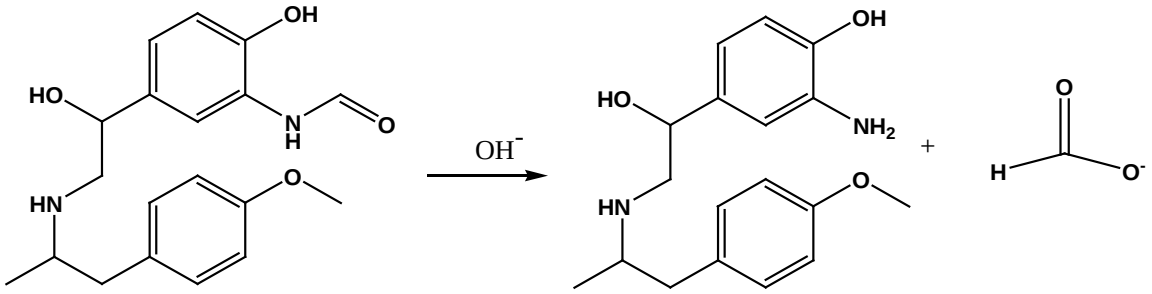

formoterol

des-formoterol

formate

aniline. Using the authentic samples as standards, calibration curves were generated and used to calculate the concentrations of the substituted formanilides, and the corresponding aniline. Mass balances were evaluated and degradation reaction schemes were proposed.

Once the degradation schemes were determined, the hydrolysis of substituted formanilides were carried out under different acid and base concentrations. The pseudo-first-order rate constants were determined for the reactions, and used to generate pH-rate profiles. pH-rate profiles were used to propose suitable rate laws for the hydrolysis of formanilides. Rate constants obtained were also analyzed using the appropriate linear free energy relationship. The effect of ionic strength, binary solvent systems, buffers, and temperature were also evaluated. The kinetic information generated was then used to propose/confirm mechanisms for hydrolysis of formanilides and to elucidate the effect of ortho substitution.

Formanilides as Model Compounds

Formanilides consist of anilines and formic acid as shown in Figure I- 5. Formanilides are labile as compared to acetanilides which permitted the study of their hydrolysis under mild experimental conditions. The electronic and hydrogen bonding capabilities of the amide bond have been studied extensively.[21-29] This amide bond is isolated, freely rotating, and does not have any significant steric restrictions due to the acyl component of the moiety. Hence any steric effect due to ortho substitution was expected to be easily observable. These properties make formanilides ideal compounds to study the effect of ortho substitution.

Several studies have been published on the acidic and alkaline hydrolysis of formanilides; however these studies are not complete and the underlying mechanisms have not been fully characterized. In strongly acidic solutions, formanilide has been reported to degrade via the $A_{AC}2$ mechanism to form the products.[30-32] At high

concentrations of acid a linear Hammett relationship was observed (Figure I-6(A)). However, at lower acid concentrations a nonlinear Hammett relationship was observed (Figure I-6(B)). These results were explained by postulating a change in the rate-determining step for the reaction. However these interactions were not quantitatively analyzed.

DeWolfe and Newcomb were the first to study the alkaline hydrolysis of formanilide.[16] The pH-rate profile for formanilide displayed nonlinear dependence on hydroxide which they explained by (a) higher than first-order dependence on hydroxide, and (b) concurrent reduction in the concentration of substrate due to formation of unreactive conjugate base. Hammett plots generated using the observed rate constant showed no difference in reactivity with change in substituent except for strongly electron withdrawing compounds such as cyano and nitro groups. The analysis of the structure-reactivity relationship was incomplete since the studies did not take into account the dependence of reaction on the ionization of substrate and also the effect of substituent on individual steps of the reaction. Kvalek and Sterba attempted to correct the rate constants for substrate ionization and isolated rate constants (k_3) for the second-order dependence on hydrolysis.[14] The Hammett plot for these rate constants showed a concave upward curve which is indicative of a change in mechanism (Figure I-6(C)). At lower hydroxide concentrations the solutions show first-order dependence on hydroxide concentrations.[31, 32] Effect of nucleophilic catalysis (imidazole), ionic strength, and temperature studies have been carried out; however no mechanistic explanation of the effects was attempted.[31-35]

Overview of Kinetic Techniques

One approach to study the kinetics of a reaction is to understand the reaction mechanism. A chemical mechanism is a complete detailed description of a reaction pathway, including any reactive intermediates. However, a mechanism is a postulate. To

Figure I- 5: Chemical structure of formanilide.

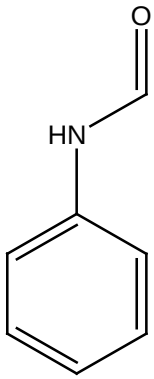

Figure I- 6 Hammett plots for formanilide: (A) acid hydrolysis at very high acid concentrations (H_A = -3.2); (B) acid hydrolysis at lower acid concentrations (H_A = 0); (C) second-order (k_3) alkaline hydrolysis of formanilide. The line in I-6 (A) is a linear regression line for the Hammett equation while the lines in I-6(B) and (C) are smooth lines not fit to the data.

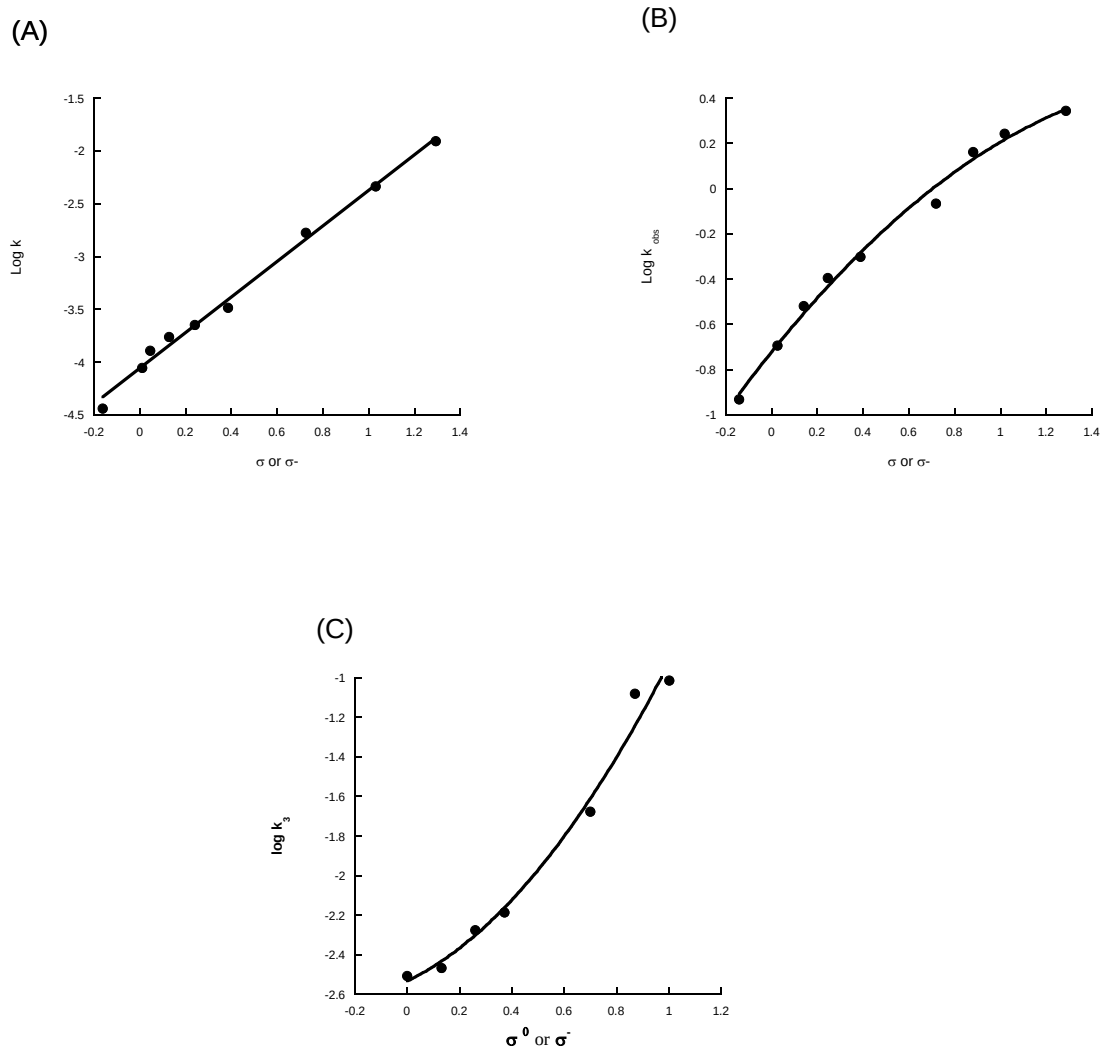

be considered valid, mechanisms have to be consistent with observed kinetic data and chemical intuition. Systematic studies of mechanisms are carried out in a stepwise fashion. The first step consists of the characterization and identification of the substrate, intermediates, and products of the reaction. The next step consists of determination of the reaction order of the reaction followed by the determination of a reaction scheme. Using pH-rate profiles, the rate law for the reaction can be proposed. Since several mechanisms are usually consistent with an observed rate law, complementary kinetic studies need to be carried out to identify the correct mechanism. To identify the mechanism for hydrolysis of formanilides, kinetic studies were carried out which included pH-rate profile determinations, temperature effect studies, ionic strength effect studies, solvent studies, and structure-reactivity relationship correlations. Brief overviews of the methods used are given below.

pH-Rate Profiles

Degradation rates of drugs in solution are markedly dependent upon the pH of the medium.[36] This implies that the degradation rate is dependent upon the concentration of hydronium ion, hydroxide ion, and water molecules. pH-rate profiles are generated by carrying out the reactions under pseudo-first-order conditions, at different pH conditions, wherein the pH remains constant, and the apparent rate constants for loss of substrate (S), appearance and loss of intermediates, and appearance of products (P) does not change over time. Reaction products for the degradation reaction are analyzed and reaction schemes are determined. If the reaction follows more than one reaction pathway, each pathway is elucidated and analyzed separately. A pH-rate profile corresponding to the pathway under consideration is prepared by plotting the logarithm of the observed pseudo-first-order rate constants (k_{Δ}) against pH. Based on the shape of the pH-rate profile the composition of the rate limiting transition-state can be deduced thereby defining a rate law.[37] The rate law defines the compositions of the rate limiting

transition-states; however it does not describe the sequence of events that led to the composition and does not describe the structure of transition-state. Hence, several different mechanisms can account for the same rate law and additional studies are needed to distinguish between kinetically indistinguishable mechanisms.

pH-rate profiles occur in different shapes; however all pH-rate profiles can be regarded as the composite of five fundamental curves, as illustrated in Figure I- 7. Each segment represents a kinetically distinguishable mechanism. These curves are connected to each other by upward bends (slope changes from 0 to ± 1), which indicate an additional, kinetically distinct, competitive mechanistic pathway.

Specific acid and base catalysis are represented by the straight lines of Figures I-7(A), and I-7(B) respectively. The specific acid catalyzed reactions generate a pH-rate profile with a straight line having a unit negative slope (-1) and can be represented by Scheme I-1where S is the substrate and P are the products. The rate is given by Equations I-1and I-2.

$$S \xrightarrow{k_1\ [H^+]} P$$

Scheme I- 1

$$rate = k_1[H^+][Substrate] \qquad \text{Equation I-1}$$

$$k_\Delta = k_1[H^+] \qquad \text{Equation I-2}$$

The rate law indicates that the rate limiting transition-state consists of substrate molecule and a proton. Examples for this type of behavior include hydrolyses of chloramphenicol and digoxin. [38, 39]

Similarly specific base catalyzed reactions generate pH-rate profiles with unit positive slope (+1) and can be represented by Scheme I-2, and the rate equations and laws are is given by Equations I-3, and I-4. Specific base catalysis has been observed for drugs such as acetaminophen and lidocaine.[29, 40]

$$S \xrightarrow{k_1\,[OH^-]} P$$

Scheme I- 2

$$rate = k_1[OH^-][Substrate] \qquad \text{Equation I-3}$$

$$k_\Delta = k_1[OH^-] \qquad \text{Equation I-4}$$

The curve observed in Figure I- 7(C), and corresponding Scheme I-3 shows no dependence on pH. It reflects a unimolecular reaction of substrate with neither acid nor base involvement as represented by the rate laws in Equations I-5 and I-6, respectively. These shapes have been observed for the hydrolysis of cefotaxime and lidocaine.[40, 41]

$$S \xrightarrow{k_1} P$$

Scheme I- 3

$$rate = k_1[Substrate] \qquad \text{Equation I-5}$$

$$k_\Delta = k_1 \qquad \text{Equation I-6}$$

Curves shown in Figure I- 7(D) and I-7(E) are termed as downward bends. The downward bend consists of a regions with unit positive (+1) or unit negative (-1) slopes connected by a short curved segments to a regions of zero slope. Both these regions in the downward bend correspond to a single mechanism. Downward bends can be explained by two situations; partitioning of substrate between two species with different reactivites (substrate ionization) or a reaction pathway involving an intermediate where its formation and breakdown is subject to different pH dependent behavior (i.e. change in rate-determining step).

The first type of mechanism that gives rise to a downward bend can involve the loss or gain of a proton by the substrate in a rapid equilibrium prior to the rate limiting step. This situation is also known as substrate ionization or substrate titration wherein the protonated and unprotonated forms have different reactivities. pH-rate profiles for aspirin and *para* benzoic acid esters exhibit such downward bends.[37, 42] The pH-rate profile in Figure I-7(D) can be described by a proposed mechanism where the protonated form of the substrate reacts to form the product. The reaction can be represented by Scheme I- 4. The fraction of ionized substrate (f_{SH}) can be represented by Equation I-7. The rate of the reaction is given by Equation I-8, and the rate law then becomes Equation I-9.

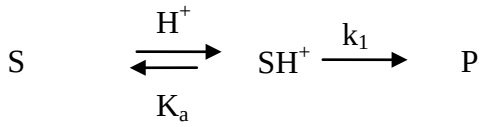

Scheme I- 4

$$f_{SH} = \frac{[H^+]}{K_a + [H^+]} \qquad \text{Equation I-7}$$

$$rate = k_1[SH^+] = k_1 f_{SH} S_{Total} \qquad \text{Equation I-8}$$

$$k_\Delta = k_1 f_{SH} \qquad \text{Equation I-9}$$

Similarly for the downward bend in Figure I- 7(E) a mechanism can be hypothesized (Scheme I-5) where the unionized form is the reactive species, and a corresponding rate law (Equation I-12**)** can be proposed.

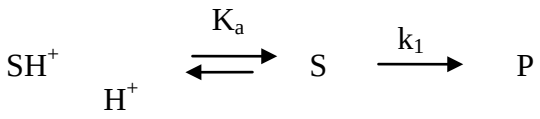

Scheme I- 5

$$f_S = \frac{K_a}{K_a + [H^+]}$$ Equation I-10

$$rate = k_1[S] = k_1 f_S S_{Total}$$ Equation I-11

$$k_\Delta = k_1 f_S$$ Equation I-12

It should be noted that for both types of downward bends alternative kinetically indistinguishable mechanisms may exist. The kinetically equivalent mechanisms for Schemes I-4 and I-5 are I-6 and I-7, respectively. These mechanisms show the same functional dependence on $[H^+]$ or $[OH^-]$ and will give identical transition-state compositions.

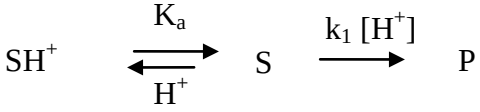

Scheme I- 6

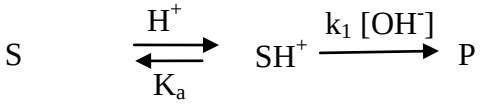

Scheme I- 7

Downward bends may also occur due to a change in rate-limiting step as seen for reactions of kynurenine and semicarbazones.[43, 44] The pH-rate profile for the mechanism shown in Scheme I-8 will give an pH-rate profile similar to Figure I- 7(E). In

this mechanism the substrate equilibrates to form the steady-state intermediate (X) which then degrades to form the products. The appropriate rate law is given by Equation I-13. In this mechanism the first step is pH independent, however the rate of the second step increases with pH. At high hydroxide concentrations the formation of the intermediate is the rate limiting step and the pH-rate profile will be essentially be flat with a slope of zero.

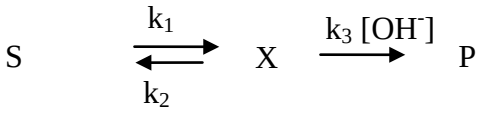

Scheme I- 8

$$k_{\Delta} = \frac{k_1 k_3 [OH^-]}{k_2 + k_3 [OH^-]}$$

Equation I-13

Over the entire pH the pH-rate profile will be a sum of several rate laws and may have complex shapes. Interpretation of pH-rate profiles is typically a useful first step towards proposing a mechanism.

Temperature Effects

For a given reaction the rate of the reaction is dependent on the temperature, and this dependence can be systematically studied using a series of isothermal studies. The energy of activation for a reaction can be calculated using the Arrhenius relationship as shown in Equation I-14; where k is the rate constant, A is the frequency factor, R is gas constant, T is absolute temperature, and E_a is activation energy. The Arrhenius equation can also be represented as a linear equation as shown in Equation I-15. Arrhenius plots can be generated by plotting the reciprocal of the reaction temperature against the natural logarithm of the rate constants. The slope and intercept can be used to generate estimates for the E_a and A respectively (Figure I-8 (A)). Activation energies are useful in

predicting the rate of reaction at different temperatures.[45] The free energy of activation ($\Delta G^{\ddagger}$), entropy of activation ($\Delta S^{\ddagger}$), and enthalpy of activation ($\Delta H^{\ddagger}$) of the reaction can also be determined from rate data by using Equation I-17 where *k* is the Boltzmann constant and *h* is the Planck's constant. As shown in Figure I-8 (B), Eyring plots are plots of ln(k/T) against (1/T) which are used to determine the enthalpy of activation ($\Delta H^{\ddagger}$) from the slope (Equation I-18). The $\Delta H^{\ddagger}$ value is then used to calculate the entropy of activation ($\Delta S^{\ddagger}$) at each temperature using Equation I-19. The reported entropy of activation value is the average value determined over the temperature range. The enthalpy of activation of the reaction provides information about the energy associated with breaking and forming of bonds while entropy of activation of the reaction gives information about the degree of disorder between the reactants and the transition-state. The extrathermodynamic parameters in some cases are used to differentiate between possible mechanisms.[46, 47]

$$k = Ae^{-\frac{E_a}{RT}} \qquad \text{Equation I-14}$$

$$\ln k = \ln A - \frac{E_a}{RT} \qquad \text{Equation I-15}$$

$$k = \frac{kT}{h} e^{-\Delta H^{\ddagger}/RT} e^{\Delta S^{\ddagger}/T} \qquad \text{Equation I-17}$$

$$\ln \frac{k}{T} = -\frac{\Delta H^{\ddagger}}{RT} + \frac{\Delta S^{\ddagger}}{R} + \ln \frac{k}{h} \qquad \text{Equation I-18}$$

$$\Delta S^{\ddagger} = \frac{\Delta H^{\ddagger}}{T} - R \ln\left(\frac{T}{k}\right) - R \ln\left(\frac{k}{h}\right) \qquad \text{Equation I-19}$$

For most reactions the rates are studied over a limited range of temperatures and the Arrhenius relationships are usually linear. Curvature in Arrhenius plots is rarely observed but the nonlinearity could occur due to three possible reasons. The first reason is the possibility that the curvature is an artifact due to systematic error in the

measurements. This possibility can be evaluated by careful analysis of the reaction data. The second possible reason is that the E_a is a function of $\Delta H^{\ddagger}$ which in turn is related to the molar heat capacity of activation at constant pressure ($\Delta C^{\ddagger}_p$) as shown in Equation I-20. $\Delta C^{\ddagger}_p$ is related to the differences in heat capacities between the transition state and the reactants. $\Delta C^{\ddagger}_p$ values are typically constant over a limited temperature range; however this value could vary when studied over a wider temperature range which in turn could lead to nonlinear Arrhenius plots. The third reason for nonlinearity in Arrhenius plots occurs in complex reactions with multiple elementary reaction steps. The observed rate constant is a function of the rate constants for all the individual elementary reactions prior to the rate-determining step with each elementary reaction having its own activation energy. Thus the presence or absence of curvature in the Arrhenius relationships could be due to the functional relationship of the observed rate constants on the elementary constants and the magnitudes of the individual activation energies of each elementary step.[45]

$$\Delta C_P^{\ddagger} = \frac{\Delta H^{\ddagger}}{\Delta T} \qquad \text{Equation I-20}$$

Ionic Strength Effects

The bulk properties of the solvent system, such as dielectric constants, ionic strength, and viscosity can directly affect the rate constant by changing the environment of the reactive species, intermediates, and transition-states. Ionic strength studies are carried out at constant pH but varying concentrations of a non-interacting salt. Ionic strength effects occur due to the effect of the ionic atmosphere on the activity coefficients of the reactive species and transition-states. Consider the simple reaction where reactants A and B react to form products via transition-state denoted by $[AB]^{\ddagger}$ as shown in Scheme I-9. The charges (z) on the three species are related to each other by Equation I-21. The rate constant (k) is related to the activity coefficients by Equation I-22 where k^0 is the rate

constant associated with the reference state, and γ_A, γ_B, and $\gamma_{[AB]‡}$ are the respective activity coefficients for the reactants and the transition-state. The activity coefficient of the ions can be calculated using the Debye Huckel Limiting law (Equation I-23). The Brønsted-Bjerrum equation(Equation I-24) can then be derived by substituting Equation I-23 in Equation I-22, where Q is a constant and μ is the ionic strength of the medium. Changing the ionic strength by addition of inert electrolytes causes the rate constants for reacting species to increase, decrease, or remain constant. Accordingly the effect is denoted as positive, negative or absent. Lack of ionic strength effects indicates that either one or both of the reactants have no charge. Occurrence of ionic strength effects imply the presence of charged reactant species are of identical or opposite charge. Thus, ionic strength effects can be used to determine the charge of the reactive species and the transition-state. The net effect and the sign of the effect are valuable aids in the interpretation of mechanisms.[48] The Debye Huckel limiting law is applicable only at low ionic strength ($\mu \leq 0.01$), however the range can be extended by using the Guntelberg approximation (Equation I-25).[49]

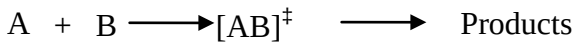

Scheme I- 9

$$z_A + z_B = z_{[AB]‡} \qquad \text{Equation I-21}$$

$$\log k = \log k^0 + \log[\gamma_A \gamma_B / \gamma_{[AB]‡}] \qquad \text{Equation I-22}$$

$$\log \gamma = -Qz^2 \sqrt{\mu} \qquad \text{Equation I-23}$$

$$\log k = \log k^0 + 2Qz_A z_B \sqrt{\mu} \qquad \text{Equation I-24}$$

Figure I-7: Fundamental curves into which most pH-rate profiles can be resolved.[37]

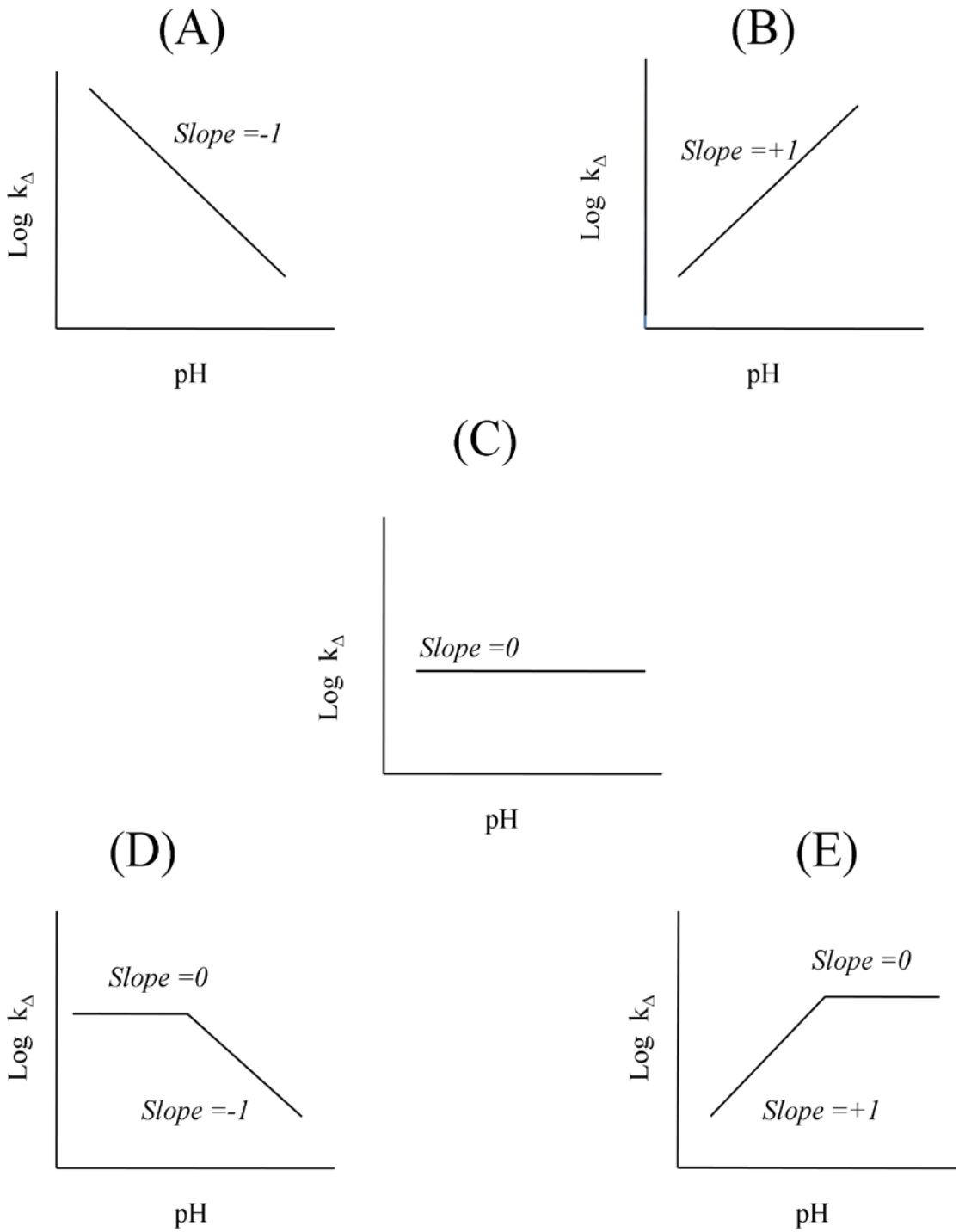

Figure I- 8: Examples for Arrhenius plot (A) and Eyring plot (B) for the hydrolysis of m-chloroformanilide in 1.0 M hydrochloric acid.

(A)

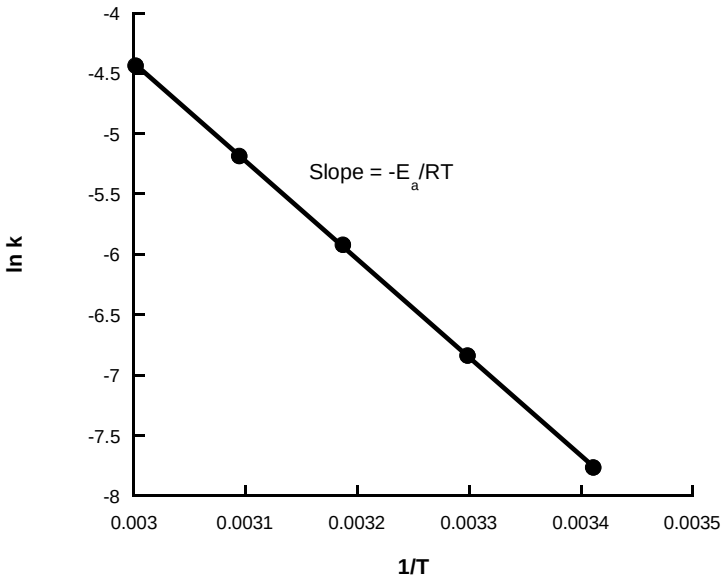

(B)

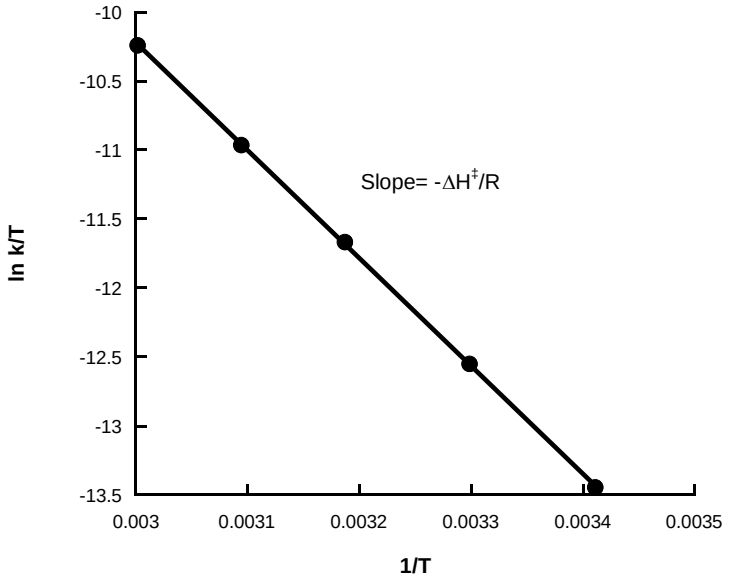

$$\log k = \log k^0 + \frac{2Qz_A z_B \sqrt{\mu}}{1+\sqrt{\mu}} \qquad \text{Equation I-25}$$

Binary-Solvent Effects

The addition of organic solvent to an aqueous system will alter the bulk properties of the aqueous system. These bulk properties include dielectric constant, viscosity, solvent structure, and the solvation characteristics of the medium.[50] Due to the variety of changes that occur, it is difficult to put forward a single universal theory for liquid-phase reaction kinetics. A qualitative theory applicable to several binary aqueous systems is the Hughes-Ingold hypothesis. The Hughes-Ingold rule indicates that if the transition-state is more polar than the initial state, increasing the polarity of the solvent will stabilize the transition-state relative to the initial state and lead to an increase in the rate of the reaction. Several reactions appear to follow this rule. However this theory holds only if the reaction is predominantly driven by enthalpy change, and entropy changes are negligible.[51] In some cases solvent effects have been used to elucidate the reaction mechanism.[52]

Buffer Catalysis

In buffered systems, in addition to catalysis by hydronium and hydroxide ions, reactions can be catalyzed by the components of the buffer.[53] The buffer acid (HB) and its conjugate base (B) can individually catalyze the degradation reaction. Linear buffer catalysis dependencies are common and can be represented by Equation I-26 where k_B and k_{HB} are the second-order rate constants for catalysis due to the buffer acid and buffer base, respectively. Nonlinear buffer effects may indicate a problem with the buffer system (i.e. buffer polymerization or uncontrolled ionic strength effect), higher than first-order dependence of buffer on reaction rate or in special cases, the change of rate-determining step.[43] Buffer catalysis studies are conducted by studying the reaction in several different buffers at various concentrations of buffer. The k_B and k_{HB} are

isolated by appropriate methods and used to generate a Brønsted plot. The Brønsted general base catalysis plot is generated plotting the log k_B against pK_a of the buffer. The Brønsted relationship for base catalysis is given by the Equation I-27 where G_B is a constant, pK_w is the ion product of water, and β is the slope. The value for β is determined from the plots of log k_B vs pK_a and the value is between 0 and 1. A value of 0 for β indicates that there is no general acid or base catalysis and β =1 indicates that proton transfer is complete before rate limiting transition-state i.e. predominating specific base catalysis exists. The value of β is an indicator of the extent of proton transfer from the solvent in the reaction process. A similar relationship can also be derived for catalysis due to buffer acid catalysis. Buffers involved in nucleophilic catalysis can be detected by deviations from the line determined by the general base or general acid catalysis.

$$rate = k_{\Delta} + k_B[B] + k_{HB}[HB] \qquad \text{Equation I-26}$$

$$\log k_B = \log(G_B - pK_w) + \beta \times pK_a \qquad \text{Equation I-27}$$

Structure-Reactivity Relationships

Structure-reactivity relationships (SRR) can be used to clarify and classify data, to predict the rate and equilibrium behavior of structurally similar compounds, and to provide information about the mechanism for the reactions.[54] SRR occur because the velocity of the reaction is dependent on the stability of the transition-state with respect to the initial state of the reactants. Therefore, the structural characteristics which stabilize either the initial or transition-state will affect reaction kinetics.

Some reactions show linear correlations between the logarithms of the rate or equilibrium constants of one reaction series and logarithm of equilibrium constants of a second reaction series when both series are subjected to the same structural variation. A typical example of such linear relationships is illustrated in the classical Hammett

relationships where linear relationships were observed between the logarithm of the rate constants (k) for *meta* and *para* substituted ethyl benzoates and the logarithm of the equilibrium ionization constants (K_a) of *meta* and *para* substituted benzoic acids.[55] The SRR can be represented by Equation I-28 where k_1 and K_1 are the rate and equilibrium constants respectively for reaction A, and ρ and c are the slope and intercept.

$$\log k_1 = \rho \log K_1 + c \qquad \text{Equation I-28}$$

The rate constant can be defined by the free energy of activation ($\Delta G^{\ddagger}$) using Equation I-29 and the equilibrium constant can be defined by the Gibbs free energy (ΔG^0) using Equation I-30. In Equations I-29 and I-30, *k* is the Boltzmann constant; T is the temperature; *h* is the Planck constant, and R is the universal gas constant. Substituting Equations I-29 and I-30 into Equation I-28 gives Equation I-31

$$\log k = -\frac{\Delta G^{\ddagger}}{2.303RT} + \log \frac{kT}{h} \qquad \text{Equation I-29}$$

$$\log K = -\frac{\Delta G^{0}}{2.303RT} \qquad \text{Equation I-30}$$

$$\Delta G^{\ddagger} = \rho \, \Delta G^{0} + c' \qquad \text{Equation I-31}$$

A linear correlation exists between the free energy changes and hence such correlations are called as linear free energy relationships (LFER). Frequently LFER are developed using reference reactions in the series where k_0 and K_0 refer to the rate and equilibrium constants for the reference reactions (Equation I-32). A substituent constant (σ) is defined (Equation I-33) and substituted in Equation I-32 to give Equation I-34. The slope ρ is defined as the reaction constant.

$$\log\left(\frac{k_1}{k_0}\right) = \rho \log\left(\frac{K_1}{K_0}\right) \qquad \text{Equation I-32}$$

$$\log\left(\frac{K_1}{K_0}\right) = \sigma \qquad \text{Equation I-33}$$

$$\log(\frac{k_1}{k_0}) = \rho\sigma$$

Equation I-34

The value and sign of σ indicates if the substituent is electron withdrawing or electron donating. The initial σ values designated as the Hammett sigma scale were determined using the ionization of benzoic acids as the reference reaction. However, these σ values could not account for resonance interactions present in aromatic compounds in which the reaction site is located very close to the aromatic ring. To account for these enhanced interactions due to the ability of the aromatic ring to transfer electron density from the substituent to the reaction site several different scales for substituent constants were developed. To account for enhanced electron donating capability due to resonance the σ^+ scale was developed which uses the solvolysis of cumyl chlorides as the reference reaction [56] To account for enhanced electron withdrawing capability due to resonance interactions the σ^- scale was developed which used the ionization of anilines and phenols. Other scales also developed include the σ^0 and the σ^n scales developed for substituents that do not show any resonance delocalization interactions.[57, 58] The reaction constant (ρ) is dependent on the reaction and is a quantitative measure of the sensitivity of reaction to the influence of substituents. The value of the reaction constant is determined by the transmission efficiency of substituent effects from substituent to the reaction center, reaction conditions, and susceptibility of the reaction to electronic or other effects. For linear Hammett plots the reaction constant can be positive, negative or almost zero as shown in Figures I-8(A-C). If the ρ is positive the reaction is accelerated by electron withdrawing substituents. [55] If the ρ is negative the reaction is accelerated by electron donating substituents.[59] If ρ is very small then either the substituent does not have any significant effect on the reaction or the reaction consists of consecutive steps that have an equal and opposite effect on the reaction rate. [60] The sign of the reaction constant can,

in some cases, be an indicator of the charge in the transition-state and the effect of changing electronic environment at the reaction center.[61]

Linear Hammett plots provide quantitative information about the reaction; however, the deviations from ideal linear behavior provide additional mechanistic insight into the reaction mechanism. Nonlinearity in a Hammett plot can be due to change in mechanism, change in rate-determining step (RDS), ortho substitution effects, and intramolecular catalysis. Such reactions are of two types: simple single step reactions or complex reactions which consist of several steps. In the elementary (single step) reactions, the Hammett reaction constant (ρ) represents the effect of the single rate-determining step on the reaction. However, for complex reactions the Hammett reaction constant (ρ) is a sum of each individual step that precedes the rate-determining step. Nonlinear Hammett relationships occur frequently in complex reactions since each step affect the overall reaction.

Occasionally the energetically preferred mechanism of a reaction changes upon altering a substituent. This is often the case if two pathways of similar activation energy are available and have very different electronic requirements. This results in a nonlinear Hammett plot with a change in the slope(i.e. concave upwards) indicative of change in mechanism as shown in Figure I- 9(d) .[62, 63] The change may be abrupt or may change smoothly as function of substituent.

In a multistep reaction the overall rate constant obtained is a function of the rate constant of each individual step in the reaction preceding the rate-determining step. Each elementary step will have a characteristic susceptibility to electronic effects and therefore its own ρ value. If the rate-determining step changes at some position along the substituent constant axis, the observed reaction constant will also change leading to curvature in the Hammett plot, concave downwards, indicative of change in RDS as shown in Figure I- 8(e). [44, 64]

Hammett plots for ortho substituted aromatic compounds can result in scatter plots whereas the corresponding *meta* and *para* substituents give linear correlations. These deviations from linearity are due to "*ortho* effects" which consist of several factors including the normal electronic effects due to inductive and resonance contributions, the proximity or field effects, and true steric effects. Taft and co-workers split the overall *ortho* effect into two components. The normal electronic effects (similar to those seen with the *meta* and *para* substituents) and steric effects. Comparing the acidic and alkaline hydrolysis of benzoic acid esters, Taft was able to define the Taft steric substituent constant (E^o_s) and steric reaction constant (δ). As shown in Equation I-35 a multiple linear free energy relationship was defined where $\rho^*\sigma^*$ correspond to the normal electronic effects and δE^o_s account for steric effects.

$$\log(\frac{k_1}{k_0}) = \rho^*\sigma^* + \delta E_s^0$$

Equation I-35

Where, k_0 is the rate constant for the *ortho* methyl substituted compound. Several excellent correlations using Equation I-28 have been achieved which indicate the presence of a significant steric effect on the reaction for substituents at the *ortho* position.[65]

In reactions where the substituent can interact directly with the reaction center, deviations from the expected Hammett plot can occur. These deviations can be due to intramolecular catalysis which requires the presence of suitably positioned substrate and reagent functions on the same molecule. The rate enhancement then could be due to the proximity of the reactive species, reduction in the distribution of conformational populations, or changes in the entropy of the reaction.[60, 61] For example, the hydrolysis of salicylamide was compared with hydrolysis of *o*-methoxybenzamide. The rate of degradation of unionized salicylamide was significantly greater than that of *o*-methoxybenzamide due to intramolecular catalysis.[66]

If temperature studies are carried out on a series of compounds then SRR between extrathermodynamic parameters, i.e. $\Delta S^{\ddagger}$ and $\Delta H^{\ddagger}$,can also be observed.[67] To study these effects temperature studies have to be carried out for all the compounds in the series, and the $\Delta S^{\ddagger}$ and $\Delta H^{\ddagger}$ values are estimated. A plot of the $\Delta S^{\ddagger}$ against the $\Delta H^{\ddagger}$ will generate an enthalpy-entropy compensation plot. If the enthalpy and entropy changes are temperature independent then enthalpy changes must be directly proportional to the entropy changes for the reaction system.[61] The relationship can be represented by Equation I-36 where β is defined as the isokinetic temperature. At the isokinetic temperature $\Delta S^{\ddagger}$ and $\Delta H^{\ddagger}$ exactly offset each other and all substituent effects vanish.

$$\Delta H^{\ddagger} = \beta \Delta S^{\ddagger} \qquad \text{Equation I-36}$$

If a linear relationship between the parameters is observed then an enthalpy-entropy compensation relationships exists.[68] The enthalpy-entropy compensation relationship can occur due to conformational equilibria, linear free energy relationships or solvation effects though none offer a specific explanation for the compensation effect.

A special case of enthalpy-entropy compensations is the isokinetic relationship where the correlation coefficient of the compensation plot is unity and there exists a common intersection point for Arrhenius plots for the series of compounds studied.[61, 68] Since $\Delta S^{\ddagger}$ and $\Delta H^{\ddagger}$ are evaluated from the same data they are highly correlated and suitable statistical methods need to be used to confirm the existence of true isokinetic relationships.[69-72] The demonstration of a valid isokinetic relationship has several implications. An isokinetic relationship is a necessary condition for the existence of a reaction series; exceptions usually indicate changes in interaction mechanisms. *Ortho* substitution can lead to deviations from the enthalpy-entropy lines defined using *meta* and *para* substituted compounds. If the reaction temperature is near the isokinetic temperature the substituent effects would be small and difficult to interpret. If a isokinetic relationship holds for the series then $\Delta S^{\ddagger}$, $\Delta H^{\ddagger}$, and $\Delta G^{\ddagger}$ all change in a parallel

fashion and so discussions of $\Delta S^{\ddagger}$ and $\Delta H^{\ddagger}$ provide no further information or insight that is not already available in effects on reactivity ($\Delta G^{\ddagger}$).[61]

Organization of the Thesis

The organization of this thesis is as follows. Chapter II deals with the selection, collection, synthesis, and characterization of substituted formanilides. Chapter III deals with the reaction kinetics of substituted formanilides in acidic solutions. Chapter IV deals with the reaction kinetics of substituted formanilides in alkaline solutions.

Figure I- 9: Types of Hammett plots showing (a) negative slope, (b) positive slope, (c) slope close to zero (d) slope changing concave upwards, and (e) slope changing concave downwards.

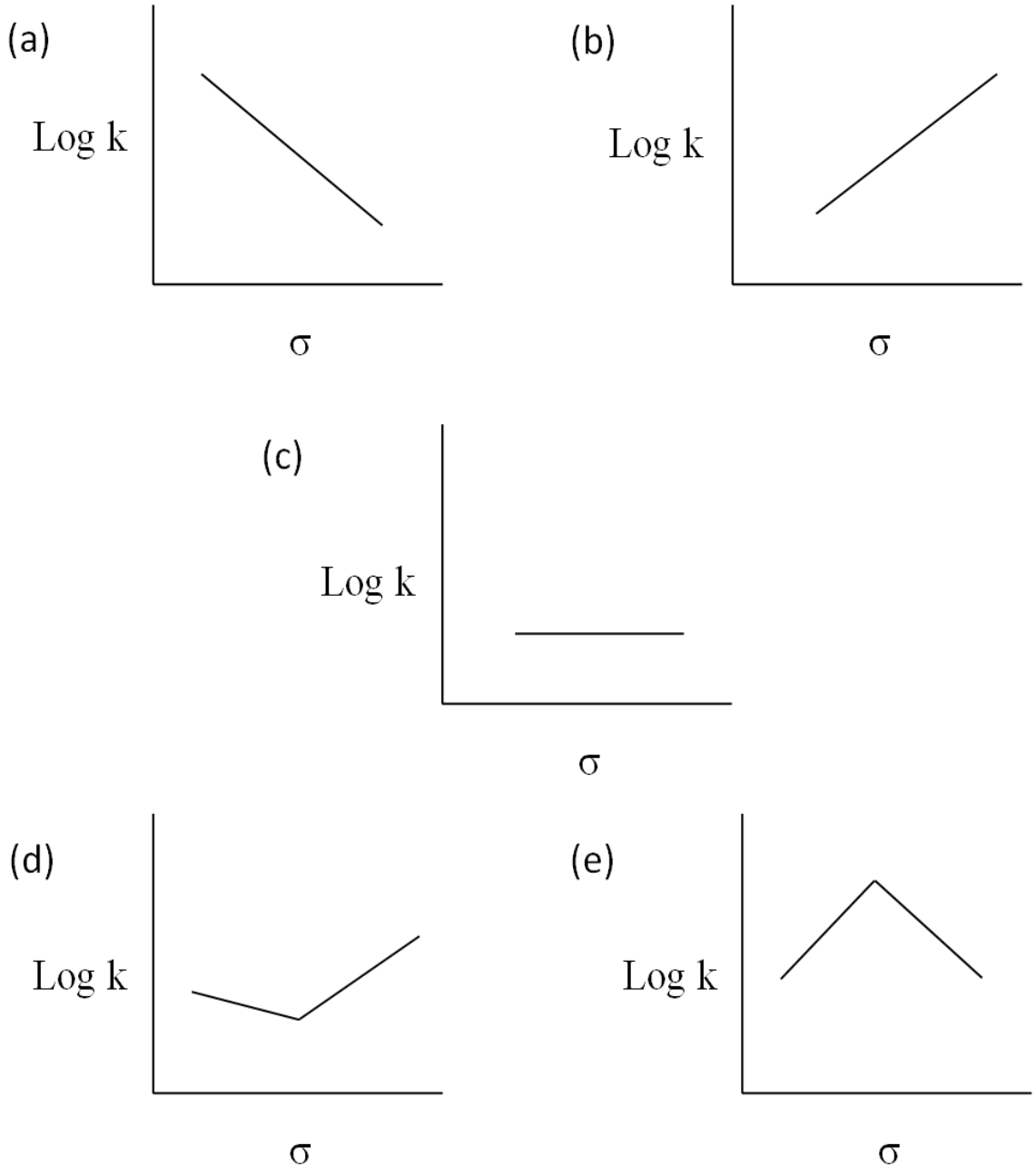

CHAPTER II

SYNTHESIS AND CHARACTERIZATION OF SUBSTITUTED FORMANILIDES

Introduction

This chapter deals with the selection, synthesis, and characterization of substituted formanilides. Substitution effects in aromatic compounds can be divided into electronic (resonance, and inductive) and steric (steric bulk and proximity) effects. Substituents were chosen such that they cover the wide range of electronic and steric effects. The substituent constants of the selected substituents are available in the literature and are listed in Table II-1. Some of the substituted formanilides in Table II-1 were procured commercially and the rest were synthesized. Table II-2 lists the compounds purchased or synthesized. After synthesis, a reaction product was structurally analyzed by nuclear magnetic resonance (NMR) spectroscopy to demonstrate consistency with intended products. A reaction product was then purified by extraction, recrystallization or vacuum distillation. The melting point and purity of the purified product was determined using differential scanning calorimetry (DSC). The pK_a values of compounds with ionizable groups were determined using ultraviolet (UV) spectroscopy or potentiometric titration.

Materials

Formanilide, *p*-chloroformanilide, *o*-chloroformanilide, *p*-bromoformanilide, *o*-bromoformanilide, *p*-methoxyformanilide, *p*-hydroxyformanilide, *o*-hydroxyformanilide, *o*-carboxyformanilide, *o*-methylformanilide, and *p*-methylformanilide were purchased from Sigma-Aldrich (St Louis, MO) with stated purities > 97%. *Para*, *meta*, and *ortho* substituted anilines of >95% purity were purchased from Sigma-Aldrich (St Louis, MO) and used without purification. Formic acid (99%) was purchased from Acros Organic

Table II- 1: Representative structure for substituted formanilides and Hammett substituent constants (σ_m, σ_p), electrophilic substituent constant (σ_m^+, σ_p^+), enhanced substituent constants (σ_p^-), and Taft steric substituent constant (E^0s) values for selected substituent groups.[61, 73]

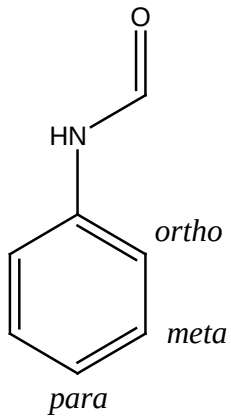

Substituent		σ_p	σ_m	σ_p^+	σ_m^+	σ_p^-	E_s^0
H	H	0	0	0	0	0	1.24
Chloro	Cl	0.22	0.37	0.114	0.399	-	0.18
Bromo	Br	0.22	0.34	0.150	0.405	-	0
Nitro	NO_2	0.78	0.74	0.790	0.674	1.27	-0.75
Methyl	CH_3	-0.17	-0.06	-0.311	-0.066	-	0
Ethyl	C_2H_5	-0.15	-0.07	-0.295	-0.064	-	-0.07
*iso*propyl	*iso*-C_3H_7	-0.15	-	-0.280	-0.060	-	-0.47
Phenyl	C_6H_5	-0.01	0.06	-0.179	0.109	-	-0.90
Methoxy	OCH_3	-0.28	0.11	-0.778	0.047	-	0.99
Hydroxyl	OH	-0.38	0.13	-0.92	-	-	-
Carboxyl	COOH	0.44	0.35	0.421	0.322	0.73	-

Table II- 2: List of substituted formanilides either obtained or synthesized. Compounds commercially available are marked with X, and synthesized compounds are marked with √

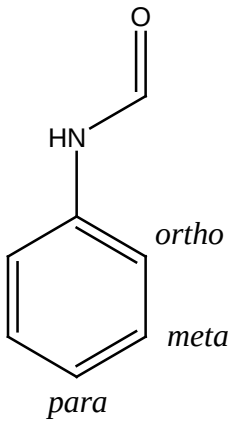

Substituent		Para	Meta	Ortho
	H	√		
Chloro	Cl	X	√	X
Bromo	Br	X	√	X
Nitro	NO_2	√	√	√
Methoxy	OCH_3	X	√	√
Hydroxyl	OH	X	√	X
Carboxyl	COOH	√	√	X
Methyl	CH_3	X	√	X
Ethyl	CH_2CH_3	√	√	√
*iso*Propyl	$isoC_3H_7$	√	√	√
Phenyl	C_6H_5	√		√

(New Jersey, USA). Sodium chloride, sodium sulfate anhydrous, diethyl ether, diisopropyl ether, ethyl alcohol, benzene, cyclohexane, chloroform, sodium bicarbonate,acetic anhydride, and concentrated hydrochloric acid were purchased from Fisher Scientific (Fairlawn, NJ). Deuterated dimethyl sulfoxide (DMSO-d6) and deuterated chloroform ($CDCl_3$) with 0.1% TMS were obtained from Sigma-Aldrich. (St Louis, MO). All other solvents and chemicals used were reagent grade.

General Methods Used for Synthesis and Characterization

Synthetic Methods

Anilines and formic acid react to form formanilides and water as products (Figure II-1). This reaction occurs by the nucleophilic attack of the aniline amine on the carbonyl group of the formic acid to form a tetrahedral intermediate which then degrades to form the corresponding formanilide. The reaction is reversible and the yield is low. To drive the reaction to completion, the water produced needs to be removed. This can be achieved either by azeotropic synthesis or by acylation reaction.

Azeotropic synthesis

Azeotropic synthesis was carried out by mixing the aniline, formic acid, and diisopropyl ether (Figure II-2). Diisopropyl ether acts as a solvent for the reaction of the aniline and formic acid. The reaction leads to the formation of water which then forms an azeotrope with diisopropyl ether. An azeotrope is a mixture of two compounds which cannot be separated by simple distillation.[74] Diisopropyl ether forms an azeotrope with 3.6 % water that boils at 61.4 °C which is lower than the boiling point of both diisopropyl ether (69 °C) or water (100 °C).[75] When the solution is heated, at the boiling point of the azeotrope, the vapor and the solution have the same composition, and the solution boils off. However when the water rich vapor cools, the equilibrium shifts, and the solubility of water in the mixture decreases causing the water to separate out. The cooled

organic solvent with lower water content can be recycled to continue the process. The *m*-chloro, *m*-bromo, *m*-nitro, *m*-methoxy, *o*-methoxy, *m*-hydroxyl, *p*-carboxyl, *m*-carboxyl, *m*-methyl, *p*-ethyl, *m*-ethyl, *o*-ethyl, *p*-isopropyl, *m*-isopropyl, *o*-isopropyl, *p*-phenyl, and *o*-phenyl substituted formanilides were prepared using azeotropic synthesis.

The method consisted of mixing 0.08 moles of the substituted aniline, and 0.16 M anhydrous formic acid (1:2 molar ratio) in a 250 mL round bottom flask. Then 170 mL of diisopropyl ether was added to the mixture. The flask was placed in a water bath and attached to a Dean-Stark trap which was attached to a water cooled condenser (Figure II-3). The water bath was heated, and the mixture was refluxed. The reaction produces water in stoichometric proportion to the aniline consumed and the reaction was monitored by following the amount of water produced. At the end of the reaction, refluxing was stopped and the apparatus was disassembled. The round bottom flask containing the reactant and product was removed. Diisopropyl ether and formic acid were removed under reduced pressure at temperatures of 50-80 °C in a rotary evaporator (Rotavap®, Buchi RE 111 with Buchi 461 Water Bath, Brinkmann Instruments; Switzerland) and the crude product was concentrated under high vacuum.

Acylation reaction

For the weakly basic p-nitroaniline, the reaction with formic acid is either too slow or the products decompose to reactants in the presence of trace quantities of water. Hence the reaction was carried out using acylation reaction. Acid anhydrides react with amines to form amides by a nucleophilic addition reaction.[5] Unsymmetrical carboxylic anhydrides can be attacked by the amine at two possible sites to form two different acylated products as shown in Figure II-4. The yield and specificity of the product is controlled by the steric and electronic properties of the substituents on the anhydride. Electron withdrawing groups on the substituents will facilitate the forward reaction. If R_2

is more electron withdrawing than R_1 , the rate of addition of amine will be greater at the carbonyl group adjacent to R_1, and $R_2CO_2^-$ will be a better leaving group than $R_1CO_2^-$. Steric effects are also important, and the amine will preferentially attack the carbonyl group next to the less bulky substituent. Substitution on the amino group is also very important for this reaction. Electron withdrawing groups attached to the amines will decrease the nulceophilicity of the amine, and the reaction will proceed slowly. However, excess acid catalyzes the forward reaction and the reaction can be used even for weakly basic amines. Since water is not formed during this reaction, the reaction is non-reversible.

Synthesis of *p*-nitroformanilide was carried out using acetic formic anhydride.[76] Acetic anhydride reacts with formic acid to form acetic formic anhydride and acetic acid as shown in Figure II-5. When the *p*-nitroaniline is mixed with acetic formic anhydride the amine attacks the formyl group of the acetic formic anhydride selectively due to the lower steric hindrance and higher electronegativity of the formyl group over the acetyl group. The reaction is catalyzed by excess acid and formanilides are formed in good yield. Only *p*-nitroformanilide was prepared using acylation.

Acylation of *p*-nitroaniline was carried out using acetic formic anhydride. Acetic formic anhydride was prepared *in situ* by mixing 17.7 grams of acetic anhydride and 8.0 grams of formic acid (1:2 molar ratio) in a 250 mL round bottom flask. The flask was attached to a condenser topped with a drying tube. The mixture was heated at 50- 60 °C with constant mixing in a water bath. The reaction mixture was cooled to 30 °C and then 12.0 grams (0.086 mole) of *p*-nitroaniline was added slowly with constant mixing. The mixture was maintained at 30 °C using an ice bath. Diethylether (50 ml) was added to the mixture and mixed overnight. Solid product was filtered and washed with water.

Figure II- 1: Reaction scheme for the formation of formanilides from aniline and formic acid

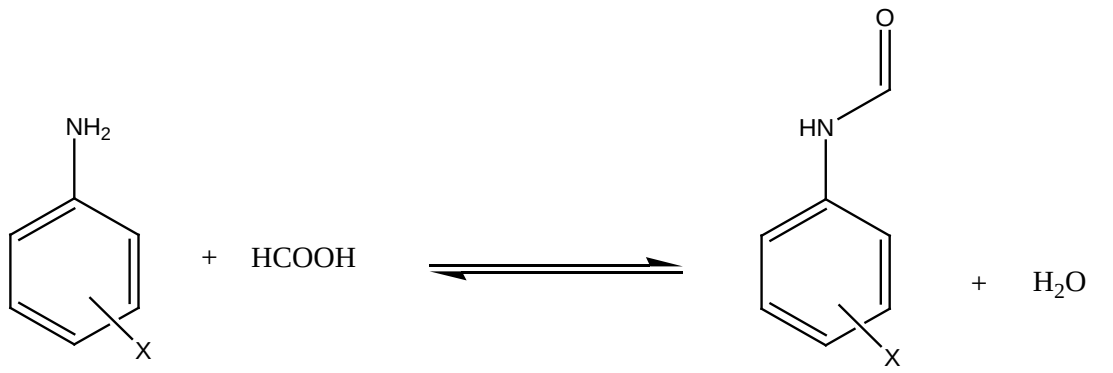

Figure II- 2: Reaction scheme for the synthesis of formanilide from aniline using azeotropic synthesis.

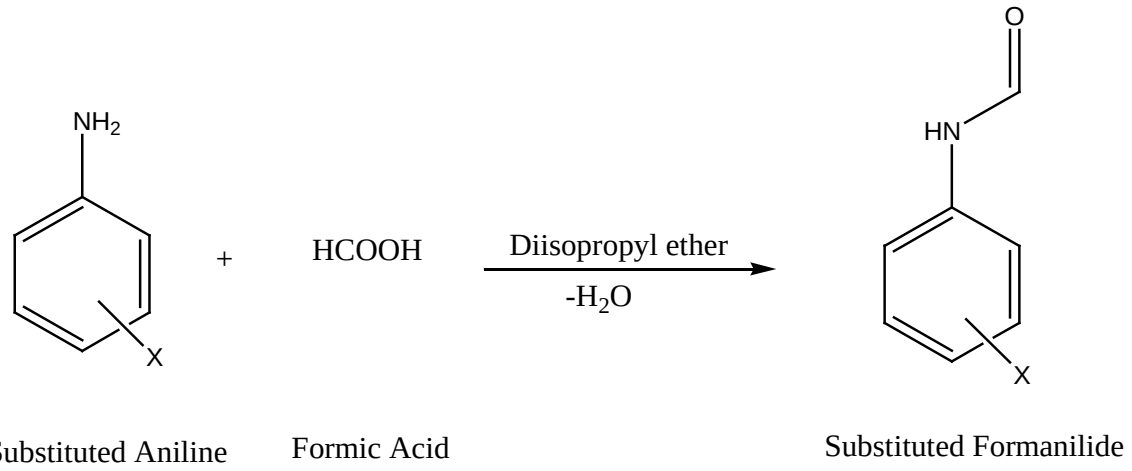

Figure II- 3: Complete reaction assembly for synthesis of substituted formanilides by azeotropic synthesis.

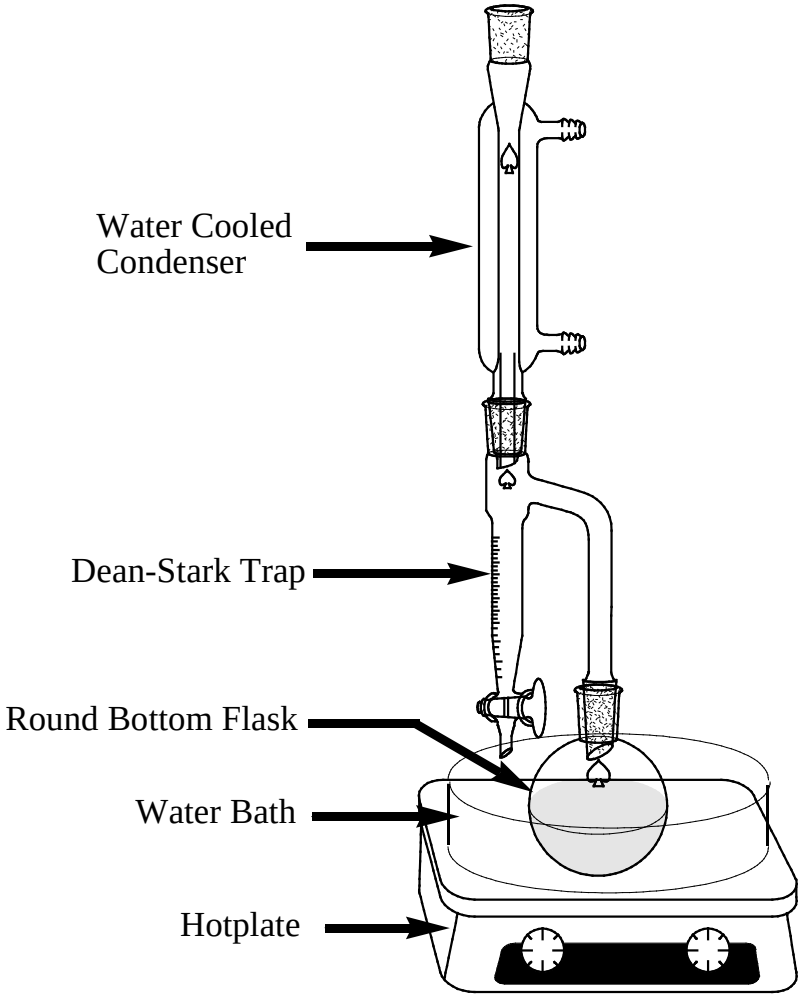

Figure II- 4: Reaction scheme for acylation of amines by unsymmetrical acid anhydrides.

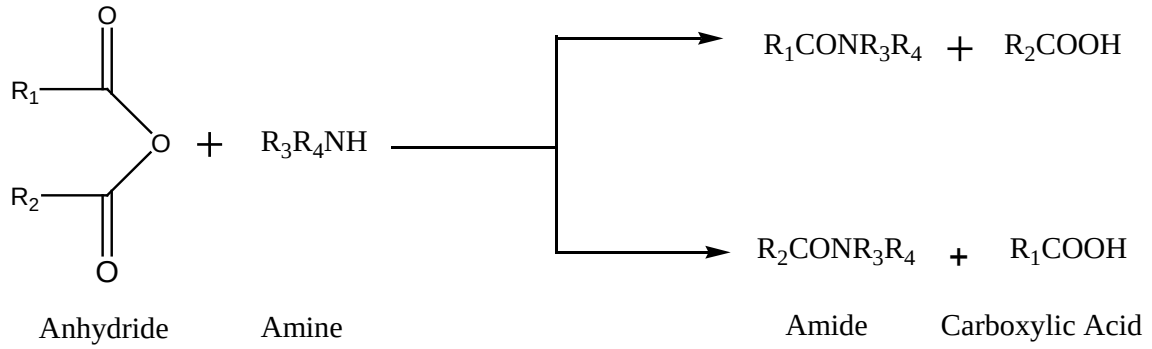

Figure II- 5 Formylation reaction for synthesis of formanilides: (A) Formation of acetic formic anhydride from acetic anhydride and formic acid and (B) Reaction of acetic formic anhydride with aniline to form formanilide.

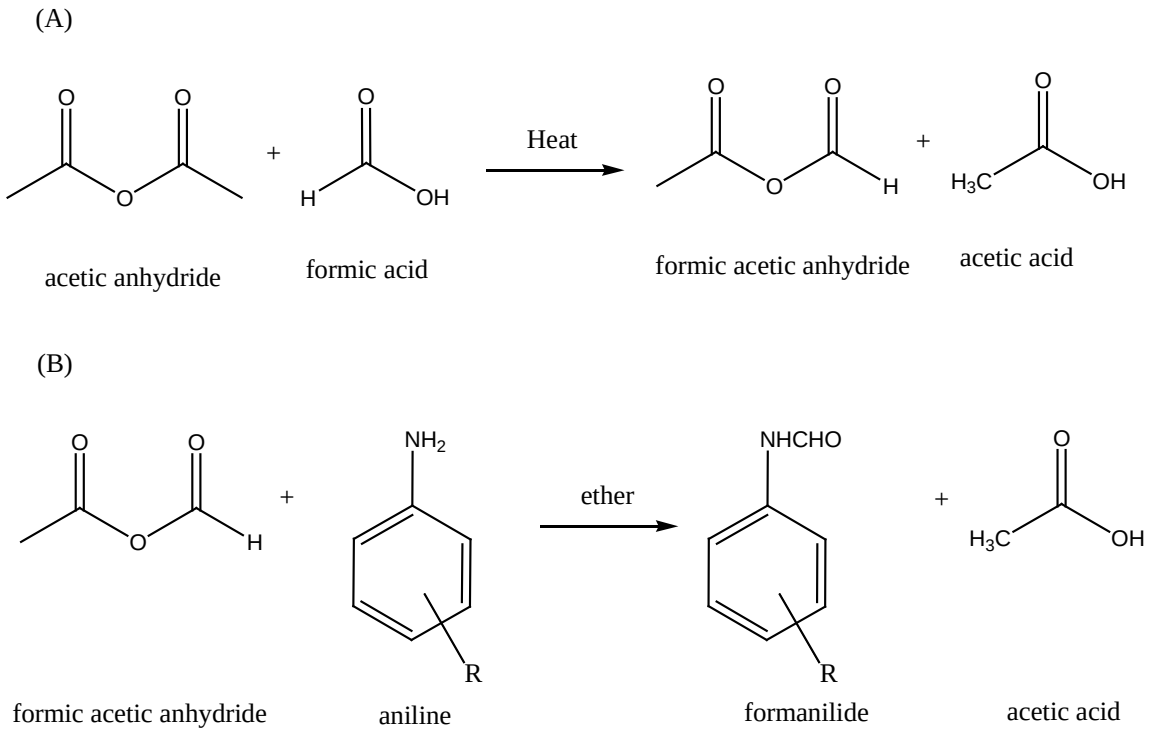

Purification of Reaction Products

Reaction products contained a mixture of the mostly formanilide and trace amounts of unreacted aniline and formic acid. The formanilide was purified either by extraction, vacuum distillation or recrystallization.

Extraction (liquid-liquid extraction) is a method to separate compounds based on their relative solubilities in two different immiscible liquids: water and an organic solvent (usually ether).[77] Usually the component to be purified is soluble in the organic solvent while the component to be removed has a lower solubility in the organic phase but has preferential solubility in the aqueous phase. By changing the properties of the aqueous solvent the solubility for the contaminant is increased to help partition it into the aqueous phase. The organic liquid is then separated and evaporated under vacuum to produce the purified product.

Extraction for formanilides was carried out by dissolving the reaction products in ethyl ether and transferred to a separating funnel. This organic layer was washed with equal volumes of dilute hydrochloric acid, saturated ammonium chloride solution, saturated sodium bicarbonate solution, and water to remove the unreacted amine and formic acid. The organic layer was then washed with saturated sodium chloride solution (brine) and passed through a layer of anhydrous sodium sulfite to dry the organic solvent. The purified formanilide was isolated by evaporating the ether under vacuum.

A compound containing trace impurities can be purified by recyrstallization. Recrystalization works by taking advantage of the differential solubilities of the components of the mixture. The mixture is dissolved in solvent systems that have a preferential solubility for the impurities. The mixture is then the heated until all the material is dissolved and then slowly cooled until the product crystallizes. High purities of products can be achieved using recrystallization.

For formanilides, recrystallization solvent systems screened included cyclohexane, chloroform, ethanol, water, water-ethanol, and benzene. Recrystallization was carried out by heating the crude product in the solvent system to dissolve the material and then cooling the mixture slowly overnight to obtain crystals. The crystals were isolated by filtration, and if needed, the process was repeated until a high purity compound was produced.

Distillation separates mixtures by using the differences in the boiling points of mixture components. Best results are possible if each component of a mixture has a boiling point which is significantly different from the boiling point of the other components. However under normal atmospheric pressures the boiling points may be so high that thermal degradation may occur. This problem can be circumvented by distilling the mixture under reduced pressure (i.e. vacuum). Vacuum distillation for formanilides was carried out in an apparatus as shown in Figure II-6. The mixture was placed in the round bottom flask, the assembly was made airtight using high vacuum grease and vacuum was applied using a vaccum pump. The oil bath was heated slowly and fractions were collected as a function of temperature. Formic acid distills at relatively low temperatures whereas anilines generally did not distill in the temperature range used. The middle fraction of distillate corresponding to the formanilides was boiled in the range of 110-140 °C.

Identification, Purity Assessment and Characterization of Products

Crude products and final products were identified using NMR and melting point determination. The purity was assessed using differential scanning calorimetry. The pK_a values of the ionizable compounds were determined using titration or UV spectroscopy.

Figure II- 6: Vacuum distillation apparatus used for the purification of formanilides.

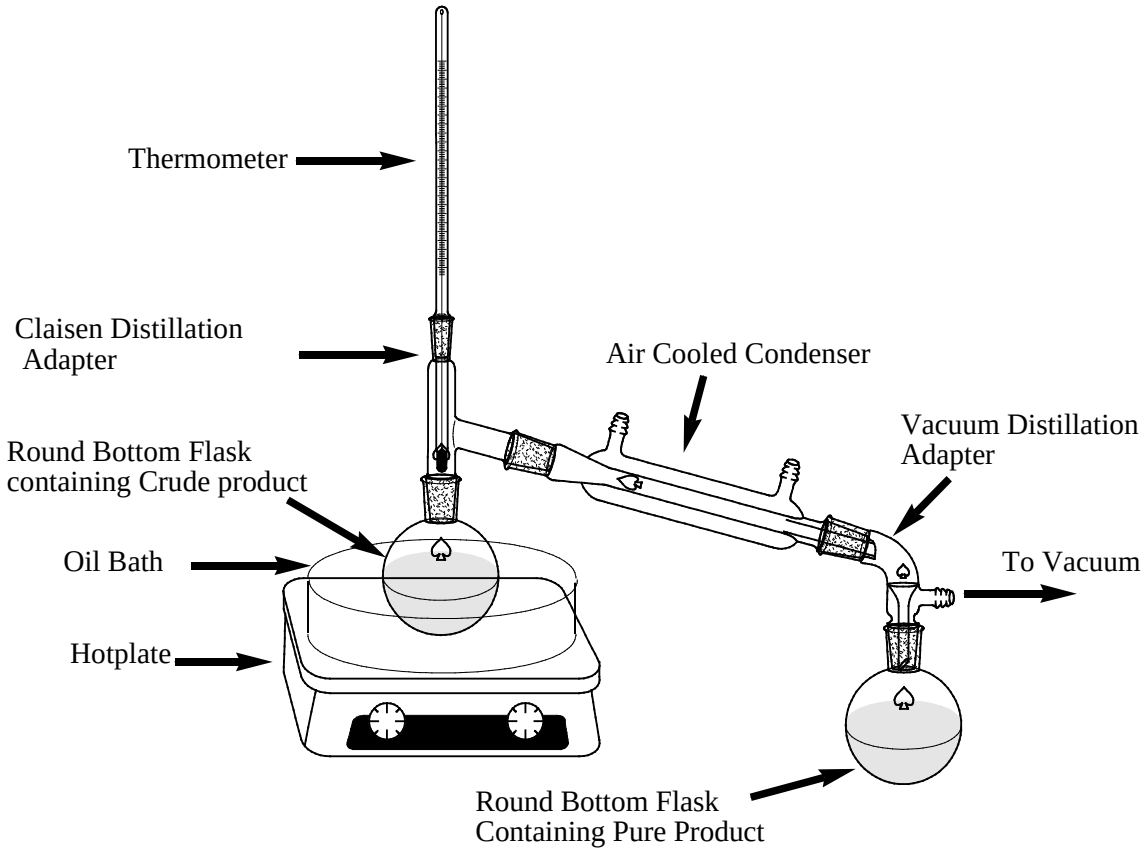

Nuclear magnetic spectroscopy

Nuclear magnetic resonance (NMR) depends on the quantum mechanical magnetic properties of an atom's nucleus. Nuclei that contain an odd number of protons or neutrons have an intrinsic magnetic moment and angular momentum. These include hydrogen (^{1}H) and carbon (^{13}C). If protons (^{1}H) are used, the spectroscopy is called proton NMR and if carbon (^{13}C) atoms are used, then the spectroscopy is called carbon NMR. The nuclei have two allowed nuclear spin states (+ ½ and - ½) which behave as tiny bar magnets since spinning charges create a magnetic field around them. When they are placed in a strong magnetic field they are aligned with the field (+½), which is the low energy state, than against the field. If radio frequency waves of appropriate energy are supplied, the nuclei aligned with the field absorb the radiation and reverse their direction of spin (flip to -½), and re-orient against the applied magnetic field in a higher energy state. The frequency of radiation (resonance frequency) required to induce spin conversion is a direct function of the applied magnetic field and varies from nuclei to nuclei within a molecule depending upon the immediate chemical environment. These environmental differences cause very slight (parts per million) differences in the frequencies at which identical nuclei resonate. This phenomenon is called the chemical shift. An NMR spectrum consists of a plot of the chemical shifts versus the intensity of the absorptions. Chemical shift ranges for protons, though not unique, have been compiled for various groups, and are used to identify the components of the compounds. Nuclei can also interact with each other to cause mutual splitting of the sharp resonance lines into multiplets, called spin-spin coupling. This provides information about the connections between the various nuclei. The intensity of the absorption gives information about the relative number of atoms. The intensity, chemical shift, and spin-spin coupling information are used with chemical intuition to identify the compound being analyzed.

The NMR spectra of the compounds were acquired by dissolving the product in a suitable NMR solvent (10 to 15 mg in 0.5 ml of solvent) in an NMR sample tube. For hydrophobic compounds deuterated chloroform ($CDCl_3$) was used and for hydrophilic compounds deuterated dimethyl sulfoxide (DMSO-d6) was used. ^{1}H and ^{13}C NMR spectra were collected on a Bruker Avance 300 NMR (Bruker BioSpin Corporation, Billerica, MA). Data were processed on WinNuts® (Acorn NMR Inc, Livermore, CA). For proton NMR spectra the proton resonance for tetramethylsilane (TMS) was used as a reference when $CDCl_3$ was used as the solvent, and the residual methyl proton signal (2.5 ppm) was used when DMSO-d6 was the solvent. For carbon NMR spectra, the solvent backbone carbon signals were used as a reference signals for $CDCl_3$ (77.23 ppm) and DMSO-d6 (39.5 ppm). NMR spectra were used to confirm the identity of the synthesized compounds and to qualitatively assess the purity of the compounds. During the synthesis and purification process, NMR spectroscopy was used to follow the progress of the reaction.

Differential scanning calorimetry

DSC was used to assess if the melting point of the reaction products was consistent with literature values and to determine purity of the samples. The purity of a sample can be determined using DSC for compounds which are fairly pure (> 98 %), heat stable, and whose impurities are insoluble in the solid phase and soluble in the melt. This method involves the estimation of purity by evaluating the area under the melting endotherm by using the van't Hoff equation (Equation II-1).[78, 79]

$$\frac{1}{F_S} = \frac{\Delta H[T_0 - T_S]}{RT_0^2 X} \qquad \text{Equation II-1}$$

In Equation II-1, T_s is the instantaneous sample temperature (K); T_0 is the melting temperature of the pure substance; ΔH is the heat of melting of the pure material (J/g); X

is the mole fraction of impurity in the sample; R is the gas constant (8.314 J/mole), and F_s is the fraction of sample melting at temperature T_s. The fraction F_s is given as A_s/A_t where A_s is the area of the melting endotherm up to temperature T_s and A_t is the total area of melting endotherm.

In some cases the van't Hoff plots deviate from the expected straight line. This usually results from the underestimation of the fraction melted which has occurred at lower temperatures but which was not observed by the DSC. This deviation is a function of the amount of the impurity in the sample and is constant for a given sample. This deviation can be corrected by using a constant (X-correction) which accounts for the amount of peak area which is undetected. The X-correction should be less than 10% for the purity values to be considered meaningful.

The DSC was calibrated using indium as a standard (melting point 156.60). The value for the heat of fusion was calculated and used for calculating the purity of all of the samples. This calibration also corrects for the thermal lag between the temperature of the sample and the temperature of the sample holder. The baseline was corrected for the temperature changes due to flow of nitrogen. About 6 mg of each formanilide was carefully weighed into aluminum DSC pans. The pan was sealed and DSC analysis was carried out on a Perkin Elmer DSC 7 instrument (Waltham, MA), and the data were acquired and analyzed using Perkin Elmer thermal analysis software version 4.0. Temperature was increased at a rate of 10 °C per minute to about 10 °C below the expected melting point of the product. The sample was allowed to equilibrate for five minutes, and then the temperature was increased gradually at the rate of 1°C per minute until the temperature reached 10 °C above the melting point of the sample. This slow rate of heating was required to achieve the quasi-equilibrium conditions for accurately determining the fractional melted areas under curve accurately. The entire run was carried out under a constant flow of nitrogen gas. Thermograms were inspected for

thermal stability. If the sample was pure and heat stable, the endotherm was a single peak. If melting led to degradation, the peak could be split into several peaks. Only compounds that exhibited a single peak were evaluated for purity using the DSC. In this analysis the limits by using areas calculated from the start of melting of the sample to a point about where the sample is half melted. The areas were calculated and the X- correction was determined to obtain a linear van't Hoff plot. If the value was under 10%, the purity was calculated was considered acceptable. Formanilide is shown as an example compound to demonstrate the purity determination using DSC, formanilide (Figure II-7). Figure II-7 (A) shows the melting endotherm for formanilide while Figure II-7 (B) shows the corrected van't Hoff plot for the determination of the X- correction. The purity determined by using DSC was 99.95% which closely matched the labeled purity for formanilide (99.9 % by gas liquid chromatography).

Determination of pK_a

The carboxyl and hydroxyl substituted formanilides have ionizable groups. The pK_a value of *p*-hydroxyl formanilide was determined using potentiometic titration. The pK_a values of *m*-hydroxyl, *o*-hydroxyl, *p*-carboxyl, *m*-carboxyl and *o*-carboxyl formanilides were evaluated using UV spectroscopy. The titration curves, UV measurements, and fittings are tabulated in Appendix A.

Potentiometric titration of *p*-hydroxyformanilide was carried out using a Mettler DL 21 titrator (Mettler, Highstown, N.J.) attached to an Accumet combination pH electrode. The pH electrode was calibrated using pH 7 and pH 10 standardized buffers at 25 ± 1° C. A 40 mL aliquot of 0.50 mM solution of *p*-hydroxy formanilide in water was prepared and equilibrated at 25 ± 1° C in a thermostatted vessel. This solution was titrated against 0.10 N standardized sodium hydroxide solution. Titration was carried out under a constant stream of nitrogen to prevent absorption of atmospheric carbon dioxide during titration. The titrant was added until the pH of the solution was around pH 12 and

the titration curve is shown in Figure II-8(A). The K_a was determined using the Gran plot method from the slope of the plot of G versus $G \times a_H$; where G is the modified volume of titrant (Equation II-2 and Figure II-8(B)), and a_H is the hydrogen ion activity during the course of the titration.[80]

$$G = V_t + \frac{(V_0 + V_t)([H^+] - [OH^-])}{V_t}$$

Equation II-2

The parameters in Equation II-2 are defined as follows: V_t = volume of titrant added in mL; V_o = initial volume of formanilide solution in mL; $[H^+]$ = concentration of hydronium ion; $[OH^-]$ =concentration of hydroxide ion, and N = normality of titrant.

The pK_a values of the sparingly water soluble substituted formanilides were determined using a UV spectrophotometric method.[81] All measurements were made with a UV spectrophotometer (Hewlett Packard HP 8453) at 25 °C. A stock solution of 20.0 mM of the substituted formanilide was prepared in ethanol. *Ortho*-hydroxyformanilide was insoluble in ethanol and the stock solution was prepared in dimethyl sulfoxide. Stock solutions of 0.02 M phosphate buffer pH 7 (0.01 M Na_2HPO_4, and 0.01 M KH_2PO_4), 0.05 M sodium phosphate monobasic (NaH_2PO_4), 0.05 M phosphoric acid (H_3PO_4), 0.1 N sodium hydroxide, 0.1 N hydrochloric acid, and formanilide stock solutions were mixed to prepare a series of solutions in the pH range of 7-12 for the hydroxy formanilides and pH 1.5-7 for the carboxy formanilides. The final concentration of the substituted formanilide was in the range of 0.1 mM to 0.05 mM. The ionic strength was not adjusted. pH was measured using a calibrated combination glass electrode at 25 °C with a Accumet model 25 pH meter. The spectra of formanilides were obtained in the range of 190-700 nm using distilled water as reference. The buffers and solvents did not interfere with the spectra beyond 255 nm.

The determination of ionization of *m*-hydroxyformanilide is used as an example. Figure II-9 is the UV spectra obtained for the *m*-hydroxyformanilide in the pH region 7.03 to 11.6. The spectra were inspected for the presence of isosbestic points and two

isosbestic points were observed at 268 nm and 287nm. The spectra of the most ionized and the least ionized species were subtracted, and wavelengths were chosen which gave the maximum difference in absorbance (278 nm and 301 nm). The absorbances at these wavelengths were then used to calculate the apparent pK_a of the formanilide. The pK_a value was estimated by non-linear regression (JMP®, SAS institute, Cary, NC) using the method of Albert and Serjeant as shown in Figures II-10 (A) and (B).[81] The initial values of $A_{unionized}$, and $A_{ionized}$ were taken as absorbance of the compounds at the highest and lowest pH values studied. These initial estimates were used in fits of the data to Equation II-3 to obtain the estimates for K_a ($K_{a,\,278}= 5.98\times10^{-10}$ and $K_{a,\,301}= 4.73\times10^{-10}$). The K_a values obtained at the two wavelengths were averaged and this average value was used to calculate the reported pK_a value (pK_a 9.27).

$$A_{Observed} = A_{ionized}\left(\frac{K_a}{10^{-pH}+K_a}\right) + A_{unionized}\left(\frac{10^{-pH}}{10^{-pH}+K_a}\right) \qquad \text{Equation II-3}$$

Results

Summary tables for the various formanilides are presented in Tables II-3 through Table II-24. The summary tables contain the chemical structure, IUPAC name, Chemical Abstract Service (CAS) registry number, molecular weight, state, pK_a value, NMR spectra (^1H and ^{13}C), melting point, and purity. The values in parentheses are the reported literature values.

The formanilides were synthesized by both azeotropic and formylation procedures in adequate yields and were purified successfully. NMR was used extensively to follow the reaction as well as identify the products. The substituted formanilides and corresponding anilines have similar spectra; however the proton NMR spectra for anilines have absorbances around 4 ppm corresponding to the aromatic amine hydrogen while the amide resonances occur around 8 ppm. The reaction could be followed by following the gradual increase in the amide resonances with the concurrent decrease in

the amine resonance. If literature values for the spectra were present, the spectra were compared, and the identities were confirmed. If the spectra were not available in the literature then the exemplar spectra were simulated using Chemdraw® (CambridgeSoft, Cambridge, MA), and values were compared.

All compounds synthesized were identified using NMR. The ^{1}H and ^{13}C spectra of formanilides are complex due to the presence of *cis* and *trans* isomers of formanilide in solution. [82] The complexity of the spectra is demonstrated by using p-ethylformanilide as an example. Figures II-11 and II-12 are the ^{1}H and ^{13}C NMR spectra for p-ethylformanilide. As shown in Figure II-11, ring protons, methyl, and methylene protons were easily identified using the expected chemical shifts. The specific shifts for the ring protons were not determined. However the ^{1}H peaks for the amino and aldehyde protons are split into two peaks each corresponding to the *cis* and *trans* isomers and appear around 8-10 ppm. The amino and aldehyde proton peaks can be identified based on splitting patterns and the coupling constants, however, due to the complexity these were not identified uniquely. Figure II-12 is the ^{13}C NMR spectrum for *p*-ethylformanilide. Based on the number and type of carbons in the molecule seven peaks were expected, however the ^{13}C shifts were also complex because of splitting due to the high resolution NMR spectrometer used.

Melting points for the formanilides agreed with the values from the literature in most cases and are presented in parentheses in the summary tables. The melting points in some cases differed slightly, probably due to different recrystallization conditions. The thermograms for *p*- carboxyformanilide, *m*-carboxyformanilide, *o*-hydroxyformanilide, *o*-nitroformanilide, and *p*- nitroformanilide formanilides showed multiple peaks at the melting point and thus their purities were not calculated. Purities reported for formanilides, in all cases, were in excess of 99%. The pK_a values for the formanilides were determined by UV spectrophotometry and potentiometric titration, and the data and

results are presented in Appendix A. The pK_a values determined for *para* and *ortho* hydroxyformanilides were close to the reported pK_a values.

Figure II- 7: Representative DSC thermogram (A) and van't Hoff plot (B) for the determination of purity for formanilide using DSC.

(A)

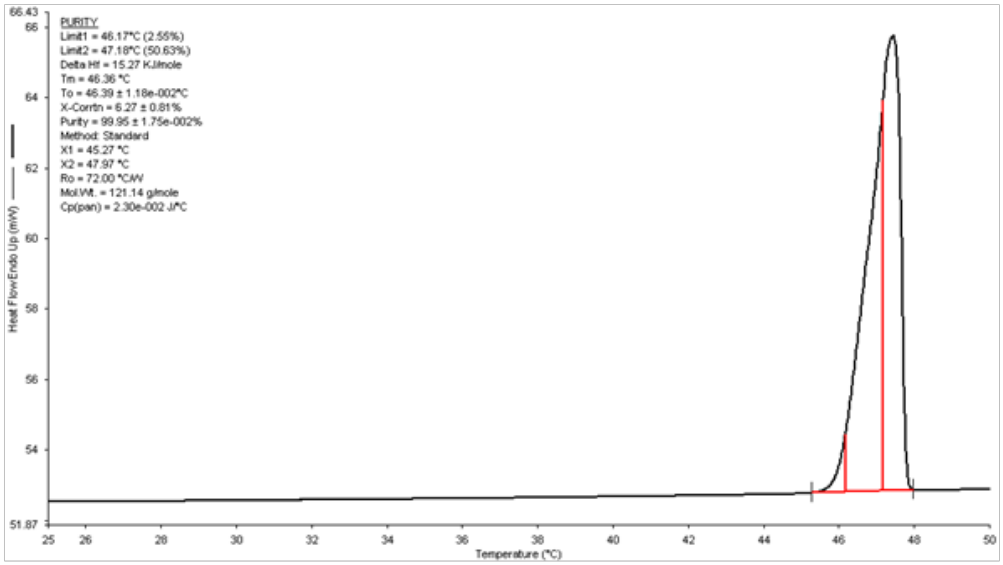

(B)

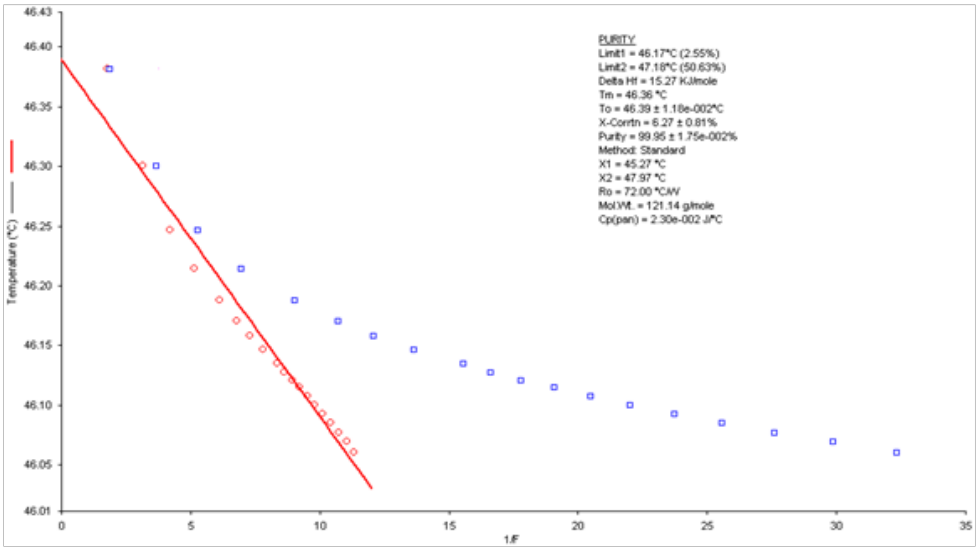

Figure II- 8 Determination of pK_a of *p*-hydroxyformanilide by potentiometric titration of a 40 mL aliquot of 5.0 mM *p*-hydroxyformanilide with 0.10 N sodium hydroxide at 25 °C. (A) Potentiometric titration curve (B) Gran's plot. G is modified term for volume of titrant at higher pH. Slope of plot gives the K_a value of 2.66×10^{-10} (pK_a of 9.57)

(A)

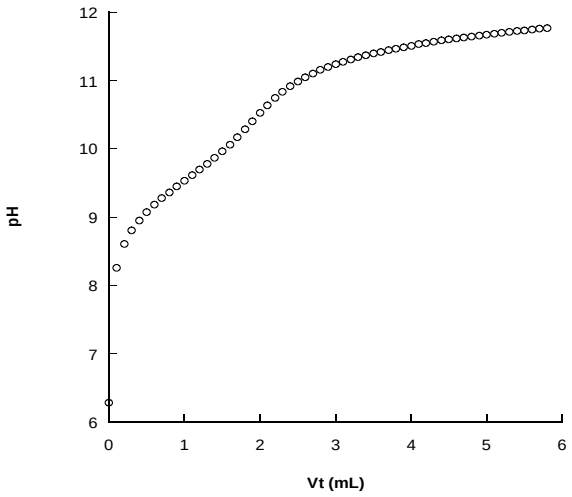

(B)

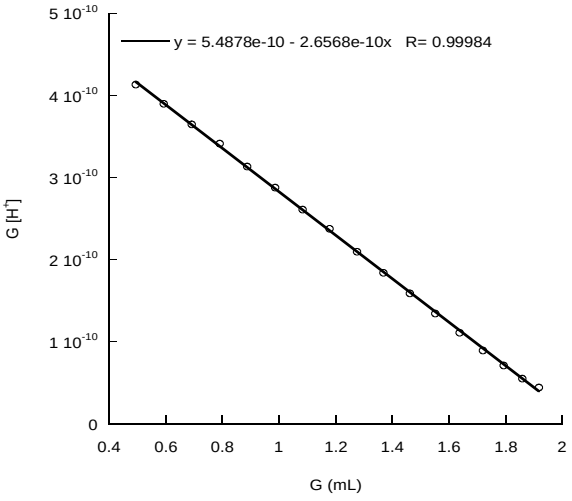

Figure II- 9Determination of the hydroxyl pK_a of *m*-hydroxyformanilide. UV spectra of 5.70×10^{-5} M *meta*-hydroxyl formanilide in the pH range 7.03-11.6 from 250 nm to 360 nm. At 278 nm highest absorbance is due to pH 7.03 and lowest absorbance is due to pH 11.6.

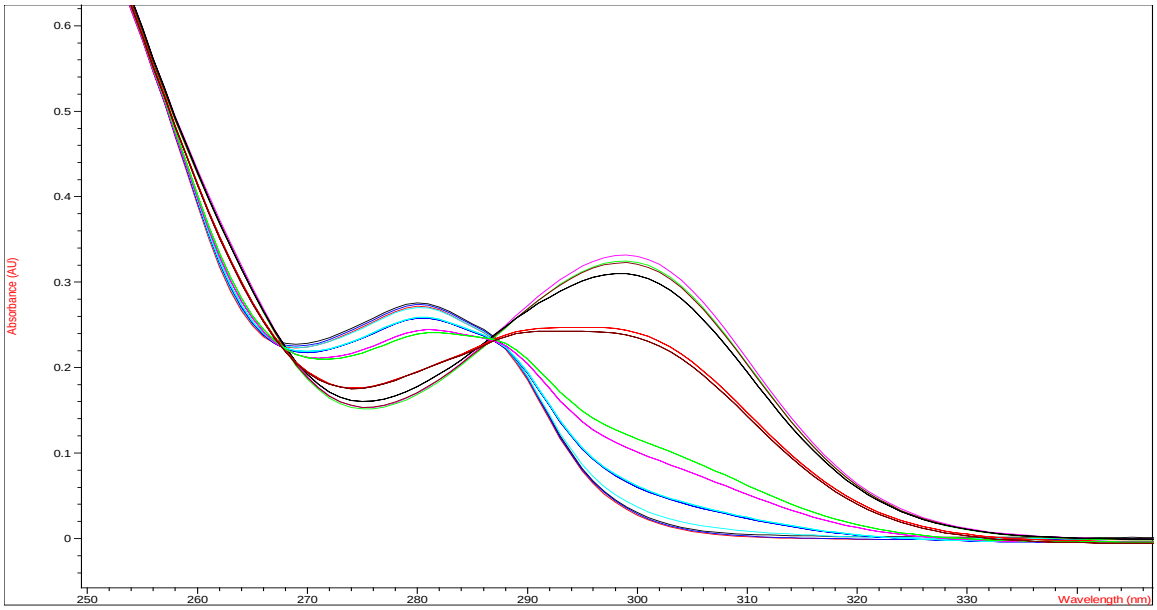

Figure II- 10 Non linear regression fits for absorbance values for 5.70×10^{-5} M *meta*-hydroxy formanilide in the pH range 7.03-11.61. Solid squares represent experimental data. Solid lines generated using Equation II-3) (A) 278 nm (estimated $K_a = 5.98\times10^{-10}$). (B) 301 nm (estimated $K_a = 4.73\times10^{-10}$). The K_a's were averaged and the average pK_a reported was 9.27.

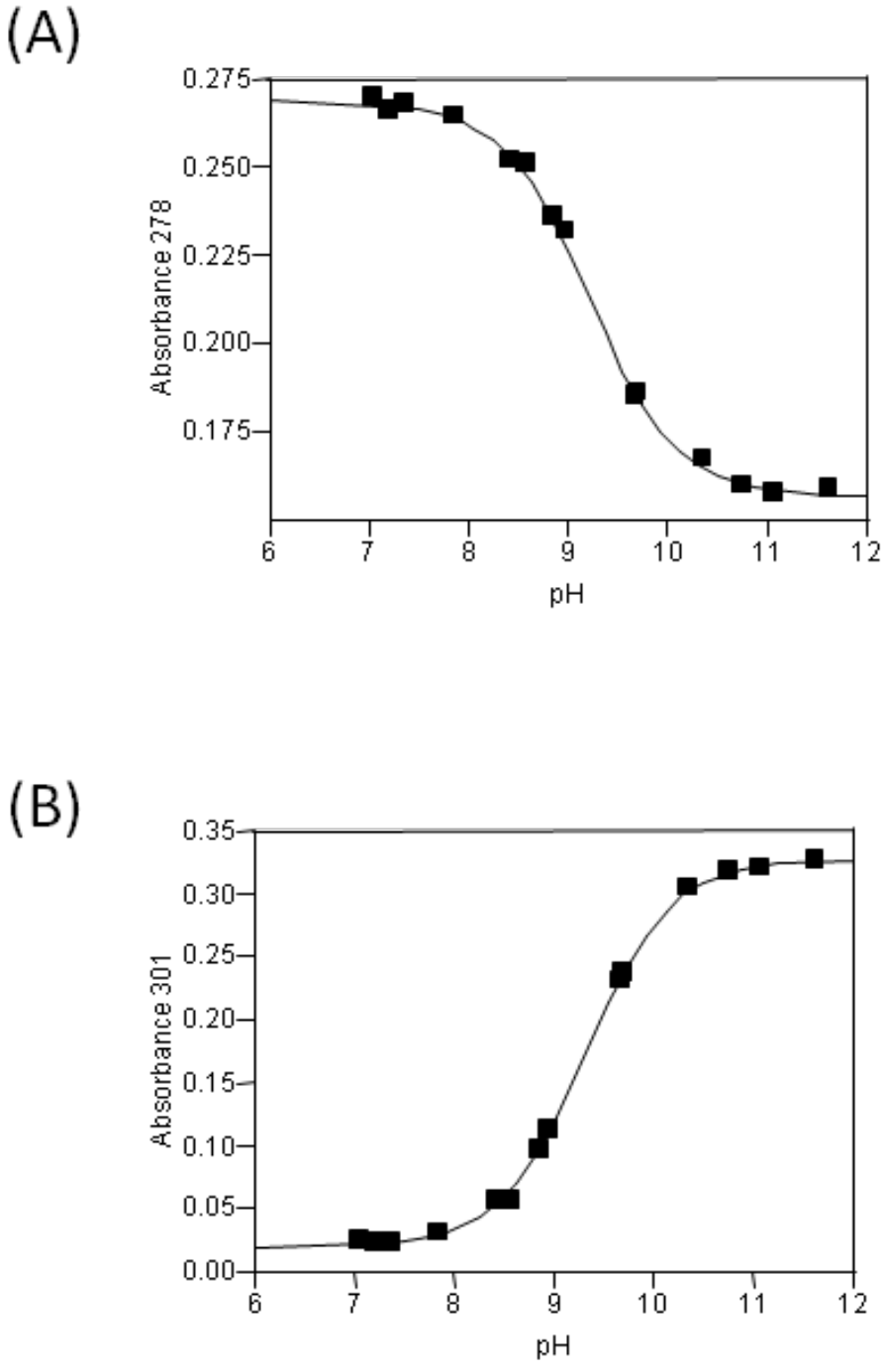

Figure II- 11: ^{1}H NMR spectrum of *p*-ethylformanilide in deuterated chloroform ($CDCl_3$) obtained on a 300 MHz NMR spectrometer. The colored boxes correspond to the protons in the compound.

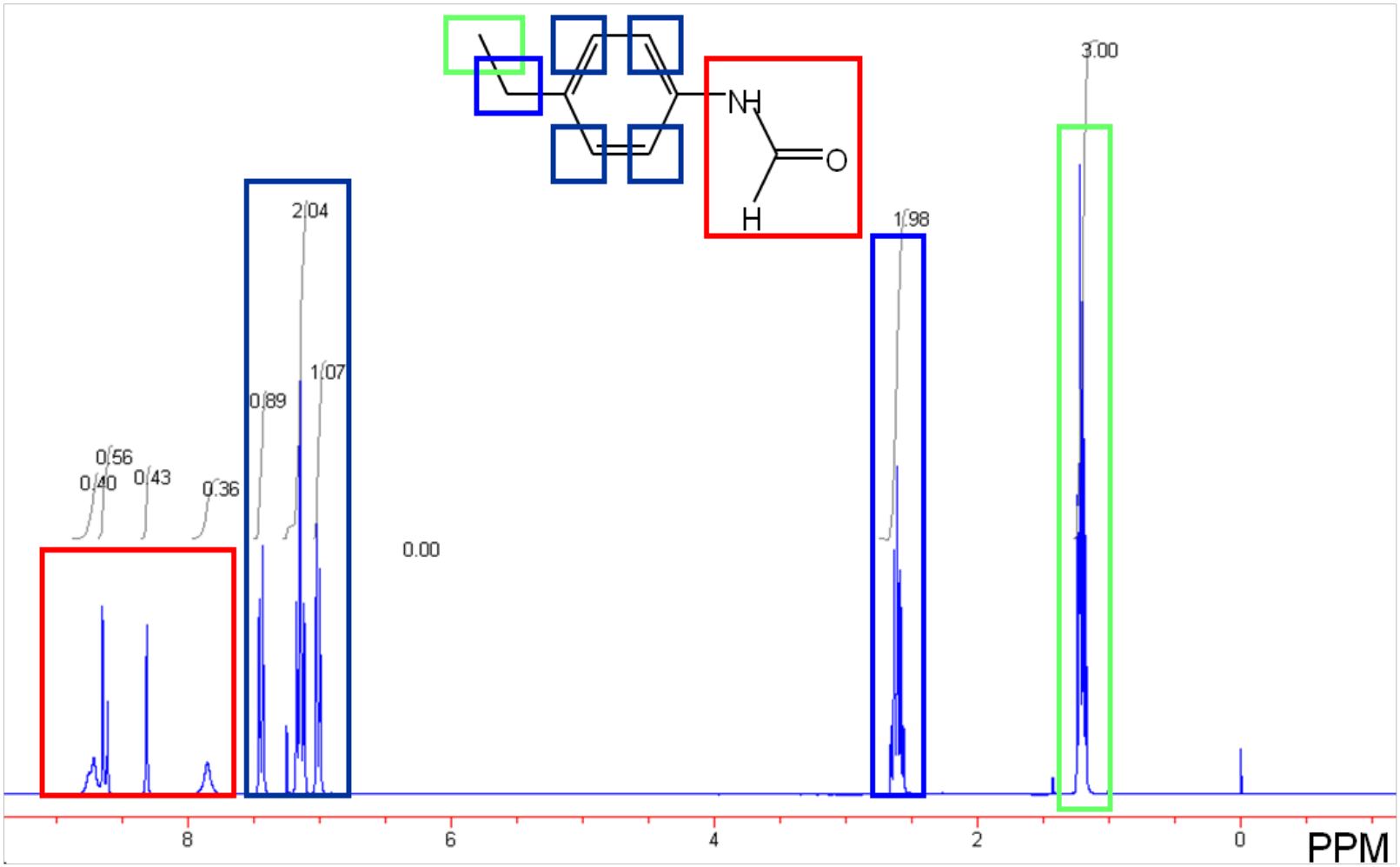

Figure II- 12: ^{13}C NMR spectrum of *p*-ethylformanilide deuterated chloroform ($CDCl_3$) obtained on a 300 MHz NMR spectrometer. The colored boxes correspond to the carbons in the compound.

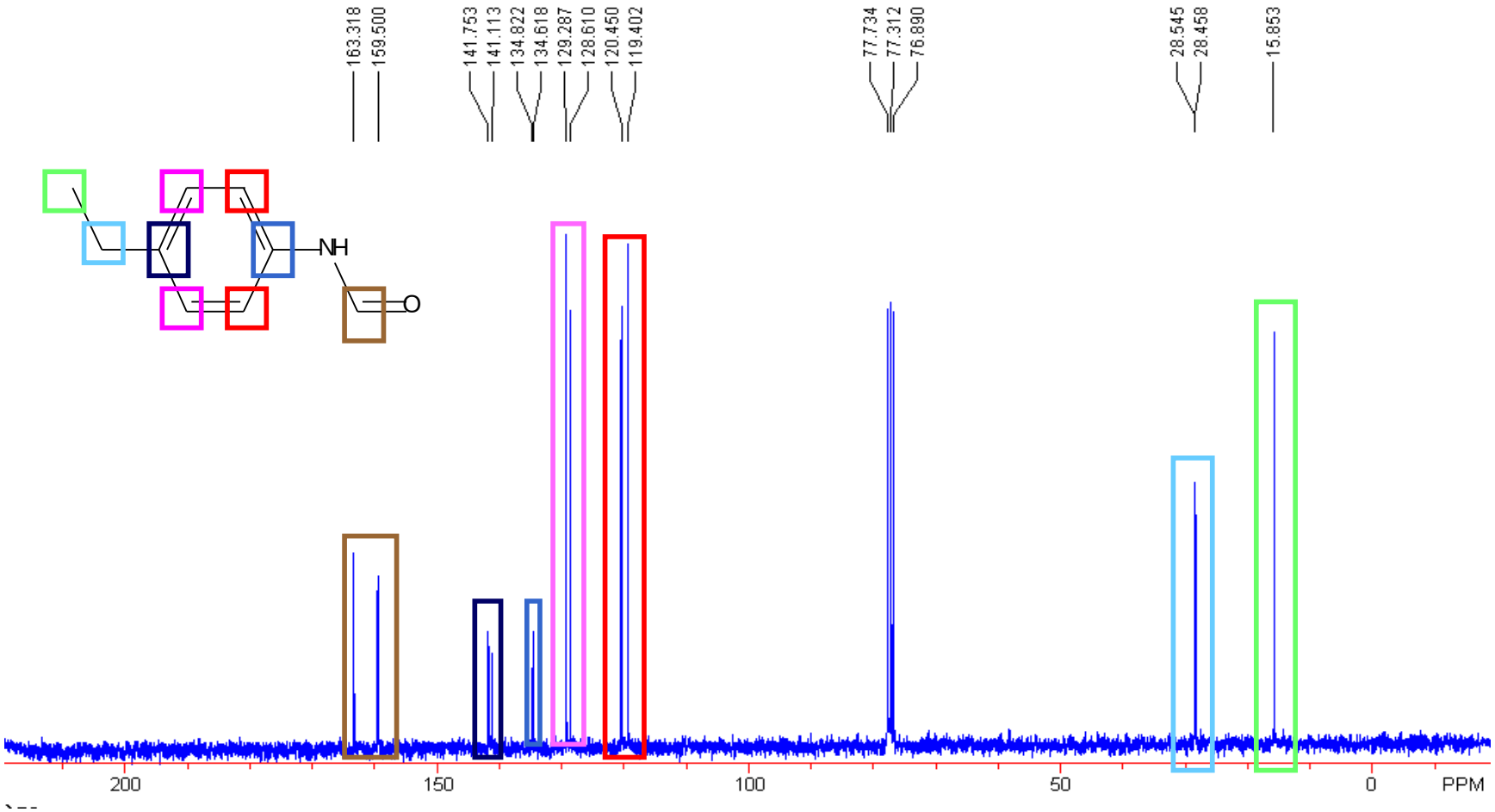

Table II- 3: Summary table for *m*-chloroformanilide

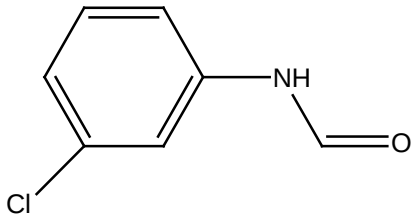

IUPAC name	N-(3-chlorophenyl)formamide
CAS No.	139-71-9
Molecular weight	155.58 g/mol
State	Solid
Synthesis method	Azeotropic synthesis
Purification	Vacuum distillation followed by recrystallization using chloroform-cyclohexane
^{1}H NMR	($CDCl_3$, δ)[83]: 8.72 (br s, ½H), 8.39 (d,½H), 7.75 (br s, ½H), 7.65 (m, ½H), 6.95-7.45 (m, 4H, Ar-H));
^{13}C NMR	($CDCl_3$, δ): 162.66, 159.35, 138.11, 135.60, 134.88, 130.98, 130.27, 125.49, 125.06, 120.28, 118.90, 118.10, 116.83,
Melting Point	52.76 °C (51-53 °C) [14]
Purity	99.98 %

Table II- 4: Summary table for *m*-bromoformanilide

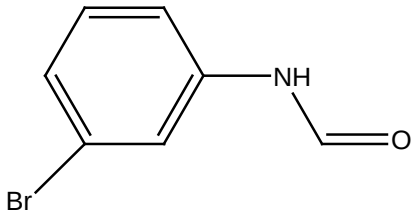

IUPAC name	N-(3-bromophenyl)formamide
CAS No.	37831-25-7
Molecular weight	200.03 g/mol
State	Solid
Synthesis method	Azeotropic Synthesis
Purification	Vacuum distillation
^{1}H NMR	($CDCl_3$, δ)[83]: 9.12 (br d, ½H), 8.50 (brs, 1H),8.7 (d, ½H), 8.34 (s, 1H), 7.02-7.81 (m, 4H, Ar-H);
^{13}C NMR	($CDCl_3$, δ):163.04, 159.90, 138.40, 131.28, 130.62, 128.47, 123.52, 123.28, 122.84, 121.82, 118.82, 117.39
Melting Point	57.89 °C (56-58 °C)[84]
Purity	99.80 %

Table II- 5: Summary table for *p*-nitroformanilide

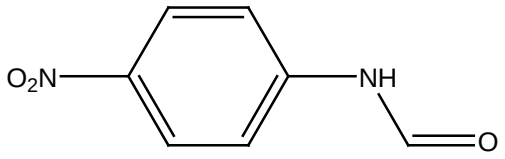

IUPAC name	N-(4-nitrophenyl)formamide
CAS No.	16135-31-2
Molecular weight	166.04 g/mol
State	Solid
Synthesis method	Acylation
Purification	Recrystallized from water-ethanol
^{1}H NMR	(DMSO-d6, δ)[83]: 10.75 (br s, 1H), 8.4 (s, 1H), 8.25-7.10 (m, 4H, Ar-H);
^{13}C NMR	(DMSO-d6, δ):161.17, 144.83, 143.17, 125.88, 119.66
Melting Point	196.00 °C (192-194°C)[16]

Table II- 6: Summary table for *m*-nitroformanilide

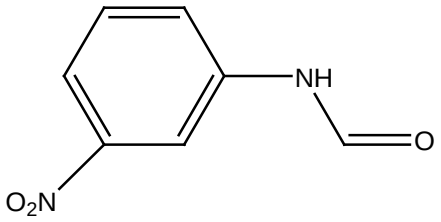

IUPAC name	N-(3-nitrophenyl)formamide
CAS No.	102-38-5
Molecular weight	166.04 g/mol
State	Solid
Synthesis method	Azeotropic synthesis
Purification	Recrystallized from chloroform
^{1}H NMR	(DMSO-d6, δ)[83]: 10.67 (s, 1H), 8.93, 10.47 (dd, 1H), 8.60 (s, 1H), 8.38(s, 1H), 7.50-7.95 (m, 3H,Ar-H);
^{13}C NMR	(DMSO-d6, δ):163.33,160.95, 149.05, 148.55, 140.54, 139.87, 131.32,130.87, 125.75, 123.70, 118.75, 118.44, 113.96, 112.17
Melting Point	134.0 °C (134 °C)[16]

Table II- 7:Summary table for *o*-nitroformanilide

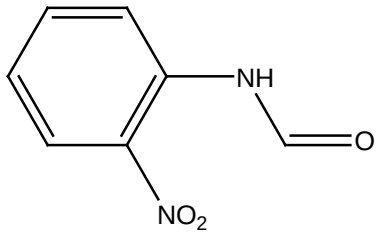

IUPAC name	N-(2-nitrophenyl)formamide
CAS No.	7418-32-8
Molecular weight	166.04 g/mol
State	Solid
Synthesis method	Azeotropic synthesis
Purification	Recrystallized from chloroform
^{1}H NMR	(DMSO-d6, δ)[83]: 10.5 (br s, 1H), 8.49 (s, 1H), 8.15 (d, 1H), 8.05 (d, 1H), 7.7 (m, 1H), 7.2 (m, 1H);
^{13}C NMR	(DMSO-d6, δ):161.14, 140.248, 135.34, 32.016, 125.88, 125.31, 124.42
Melting Point	122.20 °C (122 °C)[85]
Purity	99.45 %

Table II- 8:Summary table for *m*-methoxyformanilide

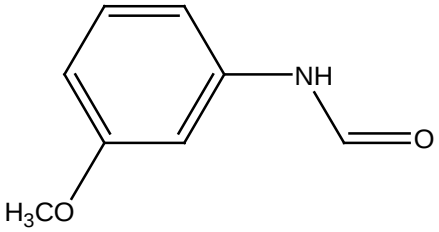

IUPAC name	N-(3-methoxyphenyl)formamide
CAS No.	27153-17-9
Molecular weight	151.06 g/mol
State	Solid
Synthesis method	Azeotropic Synthesis
Purification	Extraction
^{1}H NMR	($CDCl_3$, δ)[86]: 8.7(s, 1H), 8.27(d, ½H), 7.9 (s, ½H); 6.6-7.4 (m, 4H), 3.8 (d, 3H).
^{13}C NMR	($CDCl_3$, δ):163.04, 160.88, 160.33, 159.52, 138.38, 138.25, 130.80, 130.00, 112.34, 111.10, 110.71, 110.63, 106.15, 105.08, 55.61, 55.53
Melting Point	54.52 °C (55-57 °C)[16]
Purity	98.96 %

Table II- 9: Summary table for *o*-methoxyformanilide

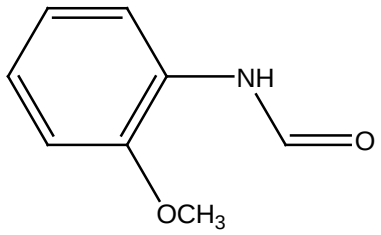

IUPAC name	N-(2-methoxyphenyl)formamide
CAS No.	23896-88-0
Molecular weight	151.06 g/mol
State	Solid
Synthesis method	Azeotropic synthesis
Purification	Vacuum distillation
^{1}H NMR	($CDCl_3$, δ)[86]: 8.4(m, 1H), 8.05 (br s, ½H), 7.85 (br s, ½H), 6.8-7.25 (m, 4H), 3.83 (m, 3H).
^{13}C NMR	($CDCl_3$, δ):161.91, 159.25, 149.05, 148.11, 126.99, 126.38, 125.49, 124.49, 121.21, 120.65, 117.09, 111.54, 110.34, 77.83, 77.61, 77.40, 76.98
Melting Point	83.79 °C (84°C) [87]
Purity	99.98 %

Table II- 10: Summary table for *p*-hydroxyformanilide

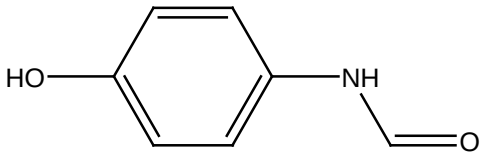

IUPAC name	N-(4-hydroxyphenyl)formamide
CAS No.	1693-39-6
Molecular weight	137.05 g/mol
State	Solid
pK_a	9.58 (9.2)[16]

Table II- 11: Summary table for *m*-hydroxyformanilide

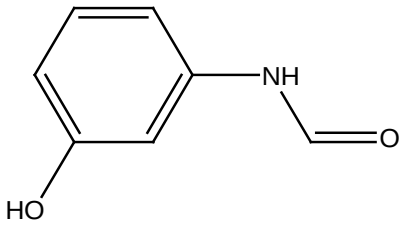

IUPAC name	N-(3-hydroxyphenyl)formamide
CAS No.	24891-35-8
Molecular weight	137.05 g/mol
State	Solid
Synthesis method	Azeotropic synthesis
Purification	Recrystallized from benzene
^{1}H NMR	(DMSO-d6): [83]10.02 (br s, 1H), 9.45 (d, 1H, OH), 9.49 (s, 1H), 8.7 (d, 1H), 8.2 (s, 1H), 6.4-7.2 (m, 4H, Ar-H)
^{13}C NMR	(DMSO-d6):163.01, 160.06, 158.89, 140.14, 139.88, 130.82, 130.18, 111.40, 110.52, 108.63, 107.00, 105.36,
Melting Point	110.57 °C (110 °C) [88]
Purity	99.98 %
pK_a	9.29

Table II- 12: Summary table for *o*-hydroxyformanilide

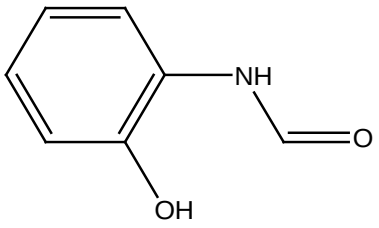

IUPAC name	N-(2-hydroxyphenyl)formamide
CAS No.	2843-27-8
Molecular weight	137.05 g/mol
State	Solid
pK_a	8.98 (8.1)[89]

Table II- 13: Summary table for *p*-carboxyformanilide

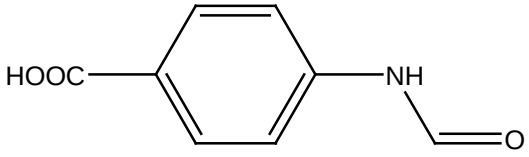

IUPAC name	4-formamidobenzoic acid
CAS No.	28533-43-9
Molecular weight	165.15 g/mol
State	Solid
Synthesis method	Azeotropic synthesis
Purification	Solid product was washed with 0.1 M hydrochloric acid, and product was filtered. The cake was dried in a oven, and under vacuum
^{1}H NMR	(DMSO-d6, δ): 12.73 (br s, 1H), 10.5 (s, 1H, COOH), 8.95 (d, 0.25H), 8.4 (s, 0.75H), 7.9 (s, 2H, Ar-H), 7.6(d, 1.5H, Ar-H), 7.25 (d, 0.5H, Ar-H)
^{13}C NMR	(DMSO-d6, δ): 167.98, 163.61, 161.15,143.63, 143.23, 132.05, 131.63, 126.68, 119.67, 117.49
Melting Point	250-270 °C (268)[90]
pK_a	4.02 by UV spectroscopy

Table II- 14: Summary table for *m*-carboxyformanilide

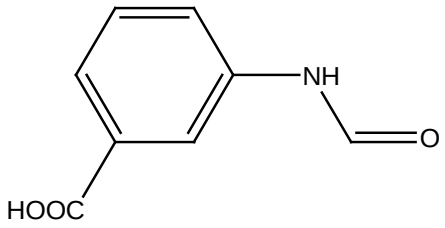

IUPAC name	3-formamidobenzoic acid
CAS No.	28533-42-8
Molecular weight	165.15 g/mol
State	Solid
Synthesis method	Azeotropic synthesis
Purification	Solid product was washed with 0.1 M hydrochloric acid, and product was filtered. The cake was dried in a vacuum oven.
^{1}H NMR	(DMSO, δ): 13.0 (br s, 1H), 10.4 (s, 1H, COOH), 8.95 (d, 0.25H), 8.2 (d, 1.75H), 7.7 (m, 2H Ar-H), 7.45(m, 2H Ar-H)
^{13}C NMR	(DMSO, δ):167.16, 167.02, 162.64, 159.93, 138.79, 138.51, 132.09, 131.52, 129.73, 129.65, 129.21, 124.53, 124.46, 123.36, 122.93, 121.37, 119.97, 118.32
Melting Point	223 °C (225 °C)[91]
pK_a	3.86

Table II- 15: Summary table for *o*-carboxyformanilide

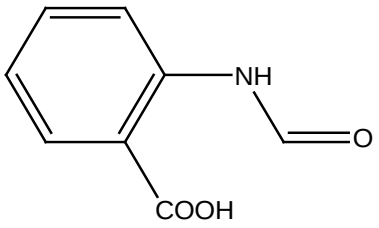

IUPAC name	2-formamidobenzoic acid
CAS No.	3342-77-6
Molecular weight	165.15 g/mol
State	Solid
pK_a	3.37

Table II- 16: Summary table for *m*-methylformanilide

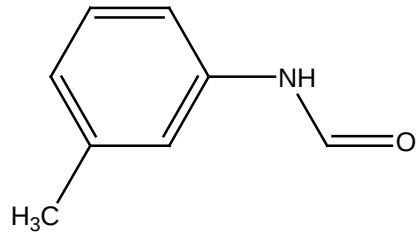

IUPAC name	N-*m*-tolylformamide, N-(3-methyl phenyl)formamide
CAS No.	3085-53-8
Molecular weight	135.07 g/mol
State	liquid
Synthesis method	Azeotropic synthesis
Purification	Vacuum distillation
^{1}H NMR	($CDCl_3$, δ): δ 9.6 (br s, ½H), 9.2 (s, ½H), 8.7 (d, ½H), 8.25 (s, ½H), 7.4 (d, 1H, Ar-H), 7.2 (m, 1H, Ar-H), 6.8 (m, 2H, Ar-H), 2.25 (m, 3H, CH_3).
^{13}C NMR	($CDCl_3$, δ): 163.20, 160.07,139.39, 138.59, 136.98, 136.77, 129.19, 128.57, 125.66, 125.29, 120.76, 119.10, 117.27, 115.39, 21.12, 21.05

Table II- 17: Summary table for *p*-ethylformanilide

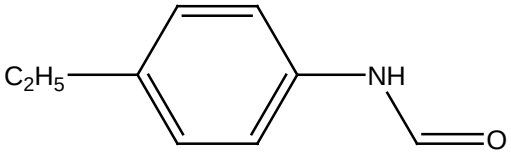

IUPAC name	N-(4-ethylphenyl)formamide
CAS No.	69753-59-9
Molecular weight	149.15 g/mol
State	Solid
Synthesis method	Azeotropic synthesis
Purification	Vacuum distillation
^{1}H NMR	($CDCl_3$, δ)[92]: 8.75 (br d, ½H), 8.63 (d, ½H), 8.3 (s, ½H), 7.85 (br s, ½H,), 7.43 (d, 1H, Ar-H), 7.15 (m, 2H, Ar-H), 7.00 (d, 1H, Ar-H), 2.60 (m, 2H, CH_2), 1.20 (m, 3H, CH_3).
^{13}C NMR	($CDCl_3$, δ):163.26, 159.45 141.7, 141.06, 134.78, 134.57, 129.24, 128.56, 120.40, 119.36, 28.51, 28.42, 15.81
Melting Point	45.45 °C (42.5-44.2 °C)[93]

Table II- 18: Summary table for *m*-ethylformanilide

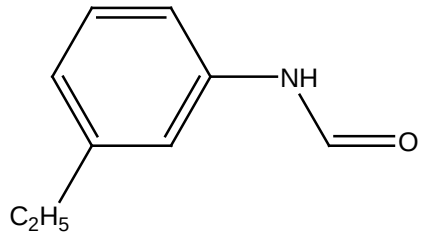

IUPAC name	N-(3-ethylphenyl)formamide
Molecular weight	149.15 g/mol
CAS No.	69753-58-8
State	liquid
Synthesis method	Azeotropic synthesis
Purification	Vacuum distillation
^{1}H NMR	($CDCl_3$, δ): 9.5 (br d, ½H,), 8.75 (d, ½H), 8.60 (br d, ½H,), 8.25 (s, ½H,), 7.40 (m, 1H, Ar-H), 7.2 (m, 1H, Ar-H), 6.9 (m, 2H, Ar-H), 2.60 (m, 2H, CH_2), 1.20 (m, 3H, CH_3).
^{13}C NMR	($CDCl_3$, δ):163.26, 161.11, 145.93, 145.11, 137.16, 136.88, 129.42, 128.74, 125.59, 124.10, 119.63, 118.16, 117.51, 115.80, 28.64, 28.57, 15.31, 15.29

Table II- 19: Summary table for *o*-ethylformanilide

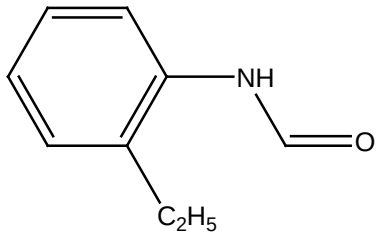

IUPAC name	N-(2-ethylphenyl)formamide
CAS No.	2860-30-2
Molecular weight	149.15 g/mol
State	Solid
Synthesis method	Azeotropic Synthesis
Purification	Vacuum Distillation
^{1}H NMR	($CDCl_3$, δ): δ 8.59 (br s, 1H), 8.4 (s, ½H), 7.82 (d, ½H), 7.6 (s, 1H, Ar-H), 7.05-7.3 (m, 4H, Ar-H), 2.62 (m, 2H, CH_2), 1.20 (m, 3H, CH_3).
^{13}C NMR	($CDCl_3$, δ): 164.00, 159.69, 136.258, 134.51, 129.47, 128.78, 127.04, 126.71, 126.52,125.91, 123.82, 121.69, 24.27, 24.21, 14.23, 14.07
Melting Point	70.10 °C (71-72°C)[94]
Purity	99.70 %

Table II- 20: Summary table for *p*-isopropylformanilide

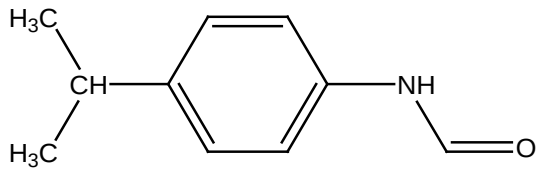

IUPAC name	N-[4-(1-methylethyl)phenyl]Formamide
CAS No.	5279-58-3
Molecular weight	163.22 g/mol
State	Solid
Synthesis method	Azeotropic synthesis
Purification	Vacuum distillation
^{1}H NMR	($CDCl_3$, δ)[95]: 8.9 (br d, ½H), 8.65 (d, ½H,), 8.3 (d, ½H), 7.9 (br s, ½H), 7.49 (d, 1H, Ar-H), 7.2 (m, 2H, Ar-H), 7.0 (d, 1H, Ar-H), 2.8 (m, H, CH), 1.29 (m, 6H, $2CH_3$).
^{13}C NMR	($CDCl_3$, δ): 163.32, 159.53, 146.38,145.72, 134.89, 134.69, 127.83, 127.15, 120.47, 119.39, 33.83, 33.78, 24.20
Melting Point	30-38 °C (multiple peaks)

Table II- 21: Summary table for *m*-isopropylformanilide

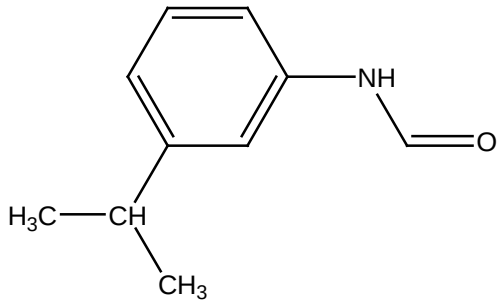

IUPAC name	N-(3-isopropylphenyl)formamide
CAS No.	74702-41-3
Molecular weight	163.22 g/mol
State	Liquid
Synthesis method	Azeotropic synthesis
Purification	Vacuum distillation
^{1}H NMR	($CDCl_3$, δ): *δ* 9.45 (br d, ½H), 9.76 (br m, 1H,), 8.35 (s, ½H), 7.50 (m, 1H, Ar-H), 7.25 (m, 1H, Ar-H), 7.0 (m, 2H, Ar-H), 2.8 (m, H, CH), 1.29 (m, 6H, $2CH_3$).
^{13}C NMR	($CDCl_3$, δ): 163.64, 160.18, 151.08, 150.21, 137.47, 137.17, 129.86, 129.17, 123.61, 123.02,118.67, 117.38, 116.44, 34.32, 24.17, 24.13, 24.08

Table II- 22: Summary table for *o*-isopropylformanilide

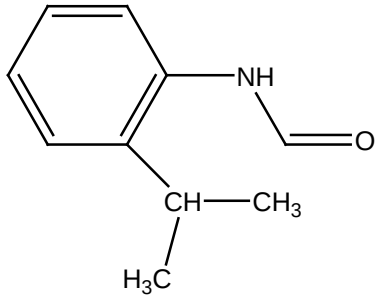

IUPAC name	N-(2-isopropylphenyl)formamide
CAS No.	90874-73-0
Molecular weight	163.20 g/mol
State	Solid
Synthesis method	Azeotropic synthesis
Purification	Vacuum distillation
^{1}H NMR	($CDCl_3$, δ): 8.5 (d, 1H), 8.25 (br s, ½H), 7.75 (m, ½H), 7.0-7.5 (m, 4H, Ar-H), 3.1 (m, H, CH), 1.25 (m, 6H, $2CH_3$).
^{13}C NMR	($CDCl_3$, δ):164.21, 159.87, 141.41, 140.29, 133.70, 133.09, 127.10, 126.99, 126.64, 126.61, 126.56, 125.90, 124.78, 122.81, 28.06, 27.97, 23.26
Melting Point	7.53 °C (71.5-72.5 °C)[96]
Purity	99.49 %

Table II- 23: Summary table for *p*-phenylformanilide

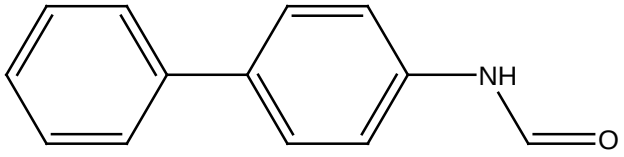

IUPAC name	N-formyl-4-aminobiphenyl
CAS No.	5472-79-7
Molecular weight	197.23 g/mol
State	Solid
Synthesis method	Azeotropic Synthesis
Purification	Recrystallization from water-ethanol
^{1}H NMR	($CDCl_3$, δ): 8.78 (d, ½H), 8.4 (s, ½H), 8.16(br d, ½H), 7.1-7.6 (m, 9H)
^{13}C NMR	($CDCl_3$, δ):162.56, 159.12, 140.55, 140.21, 138.6, 137.98, 136.28, 136.06, 129.10, 129.02, 128.63, 127.96, 127.67, 127.46, 127.09, 127.06, 120.49, 119.33
Melting Point	172.05 °C (172 °C)[97]
Purity	99.06 %

Table II- 24: Summary table for *o*-phenylformanilide

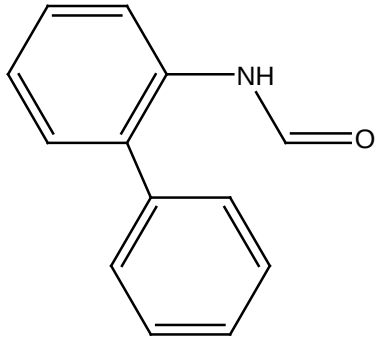

IUPAC name	N-formyl-2-aminobiphenyl
CAS No.	5346-21-4
Molecular weight	197.23 g/mol
State	Solid
Synthesis method	Azeotropic synthesis
Purification	Recrystallized from ethanol-water
^{1}H NMR	($CDCl_3$, δ)[98]: 8.7 (d, ½H), 8.4 (d, ½H), 8.25(s, ½H), 7.1-7.75 (m, 9H)
^{13}C NMR	($CDCl_3$, δ): 162.05,.159.01, 137.90, 137.44, 133.94, 133.87, 133.07, 132.08, 131.288, 130.262, 129.43, 129.28, 128.84, 128.61, 128.25, 128.22, 125.43, 124.73, 121.64, 118.37
Melting Point	73.90 °C (67-70 °C)[99]
Purity	99.06 %

CHAPTER III

ORTHO SUBSTITUTION EFFECTS ON THE ACIDIC HYDROLYSIS OF FORMANILIDES

Introduction

Kinetic studies of formanilides in acidic aqueous solutions are reported in this chapter. The reaction products were identified and reaction schemes consistent with the observed products were proposed. Effects of pH, binary solvents, ionic strength, and temperature on the rate law were determined. Structure-reactivity relationships (SRR) were used in conjunction with rate laws to propose reasonable reaction mechanisms. The effect of substitution at the ortho position on reaction mechanism was determined.

Materials

Substituted formanilides were either purchased or synthesized as described in chapter II. Substituted anilines were purchased from Sigma-Aldrich Company (Saint Louis, MO). Glacial acetic acid, anhydrous sodium acetate, potassium chloride, dioxane, dimethyl sulfoxide, sodium phosphate monobasic monohydrate, standardized hydrochloric acid (0.10 M), and anhydrous sodium phosphate dibasic were purchased from Fisher Scientific (Fair Lawn, NJ). Absolute ethanol was obtained from AAPER Alcohol and Chemical Co (Shelbyville, KY). Acetone and concentrated hydrochloric acid (12.5 M) were obtained from Sigma-Aldrich Ltd. (Saint Louis, MO). Tris(hydroxymethyl)aminomethane (Tris) was obtained from Gibco BRL (Grand Island, NY). Tris hydrochloride was obtained from Research Products International Corporation (Mount Prospect, IL). Standardized hydrochloric acid (1.0 M), pH 4 & pH 7 calibration buffers were obtained from VWR Scientific (West Chester, PA). Solvents used for chromatography were high performance liquid chromatography (HPLC) grade. All other chemicals were reagent grade or better.

Methods

Standard Protocols for Kinetic Analysis.

Reactions in concentrated hydrochloric acids (8.15-0.50 M) were followed by using UV spectroscopy and reactions in dilute hydrochloric acid (0.50-0.010 M) were followed using HPLC. For studies conducted using HPLC analysis, the following protocol was used. A 10 mM stock solution of the formanilide substrate was prepared in absolute ethanol. A 10 ml of aliquot of dilute hydrochloric acid solution was equilibrated to the reaction temperature. Reactions were initiated by adding 0.1 ml of the stock solution of the substrate to the hydrochloric acid solution to give an initial substrate concentration equal to 0.1 mM formanilide and 1% v/v ethanol. Aliquots were withdrawn and quenched with either acetate buffer (1.0 M, pH 4) or tris buffer (1.0 M, pH 8). The samples were then stored at 4 °C until HPLC analysis. The pH value was measured with an Accumet model 25 pH meter at the start and end of the reaction using a combination glass electrode calibrated with standard buffers at the reaction temperature. HPLC analysis was performed using the following protocols. Substrate and product concentrations were determined by using four to five standards prepared by dissolving authentic formanilides and their corresponding anilines in 0.1 M acetate or tris buffers. The calibration curves in the range of 0.1 mM to 0.05 mM were prepared by diluting the ethanolic stock solutions of the substrate formanilide and its corresponding aniline with the buffer solutions (0.10 M acetate or .tris). Analyses were performed on a Thermo-separations RP-HPLC system (Thermo Scientific, Waltham, MA) consisting of a UV6000LP diode array detector, AS3000 autoinjector, P4000 pump, and an online membrane degasser. Chromatograms were integrated and data stored using Chromquest® chromatography data system software (Version 4.0).

Initial HPLC method development for the degradation mixtures was carried out by evaluating different column packing materials (C18, C8, CN). The mobile phase used

consisted of 0.01 M phosphate buffer (pH 7.2) : acetonitrile (70:30), and the UV spectrum in the range 210-400 nm was monitored. The wavelength (λ) was chosen such that the sensitivities for aniline and formanilide were both maximized. Depending on the chosen column material, if the resolution between the components were adequate, then the concentration of organic solvent was varied to optimize the method for resolution and time for sample analysis. The optimized separation conditions are noted in Table III-1. The column and the autoinjector were maintained at room temperature.

Analysis of reaction mixtures was conducted with a Hewlett Packard HP8453 UV-Vis diode array spectrophotometer (Hewlett Packard, Santa Clara, CA) equipped with a Peltier thermostatted cell holder (HP 89090A). A 2.5 mL aliquot of hydrochloric acid solution was equilibrated to the reaction temperature in a closed glass cuvette in the thermostatted cell holder of the HP 8453 spectrophotometer. Reactions were initiated by adding 25 μL of stock solution (10 mM substrate in ethanol) to the reaction mixture so that the final concentration of ethyl alcohol was 1% and the final concentration of substrate in solution was 0.1 mM. Spectra were collected as a function of time using the kinetics module in the Chemstation® software. Reactions were followed until there was no significant change in spectra with time. Slow degradation reactions were followed to at least three half lives while fast reactions were followed to at least 10 half lives. The pH value was determined at the end of the reaction at the reaction temperature using a semi-micro combination glass electrode attached to a Accumet model 25 pH meter. The final and initial spectra were subtracted, and the wavelength of maximum difference was determined. Using these wavelengths the spectra were analyzed using the kinetic analysis module in Chemstation® software to determine the observed first-order rate constants. These experiments were carried out in duplicate and average rate constants are reported. To confirm the identity of the hydrolysis products of the substituted formanilide, the spectra associated with the final reaction mixture were compared to an authentic sample of the predicted end product (i.e. the corresponding aniline and formic

acid). Formic acid does not appreciable absorbance at these concentrations and cannot be detected by a UV spectrophotometer; however aniline has a stronger chromophore and could be detected. These solutions were prepared by dissolving the aniline in absolute ethanol (10 mM) and diluting a 25 μL aliquot in 2.5 mL of 1.0 M hydrochloric acid solution to a final concentration equivalent to the initial substrate concentration. The spectrum was collected and compared to the spectrum of the final products using the peak purity compare function in the Chemstation® software.

Kinetic Studies

Determination of reaction schemes for all substrates.

Reaction schemes were determined by hydrolyzing solutions of substituted 0.10 mM formanilides in hydrochloric acid solution at 40 °C or 60 °C. Samples were generated and analyzed using the standard protocol with HPLC. Degradations were also followed using UV spectroscopy as a function of time. Spectra were collected and inspected for the presence of isosbestic points.

Effect of pH on reaction kinetics

The pH-rate profile for the unsubstituted formanilide at 40 °C was determined by using aqueous hydrochloric acid solutions in the concentration range between (8.15 – 0.010 M). Hydrochloric acid solutions in the range of 8.15 M to 1.01 M were prepared by diluting concentrated hydrochloric acid in water. Dilute hydrochloric acid solutions below 1.0 M were prepared by diluting certified hydrochloric acid solutions (1.0 M or 0.10 M) in water and adjusting the ionic strength to 1.0 using potassium chloride. The conditions and experimentally determined rate constants are presented in Table III-2.

The pH-rate profiles for the remaining substituted formanilides were determined in aqueous hydrochloric acid solutions in the range of 1 M to 0.01 M. The procedures used to carry out studies using HPLC and UV-Vis spectroscopy studies for all substituted

formanilides were identical to the procedure used for the unsubstituted formanilide with one exception. *o*-hydroxy formanilide was insoluble in absolute ethanol and stock solutions were prepared in dimethyl sulfoxide. Experimental conditions and observed rate constants are tabulated in Tables III-3 to III-31.

Effect of temperature on the stability of formanilides

Formanilide was degraded in 1 M and 0.01 M hydrochloric acid solutions (adjusted to an ionic strength of 1.0 using potassium chloride). The studies were carried out at 20 °C, 30 °C, 40 °C, 50 °C, and 60 °C. Reactions in 1 M hydrochloric acid were followed using UV-Vis spectroscopy and reactions in 0.01 M hydrochloric acid solutions were analyzed using HPLC. Experimental conditions and observed rate constants are tabulated in Table III-32.

For the substituted formanilides, studies were carried out in 1 M hydrochloric acid at 20-60 °C using UV spectroscopy. The procedures were all identical except for *ortho*-hydroxyformanilide, which is insoluble in ethanol and the stock solution was prepared in dimethyl sulfoxide. Experimental conditions and rate constants are tabulated in Tables III-3 to III-31.

Effect of ionic strength on the stability of formanilide.

A series of formanilide degradation studies at 40 °C were carried out in 0.010 M hydrochloric acid by diluting 0.10 M hydrochloric acid wherein the ionic strengths of the solutions were varied from 1.0 to 0.010 by adding a neutral salt (potassium chloride). The reactions were monitored using HPLC. Experimental conditions and rate constants are tabulated in Table III-33.

Effect of binary solvents on the stability of formanilide

Reaction mixtures for formanilide degradation were prepared in 0.010 M hydrochloric acid containing 25 or 50 % v/v organic solvents (ethanol, dioxane or

acetone). Substrate was added to the reaction mixtures as previously described and reaction samples were analyzed using HPLC. The degradation proceeds very slowly and observed rate constants were determined using the initial rate method. Experimental conditions and rate constants are tabulated in Table III-34.

Results

Determination of Reaction Schemes

Since all the reaction scheme determinations follow a similar process, formanilide is used as a model compound to describe the steps involved in the HPLC chromatograms for the acidic degradation of formanilide indicate the presence of two compounds (Figure III-1) identified as the substrate and corresponding aniline by comparing the peak retention times with authentic standards. Calibration curves were generated using authentic samples of formanilide and aniline, and peak area versus concentration for formanilide and aniline (conc. range of 0.008-0.08 mM) were linear (R^2 > 0.999) (Figure III-2). The concentration-time profiles at different hydrochloric acid concentrations were generated using the calibration curves, and mass balance was determined (Figure III-3). The concentration of formanilide decreases as a function of time with a concurrent increase in the concentration of aniline. The mass balance of the reaction remained constant which indicated that formanilide was quantitatively converted to aniline (Scheme III-1). The reactions were followed to two to three half lives. The order with respect to time for the loss of formanilide was determined from plots of logarithm of the concentration versus time (Figure III-4). The linearity of the plots indicated that the loss of formanilide was first-order with respect to time. The observed first-order rate constant (k_{obs} or k) was estimated by fitting the concentration-time profile of formanilide to the first-order rate equation. In the case of formanilide the observed rate constant is equivalent to the rate constant for the formation of aniline from formanilide (k′).

Table III- 1: HPLC conditions for analysis of substituted formanilides and their reaction products.

Substituent	Flow Rate (ml/min)	Column	Wavelength (λ) nm	Retention Times minutes		Mobile Phase
				Substrate	Aniline	
H	0.8	C	235	2.8	3.6	30:70 ACN:10 mM Phosphate Buffer pH 7
p- Cl	1	C	239	2.6	3.8	38:62 ACN: Water
m-Cl	1	C	240	2.6	4.0	38:62 ACN:10 mM Phosphate Buffer pH 7.2
o-Cl	1	D	236	1.3	2.3	38:62 ACN:10 mM Phosphate Buffer pH 7.2
p-Br	1	B	242	3.6	4.2	55:45 ACN: Water
m-Br	1	D	242	1.8	2.7	35:65 ACN:10 mM Phosphate Buffer pH 7.2
o-Br	1	C	230	2.7	5.5	38:62 ACN:10 mM Phosphate Buffer pH 7
p-CH_3	1.2	C	232	2.9	3.7	30:70 ACN:10 mM Phosphate Buffer pH 7
m-CH_3	1	C	240	3.3	4.5	30:70 ACN:10 mM Phosphate Buffer pH 7
o-CH_3	1.2	C	228	2.4	4.0	28:62 ACN:23 mM Phosphate Buffer pH 7

Table III- 1-Continued

m-C_2H_5	1	D	230	3.9	5.0	30:70 ACN:10 mM Phosphate Buffer pH 7.2
o-C_2H_5	1	D	230	2.0	3.6	30:70 ACN:10 mM Phosphate Buffer pH 7.2
p-isoC_3H_7	1	D	231	4.2	5.6	32:68 ACN:10 mM Phosphate Buffer pH 7.2
m-isoC_3H_7	1	D	231	4.2	5.9	32:68 ACN:10 mM Phosphate Buffer pH 7.2
o-isoC_3H_7	1	D	231	2.7	5.3	32:68 ACN:10 mM Phosphate Buffer pH 7.2
p-NO_2	1.2	D	340	6.9	5.6	11:89 ACN:10 mM Phosphate Buffer pH 7.2
m-NO_2	1	D	236	3.3	4.3	20:80 ACN:10 mM Phosphate Buffer pH 7.2
o-NO_2	1	D	233	4.0	2.2	25:75 ACN:10 mM Phosphate Buffer pH 7.2
p-Phenyl	1	D	270	4.1	5.6	35:65 ACN:10 mM Phosphate Buffer pH 7.2
o-Phenyl	1	D	220	3.2	6.8	35:65 ACN:10 mM Phosphate Buffer pH 7.2
p-COOH	0.8	A	260	2.8	2.3	10:90 ACN:100 mM Phosphate Buffer pH 7
m-COOH	0.8	A	238	2.8	2.3	10:90 ACN:100 mM Phosphate Buffer pH 7
o-COOH	0.8	A	235	4.3	2.7	10:90 ACN:100 mM Phosphate Buffer pH 7
p-OH	1	A	230	5.7	3.7	05:95 ACN:100 mM Phosphate Buffer pH 7

Table III- 1-Continued

m-OH	1	A	210	6.8	4.0	05:95 ACN:100 mM Phosphate Buffer pH 7
o-OH	1.2	B	230	6.5	3.6	05:95 ACN:10 mM Phosphate Buffer pH 7
p-OCH_3	1	A	235	5.2	4.3	20:80 ACN:100 mM Phosphate Buffer pH 7
m-OCH_3	0.5	D	235	1.9	2.9	40:60 ACN:100 mM Phosphate Buffer pH 7
o-OCH_3	0.5	D	235	2.2	2.8	40:60 ACN:100 mM Phosphate Buffer pH 7

A = Zorbax SB-CN, 5 μ, 4.6 × 150 mm: B = Zorbax SB-C8, 5 μ, 4.6×150 mm: C = C12 HydroRP Phenomenex, 4 μ, 4.6×75mm;

D = Metasil ODS, 5 μ, 4.6 x 500 mm ; and ACN= Acetonitrile

Table III- 2: Experimental conditions and observed rate constants for the hydrolysis of formanilide in hydrochloric acid solutions at 40 °C.

HCl Conc. (M) $\times 10^2$	**Calculated H_A**	**Measured pH**	**k_{obs} $hr^{-1} \times 10^2$**
1.00	-	1.99	7.43
3.00	-	1.51	22.8
10.0	-	0.99	72.6
30.0	-	0.55	215
50.0	-	-	371
70.0	-	-	524
85.0	-	-	638
100	-	0.07	726
102	-0.20	-	812
204	-0.73	-	1640
306	-1.13	-	2490
408	-1.50	-	2980
510	-1.88	-	3480
612	-2.26	-	3160
713	-2.63	-	2420
815	-2.98	-	1530

Wavelength for UV analysis was 240 nm. Ionic strength was adjusted to 1.0 for reaction mixtures containing hydrochloric acid $\leq$ 0.85 M by addition of potassium chloride.

Table III- 3: Experimental conditions and observed rate constants for the hydrolysis of p-methylformanilide in hydrochloric acid solutions.

HCl Conc. **(M) × 10^2**	**Measured pH**	**Temperature** **°C**	**k_{obs}** **hr^{-1}× 10^2**
1.00	2.02	40	5.20
3.00	1.55	40	16.4
10.0	1.06	40	72.6
30.0	0.63	40	160
50.0	-	40	269
70.0	-	40	358
85.0	-	40	436
100	0.07	40	479
100	-	20	73.1
100	-	30	178
100	-	40	434
100	-	50	1010
100	-	60	2170

Ionic strength for all solutions was adjusted to 1.0 using potassium chloride. Wavelength for UV kinetic analysis was 243 nm.

Table III- 4: Experimental conditions and observed rate constants for the hydrolysis of m-methylformanilide in hydrochloric acid solutions.

HCl Conc. **(M) × 10^2**	**Measured pH**	**Temperature** **°C**	**k_{obs}** **hr^{-1}× 10^2**
1.00	2.03	40	7.51
3.00	1.55	40	22.7
10.0	1.04	40	70.4
30.0	0.56	40	214
50.0	0.34	40	362
100	0.07	40	653
100	-	20	98.0
100	-	30	261
100	-	50	1400
100	-	60	2970

Ionic strength for all solutions was adjusted to 1.0 using potassium chloride. Wavelength for UV kinetic analysis was 230 nm.

Table III- 5: Experimental conditions and observed rate constants for the hydrolysis of o-methylformanilide in hydrochloric acid solutions.

HCl Conc. **(M) × 10^2**	**Measured pH**	**Temperature** **°C**	**k_{obs}** **hr^{-1}× 10^2**
1.00	1.99	40	1.98
3.00	1.53	40	7.10
10.0	1.05	40	25.8
30.0	0.62	40	72.7
50.0	-	40	136
70.0	-	40	181
85.0	-	40	218
100	0.07	40	254
100	-	20	36.4
100	-	30	87.6
100	-	40	221
100	-	50	518
100	-	60	1150

Ionic strength for all solutions was adjusted to 1.0 using potassium chloride. Wavelength for UV kinetic analysis was 232 nm.

Table III- 6: Experimental conditions and observed rate constants for the hydrolysis of *p*-chloroformanilide in hydrochloric acid solutions.

HCl Conc. (M) × 10^2	**Measured pH**	**Temperature °C**	**k_{obs} hr^{-1}× 10^2**
1.00	2.03	40	8.25
3.00	1.56	40	23.9
10.0	1.04	40	76.7
30.0	0.62	40	72.7
25.0	-	40	184
75.0	-	40	522
100	0.09	40	714
100	-	20	1067
100	-	30	283
100	-	50	1490
100	-	60	3290

Ionic strength for all solutions was adjusted to 1.0 using potassium chloride. Wavelength for UV kinetic analysis was 247 nm.

Table III- 7: Experimental conditions and observed rate constants for the hydrolysis of *m*-chloroformanilide in hydrochloric acid solutions.

HCl Conc. **(M) × 10^2**	**Measured** **pH**	**Temperature** **°C**	**k_{obs}** **hr^{-1}× 10^2**
1.00	2.06	40	10.8
3.00	1.56	40	32.1
30.0	0.56	40	298
50.0	0.33	40	488
100	0.34	40	968
100	-	20	153
100	-	30	387
100	-	50	2020
100	-	60	4280

Ionic strength for all solutions was adjusted to 1.0 using potassium chloride. Wavelength for UV kinetic analysis was 243 nm.

Table III- 8: Experimental conditions and observed rate constants for the hydrolysis of *o*-chloroformanilide in hydrochloric acid solutions.

HCl Conc. (M) × 10^2	**Measured pH**	**Temperature °C**	**k_{obs} hr^{-1}× 10^2**
1.00	2.08	40	7.98
3.00	1.60	40	22.1
10.0	1.08	40	71.8
30.0	0.59	40	223
100	0.10	40	725
100	-	20	122
100	-	30	287
100	-	50	1570
100	-	60	3350

Ionic strength for all solutions was adjusted to 1.0 using potassium chloride. Wavelength for UV kinetic analysis was 238 nm.

Table III- 9: Experimental conditions and observed rate constants for the hydrolysis of *p*-nitroformanilide in hydrochloric acid solutions.

HCl Conc. (M) × 10^2	**Measured pH**	**Temperature °C**	**k_{obs} hr^{-1}× 10^2**
0.010	2.09	40	30.5
0.030	1.59	40	95.0
0.100	1.09	40	312
0.300	0.61	40	959
0.500	-	40	1440
1.000	0.13	40	2730
1.000	-	20	499
1.000	-	30	1180
1.000	-	50	5520
1.000	-	60	11050

Ionic strength for all solutions was adjusted to 1.0 using potassium chloride. Wavelength for UV kinetic analysis was 316 nm.

Table III- 10: Experimental conditions and observed rate constants for the hydrolysis of *m*-nitroformanilide in hydrochloric acid solutions.

HCl Conc. (M) × 10^2	**Measured pH**	**Temperature °C**	**k_{obs} hr^{-1}× 10^2**
1.00	2.04	40	12.6
3.00	1.56	40	37.5
10.0	1.04	40	120
30.0	0.57	40	353
50.0	0.35	40	597
100	0.11	40	1130
100	-	20	182
100	-	30	464
100	-	50	2360
100	-	60	4980

Ionic strength for all solutions was adjusted to 1.0 using potassium chloride. Wavelength for UV kinetic analysis was 240 nm.

Table III- 11: Experimental conditions and observed rate constants for the hydrolysis of *o*-nitroformanilide in hydrochloric acid solutions.

HCl Conc. (M) × 10^2	**Measured pH**	**Temperature °C**	**k_{obs} hr^{-1}× 10^2**
1.00	2.10	40	25.2
3.00	1.62	40	71.3
10.0	1.16	40	239
30.0	0.62	40	771
50.0	0.41	40	1260
100	0.15	40	2490
100	-	20	445
100	-	30	1050
100	-	50	5050
100	-	60	10260

Ionic strength for all solutions was adjusted to 1.0 using potassium chloride. Wavelength for UV kinetic analysis was 239 nm.

Table III- 12: Experimental conditions and observed rate constants for the hydrolysis of *p*-bromoformanilide in hydrochloric acid solutions.

HCl Conc. (M) × 10^2	**Measured pH**	**Temperature °C**	**k_{obs} hr^{-1}× 10^2**
3.00	1.61	40	25.5
30.0	0.60	40	250
50.0	-	40	434
70.0	-	40	606
85.0	-	40	714
100	0.09	40	825
100	-	20	114
100	-	30	306
100	-	40	743
100	-	50	1640
100	-	60	3630

Ionic strength for all solutions was adjusted to 1.0 using potassium chloride. Wavelength for UV kinetic analysis was 251 nm.

Table III- 13: Experimental conditions and observed rate constants for the hydrolysis of *m*-bromoformanilide in hydrochloric acid solutions.

HCl Conc. (M) × 10^2	**Measured pH**	**Temperature °C**	**k_{obs} hr^{-1}× 10^2**
10.0	1.10	40	95.4
30.0	0.61	40	309
50.0	0.40	40	527
100	0.09	40	926
100	-	20	156
100	-	30	367
100	-	50	1987
100	-	60	4340

Ionic strength for all solutions was adjusted to 1.0 using potassium chloride. Wavelength for UV kinetic analysis was 244 nm.

Table III- 14: Experimental conditions and observed rate constants for the hydrolysis of *o*-bromoformanilide in hydrochloric acid solutions.

HCl Conc. (M) × 10^2	**Measured pH**	**Temperature °C**	**k_{obs} hr^{-1}× 10^2**
3.00	1.59	40	21.6
30.0	0.60	40	206
50.0	-	40	369
70.0	-	40	513
85.0	-	40	593
100	0.09	40	695
100	-	20	117
100	-	30	262
100	-	40	626
100	-	50	1360
100	-	60	3000

Ionic strength for all solutions was adjusted to 1.0 using potassium chloride.
Wavelength for UV kinetic analysis was 239 nm.

Table III- 15: Experimental conditions and observed rate constants for the hydrolysis of p-ethylformanilide in hydrochloric acid solutions.

HCl Conc. (M) × 10^2	**Measured pH**	**Temperature °C**	**k_{obs} hr^{-1}× 10^2**
1.00	2.09	40	5.63
3.00	1.63	40	17.0
10.0	1.15	40	52.7
30.0	0.70	40	157
50.0	0.50	40	278
100	0.20	40	463
100	-	20	77
100	-	30	190
100	-	50	1030
100	-	60	2330

Ionic strength for all solutions was adjusted to 1.0 using potassium chloride. Wavelength for UV kinetic analysis was 230 nm.

Table III- 16: Experimental conditions and observed rate constants for the hydrolysis of *m*-ethylformanilide in hydrochloric acid solutions.

HCl Conc. (M) × 10^2	**Measured pH**	**Temperature °C**	**k_{obs} hr^{-1}× 10^2**
1.00	2.07	40	7.33
3.00	1.61	40	22.5
10.0	1.14	40	71. 9
30.0	0.71	40	201
50.0	0.57	40	310
100	0.27	40	627
100	-	20	120
100	-	30	270
100	-	50	1360
100	-	60	3040

Ionic strength for all solutions was adjusted to 1.0 using potassium chloride. Wavelength for UV kinetic analysis was 230 nm.

Table III- 17: Experimental conditions and observed rate constants for the hydrolysis of *o*-ethylformanilide in hydrochloric acid solutions.

HCl Conc. (M) × 10^2	**Measured pH**	**Temperature °C**	**kobs hr^{-1}× 10^2**
1.00	2.05	40	2.27
3.00	1.59	40	6.92
10.0	1.08	40	21.4
30.0	0.63	40	63.3
50.0	0.42	40	104
100	-	40	173
100	-	50	407
100	-	60	996

Ionic strength for all solutions was adjusted to 1.0 using potassium chloride. Wavelength for UV kinetic analysis was 230 nm.

Table III- 18: Experimental conditions and observed rate constants for the hydrolysis of *p*-isopropylformanilide in hydrochloric acid solutions.

HCl Conc. (M) × 10^2	**Measured pH**	**Temperature °C**	**k_{obs} hr^{-1}× 10^2**
3.00	1.63	40	14.9
10.0	1.15	40	54.2
30.0	0.67	40	167
50.0	0.46	40	269
100	-	40	485
100	-	30	198
100	-	50	1080
100	-	60	2500

Ionic strength for all solutions was adjusted to 1.0 using potassium chloride. Wavelength for UV kinetic analysis was 244 nm.

Table III- 19: Experimental conditions and observed rate constants for the hydrolysis of *m*-isopropylformanilide in hydrochloric acid solutions.

HCl Conc. **(M) × 10^2**	**Measured pH**	**Temperature** **°C**	**k_{obs}** **hr^{-1}× 10^2**
3.00	1.63	40	22.1
10.0	1.12	40	72.1
30.0	0.67	40	199
50.0	0.46	40	327
100	-	40	610
100	-	30	256
100	-	50	1360
100	-	60	3030

Ionic strength for all solutions was adjusted to 1.0 using potassium chloride. Wavelength for UV kinetic analysis was 244 nm.

Table III- 20: Experimental conditions and observed rate constants for the hydrolysis of *o*-isopropylformanilide in hydrochloric acid solutions.

HCl Conc. (M) × 10^2	**Measured pH**	**Temperature °C**	**k_{obs} hr^{-1}× 10^2**
3.00	1.63	40	4.91
10.0	1.12	40	15.8
30.0	0.67	40	45.0
50.0	0.46	40	73.0
100	-	40	140
100	-	30	43.2
100	-	50	317
100	-	60	769

Ionic strength for all solutions was adjusted to 1.0 using potassium chloride. Wavelength for UV analysis was 224 nm.

Table III- 21: Experimental conditions and observed rate constants for the hydrolysis of *p*-methoxyformanilide in hydrochloric acid solutions.

HCl Conc. (M) × 10^2	**Measured pH**	**Temperature °C**	**k_{obs} hr^{-1}× 10^2**
50.0	0.39	40	149
100	0.06	40	295
100	-	50	660
100	-	60	1500

Ionic strength for all solutions was adjusted to 1.0 using potassium chloride. Wavelength for UV kinetic analysis was 242 nm.

Table III- 22: Experimental conditions and observed rate constants for the hydrolysis of *m*-methoxyformanilide in hydrochloric acid solutions.

HCl Conc. **(M) × 10^2**	**Measured pH**	**Temperature** **°C**	**k_{obs}** **hr^{-1}× 10^2**	**k′** **hr^{-1}× 10^2**
3.00	1.58	40	34.0	26.1
10.0	1.09	40	106	85.4
30.0	0.61	40	328	257

Ionic strength for all solutions was adjusted to 1.0 using potassium chloride

Table III- 23: Experimental conditions and observed rate constants for the hydrolysis of *o*-methoxyformanilide in hydrochloric acid solutions.

HCl Conc. (M) × 10^2	**Measured pH**	**Temperature °C**	**k_{obs} hr^{-1}× 10^2**
3.00	1.58	40	14.0
10.0	1.07	40	63.1
30.0	0.60	40	181
50.0	0.39	40	291
100	0.06	40	524
100	-	30	221
100	-	50	1160
100	-	60	2520

Ionic strength for all solutions was adjusted to 1.0 using potassium chloride. Wavelength for UV analysis was 242 nm.

Table III- 24: Experimental conditions and observed rate constants for the hydrolysis of *p*-carboxyformanilide in hydrochloric acid solutions.

HCl Conc. (M) × 10^2	**Measured pH**	**Temperature °C**	**k_{obs} hr^{-1}× 10^2**
3.00	1.60	40	68.2
10.0	1.10	40	208
30.0	0.59	40	983
50.0	0.39	40	291
100	0.11	40	1840
100	-	20	340
100	-	30	828
100	-	50	3930
100	-	60	8280

Ionic strength for all solutions was adjusted to 1.0 using potassium chloride. Wavelength for UV kinetic analysis was 269 nm.

Table III- 25: Experimental conditions and observed rate constants for the hydrolysis of *m*-carboxyformanilide in hydrochloric acid solutions.

HCl Conc. **(M) × 10^2**	**Measured pH**	**Temperature** **°C**	**k_{obs}** **hr^{-1}× 10^2**
3.00	1.60	40	28.6
10.0	1.10	40	90.7
30.0	0.59	40	272
50.0	0.40	40	453
100	0.12	40	823
100	-	20	146
100	-	30	360
100	-	50	1800
100	-	60	3870

Ionic strength for all solutions was adjusted to 1.0 using potassium chloride. Wavelength for UV kinetic analysis was 250 nm.

Table III- 26: Experimental conditions and observed rate constants for the hydrolysis of *o*-carboxyformanilide in hydrochloric acid solutions.

HCl Conc. (M) × 10^2	**Measured pH**	**Temperature °C**	**k_{obs} hr^{-1}× 10^2**
3.00	1.59	40	78.8
10.0	1.09	40	261
30.0	0.63	40	787
50.0	0.39	40	1280
100	0.12	40	2470
100	-	20	482
100	-	30	1110
100	-	50	5100
100	-	60	10510

Ionic strength for all solutions was adjusted to 1.0 using potassium chloride. Wavelength for UV kinetic analysis was 250 nm.

Table III- 27: Experimental conditions and observed rate constants for the hydrolysis of *p*-hydroxyformanilide in hydrochloric acid solutions.

HCl Conc. (M) × 10^2	**Measured pH**	**Temperature °C**	**k_{obs} hr^{-1}× 10^2**
30.0	0.54	40	79.4
50.0	0.34	40	143
70.0	-	40	203
85.0	-	40	247
100	0.11	40	288
100	-	30	95.5
100	-	40	254
100	-	50	542
100	-	60	1310

Ionic strength for all solutions was adjusted to 1.0 using potassium chloride. Wavelength for UV kinetic analysis was 246 nm.

Table III- 28: Experimental conditions and observed rate constants for the hydrolysis of *m*-hydroxyformanilide in hydrochloric acid solutions.

HCl Conc. (M) × 10^2	**Measured pH**	**Temperature °C**	**k_{obs} hr^{-1}× 10^2**
30.0	0.59	40	272
50.0	0.38	40	445
100	0.09	40	822
100	-	30	360
100	-	50	1620
100	-	60	3590

Ionic strength for all solutions was adjusted to 1.0 using potassium chloride. Wavelength for UV kinetic analysis was 246 nm.

Table III- 29: Experimental conditions and observed rate constants for the hydrolysis of *o*-hydroxyformanilide in hydrochloric acid solutions.

HCl Conc. **(M) × 10^2**	**Measured pH**	**Temperature** **°C**	**k_{obs}** **hr^{-1}× 10^2**
30.0	0.54	40	272
50.0	0.34	40	445
100	0.30	40	393
100	-	50	806
100	-	60	1870

Stock solutions were prepared in dimethyl sulfoxide. Ionic strength for all solutions was adjusted to 1.0 using potassium chloride. Wavelength for UV kinetic analysis was 284 nm.

Table III- 30: Experimental conditions and observed rate constants for the hydrolysis of *p*-phenylformanilide in hydrochloric acid solutions.

HCl Conc. (M) × 10^2	**Measured pH**	**Temperature °C**	**k_{obs} hr^{-1}× 10^2**
3.00	1.64	40	25.8
10.0	1.13	40	83.5
30.0	0.65	40	240
50.0	0.45	40	379
100	0.18	40	643
100	-	50	1500
100	-	60	3220

Ionic strength for all solutions was adjusted to 1.0 using potassium chloride. Wavelength for UV kinetic analysis was 267 nm.

Table III- 31: Experimental conditions and observed rate constants for the hydrolysis of *o*-phenylformanilide in hydrochloric acid solutions.

HCl Conc. **(M) × 10^2**	**Measured pH**	**Temperature** **°C**	**k_{obs}** **hr^{-1}× 10^2**
3.00	1.61	40	10.8
10.0	1.14	40	34.6
30.0	0.66	40	99.1
50.0	0.45	40	161
100	0.26	40	319
100	-	50	678
100	-	60	1480

Ionic strength for all solutions was adjusted to 1.0 using potassium chloride. Wavelength for UV kinetic analysis was 250 nm.

Table III- 32: Experimental conditions and observed rate constants for the hydrolysis of formanilide in 0.010 M, and 1.00 M hydrochloric acid solutions at different temperatures.

Temperature	**k_{obs}**	
°C	**$hr^{-1} \times 10^2$**	
	0.010 M	1.0 M
20	1.34	86.6
30	2.94	224
40	7.43	727
50	17.6	1400
60	40.0	3350

The ionic strength of the 0.010 M hydrochloric acid solution was adjusted to 1.0 using potassium chloride. Wavelength for UV analysis was 240 nm.

Table III- 33: Experimental conditions and observed rate constants for formanilide degradation in 0.010 M hydrochloric acid at 40 °C.

KCl Added (M)	**Ionic Strength μ**	**k_{obs} $hr^{-1} \times 10^2$**
0.00	0.010	6.36
0.04	0.050	6.10
0.09	0.100	6.19
0.19	0.200	6.48
0.29	0.300	6.42
0.39	0.400	6.63
0.99	1.000	7.43

Ionic strength of the solutions was varied by addition of potassium chloride.

Table III- 34: Experimental conditions and observed rate constants for the hydrolysis of formanilide in 0.010 M hydrochloric acid solutions containing different amounts of organic solvents at 40 °C.

Solvent	**Concentration**	$\mathbf{k_{obs}}$
	% v/v	$\mathbf{hr^{-1} \times 10^{2}}$
Water	-	6.48
Dioxane	25	5.57
Dioxane	50	4.43
Ethanol	25	5.27
Ethanol	50	4.36
Acetone	25	5.04
Acetone	50	3.50

The UV spectra collected as a function of time during degradation of formanilide were inspected for isosbestic points (Figure III-5). The existence of isosbestic points can be used as an indicator for the number of absorbing species in the reaction mixture. An isosbestic point is typically observed when the reaction involves the presence of at two UV absorptive substrates which are inconvertible and have the molar absorptivity at specific wavelengths. The chance of more than two UV absorptive substrates having the same absorptivity at the same points point is remote. Anilinium ion in acidic solutions does not have significant absorbance, and so it was not possible to evaluate isosbestic points in acidic solutions. The spectrum of the degradation product was compared to aniline at the same concentration under the same conditions and was found to be identical using the peak purity software. This concentration-time profile and reaction scheme can then be described as Scheme III-1. UV kinetic analysis was only used if the formanilide reaction followed Scheme III-1 as determined by HPLC. The chemical reaction scheme is shown in Figure III-6.

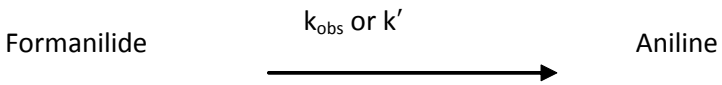

Scheme III- 1

Similar to formanilide, the other substituted formanilides evaluated exhibited the same degradation trend and kinetics, except *m*-methoxyformanilide. The reaction of *m*-methoxyformanilide was followed using HPLC and two peaks were detected corresponding to *m*-methoxyformanilide and m-*m*ethoxyaniline. As shown in Figure III-7, a decrease in the concentration of *m*-methoxyformanilide was observed with the concurrent formation of *m*-methoxyaniline. However, in this case mass balance was not maintained. This pattern was observed over 0.3-0.03 M hydrochloric acid concentrations. The analyte *m*-methoxyaniline was stable in acidic conditions as

determined by UV spectroscopy; hence the total loss in mass was probably due to loss of m-methoxyformanilide to unknown products by a different pathway. To account for the unknown degradation pathway Scheme III-2 was proposed. Under the conditions of the study the loss of *m*-methoxyformanilide occurs by first-order kinetics to form products. Thus the observed first-order rate constant (k_{obs}) for the first-order loss of *m*-methoxyformanilide is a sum of the rate constant (k') for the formation of *m*-methoxyaniline, and the rate constant (k_{unk}) for the formation of the unknown product. The value for k' and k_{unk} was estimated by simultaneously curve fitting the concentration-time profiles for *m*-methoxyformanilide and *m*-methoxyaniline using Winnonlin®. This value was used for the determination of the second-order rate constant for hydrolysis of *m*-methoxyformanilide.

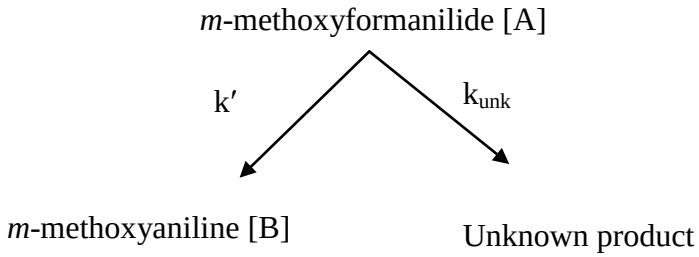

Scheme III- 2

Effect of pH

The logarithms of the deformylation rate constants (k') obtained in the absence of buffers were plotted as a function of pH or H_A to construct pH-rate profiles. For reactions in dilute hydrochloric acid solutions (< 1.0 M HCL) the pH was measured potentiometrically. At high concentrations of hydrochloric acid the conventional pH scale is not applicable. In such solutions the acidity functions (H_0) are used. Several different Hammett acidity functions have been devised based on the indicator series used and the function determined using the most structurally similar indicator molecule is used

Figure III- 1: Representative chromatogram of separation of reaction mixture of formanilide in 0.075 M hydrochloric acid using isocratic method with a C12 HydroRP Phenomenex 4µ 4.6×75 mm column using a mobile phase with 30:70 acetonitrile:water at a flow rate of 0.8 mL/min.

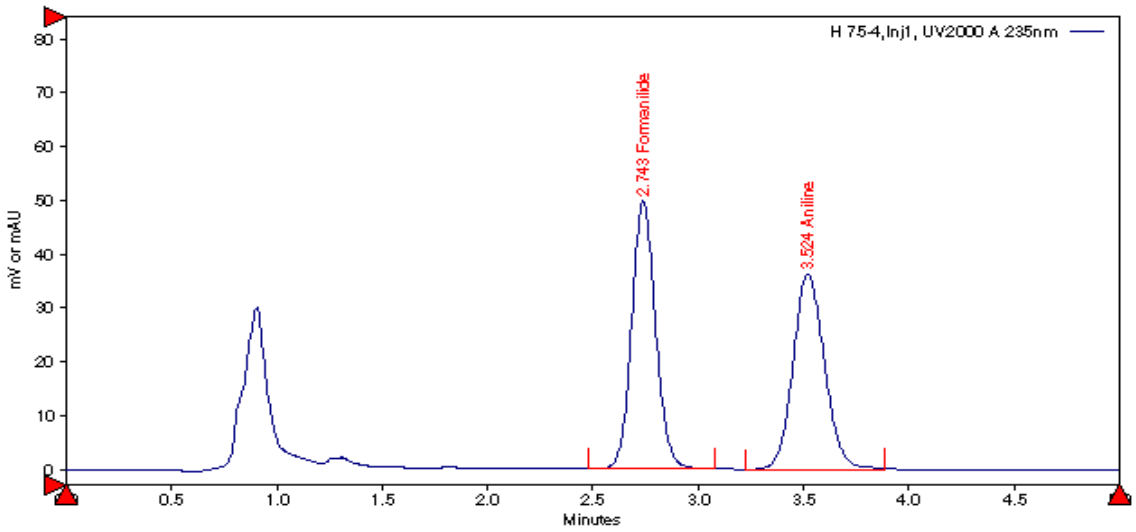

Figure III- 2: Typical HPLC calibration curves for (A) formanilide and (B) aniline.

(A)

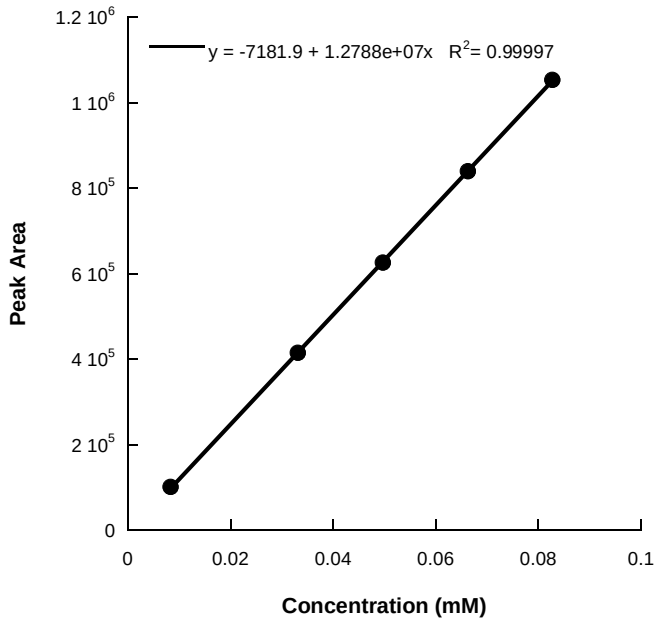

(B)

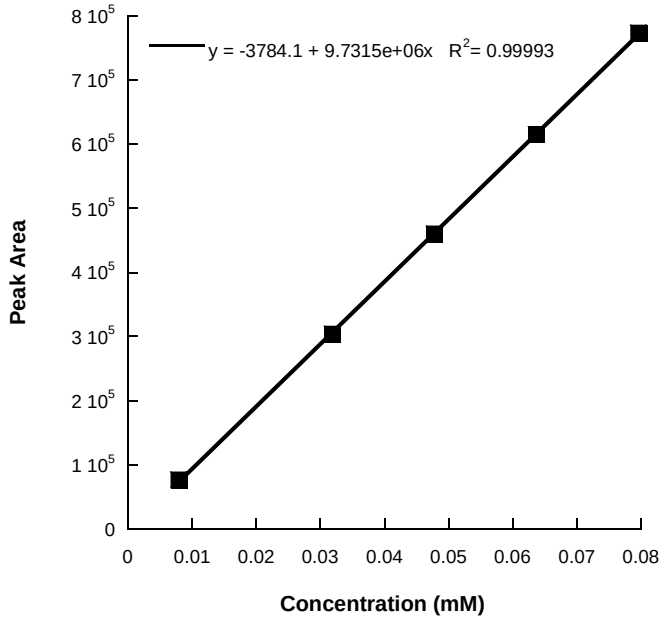

Figure III- 3: Concentration-time profiles for hydrolysis of formanilide in 0.10-0.025 M hydrochloric acid at 1.0 ionic strength and 60 °C. Solid circles (●) represent loss of formanilide, solid squares (■) represent appearance of aniline, and solid triangles (▲) represents mass balance for the reaction. The solid line is a first-order fit for formanilide loss and the broken lines are interpolations.

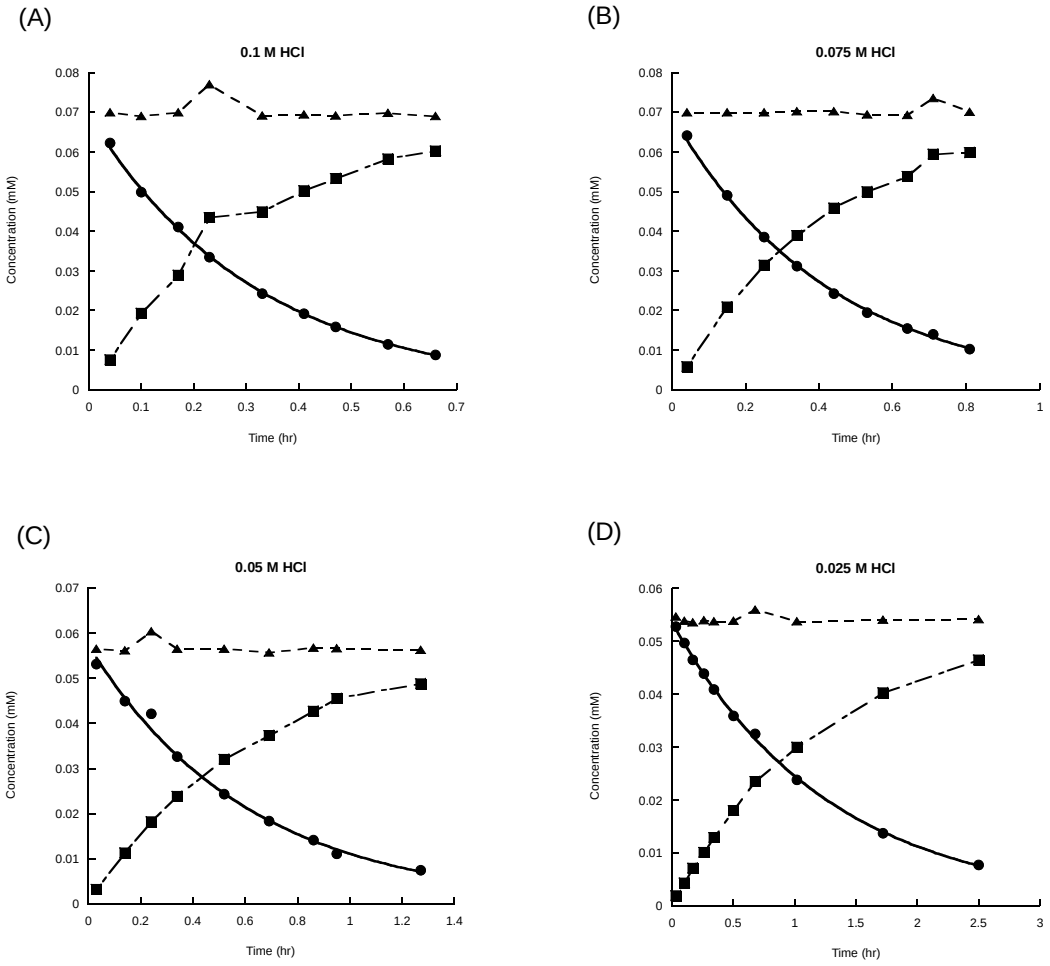

Figure III- 4: Concentration of formanilide versus time at pH 1.09 (♦), pH 1.21 (▲), pH 1.38 (■), and pH 1.68 (●) at 60 °C.

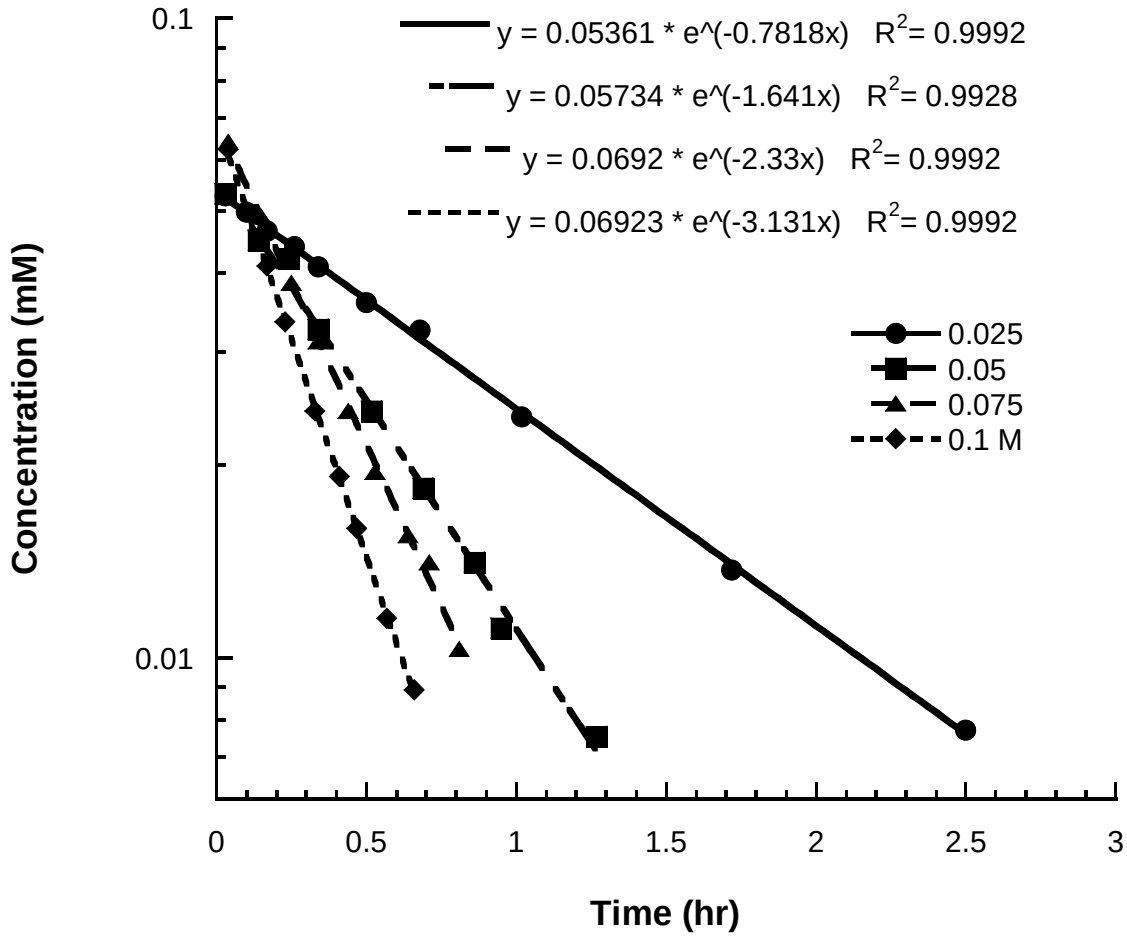

Figure III- 5: Selected UV spectra collected as a function of time for the hydrolysis of formanilide in 1.0 M hydrochloric acid solutions at 60°C. The spectrum with the highest absorbance value is that of the pure formanilide and the spectrum with the least absorbance values correspond to the reaction products.

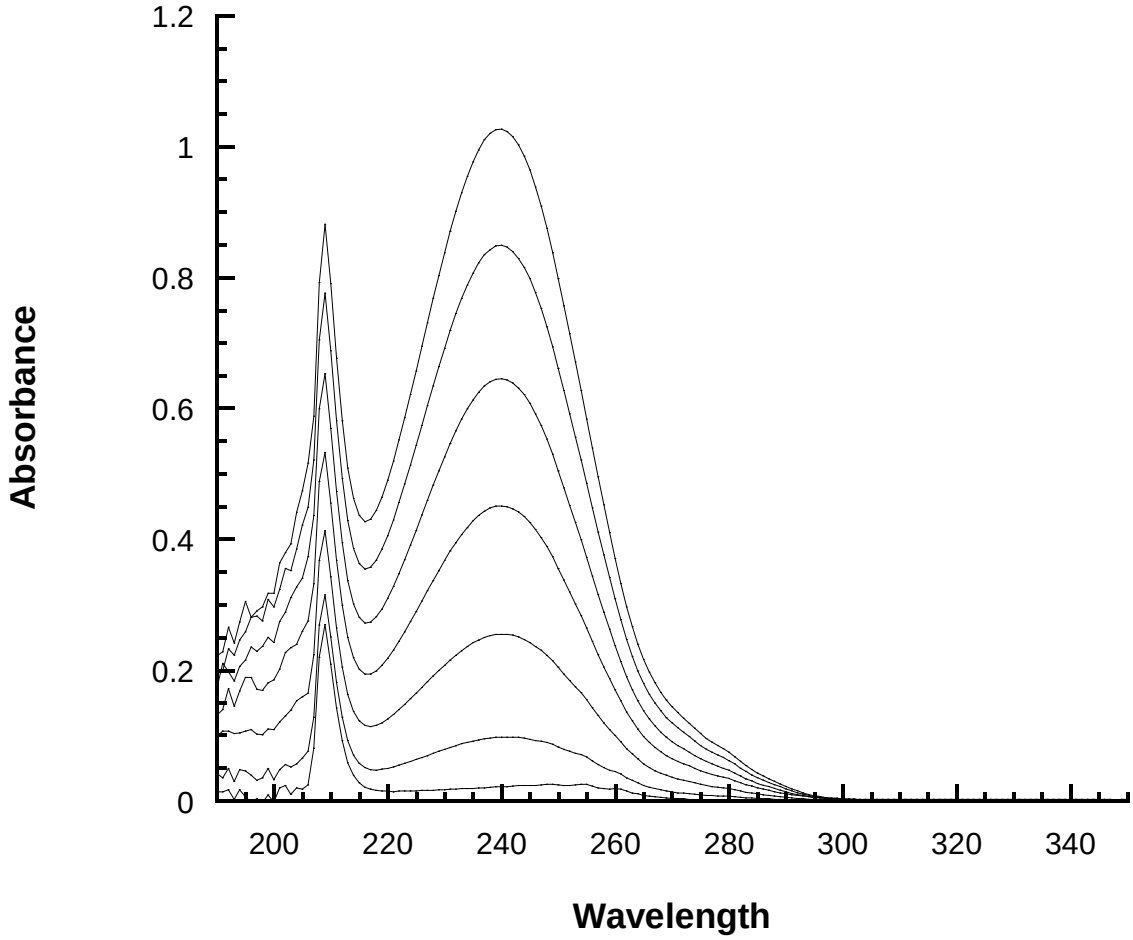

Figure III- 6: Reaction scheme for degradation of substituted formanilides in hydrochloric acid solution.

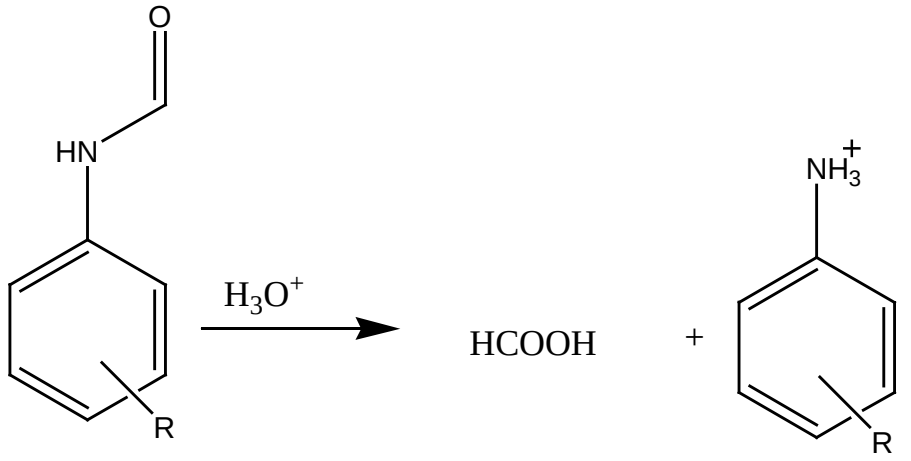

Substituted Formanilide Formic acid Substituted Anilinum ion

Figure III- 7: Concentration-time profile of hydrolysis of *m*-methoxy formanilide in 0.1 M hydrochloric acid at 1.0 ionic strength, and 40 °C. Solid circles (●) represent loss of formanilide; solid squares (■) represent appearance of aniline and solid triangles (▲) represent mass balance for the reaction. The solid lines are fitted using Scheme II-2 and estimates in Table III-22. The broken line is an interpolation.

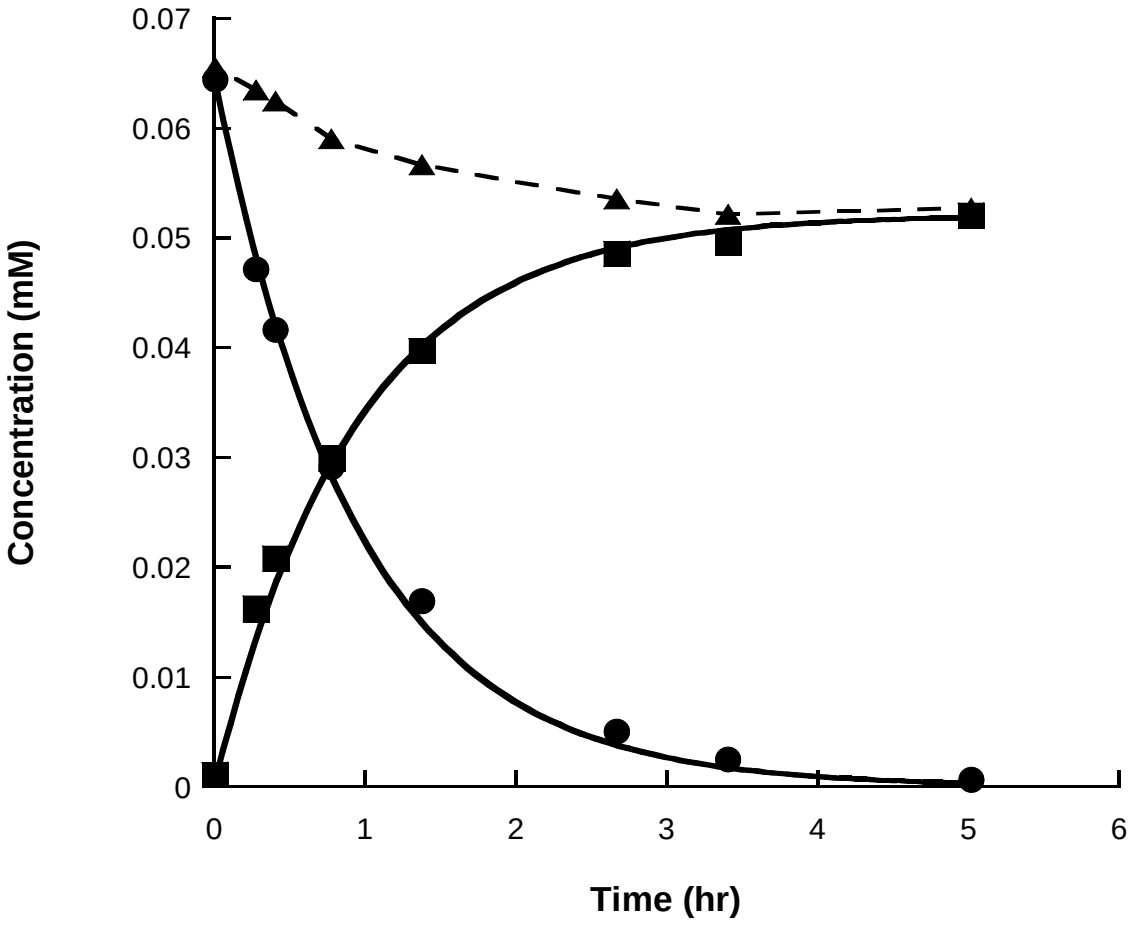

to study the effect of acidity on the reaction rates. The H_A scale which utilizes substituted benzamides as the indicators was used for formanilide since benzamides and formanilides are structurally similar. The H_A values from the literature were tabulated and H_A values corresponding to the concentrations of hydrochloric acid were interpolated and used without temperature corrections.[100] The pH-rate profile for the hydrolysis of formanilide in hydrochloric acid is depicted in Figure III-8. The bell shaped pH-rate profile is typical for amide hydrolysis where the rate increases with increasing acid concentration, reaches a maximum and then decreases.[101] Typical of acidic hydrolysis of amides, a simple pH-rate profile is predicted based on the protonation of the carbonyl oxygen at very low pH ($pK_a < -2.5$) and either specific acid catalyzed hydrolysis of the deprotonated substrate or the kinetically equivalent pathway involving solvent attack on the protonated substrate. This pH dependent behavior predicts a simple downward bend wherein the observed rate constant is pH independent in the pH regions below the substrate pK_a and has a slope of -1 in the pH regions above the pK_a. The unexpected decrease in the observed rate constant in concentrated acid (below the pK_a) is typically attributed to a decrease in water activity.[101]

The downward bend can then be described by two possible kinetically equivalent rate laws (Scheme III-3, and Scheme III-4) in which the composition of the rate-determining transition state is composed of substrate (S) and a proton (hydronium ion). In the reaction pathway described by Scheme III-3, the unprotonated form of the substrate degrades by specific acid catalysis whereas in Scheme III-4 the protonated substrate is subject to solvolysis to form products (P). Water may be involved in the reaction; however it does not appear in the rate law. The rate law for the Scheme III-3 is given by Equation III-3, and the rate law for Scheme III-4 is given by Equation III-6. The terms in these equations are defined as follows: k_1 is the second-order rate constant for specific acid catalysis; f_S is the fraction of unionized species; $[H^+]$ is the activity of the hydronium ion; S_T stands for the total substrate concentration; K_a is the ionization

constant; k_s is the second-order rate constant for solvolytic hydrolysis of the ionized substrate; and f_{SH} is the fraction of ionized species. Scheme III-3 predicts a single step reaction while Scheme III-4 predicts two steps.

$$SH^+ \underset{}{\overset{K_a}{\rightleftharpoons}} H^+ + S \xrightarrow{k_1[H^+]} P$$

Scheme III- 3

$$f_S = \frac{K_a}{K_a + [H^+]} \qquad \text{Equation III-1}$$

$$rate = k_1[H^+][S] = k_1 f_S S_{Total} \qquad \text{Equation III-2}$$

$$k = k_1[H^+] f_S = k_1[H^+] \frac{K_a}{K_a + [H^+]} \qquad \text{Equation III-3}$$

$$H^+ + S \underset{}{\overset{K_a}{\rightleftharpoons}} SH^+ \xrightarrow{k_S} \text{Products}$$

Scheme III- 4

$$f_{SH} = \frac{[H^+]}{K_a + [H^+]} \qquad \text{Equation III-4}$$

$$rate = k_S[SH^+] = k_S f_{SH} S_{Total} \qquad \text{Equation III-5}$$

$$k = k_S f_{SH} = k_S \frac{[H^+]}{K_a + [H^+]} \qquad \text{Equation III-6}$$

In dilute hydrochloric acid concentrations (1.0-0.010 M) formanilide (pK_{BH+} = -2.71 at 25 °C) is largely unionized.[30] Equations III-3 and III-6 reduce to Equation III-7. A second-order rate constant k_H can then be defined (Equation III-8) and substituted in

Equation III-7 to get Equation III-9. The apparent second-order rate constants for specific acid hydrolysis (k_H) were estimated by linear regression of plots of the k versus hydronium ion concentration ($[H^+]$). The value of the second-order rate constant (k_H) was 7.39 $M^{-1}hr^{-1}$ for formanilide (Figure III-9).

$$k = k_1[H^+] = k_S \frac{[H^+]}{K_a} \qquad \text{Equation III-7}$$

$$k_H = k_1 = \frac{k_S}{K_a} \qquad \text{Equation III-8}$$

$$k' = k_H[H^+] \qquad \text{Equation III-9}$$

The pH-rate profiles for the substituted formanilides were similar to formanilide and treated in analogous manner. The second-order rate constants (k_H) for the reactions were calculated by linear least-squares fitting of k as a function of hydrochloric acid concentrations. The second-order rate constants (k_H) were not constant and varied reflecting the different reactivities of the substituents. The results are tabulated in Table III-35.

Effect of Ionic Strength

Ionic strength (μ) studies were carried out by measuring the observed rate constant for formanilide in 0.010 M hydrochloric acid solutions at 40 °C using different ionic strength values of 0.01 to 0.40 by varying the concentration of potassium chloride. The activity coefficients (γ) were approximated using the Guntelberg equation (Equation III-10) where z_i represents the charges on the reactants. A plot of the logarithm of the observed rate constant versus substrate activity coefficient (Figure III-10), which shows a linear correlation with a slope near zero (0.076), failed to demonstrate a significant ionic strength dependence which is consistent with the rate law.[48]

$$\log \gamma = \frac{2z_i^2 \sqrt{\mu}}{1+\sqrt{\mu}}$$ Equation III-10

Binary Solvent System Studies

Degradation of formanilide in binary mixtures of aqueous organic solvents was studied using three organic solvents that were chosen to provide a range of dielectric constants and hydrogen bonding characteristics. The dielectric constants and classifications for the solvents are as follows: water (78.3, protic), ethanol (24.55, protic), acetone (20.56, dipolar aprotic), and dioxane (2.21, aprotic).[102] Kinetic studies were carried out in 0.010 M hydrochloric acid at 40 °C at different concentrations of organic solvents, and rate constants (k) were calculated for the degradation of formanilide. The k values were plotted as the function of the % v/v organic contents (Figure III-11).

Effect of Temperature

The rate of degradation of formanilide increased with temperature. The rate constants (k) were calculated from concentration-time profiles (HPLC) and from the UV studies by directly fitting UV absorbance values as a function of time. Arrhenius plots were generated using these rate constants (Figure III-12). Activation energies (E_a) and were estimated frequency factors (A) from the slopes and intercepts of the linear Arrhenius plots. The activation enthalpy and entropy changes for formanilide were calculated using Equations III-12 and III-13 over the temperature range and reported in Table III-36. Standard errors were also calculated for the estimated parameters.

$$\ln k = \ln A - \frac{E_a}{R}\frac{1}{T}$$ Equation III-11

$$\Delta H^{\ddagger} = E_a - RT_{mean}$$ Equation III-12

$$\Delta S^{\ddagger} = R\ln A - R\ln\left(\frac{kT_{mean}}{h}\right) - R$$ Equation III-13

Where, T is the absolute temperature (K), T_{mean} is the absolute temperature (K) in the middle of the experimental temperature range, R is the ideal gas constant (1.987 cal^{-1} K^{-1} mol^{-1}), k is the observed rate constant (s^{-1}), **k** is the Boltzmann constant (1.38×10^{-16} erg K^{-1}), and h is Planck's constant (6.626×10^{-27} erg s).

All of the substituted formanilides showed linear Arrhenius plots. The energies of activation, frequency factors, entropies of activation, and enthalpies of activation were calculated and are presented in Table III-37.

Discussion

The pH-rate profiles for formanilides have been described by Schemes III-3 and III-4. The rate laws indicated the presence of substrate and a proton in the rate-determining transition-state. Formanilide hydrolysis in acidic solutions does not show an ionic strength effect which is in contrast to the results from similar studies carried out by Bergstrand for hydrolysis of formanilide at 55 °C, where a positive ionic strength effect was observed.[32] This discrepancy could be due to the very high ionic strengths of 3.0 and 0.5 used by these authors at which secondary salt effects could affect the results. The absence of ionic strength effect matches the expectations of an uncharged substrate and proton involved in the rate limiting transition-state.[48]

The binary solvent studies indicate a complex relationship between the organic solvent (type and content) with the reaction rate constants (Figure III-11). All the organic solvents have lower dielectric constants than water; hence, increasing the organic content decreases the dielectric constants of the binary solutions. In addition to decreasing the dielectric constant of the system, addition of organic solvent alters several other parameters including the ionization constants for the reactants, the effective charge on the reactants and the activity of the reactants. The rate law for acidic hydrolysis of formanilide predicts that the rate-determining transition-state consists of the substrate and hydronium ion; hence the transition-state is polar. Therefore according to the Hughes

Figure III- 8: pH-rate profile for formanilide hydrolysis at 40 °C in hydrochloric acid solutions.

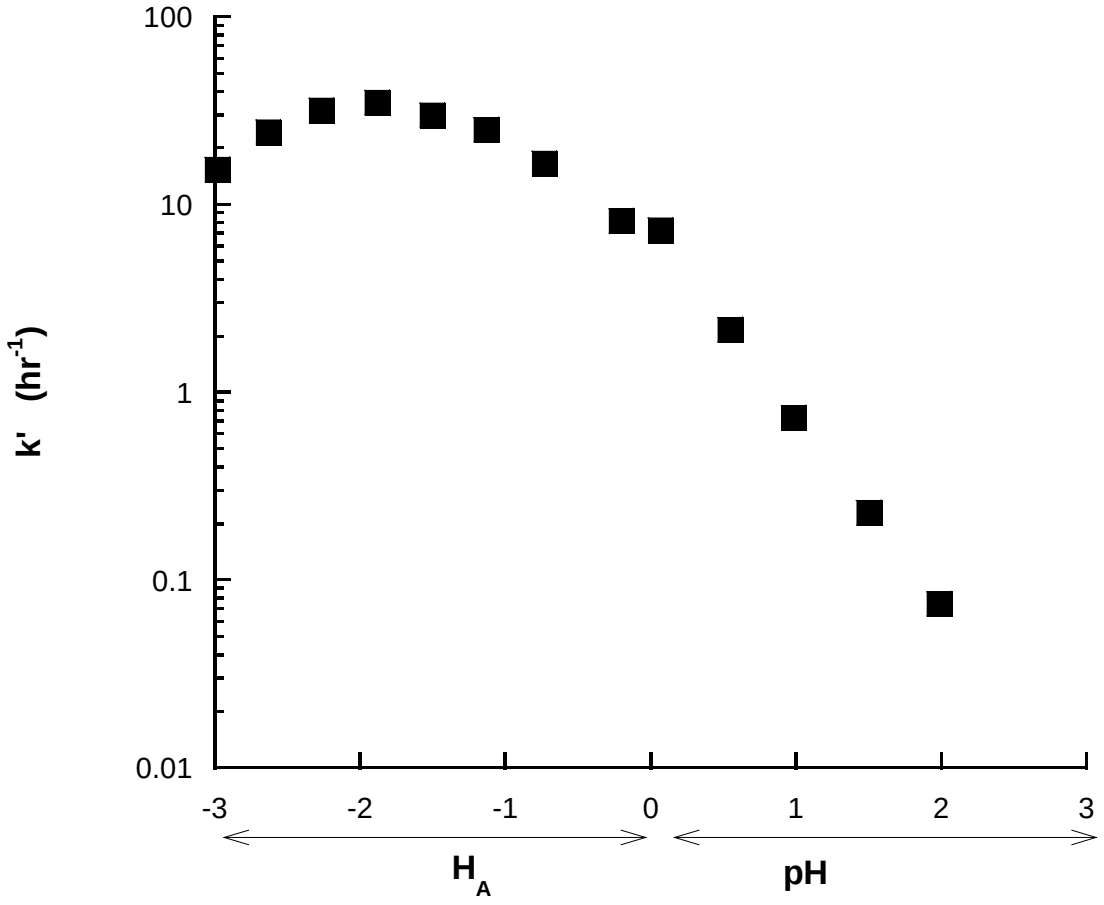

Figure III- 9: Pseudo-first-order rate constant (k′, hr^{-1}) versus hydrochloric acid concentration in the pH region of 0.07 to 1.99. The slope gives a specific acid catalytic rate constant (k_H) of 7.39 M^{-1} hr^{-1}.

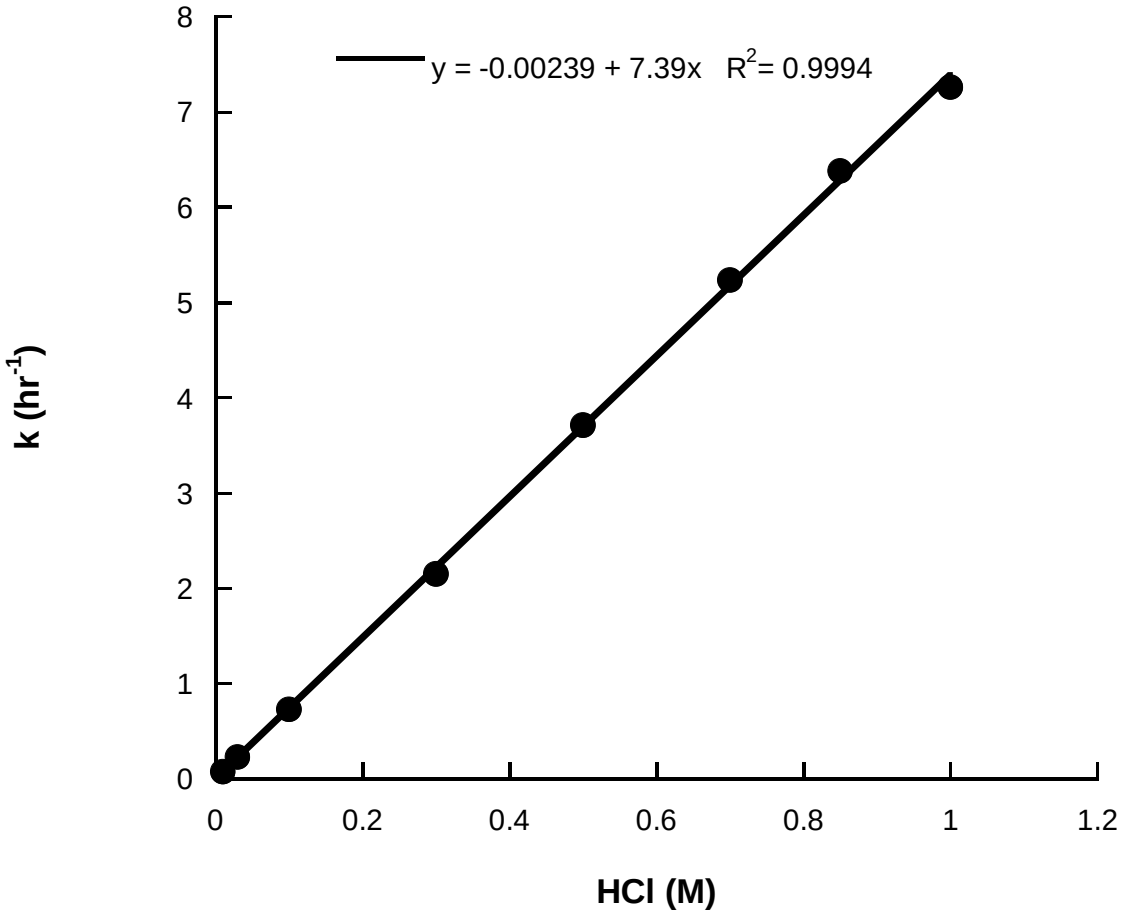

Table III- 35: Second-order rate constants for acid catalyzed hydrolysis of substituted formanilides at 40 °C in the range of 0.01-1.0 M hydrochloric acid solutions.

Substituent	**k_H ± S.E. (M^{-1} hr^{-1})**	**n**	**Substituent**	**k_H ± S.E. (M^{-1} hr^{-1})**	**n**
H	7.39 ± 0.08	8	*p*-isoC$_3$H$_7$	5.42 ± 0.10	4
p-CH$_3$	5.06 ± 0.11	7	*m*-isoC$_3$H$_7$	6.05 ± 0.13	5
m-CH$_3$	6.58 ± 0.18	6	*o*-isoC$_3$H$_7$	1.39 ± 0.02	5
o-CH$_3$	2.57 ± 0.04	8	*p*-OCH$_3$	2.95 ± 0.03	5
p-Cl	7.04 ± 0.07	7	*m*-OCH$_3$	8.59 ± 0.03	3
m-Cl	9.65 ± 0.02	8	*o*-OCH$_3$	5.23 ± 0.21	5
o-Cl	7.24 ± 0.03	5	*p*-COOH	18.2 ± 0.5	5
p-NO$_2$	27.3 ± 0.7	6	*m*-COOH	8.21 ± 0.25	5
m-NO$_2$	11.3 ± 0.2	6	*o*-COOH	24.6 ± 0.3	5
o-NO$_2$	24.9 ± 0.2	6	*p*-OH	2.67 ± 0.08	4
p-Br	8.32 ± 0.19	6	*m*-OH	7.80 ± 0.02	3
m-Br	10.8 ± 0.1	3	*o*-OH	3.81 ± 0.03	3
o-Br	2.57 ± 0.04	8	*p*-Phenyl	7.53 ± 0.18	4
p-C$_2$H$_5$	4.60 ± 0.10	5	*o*-Phenyl	3.17 ± 0.02	5
m-C$_2$H$_5$	6.21 ± 0.18	6			
o-C$_2$H$_5$	2.07 ± 0.01	5			

Figure III- 10: Plot of log of the rate constants (k) against the substrate activity coefficient of the medium. Rate constants were determined in 0.01 M hydrochloric acid at 40 °C. Ionic strength was varied using potassium chloride.

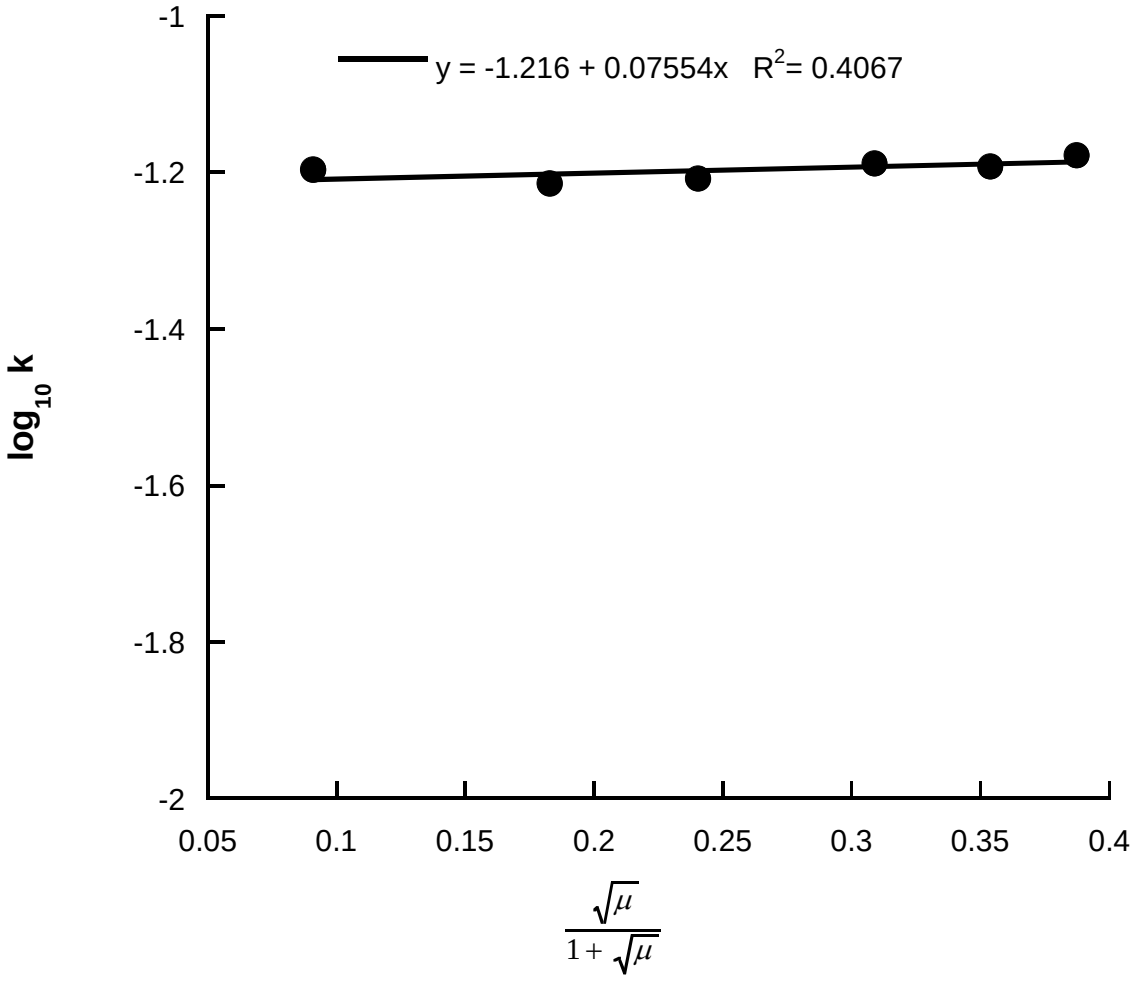

Figure III- 11: Effect of increasing organic solvent concentrations on the rate constant for hydrolysis of formanilide in aqueous organic solutions containing 0.010 M hydrochloric acid solutions at 40 °C. The lines are interpolated lines.

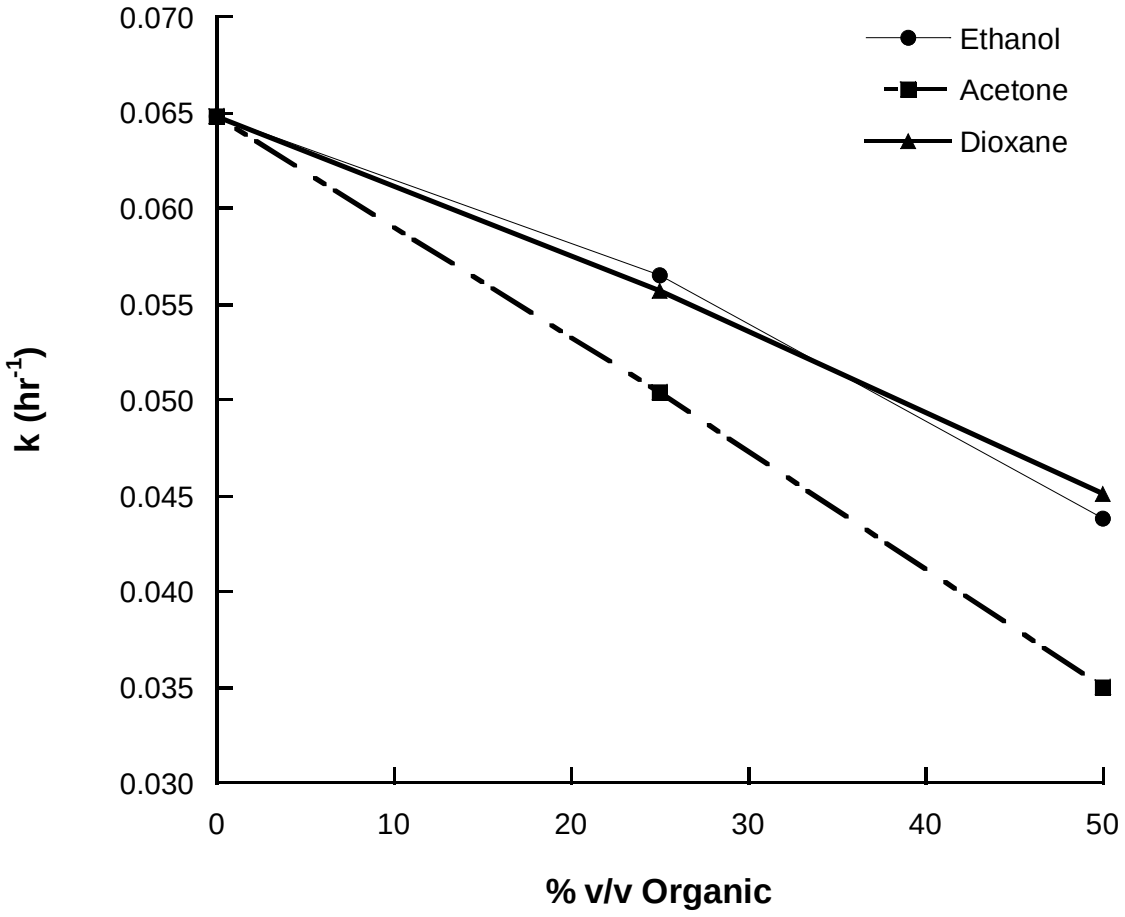

Figure III- 12: Arrhenius plot for the temperature dependence of formanilide hydrolysis in 0.010 M and 1.00 M hydrochloric acid solutions.

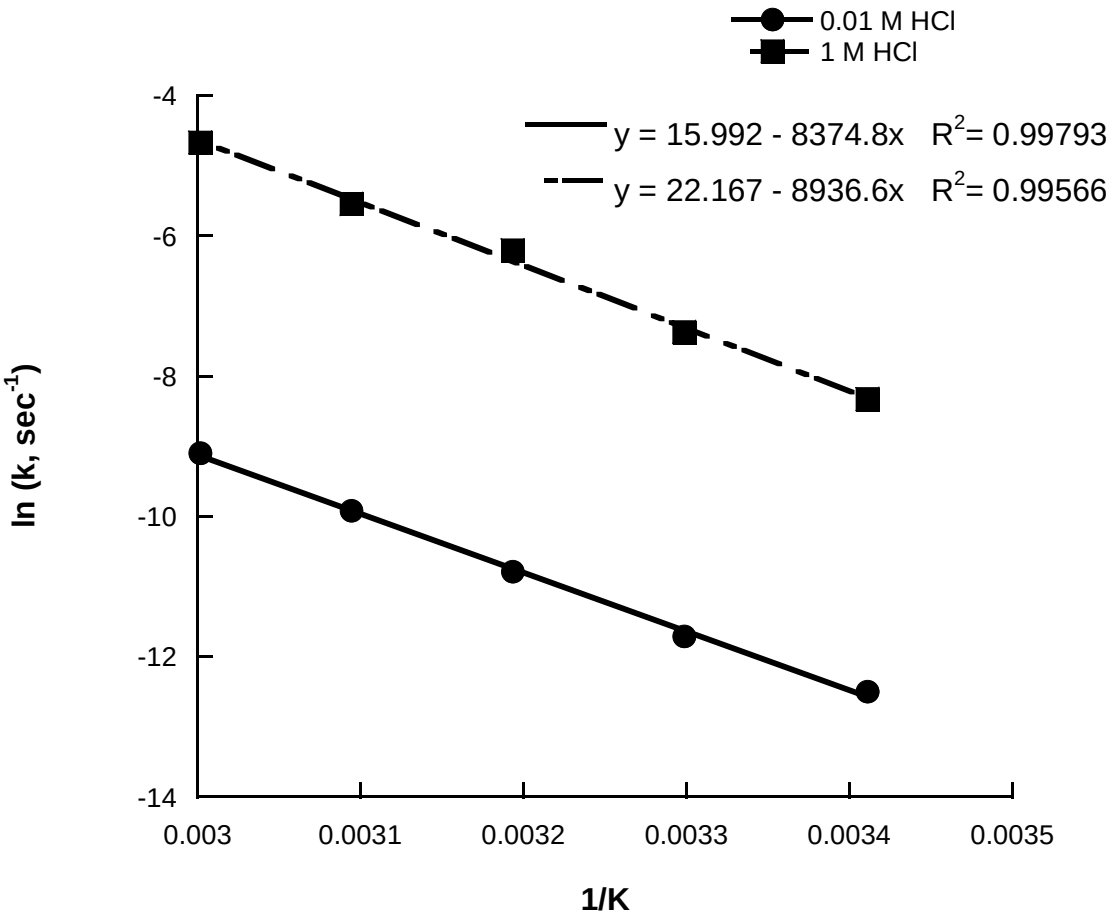

Table III- 36: Activation parameters for degradation of formanilide in 0.010 M HCl and 1.0 M HCl solutions. The ionic strength of 0.010 M hydrochloric acid solution was adjusted to 1.0 using potassium chloride.

	0.010 M HCl	**1.0 M HCl**
ln A ± S.E	16.0± 0.7	22.2± 1.1
E_a ± S.E (kJ mol^{-1})	69.9 ± 1.8	74.5 ± 2.8
$\Delta H^{\ddagger}$ ± S.E (kJ mol^{-1})	67.0 ± 1.8	71.7 ± 2.8
$\Delta S^{\ddagger}$ ± S.E (J $mol^{-1}K^{-1}$)	121 ± 6	69.3 ± 9.1

Table III- 37: Activation parameters for the hydrolysis of formanilides in 1.0 M hydrochloric acid.

Substituent	**ln A ± S.E**	**E_a ± S.E (kJ mol^{-1})**	**Δ $H^{‡}$ ± S.E (kJ mol^{-1})**	**-Δ $S^{‡}$ ± S.E (J mol^{-1} K^{-1})**
H	22.2 ± 1.1	74.5 ± 2.8	71.7 ± 2.8	69.3 ± 9.1
m-Br	20.0 ± 0.3	68.0 ± 0.8	65.1 ± 0.8	87.1 ± 2.7
m-COOH	19.4 ± 0.1	66.5 ± 0.3	63.6 ± 0.3	92.6 ± 1.0
m-Cl	20.0 ± 0.4	67.8 ± 0.9	65.0 ± 0.9	87.4 ± 3.0
m-C_2H_5	18.9 ± 0.4	65.8 ± 1.2	63.0 ± 1.2	96.8 ± 3.7
m-OH	18.3 ± 0.7	63.8 ± 1.8	61.0 ± 1.8	101 ± 6
m-isoC_3H_7	20.1 ± 0.2	69.2 ± 0.5	66.4 ± 0.5	86.4 ± 1.6
m-CH_3	20.2 ± 0.4	69.4 ± 1.0	66.5 ± 1.0	85.8 ± 3.3
m-NO_2	19.9 ± 0.3	67.3 ± 0.9	64.4 ± 0.9	87.9 ± 2.8
o-Br	19.0 ± 0.4	66.3 ± 1.1	63.4 ± 1.1	95.5 ± 3.4
o-COOH	19.0 ± 0.1	62.7 ± 0.3	59.9 ± 0.3	95.6 ± 1.0
o-Cl	19.7 ± 0.3	67.8 ± 0.8	65.0 ± 0.8	89.7 ± 2.6
o-C_2H_5	21.5 ± 0.9	76.1 ± 2.4	73.1 ± 2.4	75.4 ± 7.3
o-OH	19.1 ± 1.6	67.7 ± 4.3	64.8 ± 4.3	95.3 ± 13.2
o-isoC_3H_7	20.4 ± 1.2	74.0 ± 3.1	71.4 ± 3.1	83.9 ± 9.7
o-OCH_3	19.5 ± 0.1	68.1 ± 0.4	65.3 ± 0.8	91.1 ± 2.6
o-CH_3	19.7 ± 0.3	70.8 ± 0.9	68.0 ± 0.9	89.7 ± 2.8
o-NO_2	19.5 ± 0.3	64.0 ± 0.7	61.2 ± 0.7	91.8 ± 2.2
o-C_6H_5	18.5 ± 0.7	66.7 ± 1.8	63.8 ± 1.8	100 ± 6
p-Br	20.7 ± 0.2	70.2 ± 0.6	67.3 ± 0.6	81.9 ± 2.0

Table III-37 -Continued

p-COOH	19.5 ± 0.1	64.7 ± 0.3	61.9 ± 0.3	91.4 ± 1.1
p-Cl	20.3 ± 0.4	69.5 ± 1.1	66.7 ± 1.1	84.6 ± 3.5
p-C_2H_5	19.9 ± 0.2	69.5 ± 0.5	66.6 ± 0.5	87.9 ±1.7
p-OH	20.5 ± 0.8	72.5 ± 2.0	68.4 ± 4.3	87.6 ± 13.4
p-isoC_3H_7	20.5 ± 0.4	70.9 ± 1.0	68.0 ± 1.0	83.1 ± 3.2
p-OCH_3	19.9 ± 0.6	70.6 ± 1.6	67.7 ± 1.6	88.3 ± 4.9
p-CH_3	19.8 ± 0.2	69.4 ± 0.5	66.5 ± 0.5	88.7 ± 1.6
p-NO_2	19.3 ± 0.3	63.2 ± 0.7	60.3 ± 0.7	93.5 ± 2.1
p-C_6H_5	21.7 ± 0.7	73.3 ± 1.8	70.4 ± 1.8	73.6 ± 5.6

Ingold rule, it was expected that the rate of the reaction should decrease with the decrease in the dielectric constant. Binary solvent systems containing ethanol, acetone, and dioxane all showed a linear decrease as a function of the organic solvent content. These results are consistent with a mechanism where the transition-state is charged. The lowered dielectric constant could destabilize the transition-state and reduce the rate of reaction. The reaction mechanism may also have water molecules involved in the rate-determining transition-state even though they do not appear in the rate law. Increasing the organic content will lead to a decrease in the activity of water which could also lead to decrease in the overall rate of the reaction. However, the decreases in the rates were not proportional to the dielectric constants of the solvent mixtures. Based on the dielectric constants the expected rank order of rate constants was ethanol > acetone> dioxane; however the rate constants showed a rank order of dioxane > ethanol > acetone. This behavior could be due to several factors including specific solvation and specific interaction effects of the solvent on the substrate, intermediates, and transition-states of the reactions.[50] Since the reaction occurred at high organic content, mechanisms that require solvents with high ionizing powers, i.e. unimolecular acid catalyzed acyl oxygen cleavage ($A_{AC}1$), appear to be inconsistent with the results obtained.

Temperature studies were carried out on formanilide in 0.010 M and 1.0 M hydrochloric acid solutions and the results are tabulated in Table III-36. The activation energies for the hydrolysis of formanilide at 1.0 M hydrochloric acid and 0.010 M hydrochloric acid were 74.5 kJ mol^{-1} and 69.9 kJ mol^{-1}, respectively. The similarity of the values is consistent with a constant mechanism over this range of hydrochloric acid concentrations. The activation energies values in the range of 41-125 kJ mol^{-1} are expected for most hydrolysis reactions.[45] The enthalpies of activation ($\Delta H^{\ddagger}$) were positive and the entropies of activation ($\Delta S^{\ddagger}$) were negative. The $\Delta S^{\ddagger}$ values indicate an associative process where the formation of the transition-state leads to a decrease in the disorder of the system. The activation enthalpy and activation entropy values are similar

to the values obtained for the acidic hydrolysis of ethanoate esters ($\Delta H^{\ddagger}$ = 75 kJ mol^{-1}, $\Delta S^{\ddagger}$ = -105 kJ $K^{-1}mol^{-1}$) which degrade via the $A_{AC}2$ mechanism.[46] Temperature studies for formanilides carried out on *para*, *meta*, and *ortho* substituted formanilides gave activation energies in the range of 76.1 kJ mol^{-1} -63.2 kJ mol^{-1}, within the range expected for hydrolysis reactions (Table III-37).

The variations in second-order rate constants for hydrolysis of substituted formanilides reflect the different contributions of the substituent on the rate constant. Substituents in the *meta* position are capable of inductive effects while the *para* substituents are capable of both inductive and resonance interactions.

Second-order rate constants for *para* and *meta* substituted formanilides were used to generate Hammett plots. Under the conditions of the study all the formanilides existed as unionized substrates and the corresponding substituent constants were used (Table III-38). A plot of the logarithm of second-order rate constants (k_H) against Hammett substituent constants (σ) is shown in Figure III-13. For *meta* substituted formanilides the substituents capable of withdrawing electrons (e.g. nitro-, chloro-, bromo-, hydroxyl-, methoxy-, and carboxyl-) displayed an increase in rate constant with increasing electronegativity of the substituent, while electron donating substituents (e.g.. methyl-, isopropyl-, -phenyl and ethyl-) displayed a decrease with increasing electron donating capability of the substituent. Similarly for *para* substituents, electronegative substituents (e.g. chloro- and bromo-) exhibited an increase in the rate constant while the electron donating groups (e.g. methyl-, ethyl-, isopropyl-, phenyl-, methoxy-, and hydroxyl-) showed a decrease. These two types of substituents appeared to fall on two separate lines which intersect at formanilide. The slope for the line encompassing the electron donating groups has a slope of 1.31 while the slope of the line encompassing the electron withdrawing groups is 0.33. Strongly electron withdrawing substituents capable of resonance interactions (*p*-nitro and *p*-carboxyl) displayed positive deviation from the expected rates.

Since the Hammett substituent constants (σ) were developed from benzoic acid ionization, these constants are more reflective of inductive effects. Hence nonlinearity using Hammett substituent constants indicate that both inductive and resonance effects are significant. Hammett plots were then generated using electrophilic substitution constants (σ^+). The σ^+ scale is used in reactions that occur with the development of an electron deficiency, such as aromatic electrophilic substitutions.[56] The σ^+ values are present for most of the para substituents and some of the meta substituents. If, however, a the σ^+_m value was unavailable the σ_m value was substituted. Figure III-14 is a plot of the log of the second-order rate constants against the electrophilic substituent constants. The Hammett plot for *meta* and *para* substituents showed that all the *meta* and most of the *para* substituents fell on a single straight line.

However, the *p*-nitro, *p*-carboxyl, and *p*-phenyl formanilides deviated significantly from the linear relationships observed in the Hammett plot using σ^+ values. The *p*-nitro and *p*-carboxyl groups are capable of resonance effects coupled with strong electron withdrawing inductive effects. This ability to withdraw electrons through resonance leads to an increase in the electron withdrawing capability of these substituents above the values seen in benzoic acid ionizations. To account for this increased electron withdrawing ability the enhanced sigma constants (σ^-) were used. These values are applied primarily to electron withdrawing groups in reactions aided by low electron density at the reaction site.[61] The data point for the *p*-phenyl substituent deviated significantly from the correlation line using the σ^+ value. Phenyl rings in the para position are capable of resonance interactions only if the phenyl group is planar to the formanilide benzene group. However, if the rings are not planar then the phenyl substituent can interact only through inductive effects. A better correlation was achieved if the σ value for the *para* phenyl substituent is used indicating that the phenyl ring is not planar. Substituting the appropriate σ values, a Hammett plot with selected sigma values (σ^+, σ or σ^-) for the *para* and *meta* substituents resulted in the LFER relationship

displayed in Figure III-15. This plot was linear with a slope (ρ) of 0.457 and an correlation coefficient (R^2) value of 0.957. The intercept was 0.843 which corresponded well to the value for the unsubstituted formanilide (0.869). The value of ρ is positive and indicates that the reaction is accelerated by electron withdrawing groups. The value of ρ is a composite value and corresponds well to the ρ value published for the acidic hydrolysis of acetanilide (ρ = 0.293, 50% ethanol, 70 °C).[103]

The increase in the linearity of the Hammett plot using σ+ indicates that one of the steps in the reaction mechanism is accelerated by electron donating groups. While correlation with the σ^- suggests that another step in the reaction mechanism is accelerated by electron withdrawing groups. Thus the Hammett plots for the reaction are consistent with a mechanism involving at least two steps with opposing susceptibilities to electronic and resonance effects. These results are consistent with the rate law corresponding to Scheme III-4 which consists of two steps.

This interpretation is consistent with the work of Kavalek and Sterba for the hydrolysis of formanilides at 25 °C in hydrochloric acid solutions. [30] In these studies Hammett plots obtained at very high hydronium ion concentrations (H_A = -3.2) was linear, however at lower strengths (H_A = 0) the plots were nonlinear. The authors had explained these results by postulating a two step reaction mechanism; (1) protonation of the carbonyl oxygen and (2) rate determining attack of water on the carbonyl carbon. They proposed that at high hydronium concentration the first step (ionization of the carbonyl oxygen) was not kinetically important since most of the substrate is ionized and thus overall ρ (1.75) was a function of the second step (water attack), which is influenced by resonance effects. At lower acid concentrations the first step becomes kinetically important since fraction ionized of the substrate is significantly reduced and the ρ is a function of both the steps. Since the ionization of formanilides is controlled mainly by inductive effects (ρ_{Ka} = -0.48) the overall ρ becomes a function of both resonance and inductive effects. This leads to nonlinearity in the Hammett plot due to incomplete

cancellation of substituent effects on the two steps of the reaction in which the second step is rate-determining.[104] The results from this study agree with their explanation and the existence of a two step reaction.

Substituent effects can also be reflected in activation entropies and enthalpies of the reaction. If the activation entropies are linearly correlated with enthalpies for a series of substituted reactive analogs then the result is an enthalpy-entropy relationship. The enthalpy –entropy plots can be generated either by using E_a and lnA or by using activation parameters $\Delta H^{\ddagger}$ and $\Delta S^{\ddagger}$. In both cases the same information will be evaluated. An activation enthalpy-entropy compensation plot using the activation parameters is shown in Figure III-16 where the error bars represent the standard errors for the measurement. Since both $\Delta H^{\ddagger}$ and $\Delta S^{\ddagger}$ are evaluated from the same Arrhenius plot the parameters are highly correlated and the interpretation has to be carried out carefully since there is no apparent simple correlation.

However, if the substituents are classified in to three groups a clearer picture emerges (Figure III-17). The first group contains substituents capable of mainly inductive effects which include the *meta* substituted formanilides and *p*-phenylformanilide. The second group consists of substituents that show strong electron withdrawing capabilities through resonance (-R effects) and include the *p*-carboxyl and *p*-nitro substituents. The third group consists of substituents that show strong electron donating capabilities through resonance (+R) and include the rest of the *para* substituted formanilides. It was observed that the substituents showing the inductive effects were dispersed over the entire range and showed a good linear correlation (R^2 =0.974) with a slope (β) of 0.334. This indicates that these substituents have a common interaction mechanism. A single interaction mechanism is defined as one in which a single property (polarizability, size, charge, group dipole moment) affects the free energy of the system between the substituent and the reaction site. Several interaction mechanisms could be responsible for the effect of substitution on the rate of a reaction.[105] The slope is the

compensation temperature and corresponds to a temperature of 61.6 ± 17.2 °C. At the compensation temperature, the differences in reactivities due to free energy changes become negligible and the substituent effects are muted. The compensation temperature for these substituents is very close to the reaction temperature and this could account for the small values for the Hammett reaction constant. This is a very important since most of the kinetic studies on anilides have been carried out in experimentally accessible range between 25 to 100 °C and hence the substituent effects determined could have been underestimated.

The substituents capable of donating electrons through resonance (+R) are clustered in the center of the plot above the correlation line for the substituents with inductive effects which indicate they degrade slower than the substituents capable of inductive effect. Similarly the substituents capable of electron withdrawing effects (-R) show a negative deviation which indicate they undergo hydrolysis rapidly. This behavior for the +R and –R substituents suggests that several interaction mechanisms are involved in the hydrolysis for these substituents and these change with the electronic capabilities of the substituents. These results are in agreement with the results from the Hammett plot

A special case of enthalpy-entropy relationship is termed an isokinetic relationship, wherein the Arrhenius or van't Hoff lines intersect at a single point- the isokinetic temperature. The presence of an isokinetic relationship indicates that the interaction mechanism changes linearly with the substituent.[68] The presence of an isokinetic effect for substituted formanilides was evaluated by extrapolating the Arrhenius relationships over the temperature range (20 to 60 °C) backward to observe a common intersection. Figure III-18 shows Arrhenius extrapolations for *para* and *meta* substituted formanilides using their Arrhenius plots. No intersection point was observed. The absence of an isokinetic relationship is consistent with a complex rate law.[67]

The results for the pH-rate profile, ionic strength studies, temperature studies, and the Hammett plots can be summarized as follows: (1) the rate law and ionic strength

studies indicate a rate limiting transition-state composed of an unionized substrate and a proton; (2) the temperature studies for unsubstituted formanilide point to the formation of the transition-state by an association process; (3) the Hammett plots point to a complex reaction mechanism of two or more steps with opposing dependence on electronic effects consistent with Scheme III-4.

These observations are consistent with the acid catalyzed acyl cleavage bimolecular mechanism ($A_{AC}2$) as shown in Figure III-19. The mechanism involves stepwise reactions in which the protonation of the carbonyl oxygen is followed by the rate-determining attack of the water molecule to form the tetrahedral intermediate. The tetrahedral intermediate can either break down into the reactants or form products through a series of fast proton transfers. The transition-state consists of the unionized substrate, water, and a proton in the rate-determining transition-state. The simplified kinetic scheme for the mechanism is the same as Scheme III-4. Assuming solvolytic attack on the protonated substrate (Scheme III-4) is the degradation pathway then the specific-acid catalytic constant (k_H) is the ratio of the second-order rate constant for solvolytic attack (k_s), and ionization constant (K_a) (Equation III-8). Thus, the Hammett reaction constant (ρ) for the reaction is the sum of the reaction constants for the individual steps ($\rho_S+\rho_{Ka}$) as shown in Equation III-13. The protonation is enhanced by the electron donating substituents (ρ_{Ka} = -ive), while the second step (formation of the tetrahedral intermediate) is accelerated by the electron withdrawing substituents (ρ_1 = +ive).

$$\log k_H = Log k_S - \log K_a = \log k_S + pK_a \qquad \text{Equation III-12}$$

$$\log k_H = (\rho_S + \rho_{Ka})\sigma = \rho\sigma \qquad \text{Equation III-13}$$

In addition to inductive and resonance effects, ortho substituents are also capable of steric interactions. Steric interactions include the ability to accelerate or decelerate the reactions due to steric bulk, proximity effects, and anchimeric assistance. A Hammett

plot for the ortho substituted formanilides was prepared by assuming that the electronic effects (inductive and resonance) in the ortho position were similar to the electronic effects seen in the *para* position. Figure III-20 is the Hammett plot for *ortho* substituted formanilides overlaid on the Hammett plots for the *para* and *meta* formanilides. The Hammett correlation line for the *para* and *meta* substituents splits the *ortho* substituted formanilides into two groups. The group of compounds above the correlation are oxygen containing substituents (i.e, *o*-methoxy, *o*-hydroxyl, and *o*-carboxyl). The increase in the rate of hydrolysis by the methoxy group was surprising since it has a substantial steric bulk in the ortho position and generally displays a decrease in rate as compared to the para substituted compound. The second group consists of substituents incapable of hydrogen bonding but with substantial steric bulk (i.e., methyl, ethyl, nitro, chloro, bromo, isopropyl, and phenyl). The Taft-Kutter-Hansch (TKH) steric substituent values (E_s) are noted in the Figure III-20. These values have been derived from the van der Waals dimensions and are indicative of the steric bulk of the substituent. In the ortho position the inductive effect is higher and it was expected that in the absence of steric bulk effects that the rate of hydrolysis of both *o*-carboxyl and *o*-nitro substituent groups would increase. However the rate constant for *o*-carboxyl group was nominally higher and the rate constant for *o*-nitro group actually decreased as compared to their para substituted counterparts. This behavior is indicative of steric inhibition of resonance for carboxyl and nitro groups.

To investigate the presence of steric inhibition of resonance the ortho substituents were plotted using Hammett sigma values instead of the enhanced sigma values (Figure III-21). The *o*-hydroxyl and *o*-methoxy substituents fell closer to the correlation line. This methoxy substituent now shows a steric substituent effect consistent with its steric bulk. However the *o*-nitro and *o*-carboxyl groups still deviate from the correlation line. The nitro and phenyl group have two values associated with them since they are planar groups and their cross sectional areas change with the rotation of the group. The

reduction in the rate of hydrolysis for the nitro group and the phenyl group are consistent with the value corresponding to the lower E_s value i.e the plane of the substituent is perpendicular to the plane of the formanilide benzene ring. Since these substituents are not planar to the ring it is expected that resonance effects of the nitro and phenyl group are minimal and only the steric and inductive effects are important. The rates of reactions involving additional substituents (chloro, bromo, methyl, ethyl, and *iso*-propyl) all decrease in proportion to their E_s values.

The Fujita-Nishioka equation (Equation III-14) was used to understand and delineate the steric effects.[106] The equation assumes that the overall rate constant for ortho substituted compounds is a linear function of three components, i.e. electronic effects, steric effects, and the proximity polar effects. The first term ($\rho\sigma$) corresponds to the electronic effects which are approximated using the substituent constants (σ_m, σ_p, σ^+, σ^-, σ^0). The second term (δE_s) corresponds to the steric substituent constants (E_s) which account for the steric effect due to the space filling factor of the substituent. The third term (f F) corresponds to the proximity polar effects which are approximated by the Swain Lupton (F) constant. The reaction constants ($\rho_{o,m,p}$, δ, f) correspond to the electronic, steric, and proximity reaction constants respectively. The proximity effects and steric terms are only used for ortho substituted compounds. The last term (c) is a constant.

Second-order rate constants were analyzed using multiple linear regression analysis in JMP® (SAS Institute, Cary, NC). The substituent constants used for the *para* and *meta* substituents were the same ones used to fit the Hammett plot in Figure III-15. The *meta* and *para* substituent constants were the σ^+ with *p*-nitro, *p*-carboxyl, and *p*-phenyl being the exceptions. Substituent constants used for *p*-nitro and *p*-carboxyl substituents were σ^- values. *p*-phenyl substituent used the σ value. In the *ortho* position the resonance effects are muted due to the inhibition of resonance hence the Hammett sigma (σ) values were used. The E_S values and F values were for the *ortho* substituted

formanilides as given in Table III-38. The *o*-hydroxyl and *o*-carboxyl substituents were not included in the analysis since E_s and F values are not available for these substituents.

$$\log k_H = \rho\sigma_{o,m,p} + \delta E_S^{ortho} + fF + c \qquad \text{Equation III-14}$$

The data were fit to Equation III-14 using multiple linear regression using JMP® (Appendix C). Figure III-22 shows the plot of the actual versus predicted log k using the model. The adjusted squared correlation constant ($R^2_{adjusted}$) value was 0.974. All four terms (ρ, δ, c, and *f)* were found to be statistically significant by t-test ($p < 0.05$). The F-test for the model was significant ($p < 0.05$).

The reaction constant value for electronic effects (ρ) was 0.469 and similar to the value obtained from the Hammett plot for the *para* and *meta* substituted formanilides (0.457). The reaction constant for steric effects (δ) has a value of 0.327. The positive sign indicates that steric inhibition of reaction due to steric bulk. The magnitude of the steric constant can be considered as a function of crowding at the rate-determi*n*ing, sterically critical, reaction site.[106] Hence the small value indicates that the distance between the reaction site and the substituent is considerable (i.e. crowding is minimal). This can be explained by the ability of the unhindered amide bond to rotate freely in solution away from the space filling effect of the ortho substituent. The value is consistent with similar reactions i.e acidic hydrolysis of phenyl acetates.[107]

The reaction constant value for the proximity effects (*f*) was 0.697 which is similar to values seen for other acid catalyzed hydrolysis reactions.[106] This value is expected to be small as it is the sum of the proximity polar effects of the two steps (i.e., ionization of the substrate (-*f* value), and rate-determining nucleophilic attack (+*f* value). The intercept value (c) was 0.836 which corresponds well to the value of log k_H for the unsubstituted formanilide (0.869).

The activation enthalpy-entropy plot for the *ortho* substituted formanilides was also examined (Figure III-23). The *ortho* substituted formanilides appear to be scattered.

Around the *para* and *meta* substituted formanilides. On overlaying the *ortho* effects against the relationship developed for the *meta* and *para* relationships it is clear that the ortho substituents are split in to two groups (Figure III-24). The *ortho* nitro and carboxyl substituted formanilides lie close to their *para* counterparts which is consistent with the expectation of minimal steric effects and controlling electronic effects as determined by the analysis of the *ortho* effect. The rest of the *ortho* substituents lie above the correlation line for the substituents showing inductive effects, indicating the presence of significant *ortho* effects on the hydrolysis reaction.[67] The substituents appear to be distributed randomly without a clear dependence on E_s. Hence, the *ortho* effect for these substituents appears to be a function of both the steric and proximity effects in agreement with the Fujita Nishioka analysis.

Conclusion

The reaction order, reaction scheme and pH effects on the acidic hydrolysis of formanilides were determined. The substituent effects for the *para* and *meta* substituents showed the presence of significant inductive and resonance effects leading to nonlinear Hammett plots. A linear Hammett plot was prepared by using selected sigma values to compensate for the enhanced resonance effects. The activation entropies and enthalpies of *para* and *meta* substituted formanilides were also studied. The activation enthalpy-entropy plot showed that the *para* substituents exhibiting enhanced resonance effects deviated significantly from the substituents showing mainly inductive effects. The activation enthalpy-entropy plot revealed the presence of a compensation relationship with a compensation temperature of 61.6 ± 17.2 °C which is close to the reaction temperature. At the compensation temperature the substitution effects are muted and could lead to underestimation of the substituent effects for the series. These results, in conjunction with the Hammett plot give a clearer picture of the interaction mechanisms controlling the hydrolyses of *meta* and *para* substituents. The Hammett plot using the

selected sigma showed a reaction constant (ρ) of 0.457. This value can be used to predict the stability of substituted formanilides. The pH rate plots, Hammett plot, binary solvent studies, ionic strength studies and activation enthalpy-entropy relationships were explained using the two step $A_{AC}2$ mechanism. Substitution at the *ortho* position displayed electronic as well as steric effects. The *ortho* substituent effects (steric, electronic and proximity polar effects) were quantitatively studied using the Fujita-Nishioka analysis. The steric effect presented itself in two ways (1) steric inhibition of resonance and (2) steric bulk effect. The ortho substituents twist the amide bond out of the plane of the phenyl ring leading to a complete obstruction of the resonance effect. Substitution at the ortho position lead to a decrease in the access of solvent to the reaction site due to steric bulk effect ($\delta = 0.467$) leading to a decrease in the rate of hydrolysis. The proximity polar effects were also substantial, which when analyzed in the context of the two step $A_{AC}2$ mechanism show the effect of two complementary reaction steps on the overall rate. These conclusions drawn from the Fujita Nishioka analysis were supported by the effects on the entropy and enthalpies of activation of the ortho substituents which showed the presence of steric and proximity effects. In conclusion, the mechanism of acidic hydrolysis of formanilides was confirmed and the effect of *ortho* substitution was analyzed successfully.

Table III- 38: Substituent parameters used for correlation[73, 103].

Substituent		**σ_m**	**σ_p**	**σ_m^+**	**σ_p^+**	**σ_p^-**	**σ_m^0**	**σ_p^0**	**E_s^a**	**F**
	H	0							0	0
Methyl	CH_3	-0.07	-0.17	-0.07	-0.31			-0.12	-1.24	-0.04
Chloro	Cl	0.37	0.23	0.40	0.11			0.27	-0.97	0.41
Nitro	NO_2	0.71	0.78	0.67	0.79	1.24		0.82	-1.01[b], -2.52[c]	0.67
Bromo	Br	0.39	0.23	0.41	0.15			0.26	-1.16	0.44
Hydroxyl	OH	0.12	-0.37		-0.92		0.04	-0.13		0.29
Phenyl	C_6H_5	0.06	-0.01		-0.18			0.04	-1.01[b], -3.82[c]	0.08
Methoxy	OCH_3	0.12	-0.27	0.05	-0.79		0.06	-0.16	-0.55	0.26
Ethyl	C_2H_5	-0.07	-0.15	-0.06	-0.30			-0.13	-1.31	-0.05
Isopropyl	*Iso*-C_3H_7	-0.07	-0.15		-0.28			-0.16	-1.71	-0.05
Carboxyl	COOH	0.36	0.45	0.32	0.42	0.73				

[a] point of reference of E_s values is shifted to H; [b] minimum perpendicular dimension, and [c] maximum coplanar dimension,

Figure III- 13: Hammett plot for *para* and *meta* substituted formanilides. Open squares denote *para* substituted compounds (□) and open circles denote *meta* substituted compounds (○). Lines are not fitted to the data.

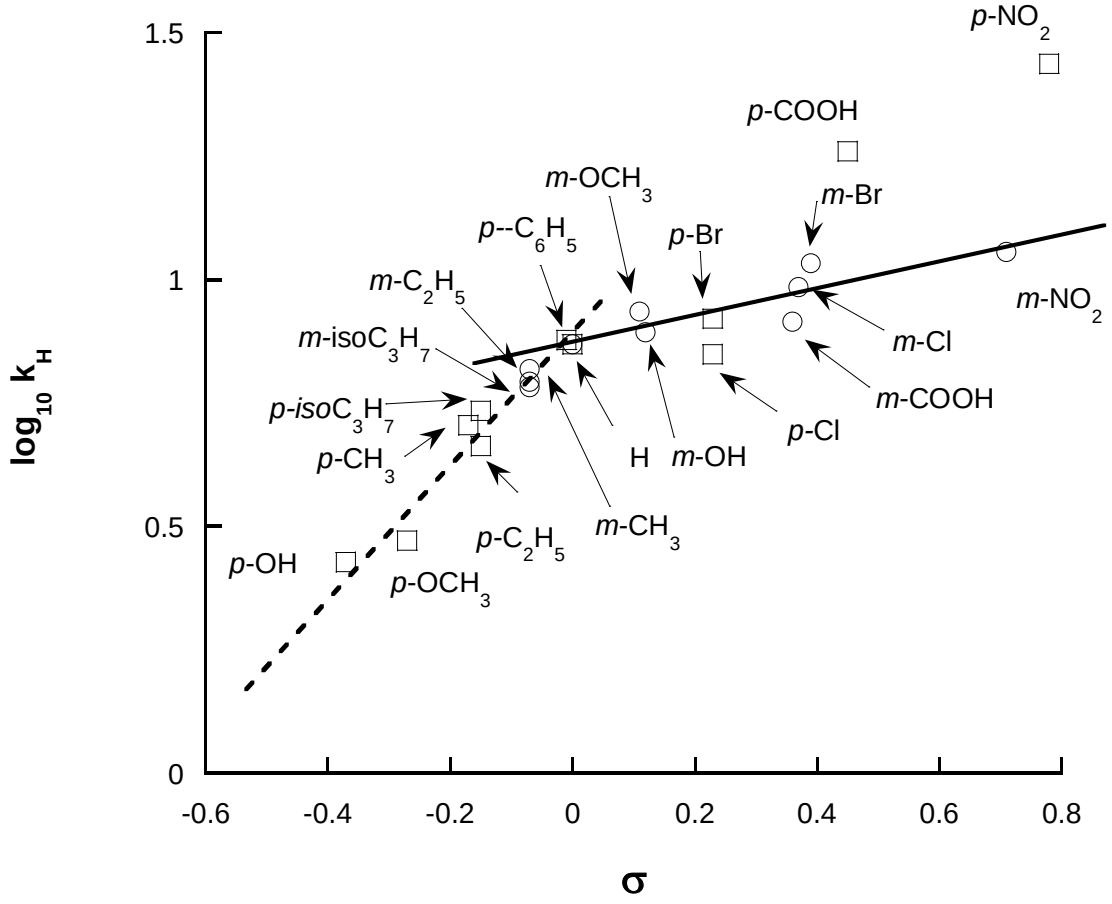

Figure III- 14 Hammett plots for *meta* and *para* substituents using electrophilic substituent constants. Open squares denote *para* substituted compounds (□) and open circles denote *meta* substituted compounds (○). The solid line is a linear fit to the Hammett equation which does not include *p*-nitro, *p*-carboxy, and *p*-phenyl substituents.

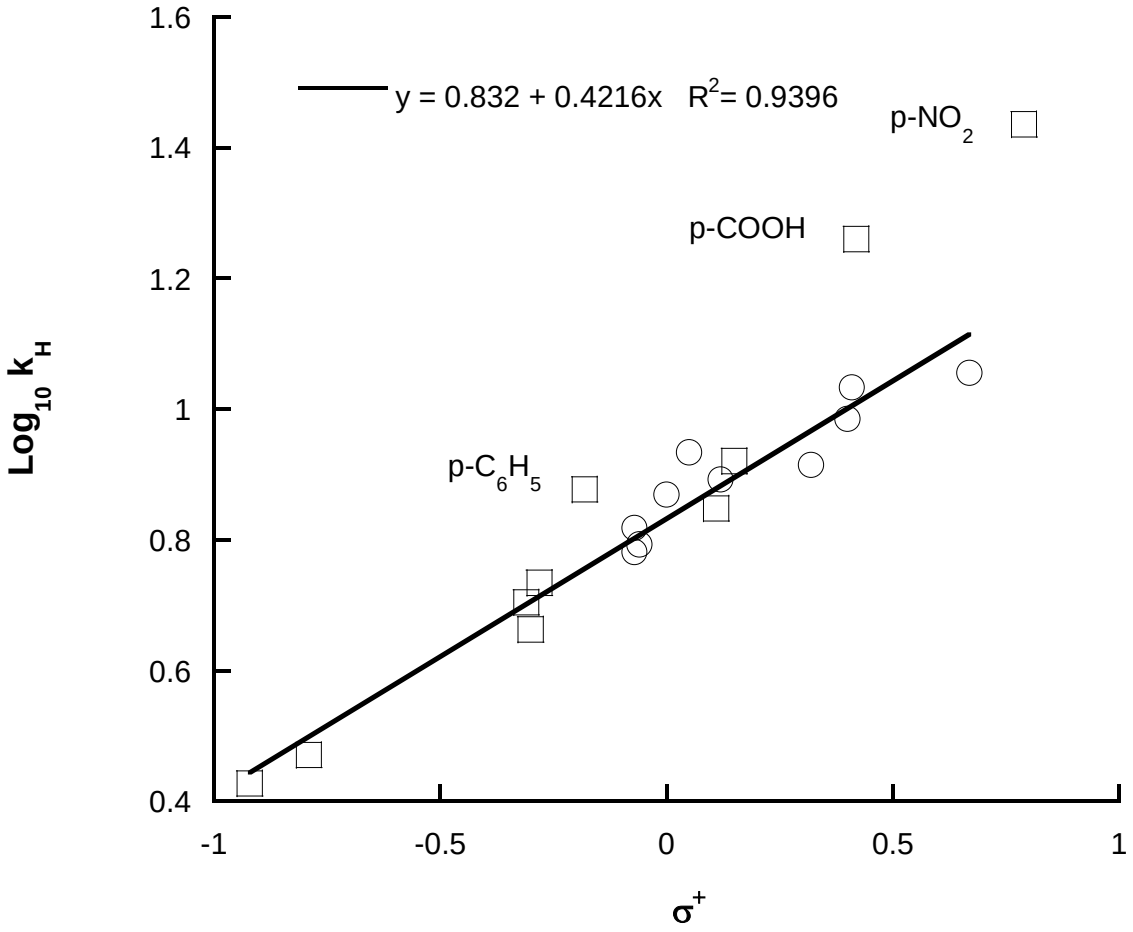

Figure III- 15: Hammett plot for *para* and *meta* substituents using various sigma values. The dotted line is a linear fit to the Hammett equation.

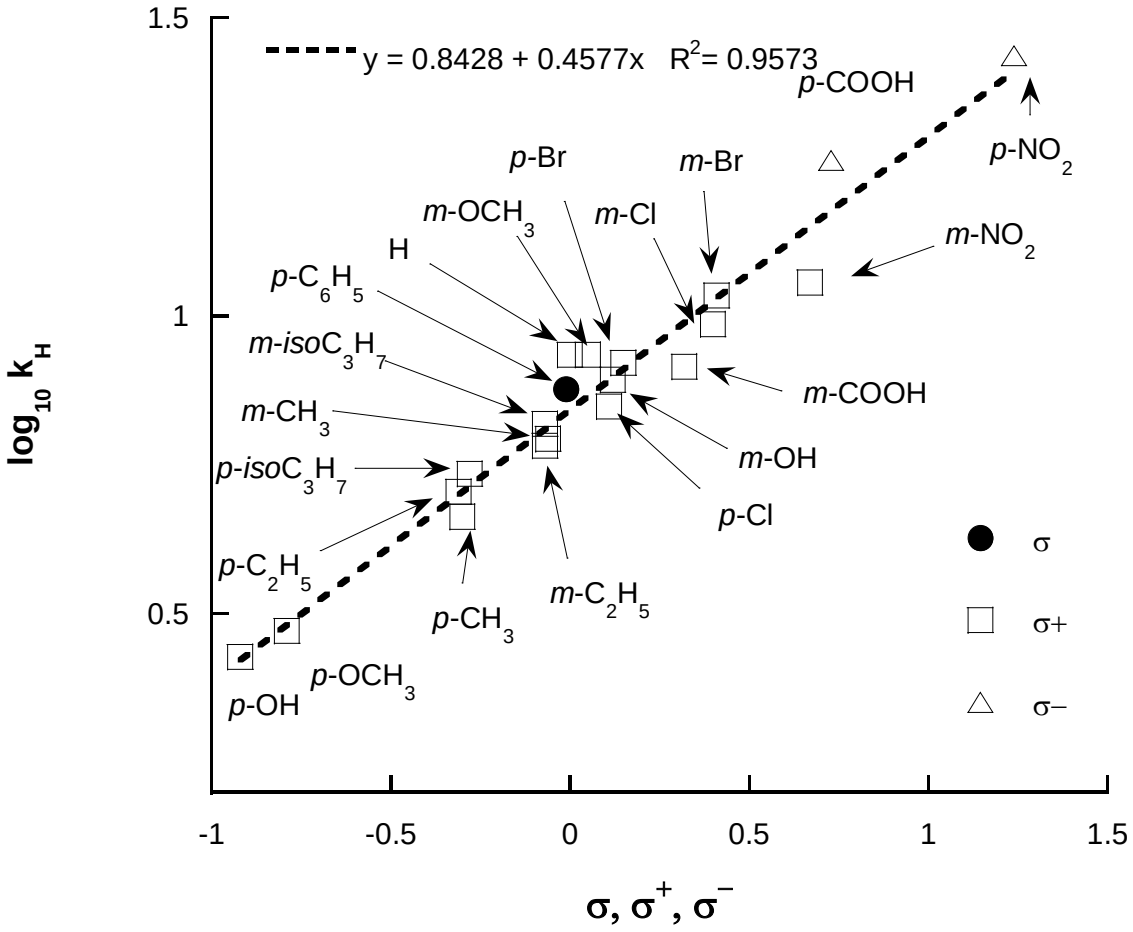

Figure III- 16: The enthalpy-entropy compensation plots for *para* and *meta* substituted formanilides using activation parameters. Solid squares denote *para* substituted compounds (■) and solid circles denote *meta* substituted compounds (●). The error bars represent the standard errors.

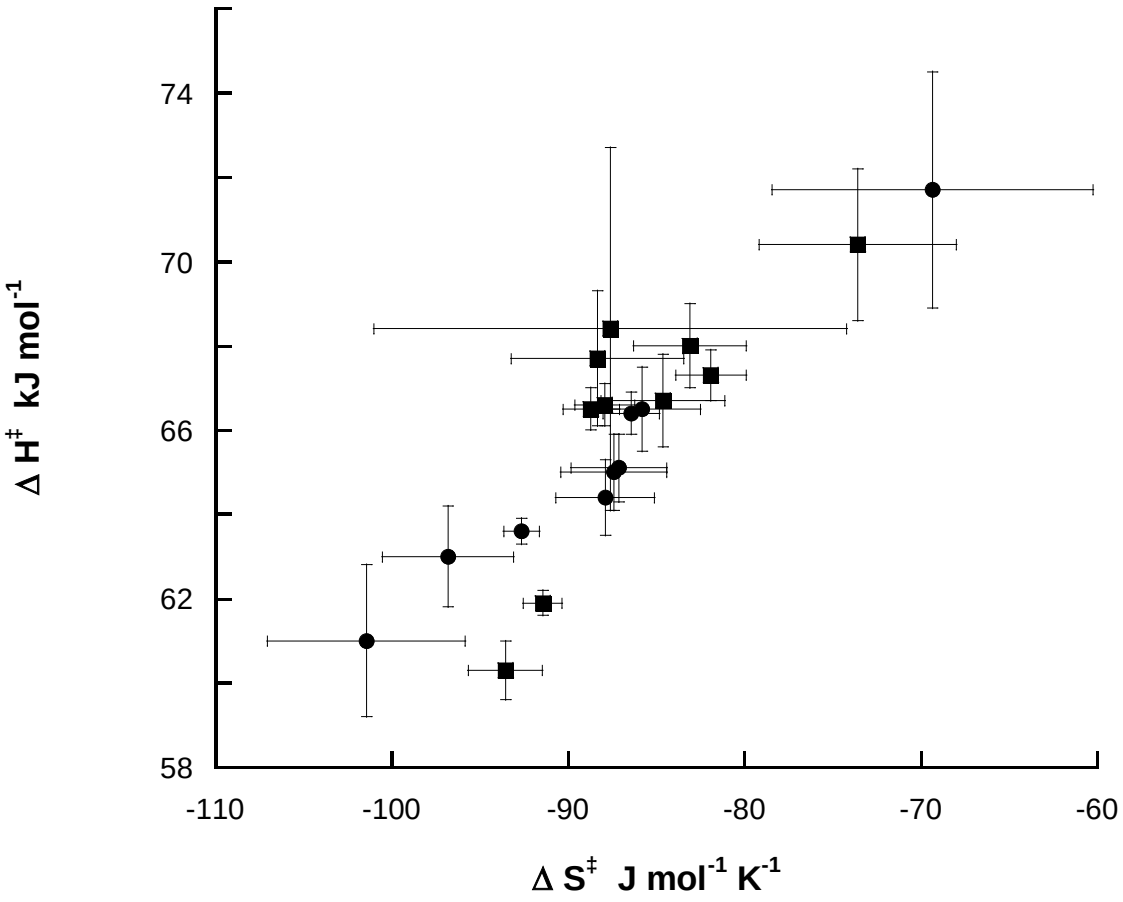

Figure III- 17: Activation enthalpy-entropy compensation plots for *para* and *meta* substituted formanilides The line is a linear regression fit to the substituents showing inductive effects.

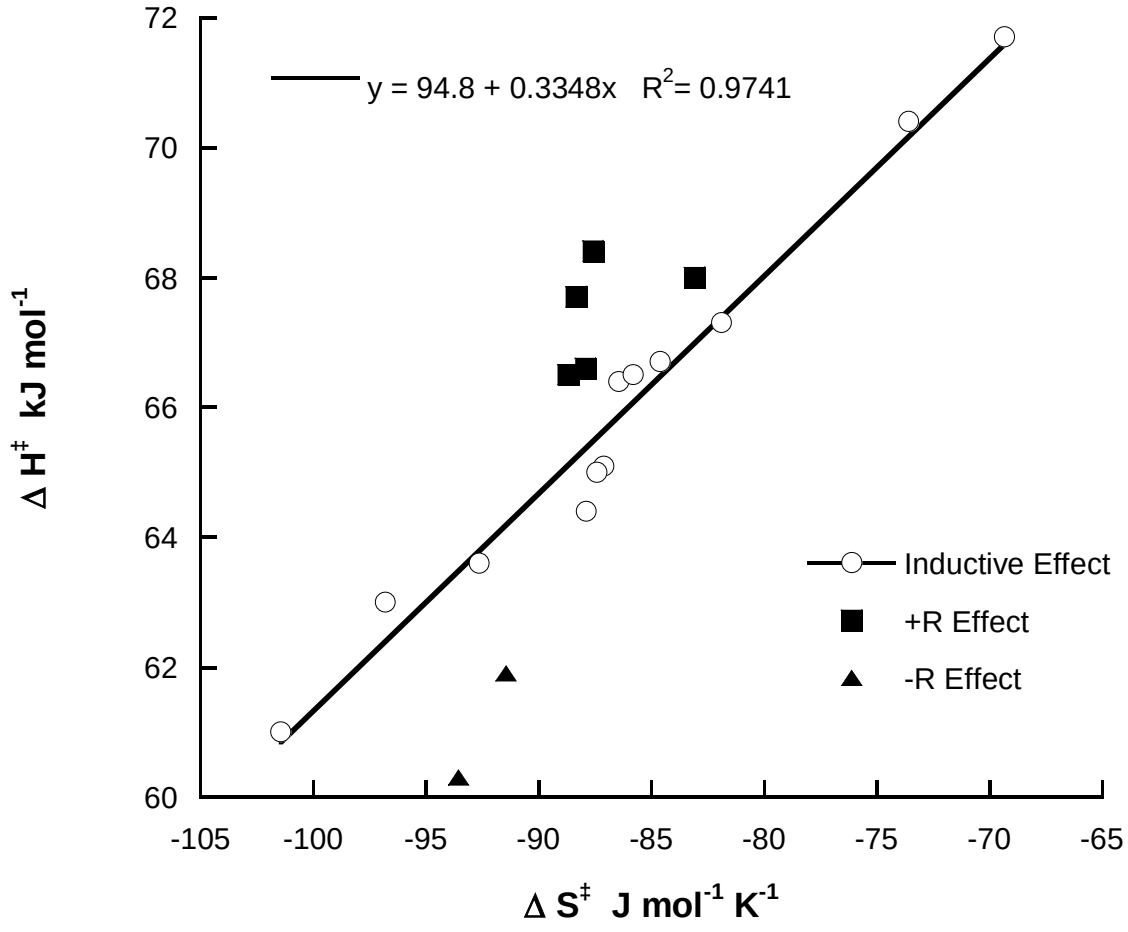

Figure III- 18: Extrapolated Arrhenius plots for (A) *meta* and (B) *para* substituted formanilides. Solid squares denote para substituted compounds (■) and solid circles denote *meta* substituted compounds (●).The lines are linear fits of the data to the Arrhenius equation.

(A)

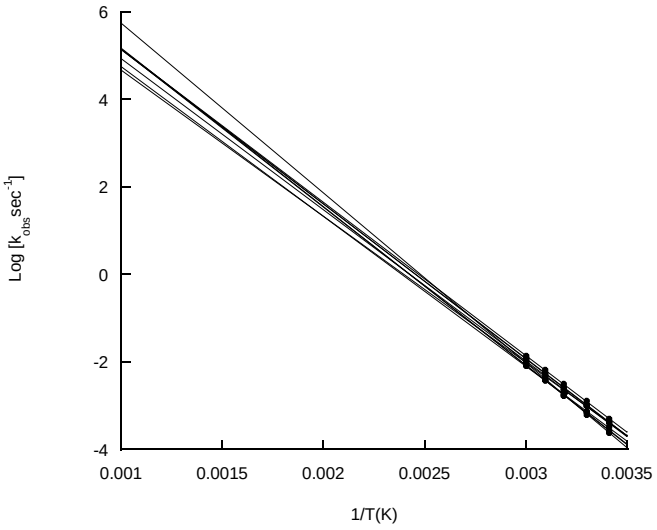

(B)

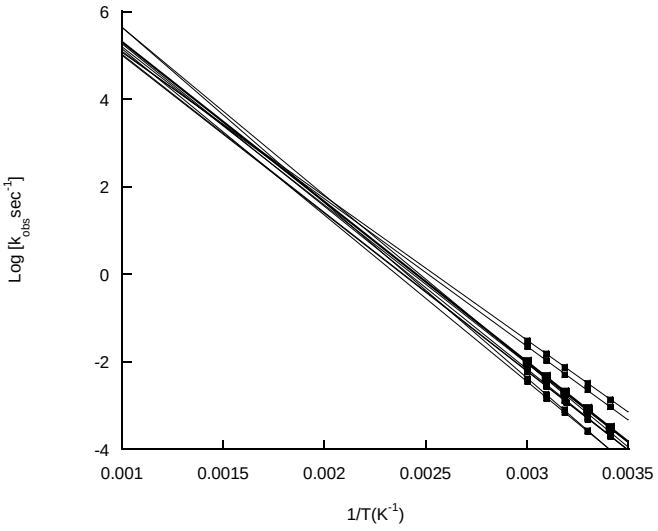

Figure III- 19 $A_{AC}2$ mechanism for acid hydrolysis of amides

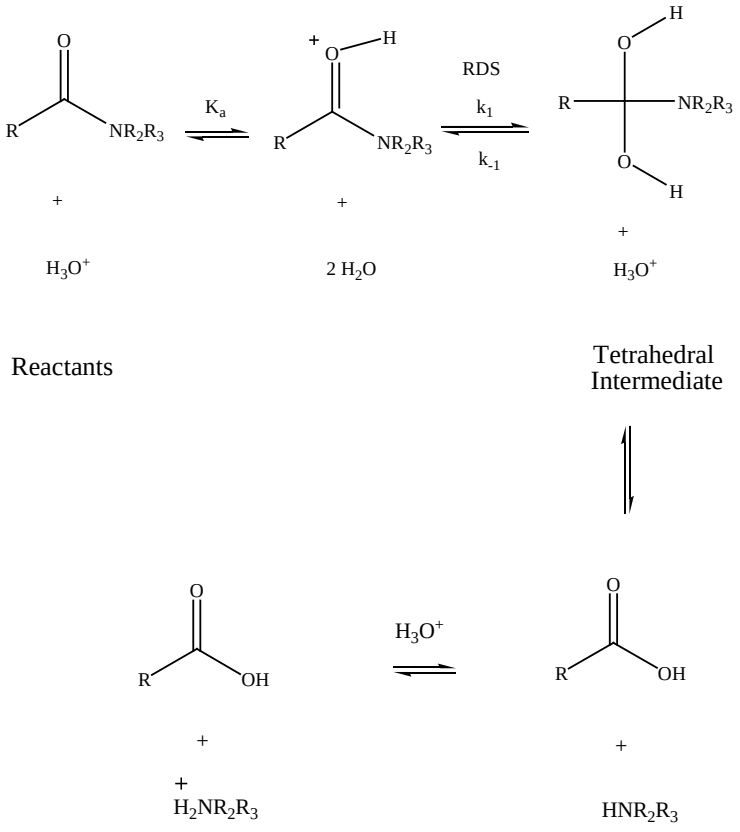

Figure III- 20 Hammett plots for *para*, *meta*, and *ortho* substituted formanilides using Hammett sigma values for ortho substituents. Solid squares denote *para* substituted compounds (■), solid circles denote *meta* substituted compounds (●), and open squares denote *ortho* substituted compounds (□). The values in parenthesis are the Taft-Kutter-Hansch values for the steric substituent E_s.

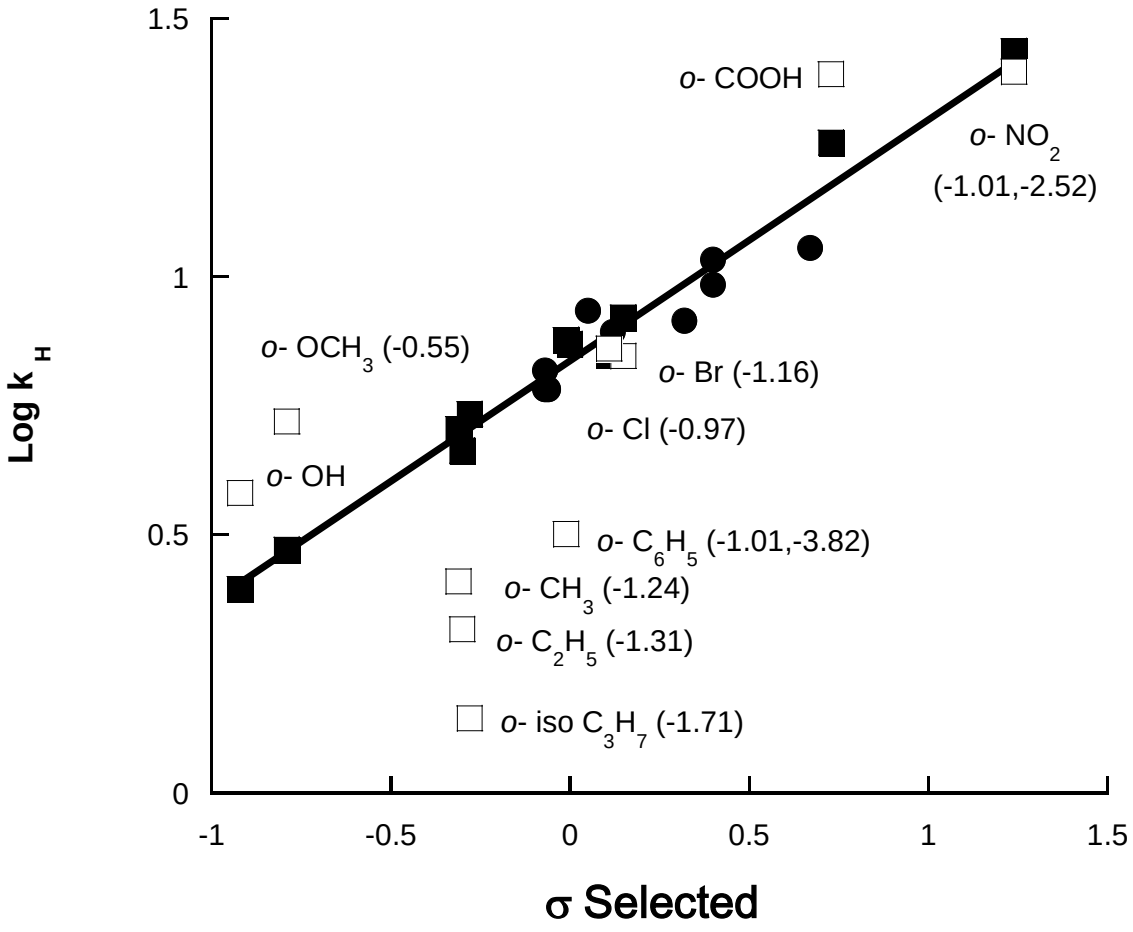

Figure III- 21 Hammett plots for *para*, *meta*, and *ortho* substituted formanilides using Hammett sigma values for *ortho* substituents (assuming steric inhibition of resonance). Solid squares denote *para* substituted compounds (■), solid circles denote *meta* substituted compounds (●), and open squares denote *ortho* substituted compounds (□). The line is a linear fit for the *para* and *meta* substituted formanilide using the selected sigma values and is used for comparison.

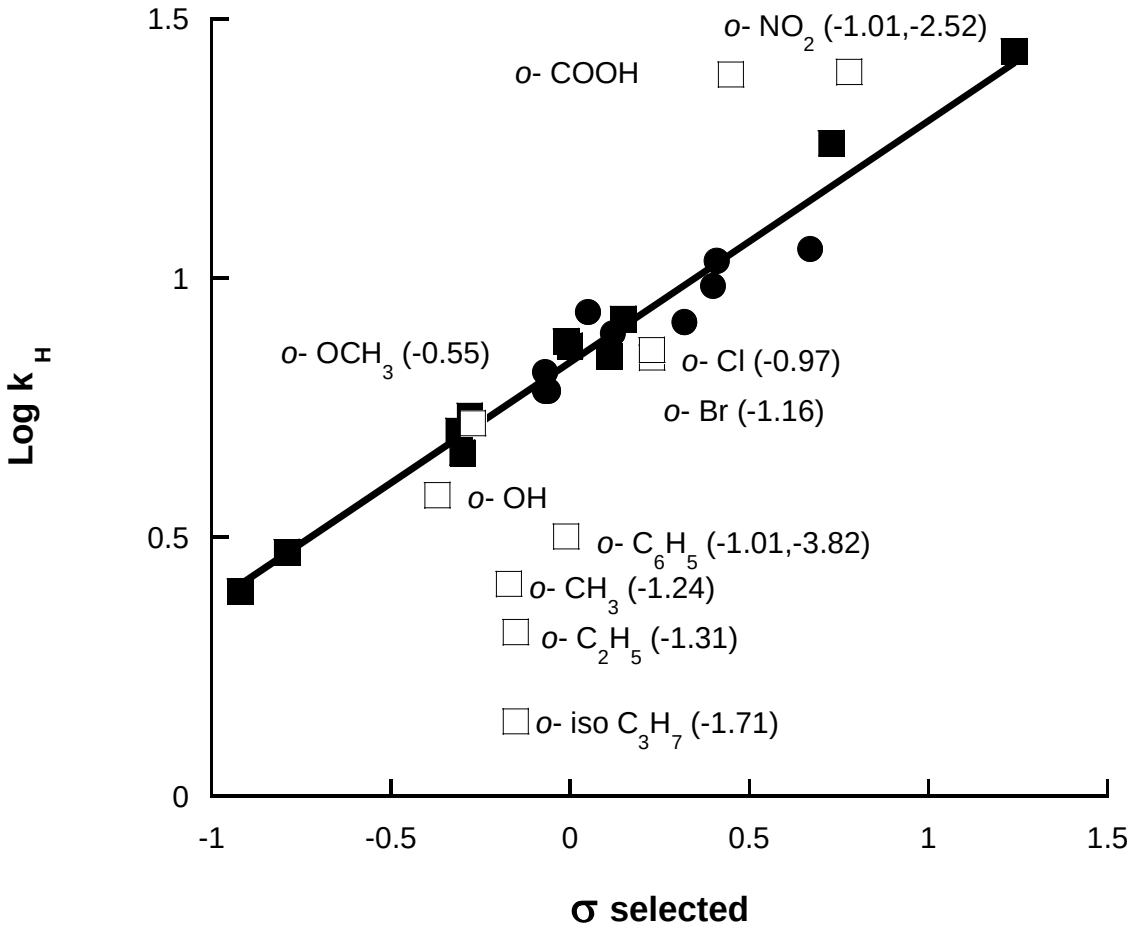

Figure III- 22: The actual versus predicted plot for log of the rate constants using the Fujita Nishioka equation. Open squares denote *para* substituted compounds (□), open circles denote *meta* substituted compounds (○), and the open triangles denote *ortho* substituents. The line is the correlation line with a slope of 1 and the dotted lines are 95% mean confidence intervals for the fitted equation.

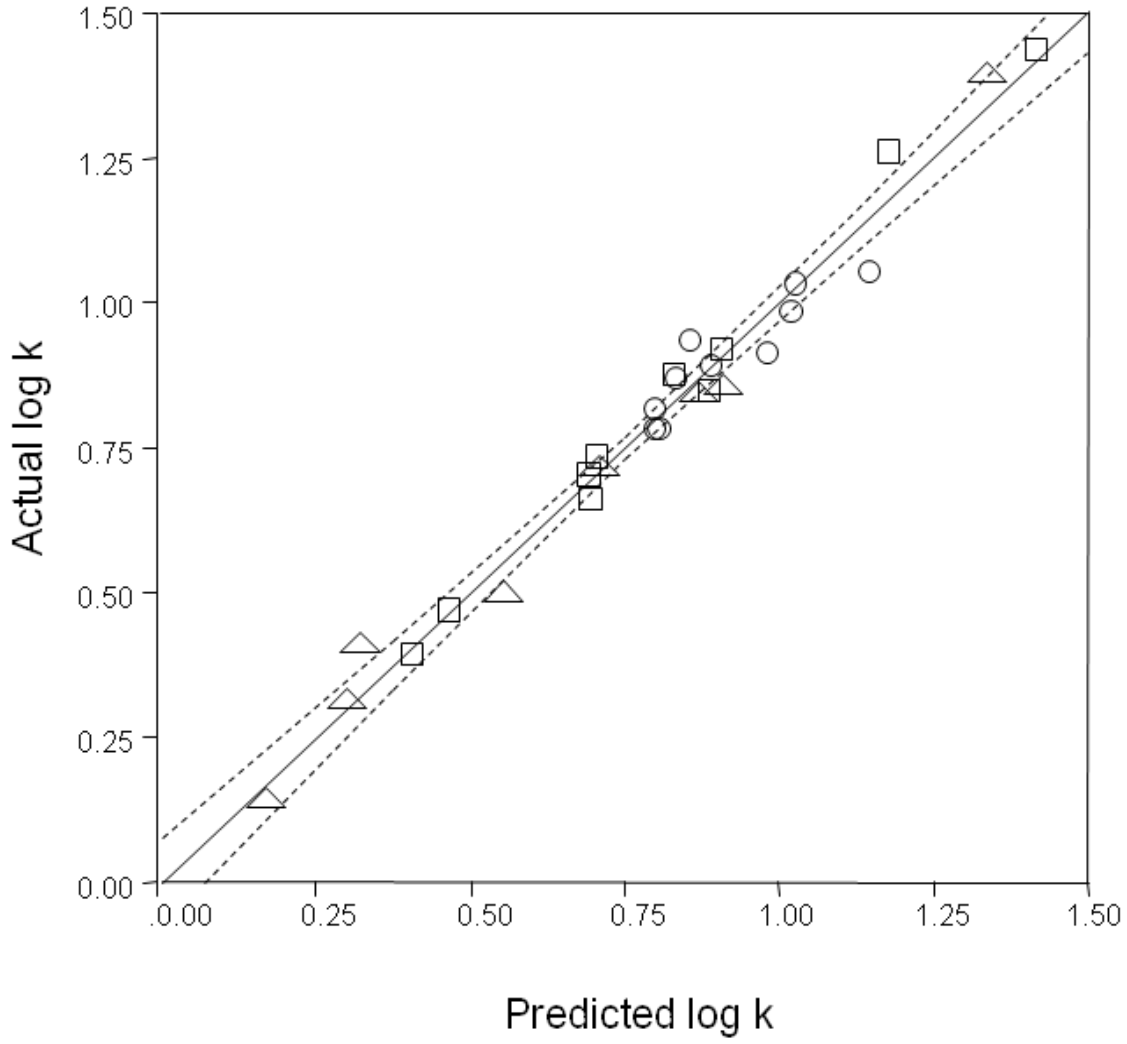

Figure III- 23: Activation enthalpy-entropy compensation plot for *ortho* substituted formanilides. Solid squares denote *para* substituted compounds (■), solid circles denote *meta* substituted compounds (●), and the open triangles denote *ortho* substituted compounds (Δ).The data for the para and meta substituted formanilides is used for comparison. The error bars represent standard errors.

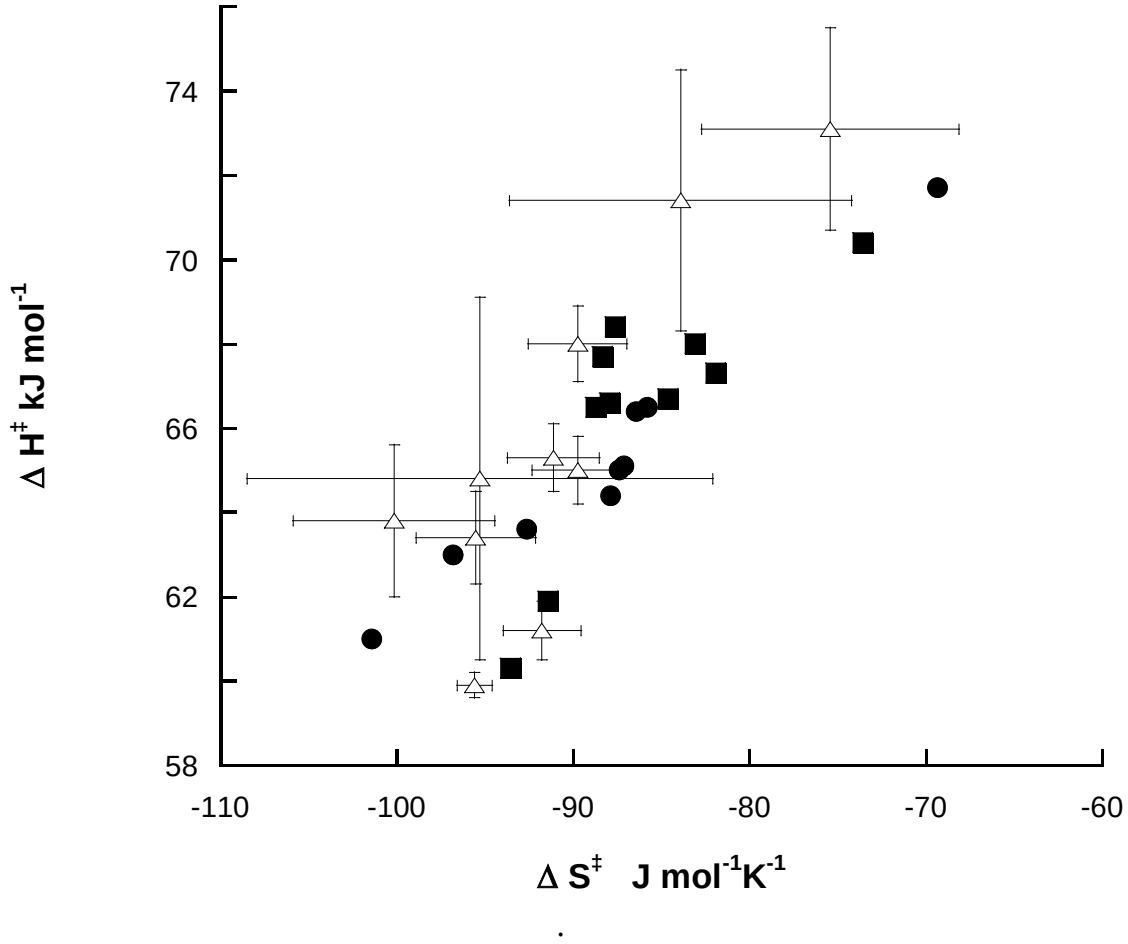

Figure III- 24 Enthalpy-entropy compensation plot for *ortho* substituted formanilides. Solid squares denote *para* substituted compounds (■), solid circles denote *meta* substituted compounds (●), and the open triangles denote *ortho* substituted compounds (Δ).The data for the *para* and *meta* substituted formanilides is used for comparison and the line is a straight line fit to the substituents which display pure inductive effects. The values in parenthesis are the E_s values.

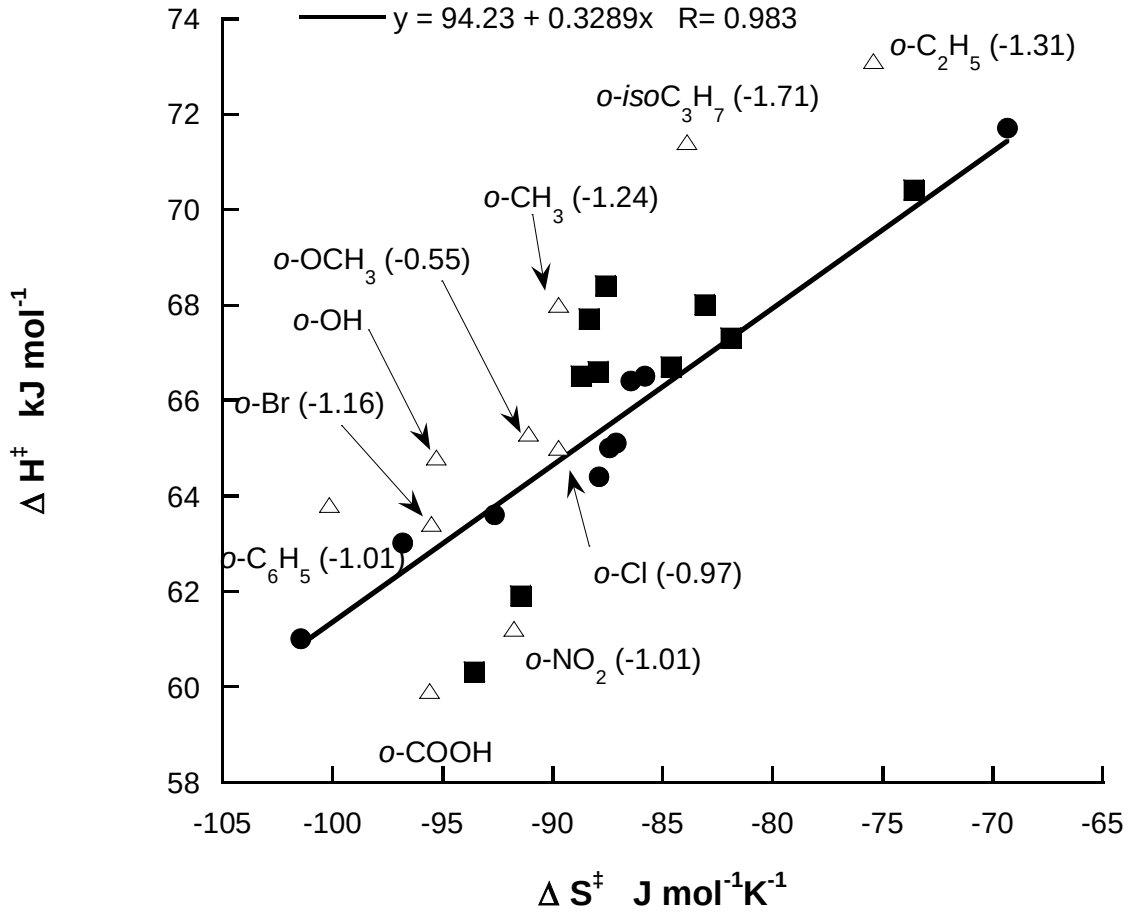

CHAPTER IV

ORTHO SUBSTITUTION EFFECTS ON THE ALKALINE HYDROLYSIS OF FORMANILIDES

Introduction

The kinetic studies of formanilides in alkaline aqueous solutions are reported in this chapter. The reaction products were identified, and reaction schemes consistent with the observed products are proposed. Effects of pH, binary solvents, ionic strength, and temperature on the rate law were determined. Structure-reactivity relationships were used in conjunction with rate laws to propose reasonable reaction mechanisms. The effect of substitution at the ortho position on reaction mechanism was determined.

Materials

Substrates were either purchased or synthesized as described in Chapter II. Substituted anilines were purchased from Sigma-Aldrich (Saint Louis, MO). Glacial acetic acid, anhydrous sodium acetate, dioxane, dimethyl sulfoxide, sodium phosphate monobasic monohydrate, sodium chloride, standardized sodium hydroxide solutions (0.10 M, 10.0 M , 0.010 M NaOH), and anhydrous sodium phosphate dibasic were purchased from Fisher Scientific (Fair Lawn, NJ). Absolute ethanol was obtained from AAPER Alcohol and Chemical Co (Shelbyville, KY). Tris hydrochloride was obtained from Research Products International Corporation (Mount Prospect, IL). Tris base was obtained from Gibco BRL (Grand Island, NY). Calibration buffers for pH measurement (pH 4, 7 & 10) were obtained from VWR Scientific (West Chester, PA). Solvents used for chromatography were HPLC grade.

Methods

Standard protocols for kinetic analysis.

Reactions in concentrated sodium hydroxide solutions (5.0 to1.0 M) were followed using ultraviolet-visible (UV-Vis) spectroscopy, and reactions in dilute sodium hydroxide solutions (0.5-0.01 M) were followed using HPLC. For studies conducted using HPLC analysis, the following methods were used. A 10 mM stock solution of the formanilide substrate was prepared in absolute ethanol. A 10 mL aliquot of the dilute sodium hydroxide solution was equilibrated to the reaction temperature. Reaction was initiated by adding 0.1 mL of the stock solution of formanilide to the sodium hydroxide solution to give an initial substrate concentration equal to approximately 0.10 mM formanilide and 1% v/v ethanol. Aliquots were withdrawn and quenched with either acetate buffer (1.0 M, pH 4.0) or tris buffer (1.0 M, pH 8.0). The samples were then stored at 4 °C until HPLC analysis. The pH value of the reaction mixture was measured at the start and end of the reaction using an Accumet model 25 pH meter with a combination glass electrode calibrated with standard buffers at the reaction temperature. Substrate and product calibration curves were determined using four to five standards. The calibration curves in the range of 0.01 mM to 0.1 mM were prepared by diluting the ethanolic stock solutions with buffer solutions (0.10 M acetate pH 4 or 0.10 M tris pH 8). Analyses were performed on a Thermo-separations RP-HPLC system (Thermo Scientific, Waltham, MA) consisting of UV6000LP diode array detector, AS3000 autoinjector, P4000 pump, and an online membrane degasser. Chromatograms were integrated and data stored using Chromquest® chromatography data system software (Version 4.0). The column and the autoinjector were maintained at room temperature. Analysis conditions are the same as the conditions given in Table III-1 in Chapter III.

UV spectroscopy was used to study fast kinetic reactions that occurred at high hydroxide concentrations. Analyses of reaction mixtures were conducted with a Hewlett

Packard HP8453 UV-Vis diode array spectrophotometer (Hewlett Packard, Santa Clara, CA) equipped with a Peltier thermostatted cell holder (HP 89090A). A 2.5 mL aliquot of sodium hydroxide solution was equilibrated to the reaction temperature in a closed glass cuvette in the thermostatted cell holder of the HP 8453 spectrophotometer. Reactions were initiated by adding 25 μL of stock solution (10 mM substrate in ethanol) to the reaction mixture so that the final concentration of ethyl alcohol was 1% and the final concentration of substrate in solution was 0.1 mM. Spectra were collected as a function of time using the kinetics module in the Chemstation® software. Reactions were followed until there was no significant change in spectra with time. Slow degradation reactions were followed to at least three half lives while fast reactions were followed to at least 10 half lives. The pH value was determined using an Accumet model 25 pH meter equipped with a semi-micro combination glass electrodebefore the reaction was initiated and at the end of the reaction at the reaction temperature. The final and initial spectra were subtracted and the wavelength of maximum difference was determined. Spectral data were analyzed using the kinetic analysis module in Chemstation® software to determine the observed first-order rate constants. Kinetic experiments were carried out in duplicate and average rate constants are reported. To confirm the identity of the hydrolysis products of the substituted formanilide, the spectra associated with the final reaction mixture were compared to an authentic sample of the predicted end product i.e. the corresponding aniline and formate ion. Formate ion does not have appreciable ultraviolet absorbance at the concentrations studied and cannot be easily detected by UV spectroscopy; however aniline has a strong chromophore and could be easily detected. The test solutions were prepared by dissolving the aniline in absolute ethanol (10 mM) and diluting a 25 μL aliquot in 2.5 mL of 1.0 M sodium hydroxide solution to a final concentration equivalent to the initial substrate concentration. The spectrum was collected and compared to the spectrum of the final products using the peak purity compare function in the Chemstation® software.

Kinetic Studies

Determination of reaction schemes for all substrates.

Reaction schemes were determined by degrading solutions of substituted 0.10 mM formanilides in sodium hydroxide solutions at 25°C, 40 °C or 60 °C. Samples were generated and analyzed using the standard protocol with HPLC. Degradation kinetics were also followed using UV-Vis spectroscopy as a function of time. Spectra were collected and inspected for the presence of isosbestic points.

Effect of pH

Initial studies to determine the effect of hydroxide concentration on reaction rates for selected formanilides (formanilide, *p*-chloroformanilide, *p*-methylformanilide, *p*-bromoformanilide, *p*-hydroxyformanilide, *o*-methylformanilide, *o*-bromoformanilide, and *o*-hydroxyformanilide) were carried out at 40 °C in sodium hydroxide solutions in the concentration range between 3.04 to 0.010 M. Sodium hydroxide solutions in the range of 3.04 M to 1.0 M were prepared by diluting certified sodium hydroxide solution (10.0 M) in carbonate free water. Dilute sodium hydroxide solutions (<1 M) were prepared by diluting certified sodium hydroxide solutions and adjusting the ionic strength (μ) to 1.0 using sodium chloride. *o*-hydroxyformanilide was insoluble in absolute ethanol and stock solutions were prepared in dimethyl sulfoxide. Experimental conditions and observed rate constants are tabulated in Tables IV-1 to Table IV-8

The pH-rate profiles for selected formanilides (formanilide, *p*-chloroformanilide, *p*-methylformanilide, *p*-methoxyformanilide, and *m*-nitroformanilide) at 25 °C were determined by using aqueous sodium hydroxide solutions in the concentration range between 5.0 M to 0.010 M. Sodium hydroxide solutions in the range of 5.0 M to 1.0 M were prepared by diluting 10.0 M certified sodium hydroxide solution in carbonate free water. Dilute sodium hydroxide solutions (<1 M) were prepared by diluting certified sodium hydroxide acid solutions (1.0 M or 0.10 M) in water. Ionic strength was not

adjusted for these studies. Experimental conditions and observed rate constants are tabulated in Tables IV-9 to Table IV-13

Effect of Ionic Strength

A series of formanilide degradation studies at 40 °C were carried out in 0.010 M sodium hydroxide solutions by diluting 0.10 M standardized sodium hydroxide solutions wherein the ionic strengths of the solutions were varied from 1.0 to 0.010 by adding solid sodium chloride. The reactions were monitored using HPLC. Experimental conditions and rate constants are tabulated in Table IV-14.

Binary-Solvent System Studies

Reaction mixtures for formanilide degradation were prepared in 0.10 M sodium hydroxide solutions containing 25 or 50 % v/v organic solvents (dioxane or dimethyl sulfoxide). Substrate was added to the reaction mixtures as previously described and reaction samples were analyzed using HPLC. The degradation proceeds slowly and observed rate constants were determined using the initial rate method. Experimental conditions and rate constants are tabulated in Table IV-15.

Effect of Temperature

Formanilide was degraded in 0.10 M sodium hydroxide solutions at different temperatures (25 °C, 40 °C, and 60 °C). Reactions were followed using HPLC. Experimental conditions and observed rate constants are tabulated in Table IV-16

Structure-Reactivity Relationship Studies

The effect of structure on the rate of alkaline hydrolysis of substrates was evaluated by hydrolyzing them in 0.10 M sodium hydroxide solutions at 40 °C. The ionic strengths of these solutions were not adjusted and reactions were followed using HPLC. The *p*-nitroformanilide and *o*-nitro formanilide degrade very rapidly even at low

hydroxide concentrations; hence the rate of degradation of these compounds was studied using UV spectroscopy. The results are tabulated in Table IV-17.

Results

Determination of reaction schemes

Reaction schemes were determined for all of the formanilides. Formanilide is used as a model compound to demonstrate the steps involved since the steps were similar for all the formanilides. HPLC chromatograms for the alkaline degradation of formanilide indicate the presence of two compounds (Figure IV-1) identified as the substrate and corresponding aniline by comparing the peak retention times with authentic standards. Calibration curves were generated using authentic samples of formanilide and aniline, and peak area versus concentration for formanilide and aniline (conc. range of 0.01-0.10 mM) were linear (Figure III-2 in Chapter III). The concentration-time profiles for formanilide hydrolysis at different hydroxide concentrations were generated using calibration curves and mass balance was determined (Figure IV-2). The concentration of formanilide decreases as a function of time with a concurrent increase in the concentration of aniline. The mass balance of the reaction remained constant, which indicated that formanilide quantitatively converted to aniline (Scheme IV-1). The reactions were followed for two to three half lives. The order with respect to time for the loss of formanilide was determined from plots of logarithm of the concentration versus time (Figure IV-3). The linearity of the plots indicated that the loss of formanilide was first-order with respect to time. The observed first-order rate constant (k_{obs}) was estimated by fitting the concentration-time profile of formanilide to the first-order rate equation. In the case of formanilide the observed rate constant is equivalent to the rate constant for the formation of aniline from formanilide, i.e. the deformylation rate constant (k′).

Table IV- 1: Sodium hydroxide concentrations and observed rate constants for the hydrolysis of formanilide at 40 °C.

NaOH Conc. $\mathbf{M \times 10^2}$	$\mathbf{k_{obs}}$ $\mathbf{hr^{-1} \times 10^2}$
0.980	2.65
2.47	7.66
5.04	16.7
7.50	28.3
10.1	40.8
25.0	146
49.7	367
74.6	682
100	970
124	1370
149	1770
173	2240
199	2640
248	3560
304	4530

The wavelength used for UV studies was 252 nm. Ionic strength was adjusted to 1.0 for reaction mixtures <1.0 M NaOH.

Table IV- 2: Sodium hydroxide concentrations and observed rate constants for the hydrolysis of *p*-methylformanilide at 40 °C. x

NaOH Conc. $\mathbf{M \times 10^2}$	$\mathbf{k_{obs}}$ $\mathbf{hr^{-1} \times 10^2}$
0.980	2.61
2.47	7.14
5.04	16.6
7.50	26.7
10.1	37.3
25.0	139
49.7	405
74.6	737
100	1080
124	1550
149	2030
173	2530
199	2990
248	4100
304	5100

The wavelength used for UV studies was 251 nm. Ionic strength was adjusted to 1.0 for reaction mixtures <1.0 M NaOH.

Table IV- 3: Sodium hydroxide concentrations and observed rate constants for the hydrolysis of *o*-methylformanilide at 40 °C.

NaOH Conc. $\mathbf{M \times 10^2}$	$\mathbf{k_{obs}}$ $\mathbf{hr^{-1} \times 10^2}$
0.980	0.730
2.47	2.23
5.04	5.06
7.50	8.54
10.1	12.9
25.0	46.2
49.7	128
74.6	245
100	363
124	521
173	911
199	1100
248	1450
304	1940

The wavelength used for UV studies was 249 nm. Ionic strength was adjusted to 1.0 for reaction mixtures <1.0 M NaOH.

Table IV- 4: Sodium hydroxide concentrations and observed rate constants for the hydrolysis of *p*-bromoformanilide at 40 °C.

NaOH Conc. $\mathbf{M \times 10^2}$	$\mathbf{k_{obs}}$ $\mathbf{hr^{-1} \times 10^2}$
0.980	2.18
2.47	6.79
5.04	16.7
7.50	27.6
10.1	43.3
25.0	133
49.7	325
74.6	564
100	789
124	1050
149	1340
173	1590
199	1970
248	2560
304	3120

The wavelength used for UV studies was 261 nm. Ionic strength was adjusted to 1.0 for reaction mixtures <1.0 M NaOH.

Table IV- 5: Sodium hydroxide concentrations and observed rate constants for the hydrolysis of *o*-bromoformanilide at 40 °C.

NaOH Conc. $\mathbf{M \times 10^2}$	$\mathbf{k_{obs}}$ $\mathbf{hr^{-1} \times 10^2}$
0.980	1.86
2.47	7.27
5.04	19.6
7.50	33.3
10.1	48.6
25.0	149
49.7	403
74.6	530
100	750
124	937
149	1220
173	1460
199	1770
248	2340
304	2810

The wavelength used for UV studies was 255 nm. Ionic strength was adjusted to 1.0 for reaction mixtures <1.0 M NaOH.

Table IV- 6: Sodium hydroxide concentrations and observed rate constants for the hydrolysis of *p*-chloroformanilide at 40 °C.

NaOH Conc. $M \times 10^2$	k_{obs} $hr^{-1} \times 10^2$
1.00	1.44
5.00	16.4
7.50	27.1
10.0	44.8
25.0	138
50.0	331
75.0	542
100	801
125	1090
150	1440
175	1710
200	1960
248	2590
304	3350

The wavelength used for UV studies was 259 nm. Ionic strength was adjusted to 1.0 for reaction mixtures <1.0 M NaOH.

Table IV- 7: Sodium hydroxide concentrations and observed rate constants for the hydrolysis of *o*-hydroxyformanilide at 25 °C.

NaOH Conc. $\mathbf{M \times 10^2}$	$\mathbf{k_{obs}}$ $\mathbf{hr^{-1} \times 10^2}$
1.00	1.74
2.50	4.49
5.00	9.33
7.50	14.6
10.0	28.0
25.0	66.3
50.0	180

Ionic strength was adjusted to 1.0 for reaction mixtures <1.0 M NaOH.

Table IV- 8: Sodium hydroxide concentrations and observed rate constants for the hydrolysis of *p*- hydroxyformanilide at 25 °C.

NaOH Conc. $\mathbf{M \times 10^2}$	$\mathbf{k_{obs}}$ $\mathbf{hr^{-1} \times 10^2}$
1.00	2.97
2.50	7.74
5.00	18.4
7.50	28.4
10.0	41.3
25.0	122
50.0	374

Ionic strength was adjusted to 1.0 for reaction mixtures <1.0 M NaOH.

Table IV- 9: Sodium hydroxide concentrations and observed rate constants for the hydrolysis of formanilide at 25 °C.

NaOH Conc. **M**	**Calculated pH or H$^-$**	**k_{obs}** **hr^{-1}**
5.0	15.08	26.6
3.0	14.65	18.2
2.0	14.37	11.8
1.0	13.97	4.34
0.10	13.01	0.144
0.010	12.03	7.01×10^{-3}

Ionic strengths were not controlled. The wavelength used for UV studies was 254 nm.

Table IV- 10: Sodium hydroxide concentrations and observed rate constants for the hydrolysis of *p*-chloroformanilide at 25 °C.

NaOH Conc. **M**	**Calculated pH or H_-**	**k_{obs}** **hr^{-1}**
5.0	15.08	18.2
3.0	14.65	13.0
2.0	14.37	8.18
1.0	13.97	3.34
0.10	13.01	0.148
0.010	12.03	7.82×10^{-3}

Ionic strengths were not controlled. The wavelength used for UV studies was 263 nm.

Table IV- 11: Sodium hydroxide concentrations and observed rate constants for the hydrolysis of *p*-methoxyformanilide at 25 °C.

NaOH Conc. **M**	**Calculated pH or H$_-$**	**k_{obs}** **hr^{-1}**
5.0	15.08	25.1
3.0	14.65	20.2
2.0	14.37	12.8
1.0	13.97	5.03
0.10	13.01	0.156
0.010	12.03	9.01×10^{-3}

Ionic strengths were not controlled. The wavelength used for UV studies was 256 nm.

Table IV- 12: Sodium hydroxide concentrations and observed rate constants for the hydrolysis of *p*-methylformanilide at 25 °C.

NaOH Conc. **M**	**Calculated pH or H**$_-$	$\mathbf{k_{obs}}$ **hr**$^{-1}$
5.0	15.08	28.5
3.0	14.65	20.2
2.0	14.37	12.3
1.0	13.97	4.61
0.10	13.01	0.142
0.010	12.03	8.23×10^{-3}

Ionic strengths were not controlled. The wavelength used for UV studies was 255 nm.

Table IV- 13: Sodium hydroxide concentrations and observed rate constants for the hydrolysis of *m*-nitroformanilide at 25 °C.

NaOH Conc. **M**	**Calculated pH or H**$_-$	$\mathbf{k_{obs}}$ **hr**$^{-1}$
5.0	15.08	19.1
3.0	14.65	11.6
2.0	14.37	7.62
1.0	13.97	3.04
0.10	13.01	0.172
0.010	12.03	8.95×10^{-3}

Ionic strengths were not controlled. The wavelength used for UV studies was 261 nm.

Table IV- 14: Adjusted ionic strengths and observed rate constants for ionic strength studies for the hydrolysis of formanilide in 0.010 M sodium hydroxide solutions at 40 °C.

NaCl Added (M)	**Ionic Strength (μ)**	**k_{obs} $hr^{-1} \times 10^2$**
0	0.010	2.78
0.10	0.11	2.48
0.20	0.21	2.39
0.50	0.51	2.39
0.99	1.00	2.65

Ionic strength of the solutions was varied by addition of sodium chloride.

Table IV- 15: Concentrations of organic solvents and observed rate constants for the hydrolysis of formanilide in 0.10 M sodium hydroxide solutions containing different amounts of organic solvents at 40 °C.

Solvent	**% v/v**	**k_{obs}** $hr^{-1} \times 10^{1}$
Water	-	4.07
dioxane	25	1.28
dioxane	50	0.534
dimethyl sulfoxide	25	1.40
dimethyl sulfoxide	50	0.354

Table IV- 16: Reactions temperatures and observed rate constants for the hydrolysis of formanilide in 0.10 M sodium hydroxide solutions.

Temperature	**Ionic Strength**	$\mathbf{k_{obs}}$
°C	**μ**	$\mathbf{hr^{-1} \times 10^{1}}$
60	1.0	11.4
40	1.0	4.08
25	0.10	1.44

Ionic strength was adjusted with sodium chloride.

Table IV- 17: Observed rate constants for the hydrolysis of substituted formanilides in 0.10 M sodium hydroxide solutions at 40°C.

Substituent	**k_{obs}** **$hr^{-1} \times 10^1$**	**Substituent**	**k_{obs}** **$hr^{-1} \times 10^1$**
H	4.08	*p*-C_2H_5	3.58
p-CH_3	3.51	*m*-C_2H_5	3.01
m-CH_3	3.24	*o*-C_2H_5	0.750
o-CH_3	0.990	*p*-isoC_3H_7	3.43
p-Cl	3.56	*m*-isoC_3H_7	2.84
m-Cl	3.20	*o*-isoC_3H_7	0.675
o-Cl	2.05	*p*-OCH_3	3.61
p-NO_2	1510	*m*-OCH_3	3.09
m-NO_2	4.13	*o*-OCH_3	2.54
o-NO_2	2950	*p*-OH	4.13
p-Br	3.39	*o*-OH	2.80
m-Br	2.71	*p*-Phenyl	2.95
o-Br	3.30	*o*-Phenyl	0.750

Ionic strength of the medium was not adjusted except for *p*-hydroxyformanilide and *o*-hydroxyformanilide where it was 1.0. Wavelengths of UV-Vis analysis for *p*-nitroformanilide and *o*-nitroformanilide substituents were 398 nm and 418 nm, respectively.

The UV spectra collected as a function of time during degradation of formanilide was inspected for isosbestic points (Figure IV-4). The existence of isosbestic points can be used as an indicator for the number of absorbing species in the reaction mixture. An isosbestic point is typically observed when the reaction involves the presence of at two UV absorptive substrates which are inconvertible and have the same molar absorptivity at specific wavelengths. The chance of more than two UV absorptive substrates having the same absorptivity at the same points point is remote, and hence presence of isosbestic points is usually taken as confirmatory evidence for two UV absorbing species in solution. Aniline and formanilide in alkaline solutions have appreciable absorbance and isosbestic points were observed. The formate ion formed does not have appreciable absorbance at the concentrations tested and is not seen in the UV spectrum of the reactants. The spectrum of the degradation product was compared to aniline at the same concentration and was found to be identical using the peak purity software. The concentration-time profile and reaction scheme can then be described as Scheme IV-1. UV kinetic analysis was only used if the formanilide reaction followed Scheme IV-1 as determined by HPLC. The chemical reaction scheme is shown in Figure IV-5.

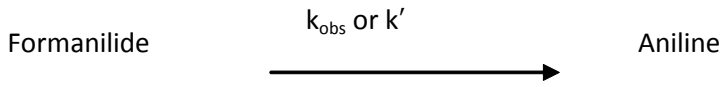

Scheme IV- 1

Similar to formanilide, the other substituted formanilides evaluated exhibited the same degradation scheme except the *ortho*- and *para*- hydroxyformanilides. The mass balance was not maintained for hydroxyl formanilides (*para* and *ortho*) due to the degradation of the aniline in alkaline solutions (Figure IV-7). This result was expected as aminophenols are unstable in solution and degrade rapidly.[29] The observed rate constant for loss of formanilide was attributed to conversion of formanilide to aniline.

Figure IV- 1: Representative chromatogram for the degradation of formanilide in 0.075 M sodium hydroxide solution using isocratic method with a C12 HydroRP Phenomenex 4µ 4.6×75 mm column using a mobile phase with 30:70 acetonitrile:water, at a flow rate of 0.8 mL/minute, an analytical wavelength of 235 nm and a runtime of 5 minutes. Peak at 2.7 minutes is formanilide and 3.5 minutes is aniline.

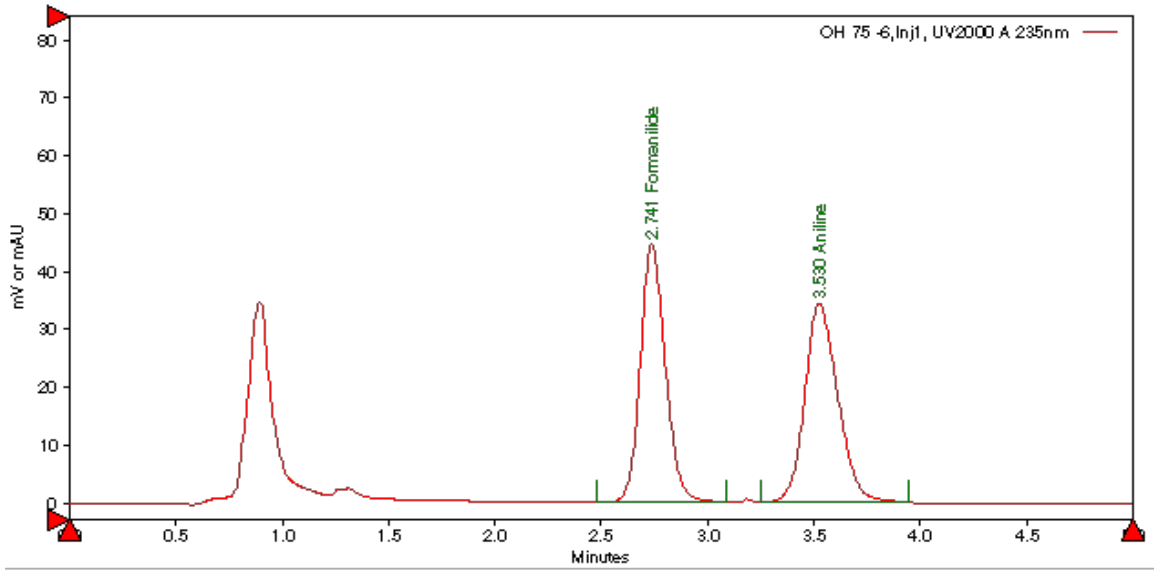

Figure IV- 2: Concentration-time profiles of hydrolysis of formanilide in 0.10-0.025 M sodium hydroxide at 1.0 ionic strength and 60 °C; (A) pH 11.77 (0.10 M) (B) pH 11.69 (0.075 M) (C) pH 11.55(0.050 M) and (D) pH 11.29 (0.025 M). Solid circles (●) represent loss of formanilide; solid squares (■) represent appearance of aniline and solid triangles (▲) represent mass balance for the reaction. The lines are interpolations.

(A)

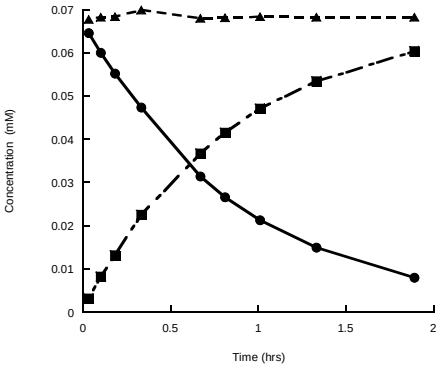

(B)

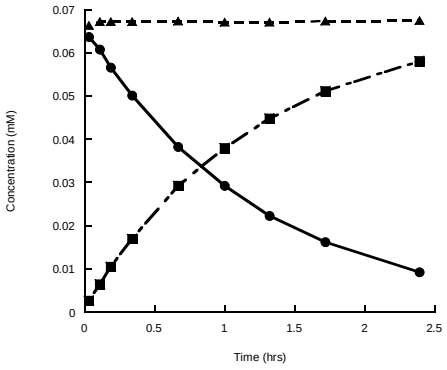

(C)

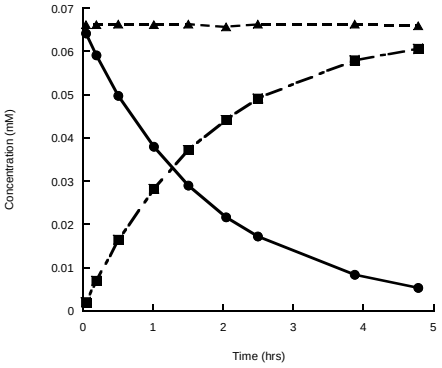

(D)

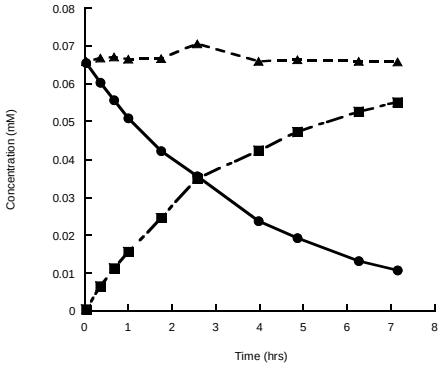

Figure IV- 3: Plot of concentration of formanilide versus time at pH 11.8 (●), pH 11.7 (■), pH 11.6 (▲), pH 11.3 (□) at 60 °C. The lines are first order fits to the data.

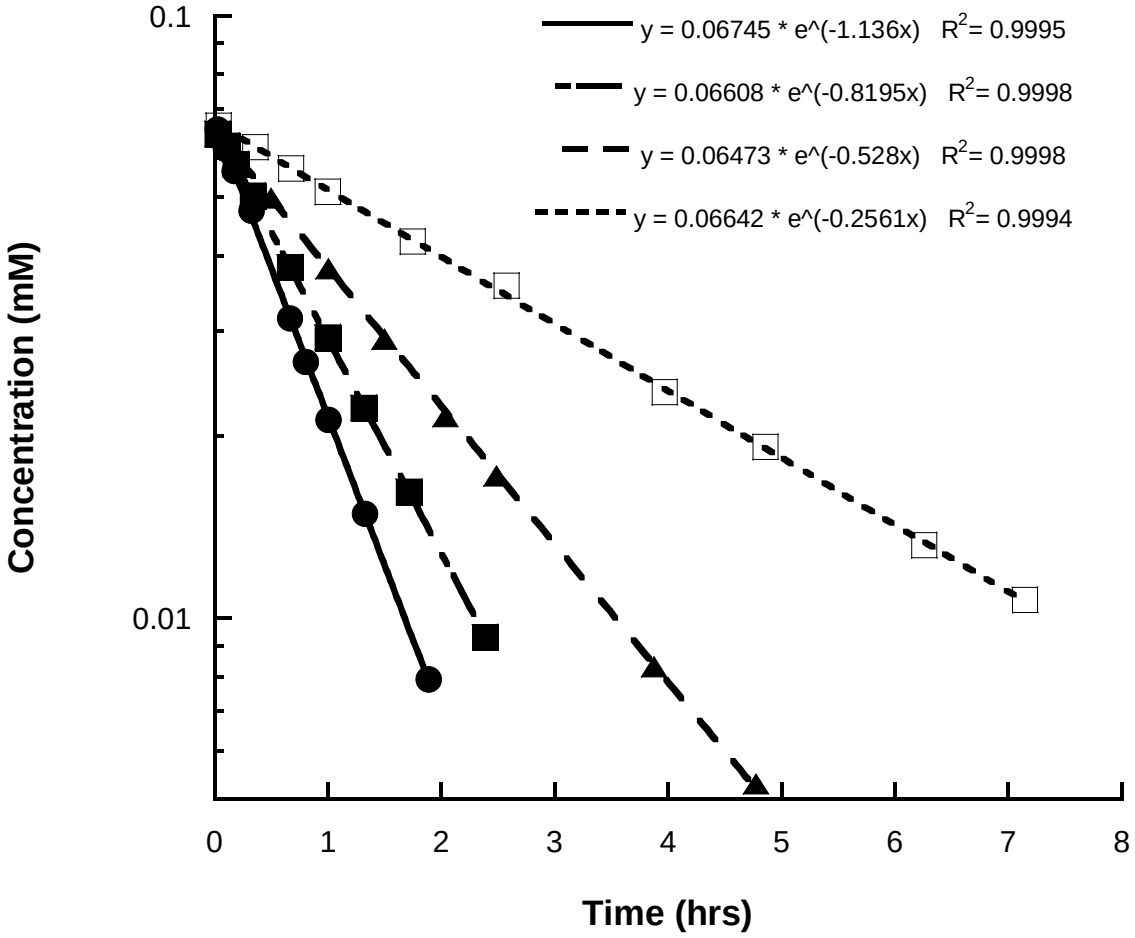

Figure IV- 4: UV Spectra collected as a function of time for the hydrolysis of formanilide in 1.0 M sodium hydroxide solution at 60 °C. The arrows point to the isosbestic points. The spectrum with the highest absorbance at 250 nm corresponds to formanilide while the spectrum with the lowest absorbance corresponds to the reaction products.

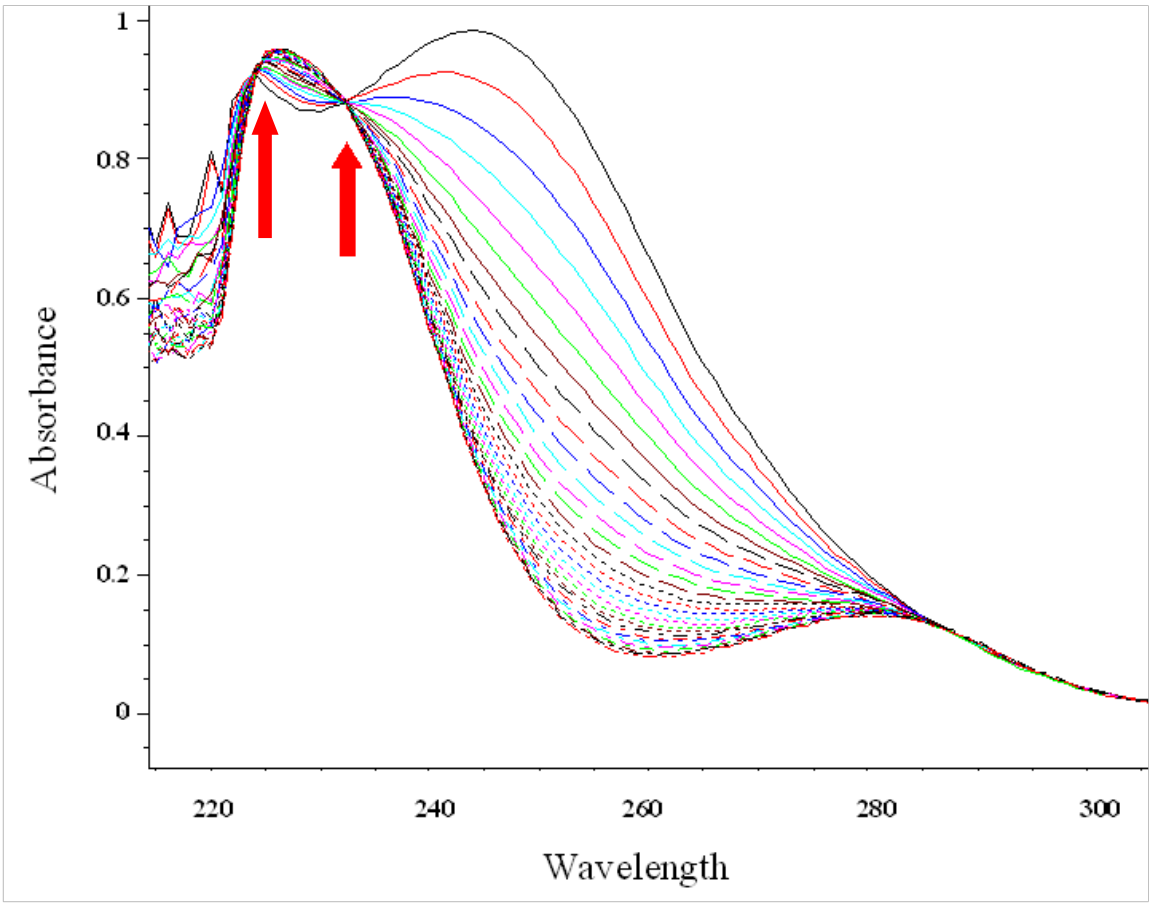

Figure IV- 5: Reaction scheme for hydrolysis of substituted formanilides in sodium hydroxide solution.

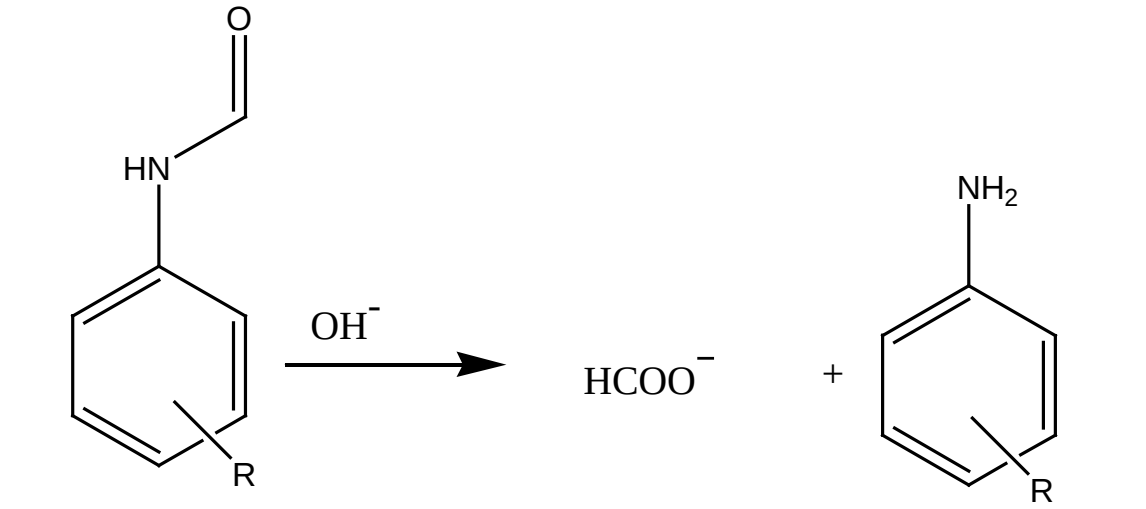

substituted formanilide formate substituted aniline

Figure IV- 6: Concentration-time profile for the hydrolysis of *p*-hydroxyformanilide in 0.010 M NaOH at 40 °C. The ionic strength of the solution was adjusted to 1.0 using sodium chloride. The filled circles (●) represent the concentration of formanilide while the open boxes (□) represent the mass balance for the reaction. The line is a first-order fit for the hydrolysis of *p*-hydroxyformanilide.

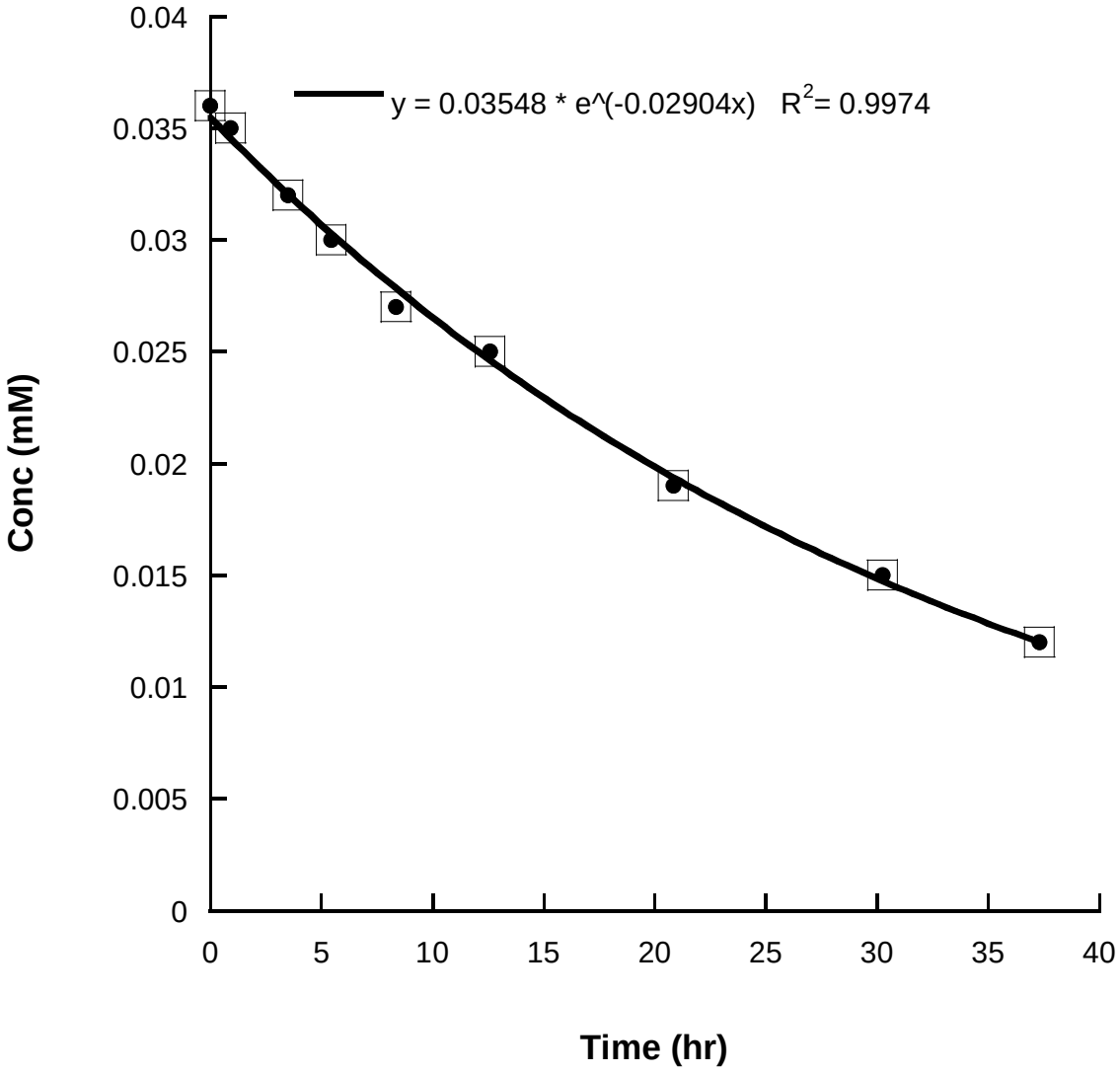

Effect of pH

The plot of k_{obs} at 40 °C against concentration of hydroxide for selected formanilides (formanilide, *p*-chloroformanilide, *p*-methylformanilide, *p*-bromoformanilide, *o*-methylformanilide, and *o*-bromoformanilide) was complex (Figure IV-7). The rate of hydrolysis increases nonlinearly with increasing concentration and the reaction shows specific base catalysis. At the high concentrations of hydroxide used (> 1.0 M) the activity of the hydroxide ion changes nonlinearly due to the reduction in the water activity. Therefore these data were not used in the construction of pH-rate profiles.

At 25 °C the observed rate profile for formanilide showed the same behavior as seen at 40 °C. At high concentrations of sodium hydroxide the conventional pH scale is not applicable. In such solutions the acidity functions (H_-) are used. Several different Hammett acidity functions for alkaline solutions have been devised based on the indicator series used and the function determined using the most structurally similar indicator molecule is used to study the effect of acidity on the reaction rates.[104] The H_- scale which utilizes thioacetamide as the indicator was used for formanilide since thioacetamide and formanilides are structurally similar. The H_- values from the literature were tabulated and H_- values corresponding to the known concentrations of sodium hydroxide were interpolated.[105, 106] These values were used to construct the pH-rate profile for formanilide by plotting the logarithm of the rate constant (k′) versus the calculated pH or H_- values as shown in Figure IV-8. The pH-rate profile displayed a downward bend consisting of a linear region with a slope 1.41 that decreases at $H_- > 14$. The slope value indicates a hydroxide concentration reaction order greater than first-order, while the presence of a plateau is likely due to formanilide ionization (pK_a 13.89 at 20 °C).[14] To account for substrate ionization, the observed rate constants (k_{obs}) were divided by the fraction of uncharged substrate and used to reconstruct a pH-rate profile (Figure IV-9) that is linear with a slope of 1.62. This higher than first order but less than second order dependence on hydroxide concentration, type of behavior has been noted

for anilides, and a scheme involving both a higher order dependence on hydroxide concentration and reduction in reactive substrate due to ionization has been proposed (Scheme IV-2).[13, 15, 17] The unionized substrate (F_{HA}) can deprotonate to form a conjugate base (F_A^-) which is unreactive. The unionized formanilide (F_{HA}) can be attacked by hydroxide ion to form a tetrahedral intermediate (I). This tetrahedral intermediate can degrade to starting materials or products. According to the proposed scheme the formation of products is catalyzed by water or hydroxide ion. In Scheme IV-2 k_{obs} is the observed rate constant, k_a is the rate constant for the addition of hydroxide ion to the unionized substrate, k_{-a} is the rate constant for the degradation of the intermediate to reactants, k'_1 is the rate constant for the conversion of the intermediate to the products via the water catalyzed pathway, k'_2 is the rate constant for the conversion of the intermediate to the products via the hydroxide ion pathway, and K_a is the ionization constant for the formanilide. Using the steady state assumption, the rate law is given by Equation IV –1, where k_1 is the complex rate constant for the conversion of reactants to products via the water catalyzed pathway (Equation IV-2), k_2 is the complex rate constant for the conversion of reactant to products via the hydroxide catalyzed pathway (Equation IV-3), and K_w is the autoprotolysis constant for water. The rate law as derived (Equation IV-1) is applicable in dilute solutions and does not take into account the water molecules involved in the reaction. At high hydroxide concentrations (>0.1 M) there is an increase in the hydration of the hydroxide ion with an concurrent decrease in the activities of the hydroxide ion and water in the solution which affect the observed rate constant.[107, 108] The change in the hydration of hydroxide ion with increasing concentration was accounted for by using the H_- values instead of hydroxide concentrations. In the sodium hydroxide concentration range studied (0.010 M to 3.0 M) the activity of water drops from 1 to 0.88.[109] Water molecules are involved in all the aspects of the reaction i.e, hydration of the formate and hydroxide ions; solvation of the reactants, intermediates and products; and water catalyzed pathway for decomposition of the intermediate. The net

effect of decrease in water activity on the reaction is not clear and due to the complexity of the model the effect of water activity on the rate constant was not evaluated.

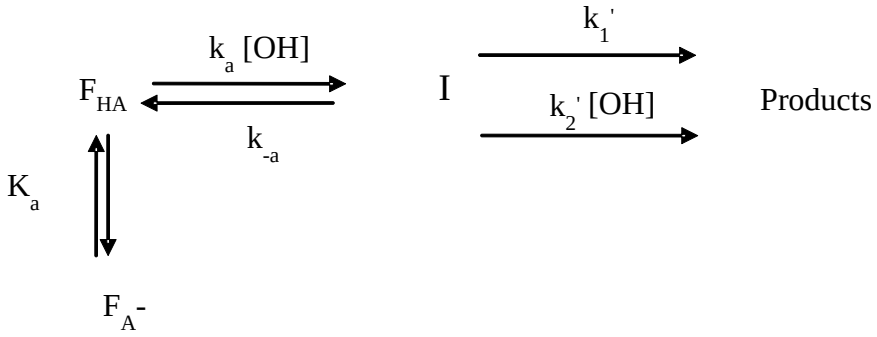

Scheme IV- 2

$$k_{obs} = \frac{k_1 + k_2[OH]}{k_a + k_1 + k_2[OH]} k_a[OH](\frac{K_w}{[OH]K_a + K_w})$$ Equation IV-1

$$k_1 = k_1' \frac{k_a}{k_{-a}}$$ Equation IV-2

$$k_2 = k_2' \frac{k_a}{k_{-a}}$$ Equation IV-3

pH-rate profiles for selected substrates (*p*-chloroformanilide, *p*-methylformanilide, *p*-methoxyformanilide, and *m*-nitroformanilide) at 25 °C in hydroxide solutions were also constructed. The substituents were chosen since their sigma values represent the range of electronic effects. The rate constants for *p*-methoxy, *p*-methyl, *p*-chloro, and *m*-nitro substituted formanildes also displayed profiles similar to formanilide. Attempts to determine the pK_a of these formanilides were not successful since the compounds degrade rapidly in alkaline solutions, and even at the highest hydroxide concentration tested some of the formanilides were not completely deprotonated. Hence pK_a values for formanilide and *m*-nitroformanilide were taken from literature. The pK_a values for the *p*-chloro, *p*-methyl and *p*-methoxy substituted formanilides were calculated

using a Hammett relationship (Equation IV-4) for the reported ionization constants for formanilides at 20 °C using σ^0 (Taft substituent constants for well behaved substituents that do not show resonance delocalization interactions) and are given in Table IV-18. [14, 110]

$$pK_a = -1.52 \times \sigma^0 + 13.8 \qquad \text{Equation IV-4}$$

The k_1, k_2 , k_a values were estimated by fitting the data to Equation IV-11 using nonlinear regression in JMP®. The corrected hydroxide concentrations using H- was the independent variable and observed rate constants (k_{obs}) were the dependent variables. Since the rate constants at higher concentrations are several magnitudes of order higher than the rate constants for the reactions at lower concentrations these rate constants had a larger influence on the sums of squares values leading to a bias in the parameter estimates. To ensure that all the data were evaluated uniformly the rate constant data were weighed using the square of reciprocal of the rate constant (k^{-2}).[111] Figure IV-10 shows the agreement between model estimated and observed data for formanilide hydrolysis. The estimated rate constants are tabulated in Table IV-18. For methoxy, methyl, chloro, and unsubstituted formanilides the model fit well and the confidence intervals could be estimated at 95 % and the coefficients of variation were less than 20%. However the parameter estimates for the *m*-nitroformanilide showed higher variation with a coefficient of variation around 60%. The confidence intervals could not be estimated for both k_a and k_2 at 95% confidence intervals, however they could be estimated at 90% confidence intervals for all the parameters for *m*-nitro substituted compound. This increase in the variability of the estimates could be due to the inaccuracy in the determination of the rate constants or ionization constants for *m*-nitroformanilide due to the instability of this formanilide in alkaline solutions.

Figure IV- 7: Plot of k_{obs} against sodium hydroxide concentrations for hydrolysis of formanilides in alkaline solutions at 40 °C. The formanilides shown are formanilide (○), *p*-bromoformanilide (▲), *o*-bromoformanilide (♦), *o*-methylformanilide (■), and *p*-methylformanilide (●). The curves are interpolations.

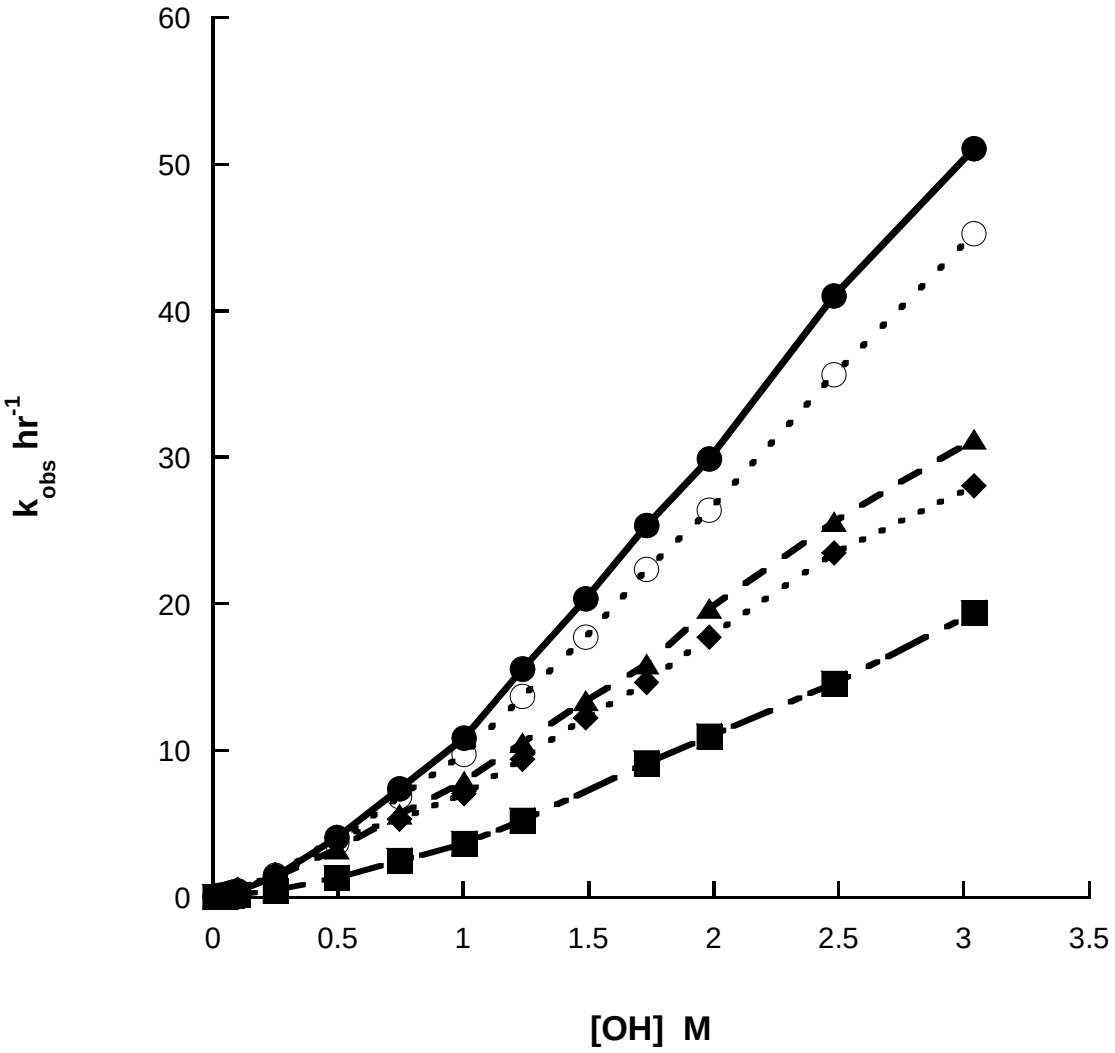

Figure IV- 8: pH-rate profile for hydrolysis of formanilide using the k_{obs} at 25 °C. The dotted line is a linear regression fit to the data for the linear portion of the pH-rate profile.

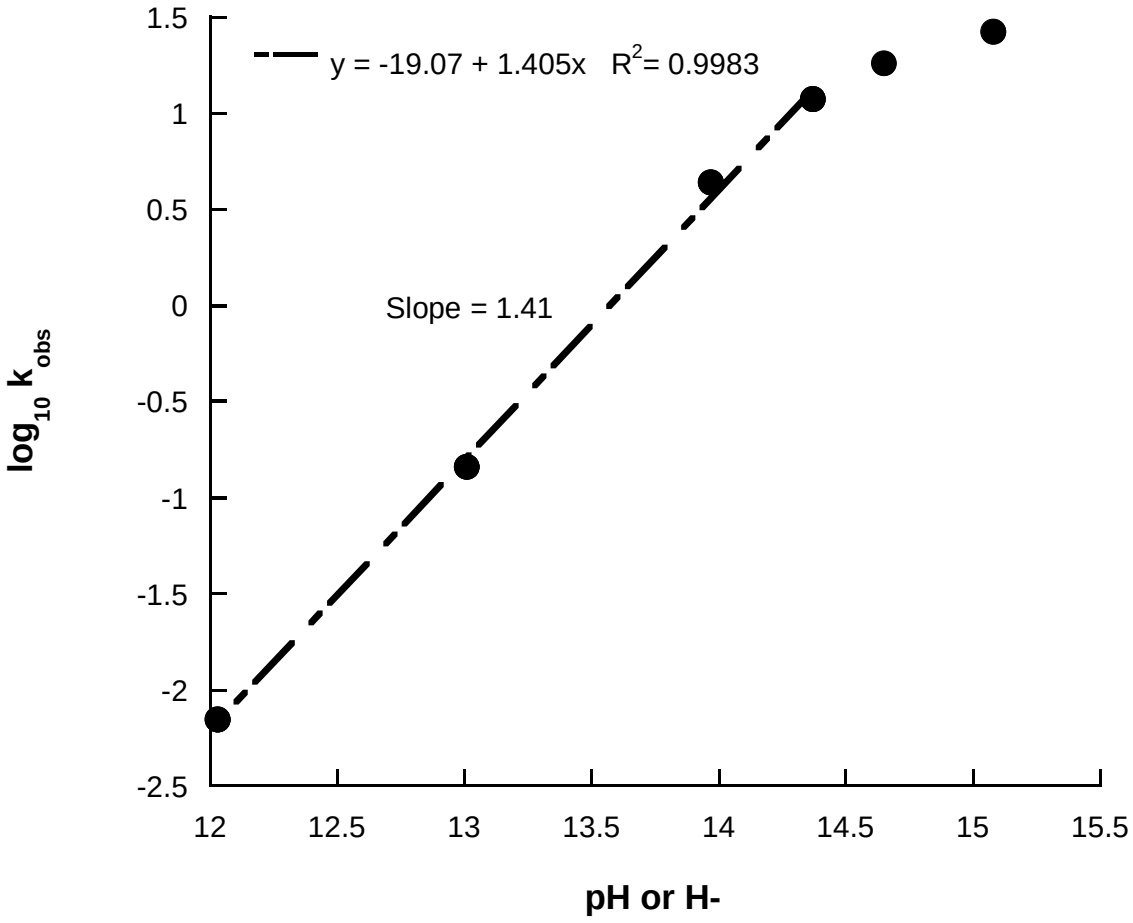

Figure IV- 9: pH-rate profile for hydrolysis of formanilide using the observed rate constants (k_{corr}) corrected for ionization of the substrate at 25 °C. The solid line is represents a line obtained by linear regression.

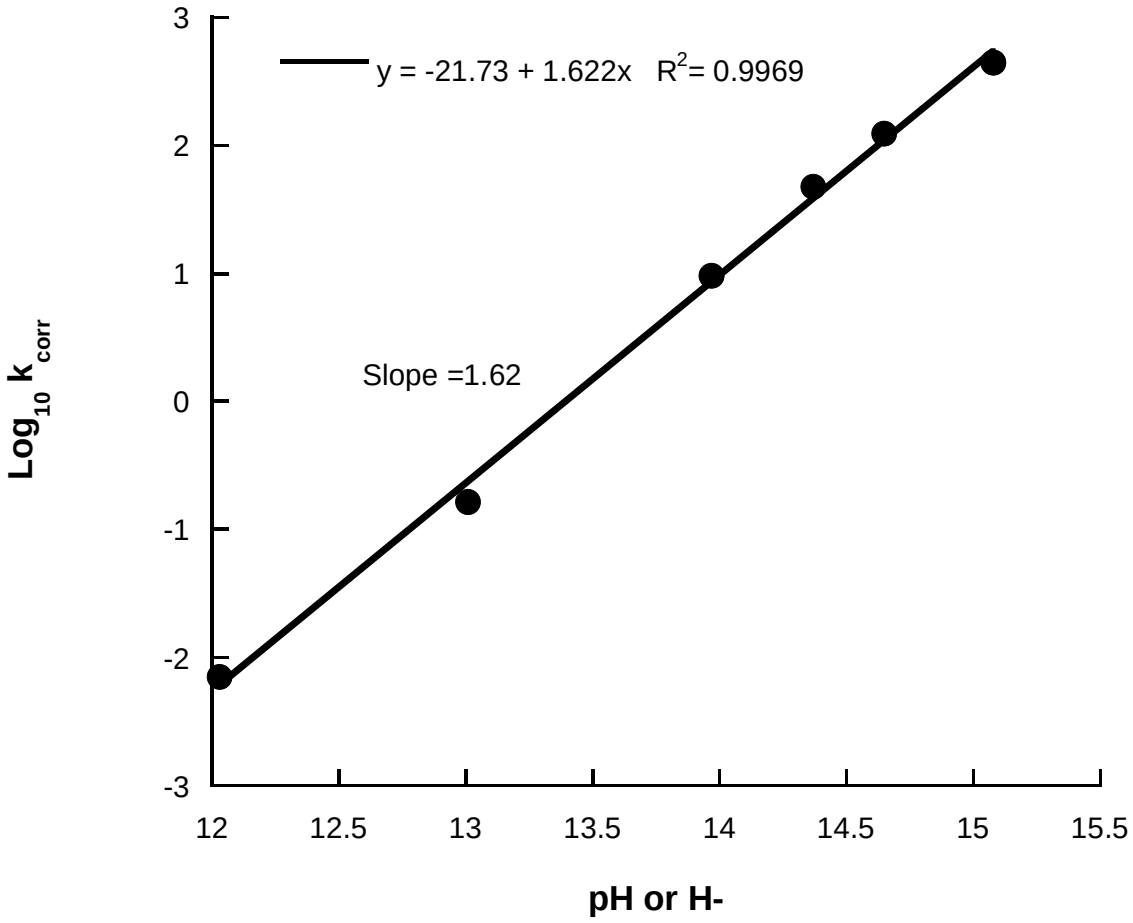

Figure IV- 10 pH-rate profile for hydrolysis of formanilide using the observed rate constants (k_{obs}) at 25 °C. The solid line was simulated using Equation IV-1 and estimates from Table IV-18.

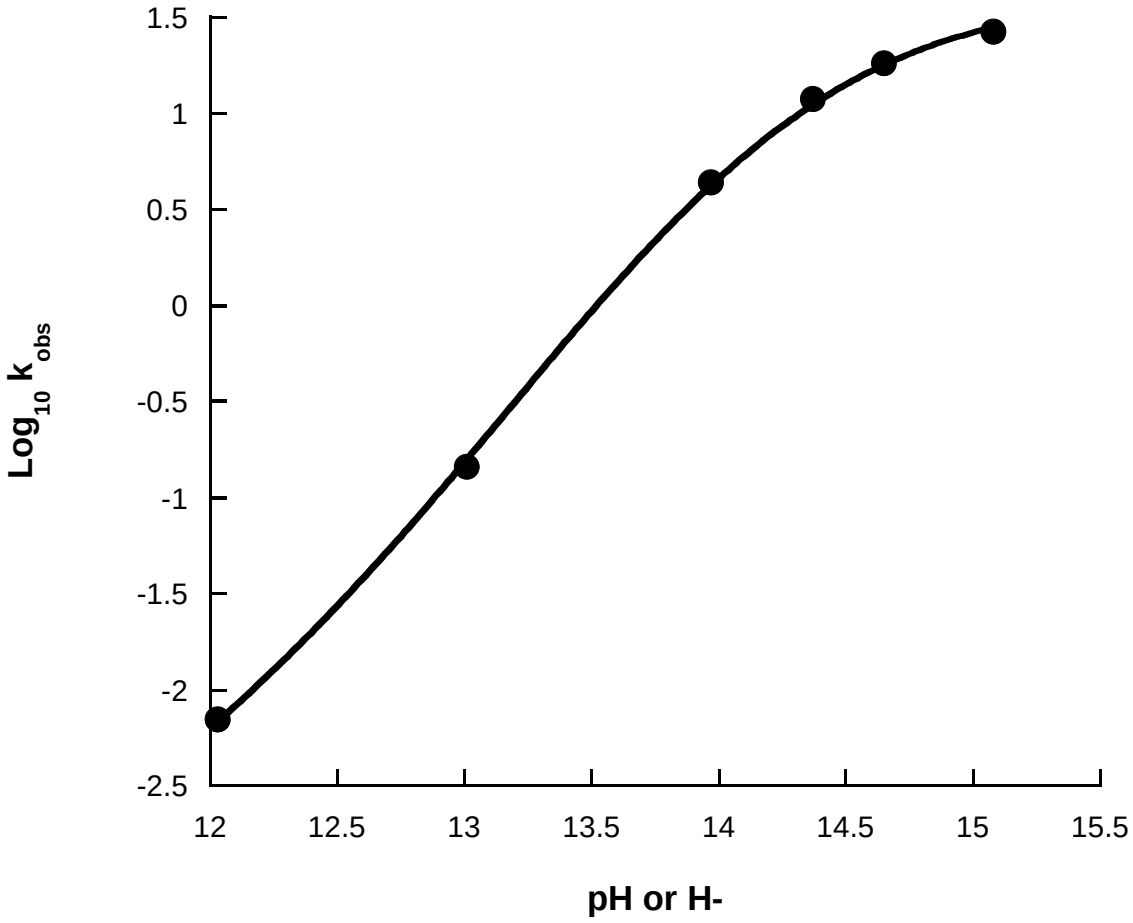

Table IV- 18: Rate constants and ionization constants for the base catalyzed hydrolysis of formanilides at 25° C.

	pK_a	**k_a ± S.E.** $M^{-1}hr^{-1}$	**k_1 ± S.E.** $M^{-1}hr^{-1}$	**k_2 ± S.E.** $M^{-2}hr^{-1}$
p-methoxy[c]	14.1[b]	30.7 ± 3.9	0.684 ± 0.117	12.8 ± 1.95
p-methyl[c]	14.0[b]	40.0 ± 4.7	0.629 ± 0.079	11.2 ± 1.25
H[c]	13.9[a]	51.1 ± 5.0	0.514 ± 0.054	12.6 ± 1.00
p-chloro[c]	13.4[b]	121 ± 26	0.527 ± 0.113	18.2 ± 2.27
m-nitro[d]	12.8[a]	760 ± 366	0.389 ± 0.231	50.8 ± 7.70

[a] pK_a values from literature; [b] pK_a values calculated using the Hammett relationship (Equation IV-4); and [c] 95% confidence intervals were generated for all parameters

[d]90% confidence intervals were generated for all parameters

Effect of Ionic Strength

Ionic strength (μ) studies were carried out by measuring the k_{obs} for formanilide in 0.010 M sodium hydroxide solutions at 40 °C using different concentrations of salt (sodium chloride). Ionic strength values (0.51 to 0.01) were varied by varying the concentration of sodium chloride. The activity coefficients (γ) were approximated using the Guntelberg equation (Equation IV-5) where z_i is the charge on the ion. A plot of the logarithm of the observed rate constants versus substrate activity coefficient (Figure IV-11) showed a linear relationship with a slope near zero (-0.212) indicating the lack of significant primary salt effects.[48]

$$\log \gamma = \frac{2 z_i^2 \sqrt{\mu}}{1 + \sqrt{\mu}} \qquad \text{Equation IV-5}$$

Binary Solvent System Studies

Degradation of formanilide in binary mixtures of aqueous organic solvents at alkaline pH was studied using two organic solvents that were chosen to provide a range of dielectric constants and hydrogen bonding characteristics. The dielectric constants and classification are as follows: water (78.3, protic), dimethyl sulfoxide (49, dipolar aprotic) and dioxane (2.21, aprotic).[102] Studies were carried out in 0.10 M sodium hydroxide solutions at 40 °C at different concentrations of organic solvents and rate constants (k_{obs}) were calculated for the degradation of formanilide. The rate constants plotted as the function of the % v/v organic contents (Figure IV-12).

Effect of Temperature

The rate of formanilide degradation increases with temperature and can be described by Arrhenius plots (Figure IV-13). Activation energy (E_a) was estimated from the slope of the Arrhenius plot and the natural log of the frequency factor (ln A) was also determined (Equation IV-6). The activation enthalpy and entropy changes were

calculated using Equations IV-7 and IV-8 over the temperature range and reported in Table IV-19. Standard errors were also calculated for the estimated parameters.

$$\ln k = \ln A - \frac{E_a}{R}\frac{1}{T} \qquad \text{Equation IV-6}$$

$$\Delta H^{\ddagger} = E_a - RT_{mean} \qquad \text{Equation IV-7}$$

$$\Delta S^{\ddagger} = R\ln A - R\ln(\frac{kT_{mean}}{h}) - R \qquad \text{Equation IV-8}$$

Where T is the reaction temperature (K), T_{mean} is the absolute temperature (K) in the middle of the experimental temperature range, R is the ideal gas constant (1.987 cal $^{-1}K^{-1}$ mol^{-1}), k_{obs} is the observed rate constant (s^{-1}), k is the Boltzmann constant (1.38×10^{-16} erg K^{-1}) and h is Planck's constant (6.626×10^{-27} erg s)

Discussion

The effect of increasing hydroxide ion concentration on the rate of the reaction is complex. A Hammett plot of the k_{obs} values at different hydroxide ion concentrations (0.010 M, 0 0.10M, 1.0 M and 5.0 M) shows that the net effect of substituents was small and the estimated reaction constants (ρ) are close to zero (Figure IV-14 (A)). However the Hammett plot of the substrate ionization normalized rate constants (k_{corr}) showed that the reaction constants are dependent on the concentration of the hydroxide ion in the reaction mixture (Figure IV-18(B)). The reaction constants at 0.010 M, 0.10M, 1.0 M, and 5.0 M hydroxide concentrations were 0.09, 0.46, 0.77, and 1.13 respectively. The value of the reaction constant increased with increase in the hydroxide ion concentration.

To elucidate the reason behind this behavior the pH-rate profiles for formanilides were described by Scheme IV-2 and the rate constants k_a, k_1 and k_2 were determined by fitting the data to the rate law (Equation IV-1). Hammett plots for each pathway were constructed (Figures IV-15 to Figure IV-17). The rate constant k_a for the addition of the hydroxide to the formanilide increases with increase in the electron withdrawing

Figure IV- 11: Plot of log of the rate constants against the ionic strength of the medium. Rate constants were determined in 0.010 M sodium hydroxide at 40 °C. Ionic strength was varied using sodium chloride. The solid line is a linear regression fit to the data.

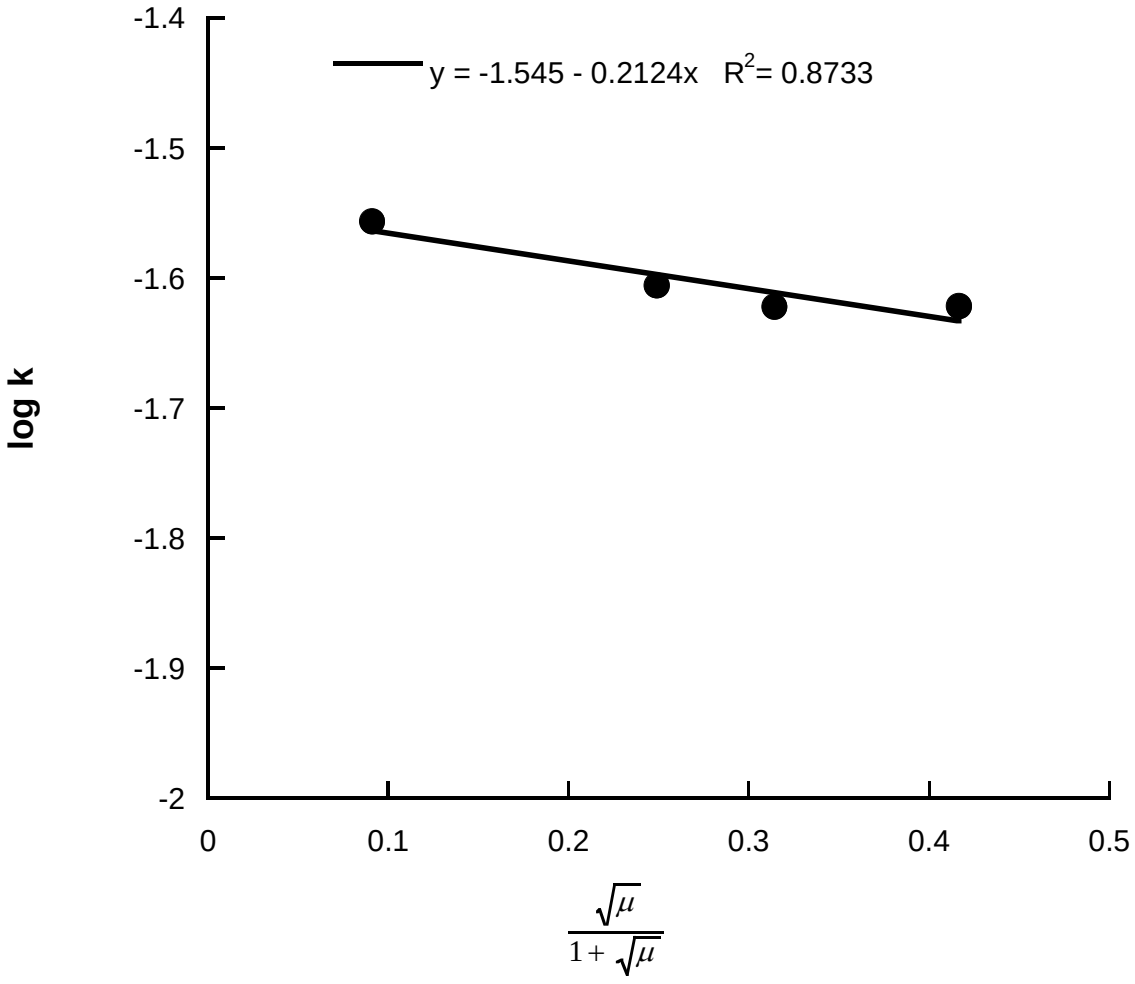

Figure IV- 12: Effect of increasing organic solvent concentrations on the rate constants for hydrolysis of formanilide in aqueous organic solutions in 0.10 M sodium hydroxide solutions at 40 °C. The closed circles (●) represent reactions in dimethyl sulfoxide solutions and closed square (■) represent reactions in dioxane solutions. The lines are interpolations.

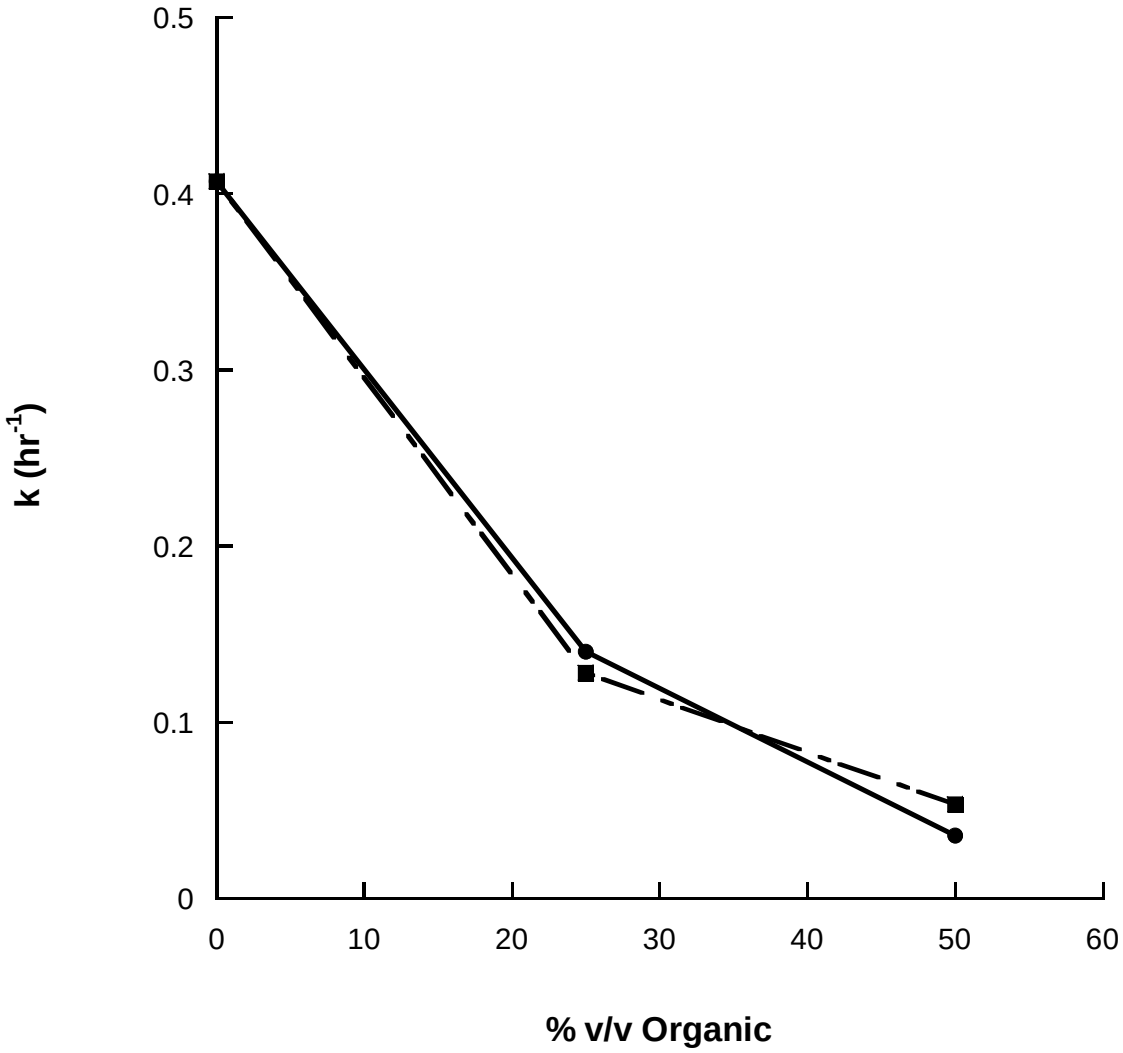

Figure IV- 13: Arrhenius Plot for the temperature dependence of formanilide degradation in 0.10 M sodium hydroxide solutions plot: Solid line is the fit to the linearized Arrhenius equation (Equation IV-6).

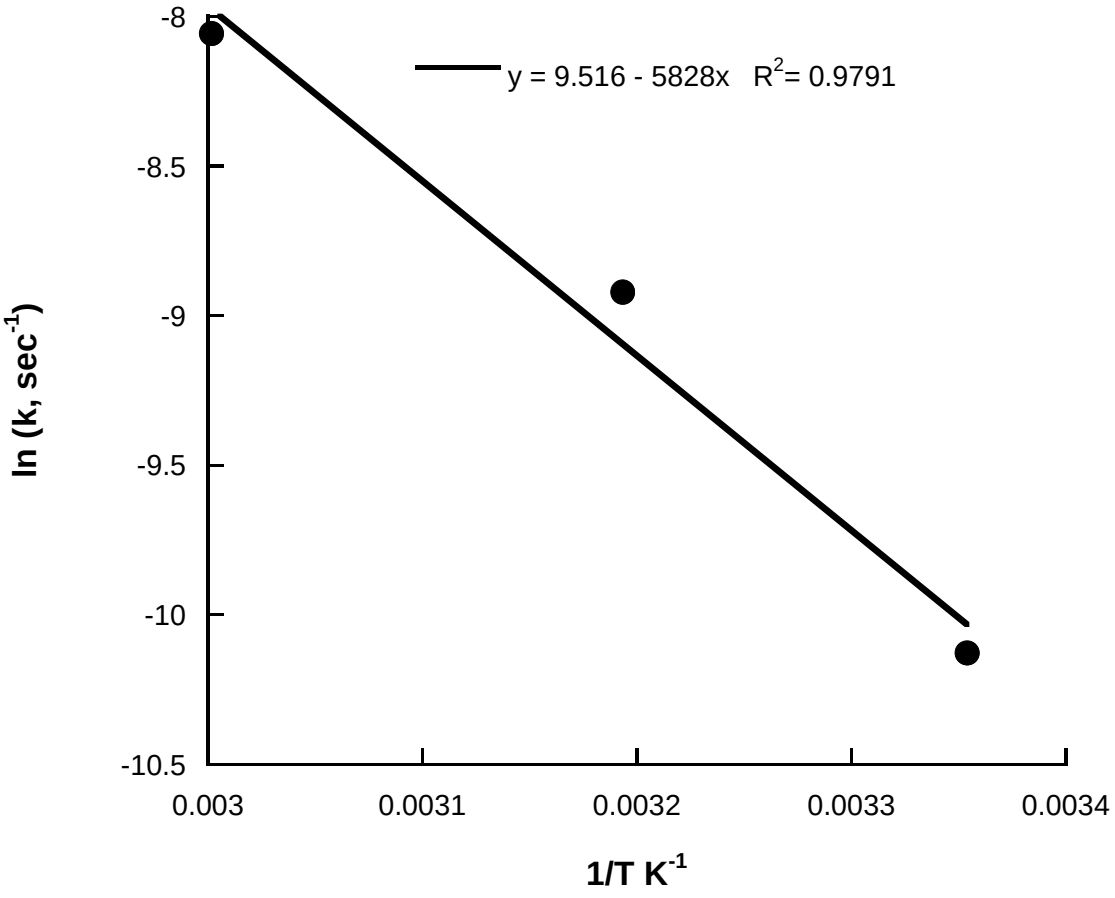

Table IV- 19: Activation parameters for degradation of formanilide in 0.10 M sodium hydroxide.

ln A ± S.E.	9.52 ± 2.71
E_a ± S.E. (kJ mol^{-1})	48.6 ± 7.1.
$\Delta H^{\ddagger}$ ± S.E. (kJ mol^{-1})	45.8 ± 7.1
$\Delta S^{\ddagger}$ ± S.E. (J $mol^{-1}K^{-1}$)	175 ± 23

capability of the substituent The Hammett plot for k_a was linear with the reaction constant (ρ_{ka}) value of 1.39, which indicated that the reaction is accelerated by electron withdrawing groups(Figure IV-15). . The complex rate constant k_1 decreased with increasing electron withdrawing capability of the substituent. The reaction constant (ρ_{k1}) was -0.23 indicating that the reaction process is accelerated by electron donating groups (Figure IV-16). The complex rate constant k_2 showed an increase with increasing electron withdrawing capability of the substituent the estimated reaction constant (ρ_{k2}) of 0.64 (Figure IV-17). The reaction steps associated with the rate constants k_1 and k_2 had opposite dependence on the electronic properties of the substituent.

The k_{obs} at low hydroxide ion concentration (<0.10 M) is a mixture of the first and second-order rate constants; however the overall rate constant is dominated by the first-order rate process. Based on the rate law, the transition-state for the rate-determining step for the first-order rate process is expected to consist of a charged intermediate and water. The absence of an ionic strength effect matches the expectations of an charged substrate, and water (uncharged species) involved in the rate limiting transition-state.[48] These results are in agreement with the results of Bergstrand for hydrolysis of formanilide at 55 °C.[32]

Since the rate-determining state for the water catalyzed pathway contains a water molecule, decreasing the activity of water would lead to a decrease in the overall rate of the reaction. Increasing the concentration of dimethyl sulfoxide (DMSO) and dioxane both lead to substantial decreases in the activity of water in the solution which leads to a decrease in the observed rate constants.[52, 112] Also since the rate-determining transition-state is expected to be polar, increasing the organic solvent concentration will decrease the dielectric constant of the solvent, negatively impacting the stability of the transition-state. This would also lead to a decrease in the rate in accordance with the Hughes Ingold rules.[113] DMSO is expected to show an increase in the rate of hydrolysis due to its ability to solvate hydroxide ions and increase their basicity.[51]

Hence if the addition step was the rate determining step was there should have been an increase in the rate of the reaction. The absence of the increase indicates that the water catalyzed decomposition of the intermediate is the rate determining step at 0.01 M sodium hydroxide concentration. It is interesting to note that both DMSO and dioxane show very similar behavior even though they have very different hydrogen bonding characteristics and dielectric constants.

Temperature studies were carried out on formanilide in 0.10 M sodium hydroxide solutions, and the results are tabulated in Table IV-23. The activation energy for the hydrolysis of formanilide was 48.6 ± 7.1 kJ mol^{-1}. The activation energy values are in the range of 41-125 kJ mol^{-1} expected for most hydrolysis reactions.[45] The enthalpies of activation ($\Delta H^{\ddagger}$) were positive, and the entropies of activation ($\Delta S^{\ddagger}$) were negative and are in agreement with earlier results.[16, 35] The large negative entropy of activation also suggests that the transition-state contains considerable bound water.[16, 106]

The results for the pH-rate profile, ionic strength studies, binary solvent studies, temperature studies, and the substituent effect studies can be summarized as follows: (1) the rate law is complicated and shows first- and second-order dependence on hydroxide ion concentration; (2) solvent studies and ionic strength studies on formanilide at low hydroxide concentrations indicate a rate-limiting transition-state composed of ionized intermediate and water molecules; (3) the temperature studies for formanilide point to the formation of the transition-state containing bound water; and (4) the Hammett plots of the individual rate constants point towards a complex reaction mechanism.

These observations are consistent with the modified base catalyzed acyl cleavage bimolecular mechanism ($B_{AC}2$) as shown in Figure IV-18.[13, 17, 114-117] The formanilide can ionize to form an unreactive conjugate base by a competitive side equilibrium. The unionized formanilide can be attacked by a hydroxide ion to form a tetrahedral intermediate (monoanion). The tetrahedral intermediate may revert to starting materials or hydrolyze to cleavage products via water or hydroxide ion catalyzed

pathways similar to Scheme IV-2. The water mediated pathway forms a dipolar ion by transferring the proton from the hydroxyl group to the amine, therefore water acts as a proton transfer agent. The hydroxide ion catalyzed pathway forms a dianion by deprotonating the hydrogen from the hydroxyl group. The dianion and dipolar ion can either revert to the monoanion or decompose to products.

The proposed mechanism is consistent with the Hammett plots. The formation of the tetrahedral intermediate (monanion) occurs by the addition of hydroxide to the carbonyl carbon. The presence of strong electron withdrawing groups will withdraw electron density away from the carbonyl carbon which enhances the ability of the hydroxide ion to attack the carbonyl carbon. Thus the predicted value for the reaction constant is positive. The ρ_{ka} value of 1.34 is in agreement with this prediction and consistent with reaction constants for similar reactions such as alkaline hydrolysis of acetanilide (1.0), and 2,2,2-trifluoroacetanlide (1.18) [12, 13, 17]

The value of k_1 and k_2 can be explained by splitting the processes into two steps (1) the formation of the intermediate and (2) degradation of the intermediate either to products or reactants. The formation of the intermediate is given by k_a while the partition of the intermediate via k_1 and k_2 processes is given by the partition ratios k'_1/k_{-a} and k'_2/k_{-a} , respectively. The partition ratios were calculated by multiplying the complex rate constant k_1 and k_2 with k_a (Equation IV-2 and IV-3). In Figure IV-19 The Hammett plot for the rate constants (k_a, k'_2/k_{-a} and k'_2/k_{-a}) are shown. The value of the reaction constant ρ_{ka} for the addition step is 1.40 while the value of reaction constant for the partition ratio ($\rho_{k'1/k-a}$) is -1.63. The overall reaction constant for the first-order process (ρ_{k2}), -0.23, is the sum of the reaction constants for the two steps and in this case the magnitude of the substituent effect for the partitioning process predominates in the net reaction constant. This value is comparable to the value of -0.4 obtained in the alkaline hydrolysis of acetanilide (recalculated for three substituents at 0.239 M hydroxide).[12]

The second-order process, denoted by k_2, has a reaction constant of +0.631 which can also be explained using a similar approach. For this process the value of the reaction constant for the partition ratio ($\rho_{k'2/k\text{-}a}$) is -0.76. This value is significantly smaller than the reaction constant for the addition process and hence the substituent effect for the formation of the intermediate predominates in the net reaction constant (ρ_{k2} =0.64).

The mechanism in Figure IV-18 implies that the hydrolysis of the amide will be affected by the basicity of the leaving group. Increase in the electron density at the amino group would stabilize the leaving group, and hence electron donating groups would enhance the breakdown of the dipolar ion and the dianion to products. The negative reaction constant values for the partition ratios ($\rho_{k'1/k\text{-}a}$ = -1.63) and ($\rho_{k'2/k\text{-}a}$ = -0.76) support this hypothesis. The basicity of the leaving groups can be estimated using an appropriate reference reaction. The leaving groups for the first- and second-order pathways resemble the protonated groups for the ionization for anilines and formanilides, and hence these were used as the reference reactions. The Hammett relationships for the protonation of the aniline and formanilide groups have the reaction constants of -2.77 and -1.53, respectively.[118] This reduction in the basicity of the leaving group could account for the differences between the reaction constants for partition ratios of the two pathways.

Due to the complex kinetic scheme it was not possible to study the effect of ortho substitution on each pathway individually. Hence substituent effects were evaluated on the k_{obs} in 0.10 M sodium hydroxide solutions at 40 °C. The Hammett plot for the *para* and *meta* substituted formanilides in 0.10 M sodium hydroxide at 40 °C is shown in Figure IV-20. The Hammett sigma values were used to prepare the Hammett plot. At this sodium hydroxide concentration the hydroxyl group is deprotonated (pK_a = 9.57) and the substituent constant corresponding to the phenoxide (-0.81) was used for p-hydroxyformanilide. Almost all of the substrates appear to lie close together in a linear trend except the *p*-nitro substituent which deviates significantly from the other

substituents. Such a deviation from the correlation line is an indication that the substituted formanilide follows a different mechanism from the rest of the formanilides. Strongly electron withdrawing substituents (*p*-nitro, *p*-cyano, and *p*-formyl) capable of strong inductive and resonance interactions appear to follow a different mechanism.[16, 115, 119] Though the mechanism is still not clear, studies on the *p*-nitro substituted derivatives of acetanilides and N-methyl acetanilides appear to hydrolyze by a mechanism where the dianion undergoes direct carbon-nitrogen bond scission.[16, 115, 120, 121]

If the p-nitro derivative is ignored, a linear Hammett plot is observed with a ρ of -0.00976; however, the correlation is very poor (R^2=0.00352). At this hydroxide concentration the rate constant (k_{obs}) is a function of both the first- and second-order pathways. Both these pathways display opposite substituent effects and the observed reaction constant is a sum of both these pathways. Hence the net effect was that the reaction constant (ρ) was approximately zero and substituent effects are not observed.

To observe the effect of ortho substitution on the rate constant, a Hammett plot of the *para* and *ortho* substituted formanilides was constructed using Hammett sigma values (Figure IV-21). For the *o*-hydroxyformanilide the sigma value for the phenoxide (-0.81) was used since the hydroxyl group is deprotonated (pK_a = 8.96) at this sodium hydroxide concentration. It was observed that most of the ortho substituted formanilides hydrolyze slower than their para substituted counterparts. The reductions in the rate constants are significant (> 80% reduction for isopropyl group). The apparent reduction in the rate constants appears to correlate with the steric substituent constants (E_s) as shown in (Figure IV-23). The Taft-Kutter-Hansch steric substituent values were used since they account only for the steric component of the reaction.

To simplify the plot (Figure IV-21) the chemical reactivities of all of the substituents were individually evaluated. The nitro and hydroxyl substituents display behaviors different from the other substituents and their reactivities were examined.

The relative instability of *p*-nitroformanilide was explained earlier as degradation via a different mechanism, and it is expected that the *ortho*-nitro substituent follows a similar mechanism since both the *p*-nitro and *o*-nitro substituent can interact with the reaction center by inductive as well as resonance interactions. In the *ortho* position the inductive effect increases due to the proximity of the substituent to the reaction site and as predicted the *o*-nitro reacts much faster than the *p*-nitro substituent. It is not clear if there is steric inhibition for this substituent since the decrease in the rate constant due to inhibition could be counteracted by the increase in the rate constant due to an increase in the inductive effects.

At 0.10 N sodium hydroxide concentration the hydroxyl group of the *o*-hydroxyformanilide is deprotonated ($pK_a = 8.96$), and the molecule exists as a phenoxide. Since the intermediate and the transition-states are negatively charged, the presence of a negatively charged ion close to the reaction site is expected to decrease the rate of the reaction due to electrostatic repulsion. *o*-hydroxyformanilide showed a decrease in the rate as compared to the *para* counterpart which could be due to both the effect of ionization and/or steric effects.

Once these substituents are removed from the Hammett plot the differences between the *para* and *ortho* substituted formanilides became clearer (Figure IV-22). Substituents in the *para* position are capable of electronic effects (inductive and resonance) while the substituents in the *ortho* position are capable of electronic and steric effects. Since the Hammett plots for the *para* and *meta* substituents did not show any significant substituent effects on the observed rate constant, the decrease in rate constants for ortho substituted derivatives was attributed to the steric component.

To observe the steric effect, the rate constants for the *ortho* substituted formanilides were plotted against the Taft-Kutter-Hansch steric substituent value (E_s), which corrects only for the steric bulk effect (Figure IV-23). A trend appears where the increase in the steric bulk leads to a corresponding decrease in the rate of the reaction.

The phenyl group, since it is a planar group, has three E_s values. The largest E_s value (-3.82) is used if phenyl ring is planar to the phenyl ring of the substituent while the smallest E_s value (-1.01) is used if the phenyl group is perpendicular to the phenyl group of the formanilide. An average E_s value is sometimes used if the reaction shows an intermediate steric effect for the phenyl group. In the case of formanilides the smallest E_s for the phenyl group lies closest to the cluster of rate constants for the other substituents, and therefore it was used for the correlation.

Figure IV-24 shows the correlation plot between the logarithm of the rate constants of the ortho substituents against their E_s values. In Figure IV-24 it appears that most of the substituents are scattered around the correlation line. The *o*-bromo and o-chloro substituents are substituents capable of strong electron withdrawing effects as compared to the rest of the substituents, and these showed the largest deviations from the rest of the substituents. If these substituents were not considered, and the data analyzed using Equation IV-9, a linear regression was observed with a δ_{app} of 0.505 and a correlation coefficient of 0.8787.

$$\log k = \delta_{app} E_s + c \qquad \text{Equation IV-9}$$

Where k is the observed rate constant, c is a constant, and δ_{app} is the apparent steric reaction constant for the reaction.

The positive sign for the value indicates that the steric bulk inhibits the reaction while the value indicates that the steric bulk inhibition of reaction is significant. . The observed rate constants used in this analysis are a function of both the first and second-order pathways for degradation of formanilide. Therefore the apparent steric substituent constant is in effect also a function of both these pathways. The expected transitions state for both the first-order and second-order pathways for alkaline hydrolysis of formanilides are similar (Figure IV-18), and therefore it is possible that the steric bulk inhibition effect

will be similar for both the pathways. Thus the overall reduction in the rate constant will be the sum of the reduction for each pathway.

Conclusion

The reaction order, reaction scheme and pH effects on the alkaline hydrolysis of formanilides were determined. The pH-rate profiles showed the specific base-catalyzed reaction with first-and second-order dependencies of hydroxide ion on the overall rate. The study of the pH rate profiles, ionic strength effects, binary solvent studies, and temperature studies supported the modified $B_{AC}2$ mechanism for the alkaline hydrolysis of formanilides. Using selected *para* and *meta* substituted formanilides, Hammett plots were used to elucidate the effect of electronic effects on both pathways. The $B_{AC}2$ mechanism predicts the reversible formation of a tetrahedral intermediate, and the water or hydroxide catalyzed breakdown of this intermediate to products. The Hammett analysis showed that the formation of the tetrahedral intermediate was accelerated by electron withdrawing groups. It also revealed that the decomposition of the intermediate to products, via either the water or the hydroxide catalyzed pathway, was a complex process dependent on the partitioning of the intermediate to products or to starting reactants. The partitioning ratio for the pathways was found to be dependent on the basicity of the leaving group. Hammett plots for the hydrolysis in 0.10 N sodium hydroxide at 40 °C of *para* and *meta* substituted formanilides showed virtually no effect on the reaction rate. This was probably due to the opposing substituents effects on the first and second order pathways for alkaline hydrolysis. The *ortho* substituted formanilides showed significant steric effects which were roughly proportional to the steric bulk of the substituent. In conclusion, the complex mechanism for alkaline hydrolysis of formanilides was evaluated and the effect of ortho substitution was determined.

Figure IV- 14: Hammett plot for observed rate constant and normalized rate constants (k_{corr}) for substituted formanilides at different hydroxide concentrations at 25 °C; 0.010 M NaOH (▲), 0.10 M NaOH (○), 1.0 M NaOH (■), and 5.0 M NaOH (●). Lines are linear fits of the data to the Hammett equation.

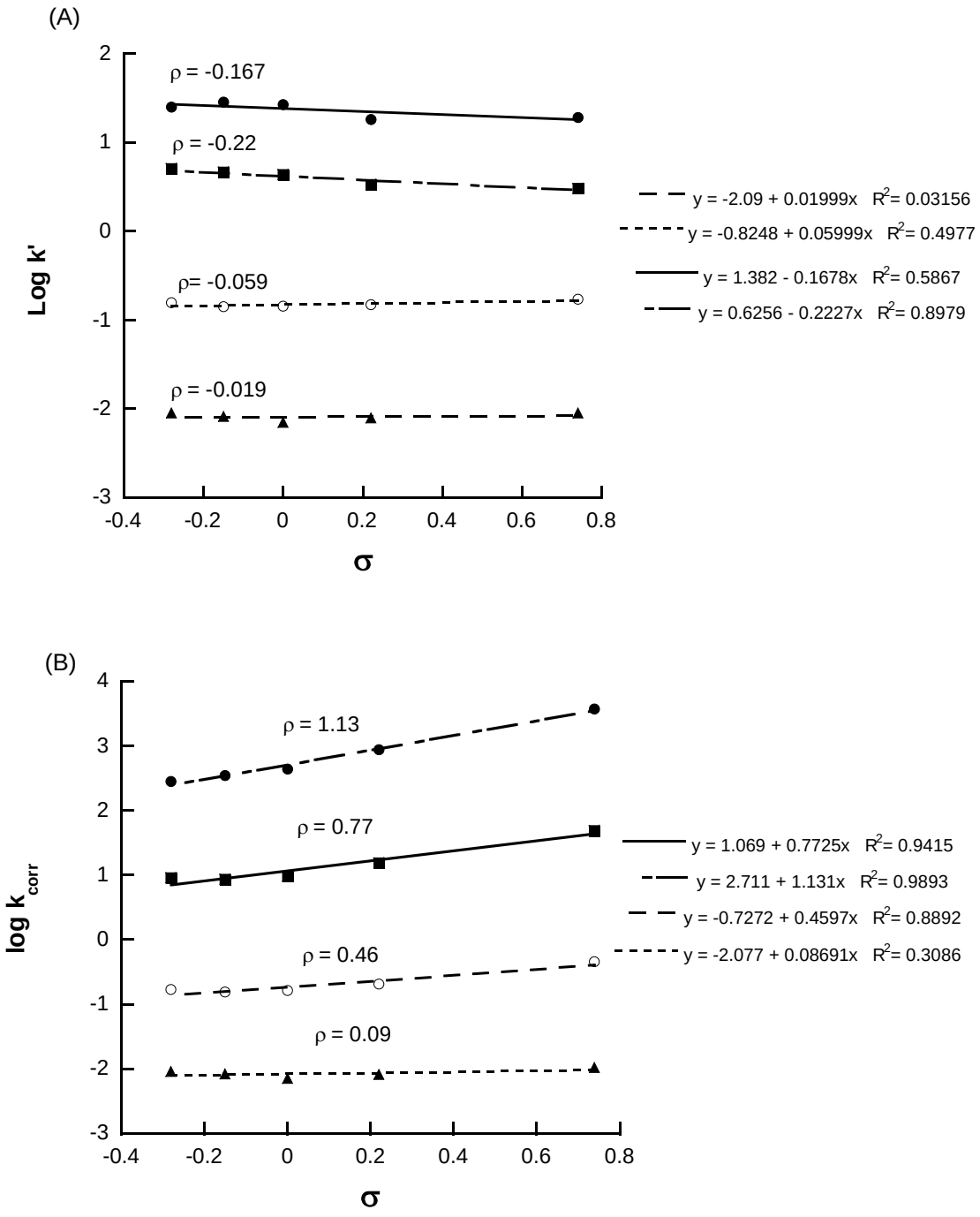

Figure IV- 15: Hammett plot for the formation of the tetrahedral intermediate by addition of hydroxide (k_a) using selected formanilides at 25 °C. The solid line is a linear regression fit of the data points to the Hammett equation and the dotted lines indicate the 95% confidence interval for the linear fit.

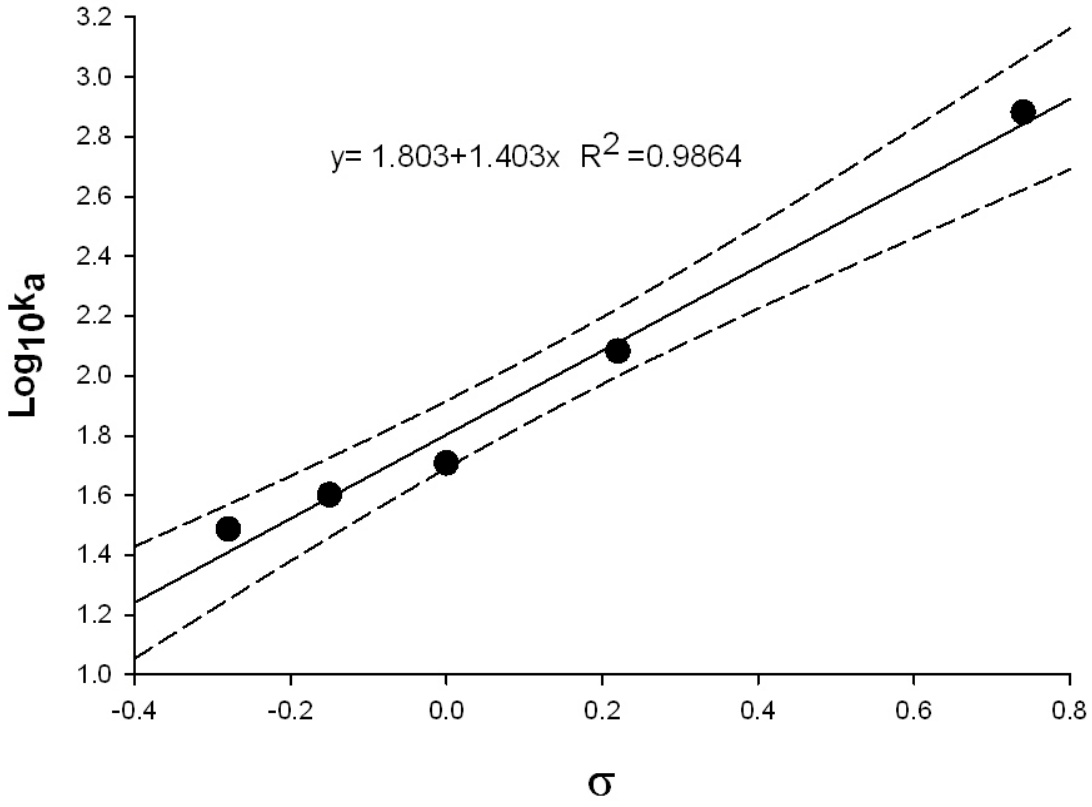

Figure IV- 16: Hammett plot for the first-order pathway for alkaline hydrolysis k_1 using selected formanilides at 25 °C. The solid line is a linear regression fit of the data points to the Hammett equation.

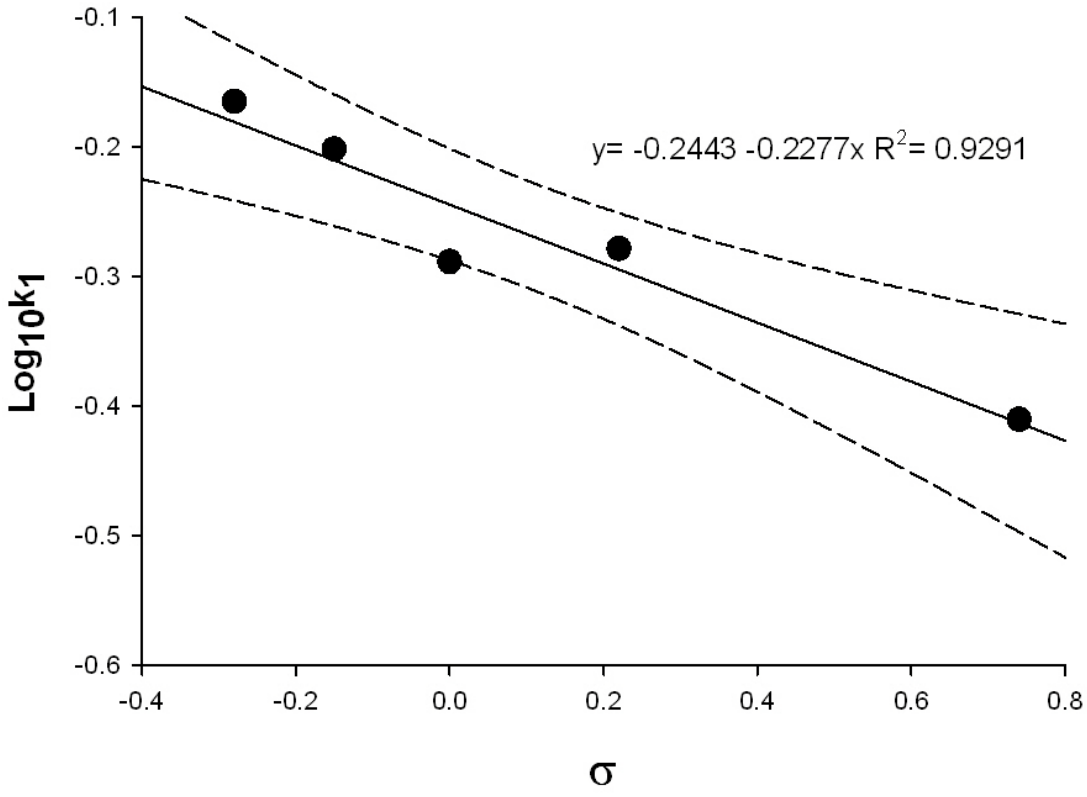

Figure IV- 17: Hammett plot for the second-order pathway for alkaline hydrolysis k_2 using selected formanilides at 25 °C. The solid line is a linear regression fit of the data points to the Hammett equation and the dotted lines indicate the 95% confidence intervals for the linear fit.

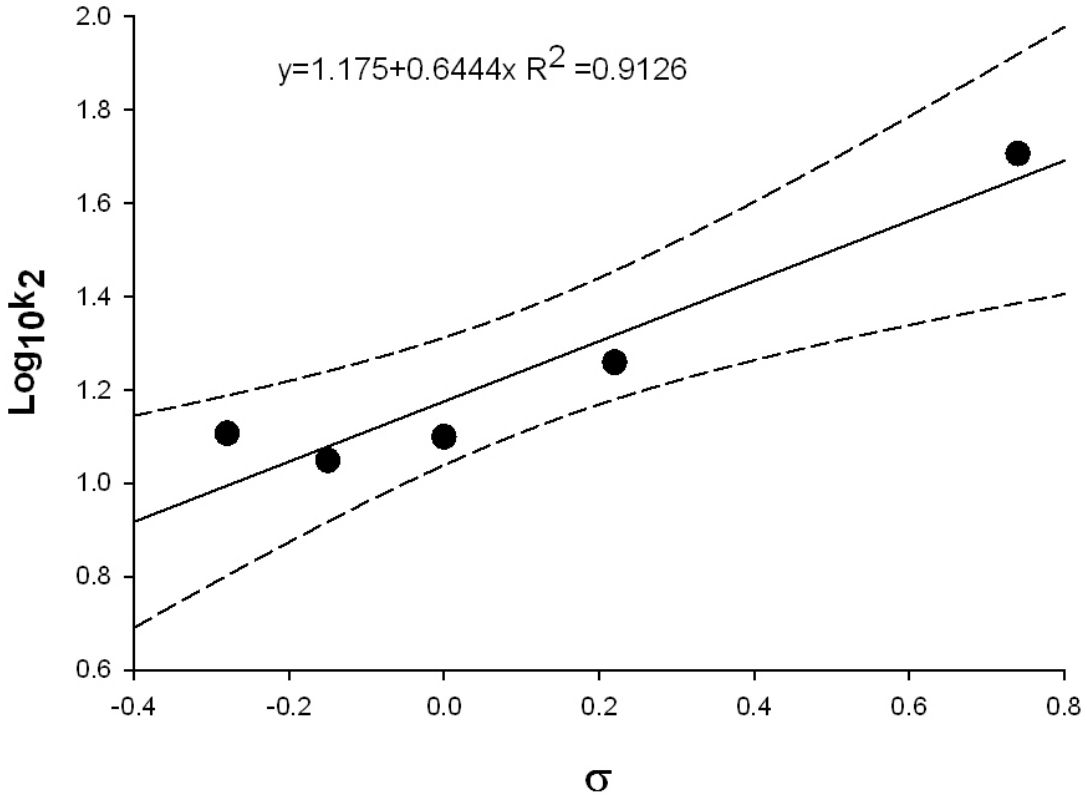

Figure IV- 18: Modified $B_{AC}2$ mechanism for formanilide hydrolysis in alkaline solutions.

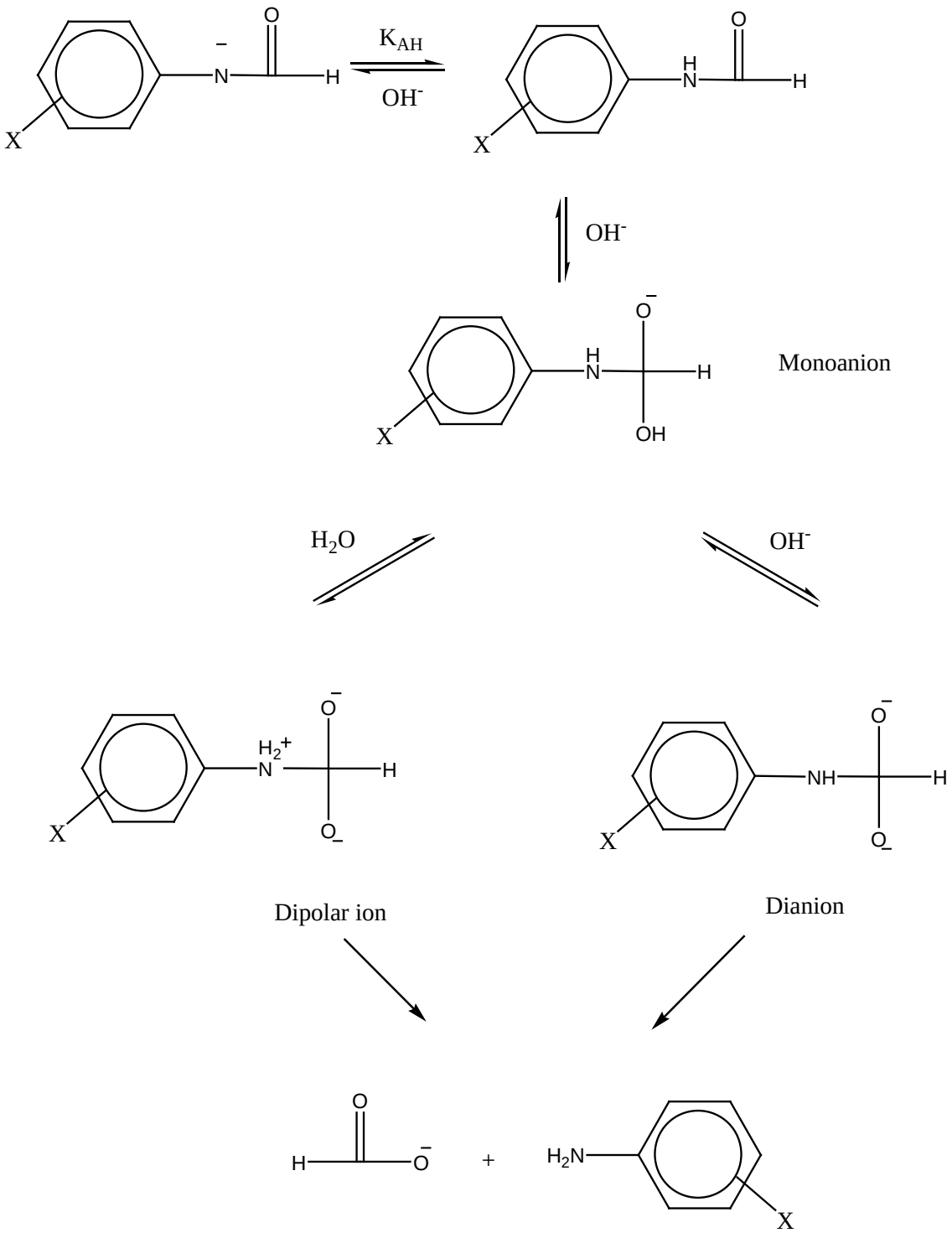

Figure IV- 19: Hammett plots for the rate constant for the formation of the intermediate, and the partition ratios for the first and second-order processes for alkaline hydrolysis of formanilides at 25 °C. The logarithm of k_a is denoted by closed circles (●) and the logarithms of the partition ratios for the first-order process and second-order processes are denoted by closed squares (■) and by closed triangles (▲), respectively. The lines are linear regression fits of the data to the Hammett equation.

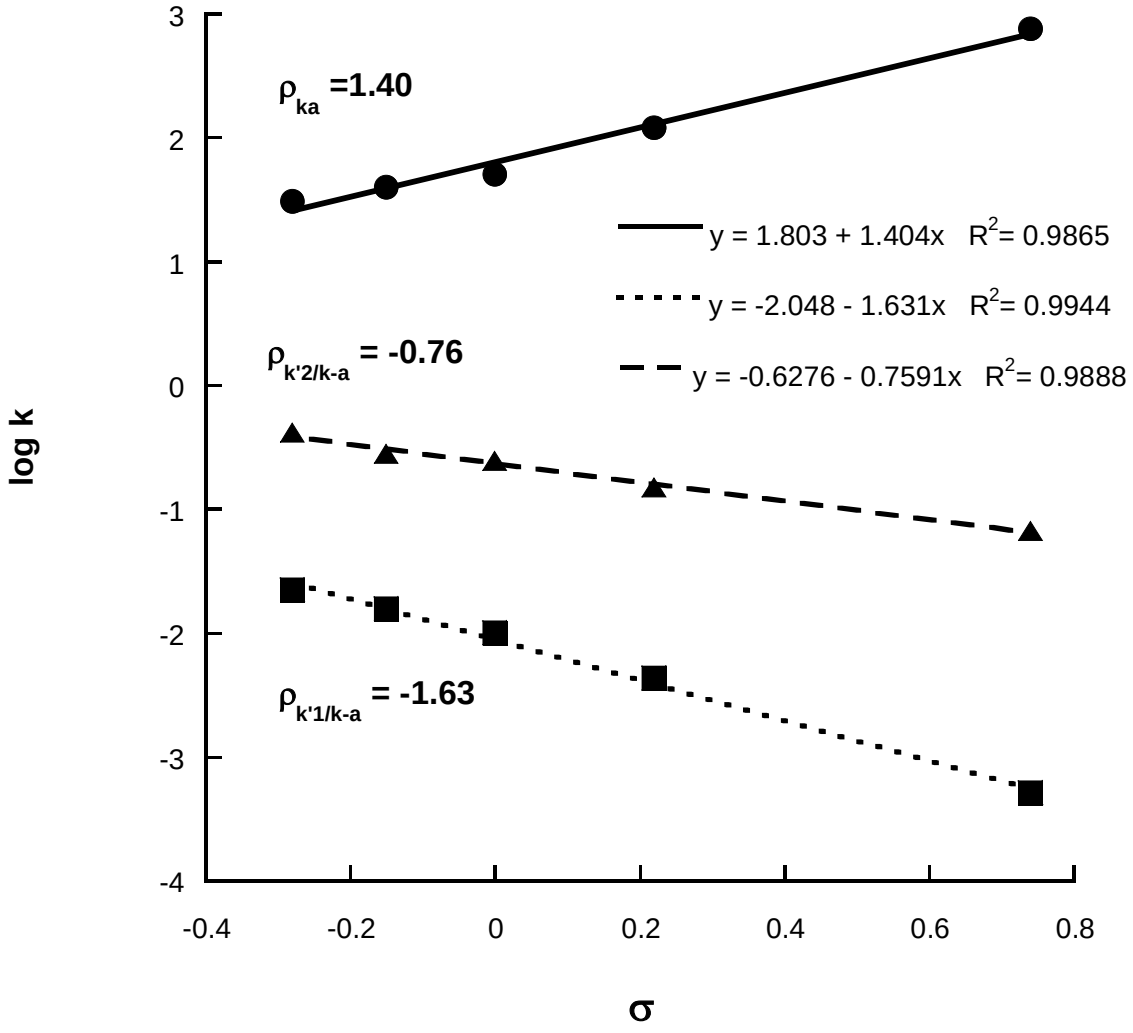

Figure IV- 20: Hammett plot using the observed rate constants k_{obs} for *para* and *meta* formanilides in 0.10M sodium hydroxide solution at 40 °C. Solid line is a linear regression fit for the rate constants for all substituents to the Hammett equation. *p*-nitroformanilide was not included in the linear regression analysis.

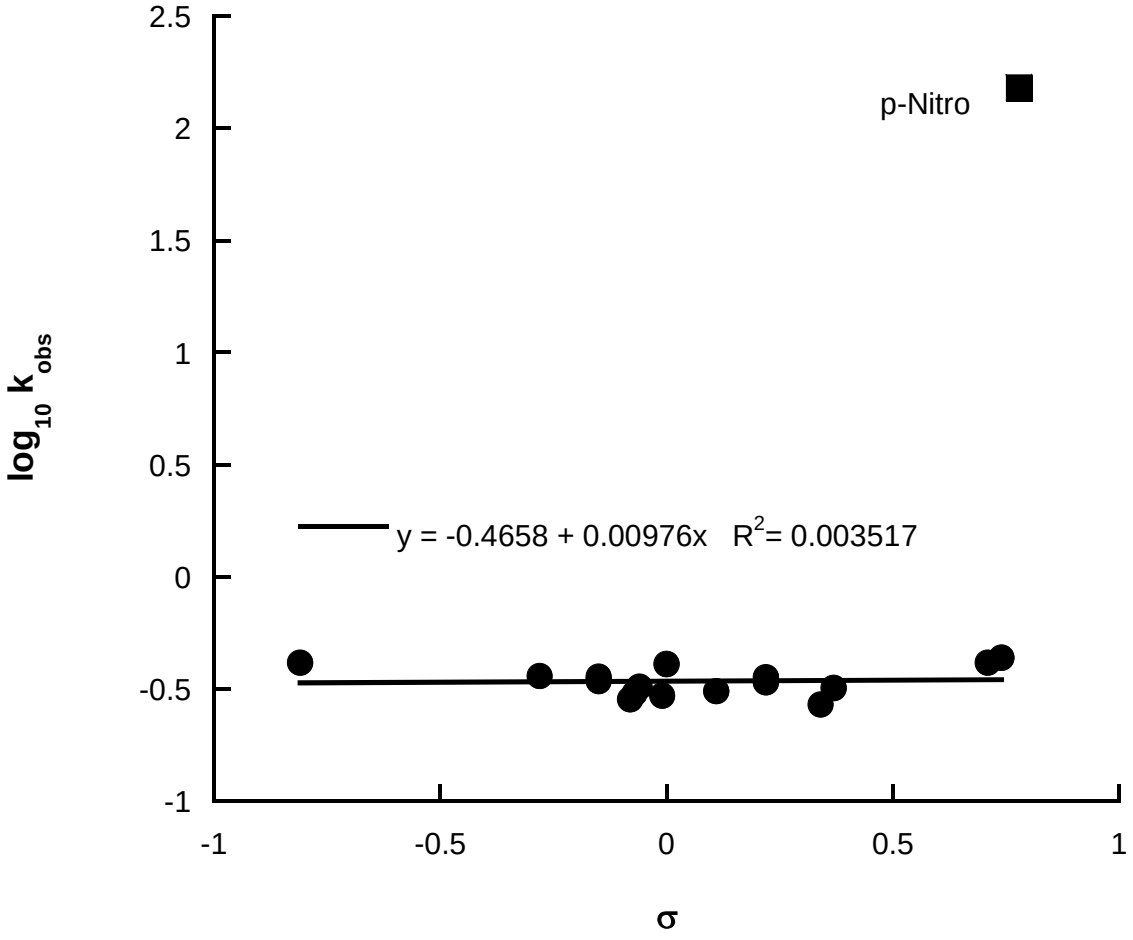

Figure IV- 21: Hammett plot for *para* and *ortho* substituted formanilides using the observed rate constants (k_{obs}) for alkaline hydrolysis of formanilides in 0.10 M sodium hydroxide at 40 °C. The *para* substituted formanilides are denoted by open squares (□) and the *ortho* substituted formanilides are denoted by open circles (○).

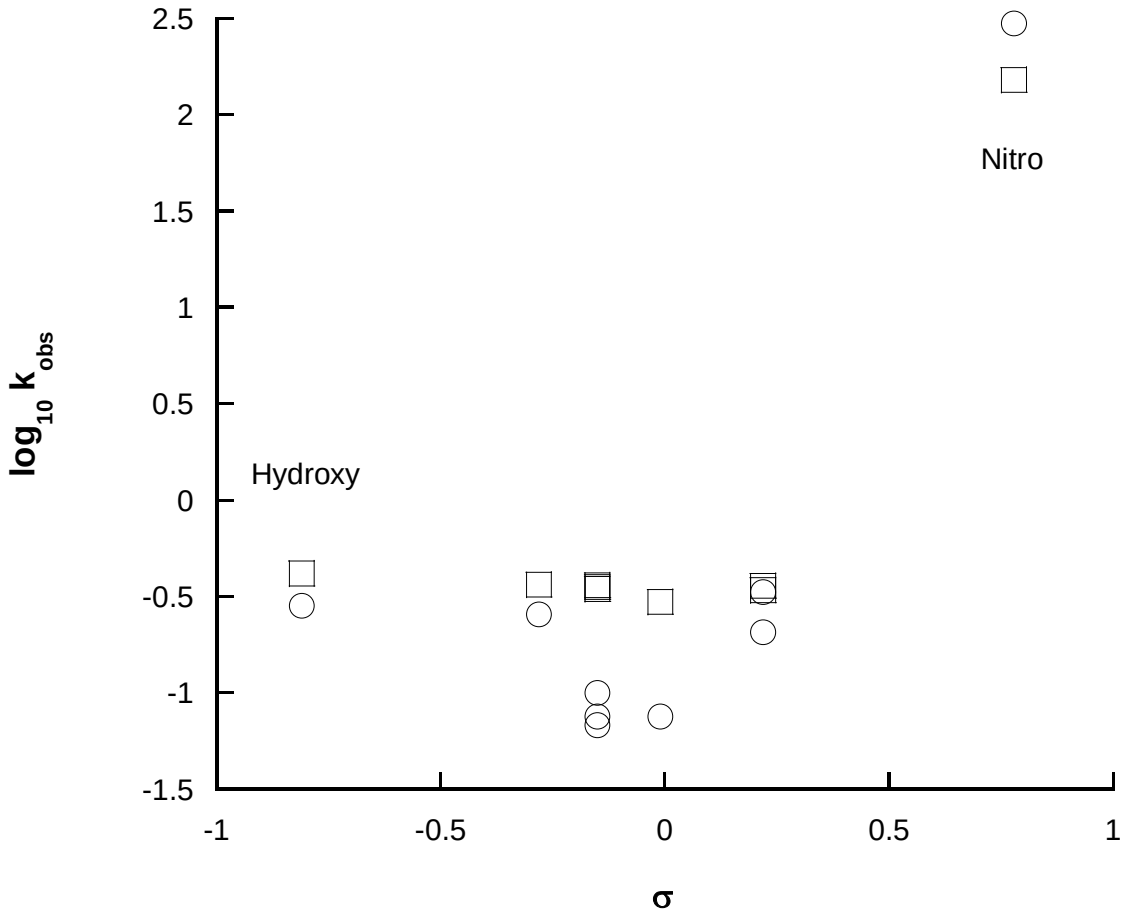

Figure IV- 22: Hammett plot for *para* and *ortho* substituted formanilides excluding nitro and hydroxyl substituted formanilides using the observed rate constants for the hydrolysis in 0.10 M sodium hydroxide solutions at 40 °C. The values in parenthesis are the Taft-Kutter-Hansch steric substituent constants (E_s). The *para* substituted formanilides are denoted by open squares (□) and the *ortho* substituted formanilides are denoted by open circles (○).

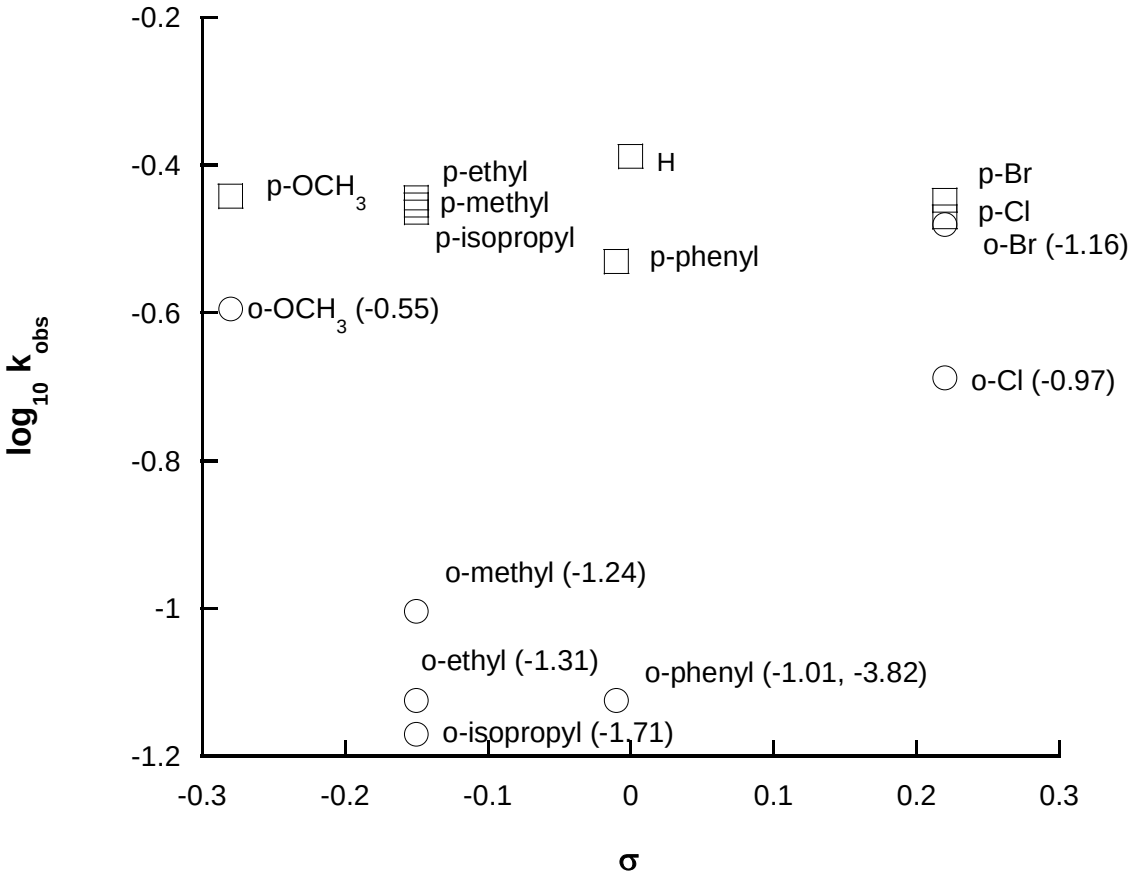

Figure IV- 23: Plot of the logarithm of the ratio of the observed rate constants of the *para* and *ortho* substituted formanilides excluding nitro and hydroxyl substituted formanilides in 0.10 M sodium hydroxide at 40 °C.

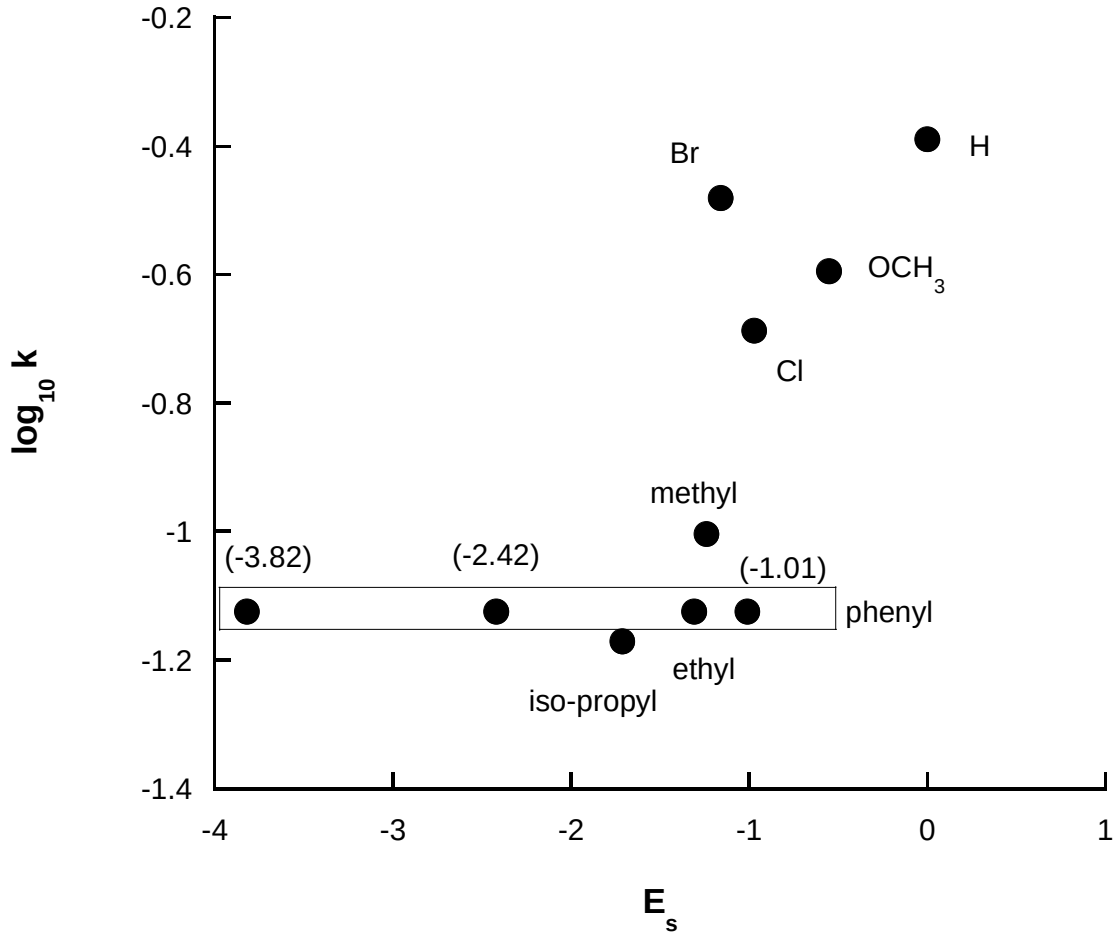

Figure IV- 24: Plot of the logarithm observed rate constants *ortho* substituted formanilides excluding nitro and hydroxyl substituted formanilides in 0.10 M sodium hydroxide at 40 °C. The solid line indicates the linear correlation line to Equation IV-9 the while the broken lines indicate the 95 % confidence intervals. The *ortho* substituents are denoted by closed circles (●). The *o*-bromo and *o*-chloro substituted formanilides are represented by the open circles (○) and are not included in the correlation but are noted for comparison.

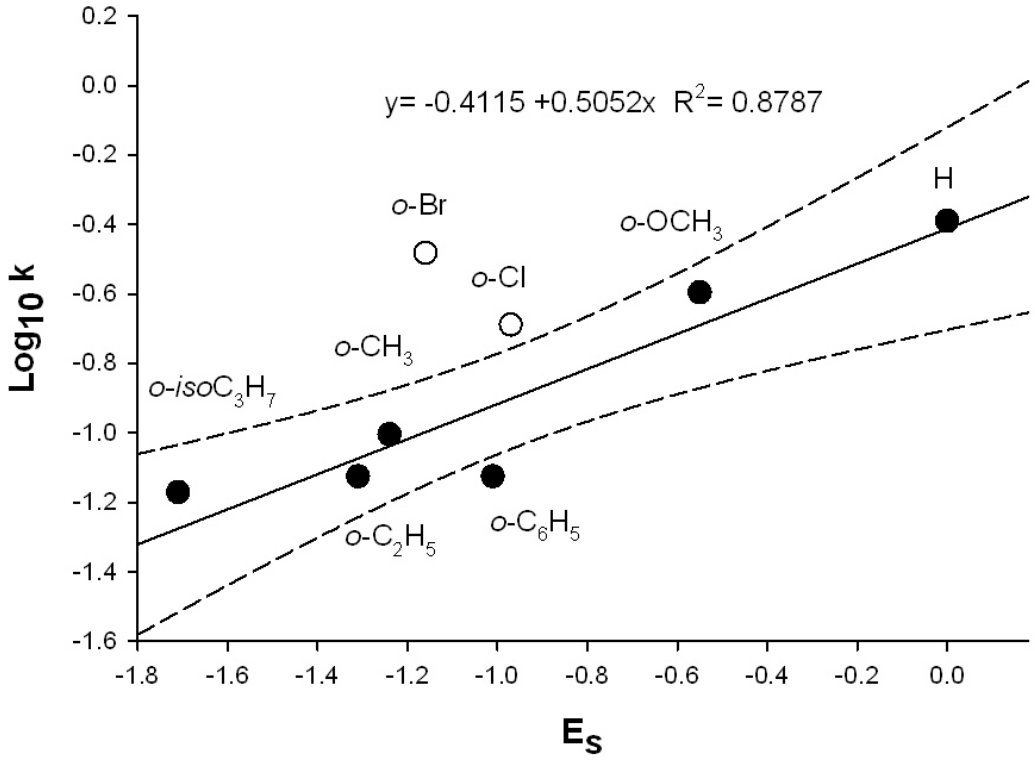

APPENDIX A

ESTIMATION OF IONIZATION CONSTANTS

Table A- 1: Potentiometric titration data for titration of a 40 mL aliquot of 5.0 mM *p*-hydroxyformanilide with 0.10 N sodium hydroxide with calculated G (modified titrant volume) used for determination of hydroxyl pK_a.

pH	Titrant Volume (mL)	$[H^+]$	G	$G\times[H^+]$	$[OH^-]$
6.283	0.00	5.21×10^{-7}	2.01×10^{-4}	1.05×10^{-10}	1.92×10^{-8}
8.257	0.10	5.53×10^{-9}	9.93×10^{-2}	5.49×10^{-10}	1.81×10^{-6}
8.606	0.20	2.48×10^{-9}	0.198	4.91×10^{-10}	4.04×10^{-6}
8.804	0.30	1.57×10^{-9}	0.297	4.67×10^{-10}	6.37×10^{-6}
8.952	0.40	1.12×10^{-9}	0.396	4.43×10^{-10}	8.95×10^{-6}
9.078	0.50	8.36×10^{-10}	0.495	4.14×10^{-10}	1.20×10^{-5}
9.182	0.60	6.58×10^{-10}	0.594	3.91×10^{-10}	1.52×10^{-5}
9.278	0.70	5.27×10^{-10}	0.692	3.65×10^{-10}	1.90×10^{-5}
9.364	0.80	4.33×10^{-10}	0.791	3.42×10^{-10}	2.31×10^{-5}
9.452	0.90	3.53×10^{-10}	0.888	3.14×10^{-10}	2.83×10^{-5}
9.534	1.00	2.92×10^{-10}	0.986	2.88×10^{-10}	3.42×10^{-5}
9.617	1.10	2.42×10^{-10}	1.08	2.62×10^{-10}	4.14×10^{-5}
9.695	1.20	2.02×10^{-10}	1.18	2.38×10^{-10}	4.95×10^{-5}
9.783	1.30	1.65×10^{-10}	1.27	2.10×10^{-10}	6.07×10^{-5}
9.871	1.40	1.35×10^{-10}	1.37	1.84×10^{-10}	7.43×10^{-5}
9.963	1.50	1.09×10^{-10}	1.46	1.59×10^{-10}	9.18×10^{-5}
10.063	1.60	8.65×10^{-11}	1.55	1.34×10^{-10}	1.16×10^{-4}
10.169	1.70	6.78×10^{-11}	1.64	1.11×10^{-10}	1.48×10^{-4}
10.283	1.80	5.21×10^{-11}	1.72	8.96×10^{-11}	1.92×10^{-4}
10.403	1.90	3.95×10^{-11}	1.79	7.09×10^{-11}	2.53×10^{-4}

Table A-1-Continued

10.526	2.00	2.98×10^{-11}	1.86	5.54×10^{-11}	3.36×10^{-4}
10.638	2.10	2.30×10^{-11}	1.92	4.41×10^{-11}	4.35×10^{-4}
10.744	2.20	1.80×10^{-11}	1.97	3.54×10^{-11}	5.55×10^{-4}
10.837	2.30	1.46×10^{-11}	2.01	2.92×10^{-11}	6.87×10^{-4}
10.916	2.40	1.21×10^{-11}	2.05	2.49×10^{-11}	8.24×10^{-4}
10.987	2.50	1.03×10^{-11}	2.09	2.15×10^{-11}	9.71×10^{-4}
11.049	2.60	8.93×10^{-12}	2.12	1.90×10^{-11}	1.12×10^{-3}
11.103	2.70	7.89×10^{-12}	2.16	1.70×10^{-11}	1.27×10^{-3}
11.153	2.80	7.03×10^{-12}	2.19	1.54×10^{-11}	1.42×10^{-3}
11.201	2.90	6.30×10^{-12}	2.22	1.40×10^{-11}	1.59×10^{-3}
11.242	3.00	5.73×10^{-12}	2.25	1.29×10^{-11}	1.75×10^{-3}
11.277	3.10	5.28×10^{-12}	2.28	1.21×10^{-11}	1.89×10^{-3}
11.308	3.20	4.92×10^{-12}	2.32	1.14×10^{-11}	2.03×10^{-3}
11.34	3.30	4.57×10^{-12}	2.35	1.07×10^{-11}	2.19×10^{-3}
11.369	3.40	4.28×10^{-12}	2.38	1.02×10^{-11}	2.34×10^{-3}
11.397	3.50	4.01×10^{-12}	2.41	9.68×10^{-12}	2.49×10^{-3}
11.421	3.60	3.79×10^{-12}	2.45	9.29×10^{-12}	2.64×10^{-3}
11.447	3.70	3.57×10^{-12}	2.48	8.84×10^{-12}	2.80×10^{-3}
11.468	3.80	3.40×10^{-12}	2.51	8.55×10^{-12}	2.94×10^{-3}
11.489	3.90	3.24×10^{-12}	2.55	8.25×10^{-12}	3.08×10^{-3}
11.510	4.00	3.09×10^{-12}	2.57	7.96×10^{-12}	3.24×10^{-3}
11.532	4.10	2.94×10^{-12}	2.60	7.63×10^{-12}	3.40×10^{-3}
11.551	4.20	2.81×10^{-12}	2.63	7.39×10^{-12}	3.56×10^{-3}
11.567	4.30	2.71×10^{-12}	2.66	7.22×10^{-12}	3.69×10^{-3}
11.586	4.40	2.59×10^{-12}	2.69	6.97×10^{-12}	3.85×10^{-3}

Table A-1-Continued

11.602	4.50	2.50×10^{-12}	2.72	6.80×10^{-12}	4.00×10^{-3}
11.617	4.60	2.42×10^{-12}	2.75	6.65×10^{-12}	4.14×10^{-3}
11.632	4.70	2.33×10^{-12}	2.78	6.49×10^{-12}	4.29×10^{-3}
11.647	4.80	2.25×10^{-12}	2.81	6.34×10^{-12}	4.44×10^{-3}
11.659	4.90	2.19×10^{-12}	2.85	6.25×10^{-12}	4.56×10^{-3}
11.673	5.00	2.12×10^{-12}	2.88	6.11×10^{-12}	4.71×10^{-3}
11.687	5.10	2.06×10^{-12}	2.90	5.97×10^{-12}	4.86×10^{-3}
11.699	5.20	2.00×10^{-12}	2.94	5.87×10^{-12}	5.00×10^{-3}
11.713	5.30	1.94×10^{-12}	2.96	5.73×10^{-12}	5.16×10^{-3}
11.725	5.40	1.88×10^{-12}	2.99	5.63×10^{-12}	5.31×10^{-3}
11.734	5.50	1.85×10^{-12}	3.03	5.59×10^{-12}	5.42×10^{-3}
11.747	5.60	1.79×10^{-12}	3.05	5.46×10^{-12}	5.58×10^{-3}
11.757	5.70	1.75×10^{-12}	3.09	5.40×10^{-12}	5.71×10^{-3}
11.766	5.80	1.71×10^{-12}	3.13	5.36×10^{-12}	5.83×10^{-3}

Table A- 2: Absorbance values at 250 nm and 310 nm for 9.99×10-4 M *o*-carboxy formanilide in the pH range 1.56-6.95

pH	**Absorbance at 250 nm**	**Absorbance at 310 nm**
1.56	1.032	0.268
1.74	1.033	0.268
2.15	1.048	0.265
2.68	1.060	0.245
2.83	1.069	0.236
3.10	1.090	0.212
3.24	1.092	0.197
4.07	1.152	0.116
4.34	1.163	0.098
4.34	1.160	0.097
4.97	1.173	0.088
6.95	1.176	0.080

Figure A- 1: Non linear regression fits for absorbance values for 9.99×10^{-4} M *o*-carboxy formanilide in the pH range 1.56-6.95. Solid squares represent experimental data. Solid lines generated using Equation II-3 (A) 310 nm (estimated $K_a = 4.83\times10^{-4}$). (B) 250 nm (estimated $K_a = 3.65\times10^{-4}$). The K_a values were averaged and the average pK_a reported was 3.37.

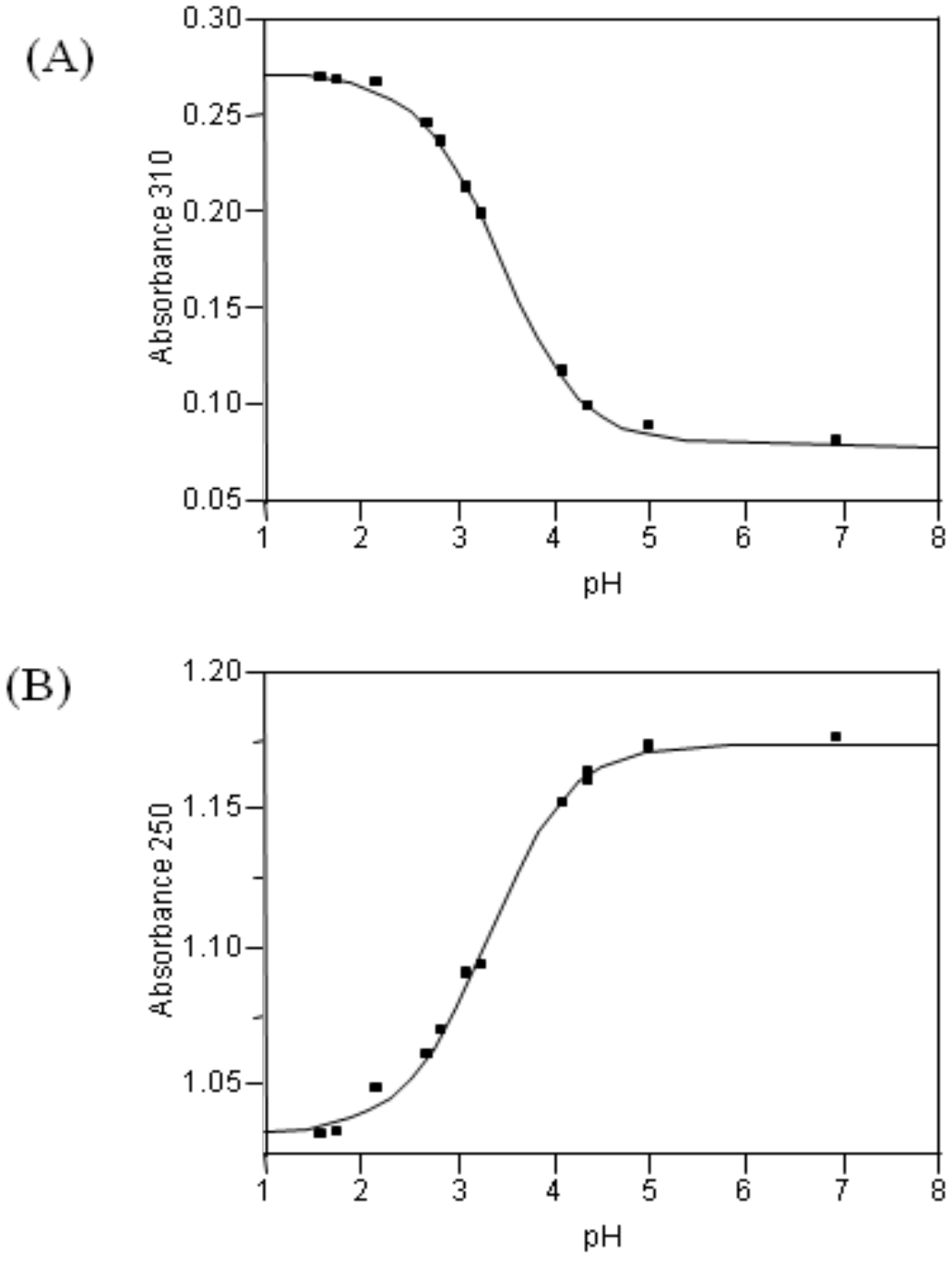

Figure A- 2: Determination of the carboxylic acid pK_a of *m*-carboxyformanilide. UV spectra of 4.98×10^{-5} M *p*-carboxyformanilide in the pH range 1.53-6.91 from 245 nm to 335 nm. At 303 nm highest absorbance is due to pH 1.53 and lowest absorbance is due to pH 6.91.

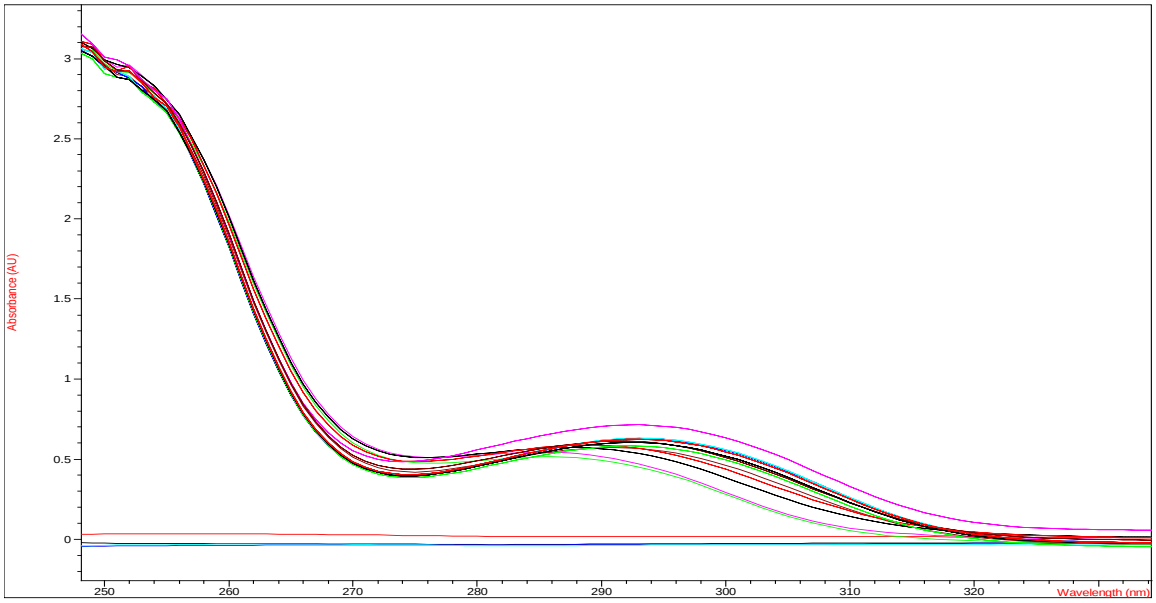

Table A- 3: Absorbance values at 303 nm for 4.98×10^{-5} M *m*-carboxy formanilide in the pH range 1.53-6.91.

pH	**Absorbance at 303 nm**
1.53	0.484
1.72	0.487
2.73	0.473
3.01	0.446
3.09	0.421
3.35	0.435
3.48	0.384
3.92	0.355
4.21	0.302
4.93	0.195
6.91	0.206

Figure A- 3: Non linear regression fits for absorbance values at 303 nm for 4.98×10^{-5} M *m*-carboxyformanilide in the pH range 1.53-6.91. Solid circles represent experimental data. Solid lines generated using Equation II-3. The estimated $K_a = 1.38\times10^{-4}$; $pK_a = 3.86$.

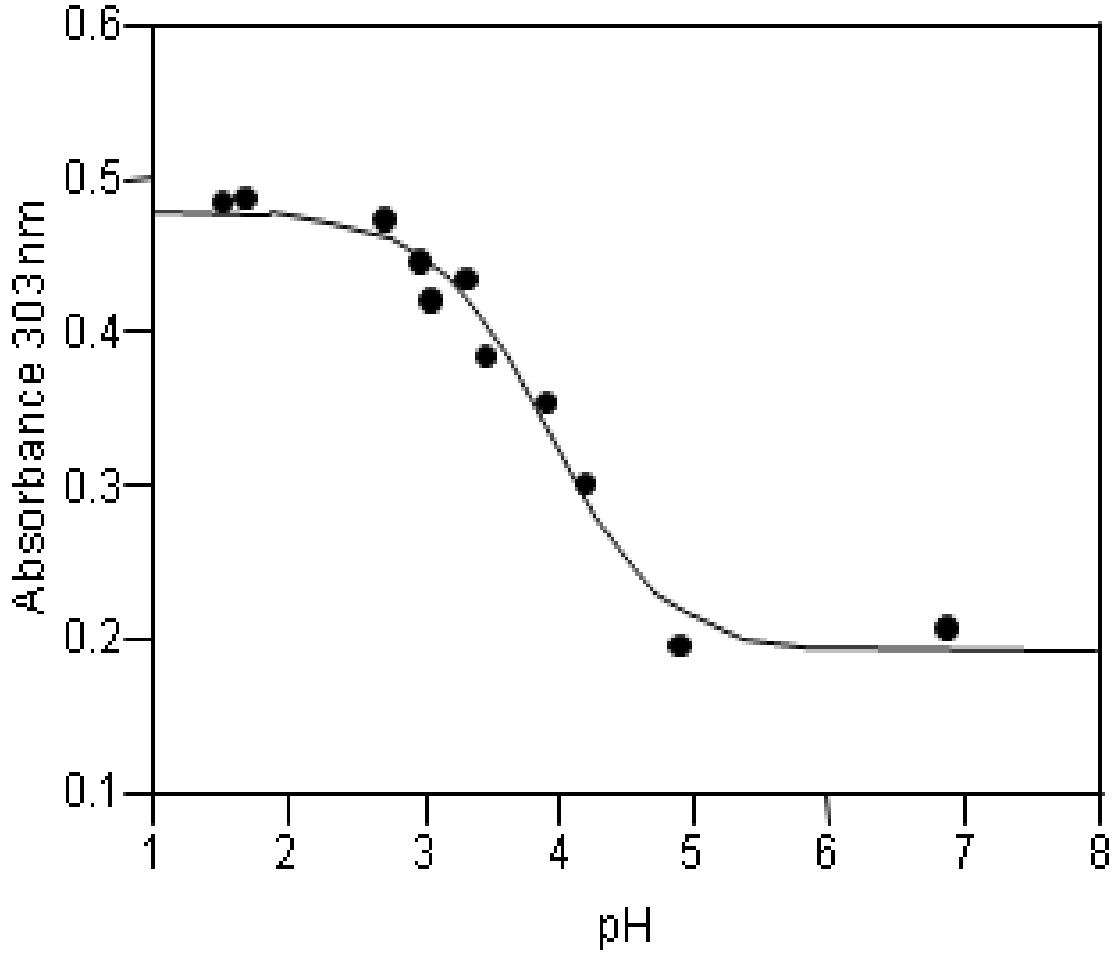

Figure A- 4: Determination of the carboxylic acid pK_a of *p*-carboxy formanilide. UV spectra of 4.99×10^{-5} M *p*-carboxyformanilide in the pH range 1.60-6.95 from 220 nm to 340 nm. At 282 nm highest absorbance is due to pH 1.60 and lowest absorbance is due to pH 6.95.

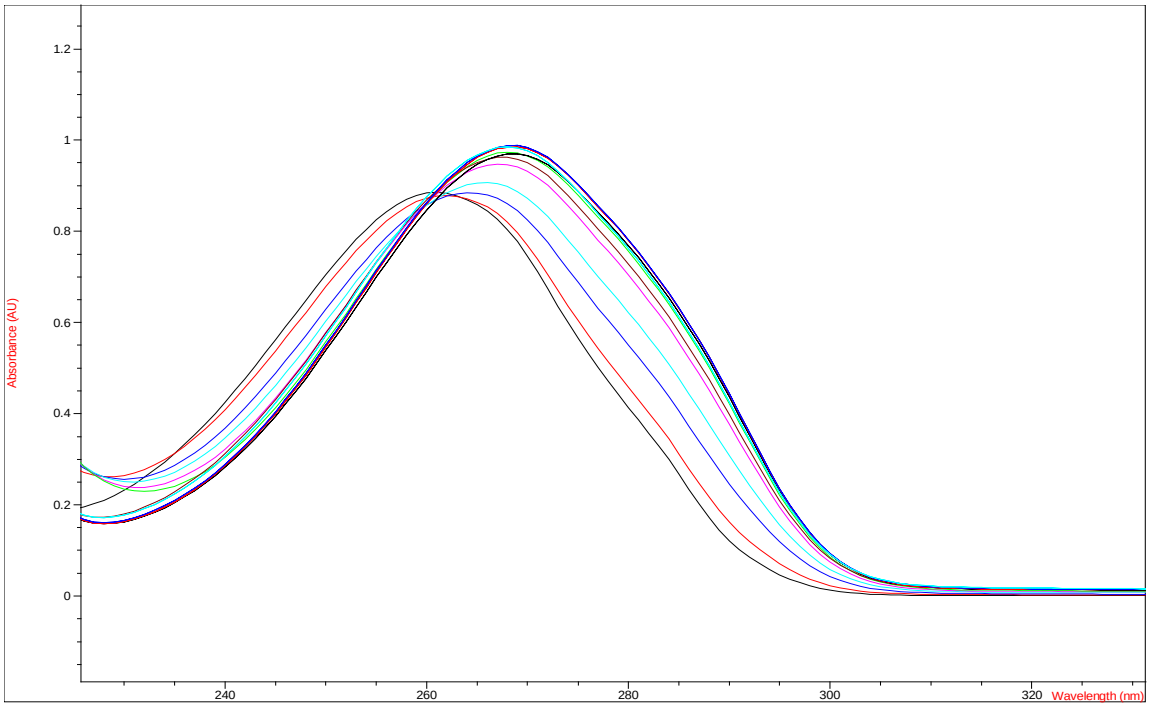

Table A- 4: Absorbance values at 282 nm for 4.99×10^{-5} M *p*-carboxyformanilide in the pH range 1.60-6.95.

pH	**Absorbance at 282 nm**
1.60	0.714
1.80	0.725
2.03	0.725
3.03	0.706
3.34	0.673
2.89	0.700
3.18	0.648
3.86	0.567
4.26	0.496
4.80	0.402
6.95	0.358

Figure A- 5: Non linear regression fits for absorbance values at 282 nm for 4.99×10^{-5} M *p*-carboxyformanilide in the pH range 1.60-6.95. Solid circles represent experimental data. Solid lines generated using Equation II-3. The estimated $K_a = 9.66\times10^{-5}$; $pK_a = 4.01$.

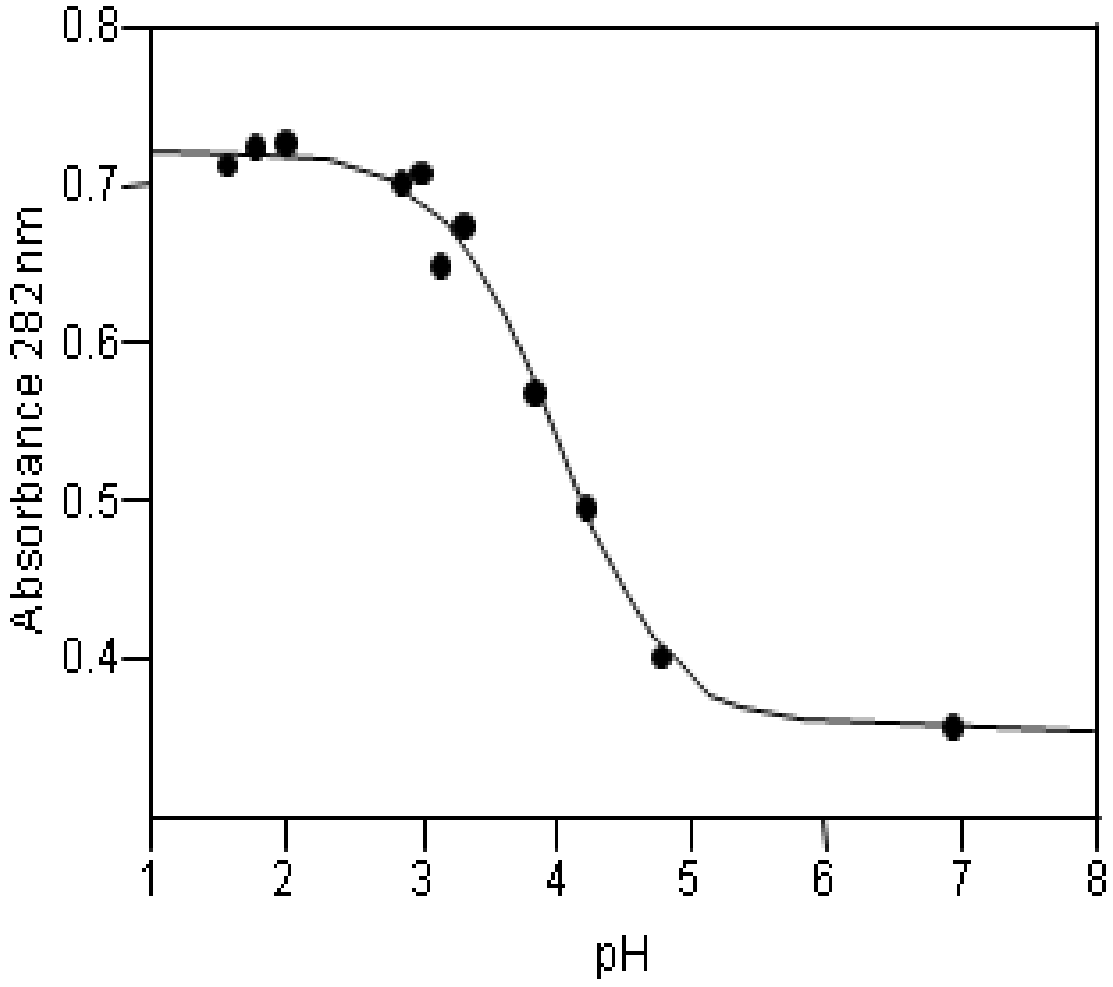

Table A- 5: Absorbance values at 278 nm and 301 nm for 5.70×10^{-5} M *m*-hydroxyformanilide in the pH range 7.03-11.61.

pH	Absorbance at 278 nm	Absorbance at 301 nm
7.03	0.270	0.025
7.18	0.266	0.022
7.35	0.268	0.023
7.83	0.264	0.031
8.41	0.252	0.056
8.56	0.251	0.055
8.84	0.236	0.096
8.95	0.232	0.111
9.65	0.185	0.231
9.68	0.186	0.237
10.3	0.167	0.304
10.7	0.160	0.317
11.1	0.157	0.320
11.6	0.159	0.327

Figure A- 6: Determination of the Hydroxyl pK_a of *o*- hydroxyformanilide. UV spectra of 1.88×10^{-4} M *o*-hydroxyformanilide in the pH range 7.07-11.75 from 225 nm to 380 nm. At 278 nm highest absorbance is due to pH 7.07 and lowest absorbance is due to pH 11.75. Stock solutions were prepared in DMSO. The spectra with the least absorbance is the sodium phosphate solution blank.

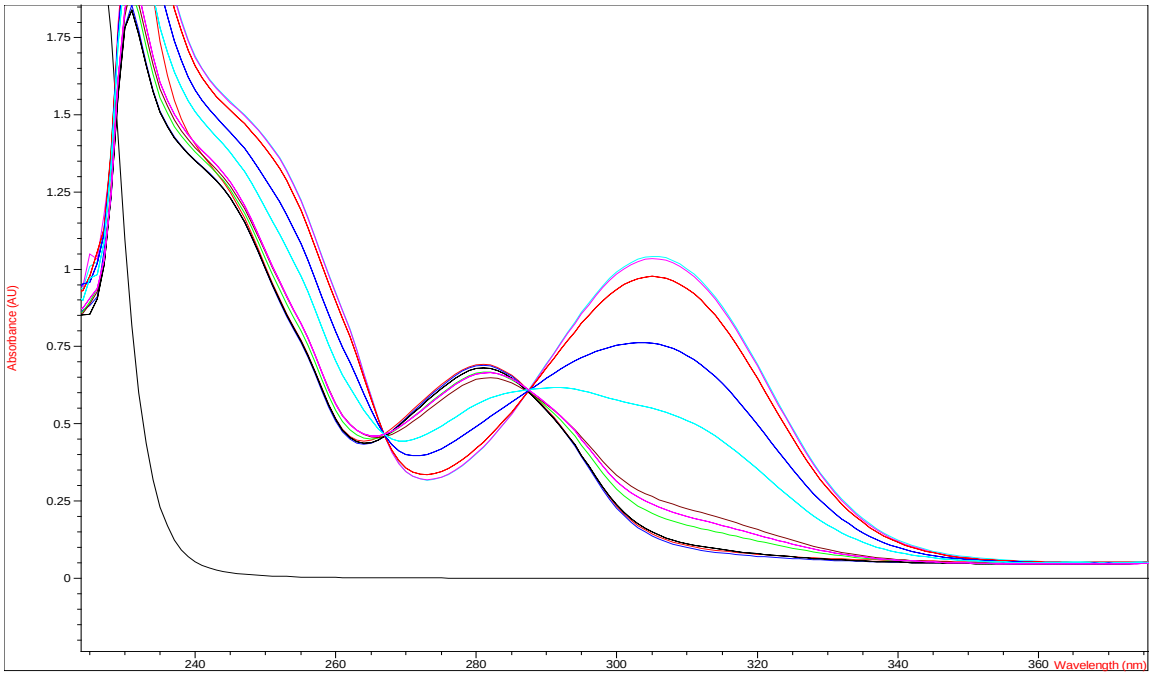

Table A- 6: Absorbance values at 308 nm and 278 nm for 1.88×10^{-4} M *o*-hydroxyformanilide in the pH range 7.07-11.75. Stock solutions were prepared in DMSO.

pH	Absorbance at 308 nm	Absorbance at 278 nm
7.07	0.111	0.670
7.40	0.124	0.662
7.92	0.185	0.645
8.06	0.214	0.642
8.20	0.239	0.624
8.85	0.529	0.536
9.40	0.744	0.460
10.1	0.963	0.384
10.9	1.021	0.365
11.8	1.028	0.364

Figure A- 7: Non linear regression fits for absorbance values for 1.88×10^{-4} M *o*-hydroxyformanilide in the pH range 7.07-11.75. Stock solutions were prepared in DMSO. Solid squares represent experimental data. Solid lines generated using Equation II-3) (A) 308 nm (estimated $K_a = 1.10\times10^{-9}$). (B) 278 nm (estimated $K_a = 1.01\times10^{-9}$). The K_a values were averaged and the average pK_a reported was 8.96.

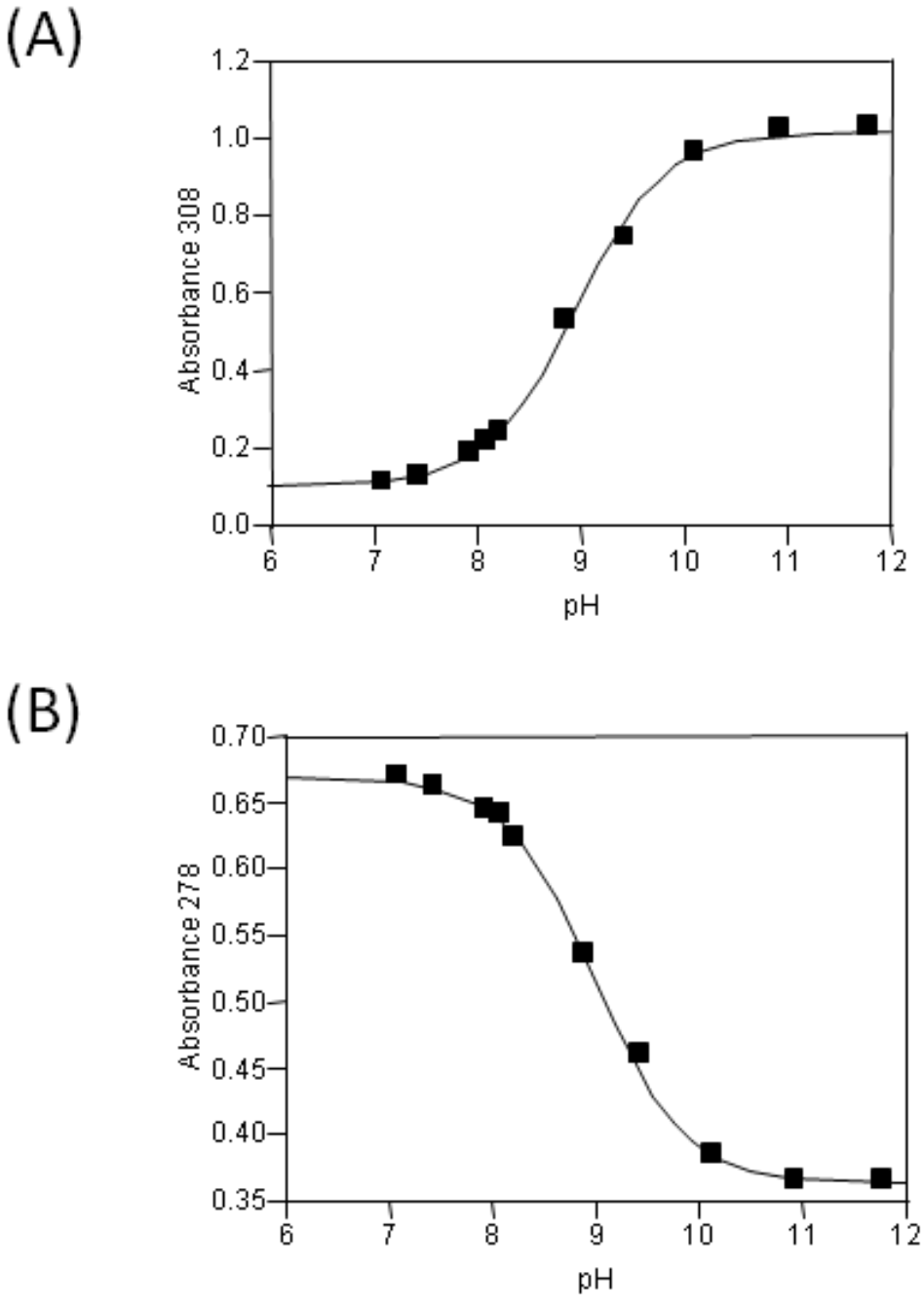

APPENDIX B

DERIVATION OF RATE LAWS

(A) First-order degradation of formanilide in dilute acidic solutions

$$\frac{dA}{dt} = -k_{obs}[A]$$

Integrating between the limits

[A]= [A_0] at t = 0

[A]=[A] at t = t

$$\int_{A_0}^{A} \frac{dA}{[A]} = -k_{obs} \int_{0}^{t} dt$$

$$A = A_0 e^{-k_{obs}t}$$

(B) First-order degradation of m-methoxyformanilide in dilute acidic solutions

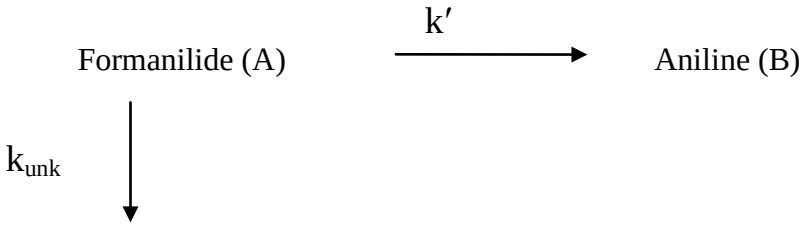

Loss of Formanilide

$$\frac{dA}{dt} = -(k' + k_{unk})[A] = -k_{obs}[A]$$

Integrating between the limits

[A]= [A_0] at t = 0

[A]=[A] at t = t

$$\int_{A_0}^{A} \frac{dA}{[A]} = -k_{obs} \int_0^t dt$$

$$A = A_0 e^{-k_{obs} t}$$

Similarly for formation of product B

$$\frac{dB}{dt} = k'[A]$$

$$\frac{dB}{dt} = k' A_0 e^{-k_{obs} t}$$

Integrating between the limits

[B]= [0] at t = 0

[B]=[B] at t = t

$$\int_0^B dB = k' A_0 \int_0^t e^{-k_{obs} t} dt$$

$$[B] = \frac{A_0 k'}{k_{obs}} (1 - e^{-k_{obs} t})$$

(C) Higher than first-order degradation of formanilide in alkaline solutions

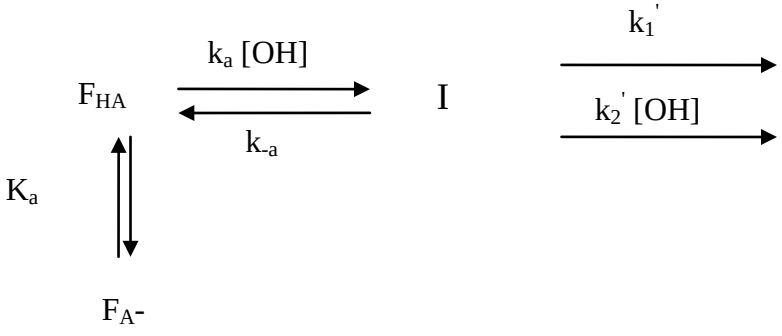

F_{HA} = Unionized substrate

F_A^- = Ionized substrate

I = Intermediate

C= Total concentration of substrate

k_a = Second-order rate constant for the formation of intermediate

k_{-a} = Rate constant for the first-order reversion of intermediate to substrate

k_1'= Rate constant for the first-order decomposition of intermediate to product

k_2'= Rate constant for the second-order decomposition of intermediate to product

K_a= Ionization constant

K_w= Autoprotolysis constant for water

f_{HA} = Fraction of unionized substrate

f_A^- = Fraction of ionized substrate

Ionization of substrate can be represented by

$$K_w = [H][OH]$$

$$K_a = \frac{[H^+][A^-]}{[HA]}$$

$$f_{HA} = \frac{[H]}{K_a + [H]}$$

$$f_{HA} = \frac{K_w}{[OH]K_a + K_w}$$

Equilibrium constant for the formation of intermediate can be given by

$$K = \frac{k_{forward}}{k_{reverse}} = \frac{k_a}{k_{-a}}$$

The differential equations for the scheme assuming the unionized substrate is the reactive species.

$$\frac{dF_{HA}}{dt} = -k_a[OH][F_{HA}] + k_{-a}[I]$$

$$\frac{dI}{dt} = k_a[OH][F_{HA}] - k_{-a}[I] - k_1'[I] - k_2'[OH][I]$$

Using steady state approximation.

dI/dt =0,

$$0 = k_a[OH][F_{HA}] - k_{-a}[I] - k_1'[I] - k_2'[OH][I]$$

$$[I] = \frac{k_a[OH][F_{HA}]}{k_{-a} + k_1' + k_2'[OH]}$$

Substituting in equation

$$\frac{dF_{HA}}{dt} = -k_a[OH][F_{HA}] + \frac{k_{-a}k_a[OH][F_{HA}]}{k_{-a} + k_1' + k_2'[OH]}$$

$$\frac{dF_{HA}}{dt} = -\left(\frac{k_1' + k_2'[OH]}{k_{-a} + k_1' + k_2'[OH]}\right)k_a[OH][F_{HA}]$$

Multiplying the numerator and denominator with the equilibrium constant (K).

$$\frac{dF_{HA}}{dt} = -\left(\frac{k_1 + k_2[OH]}{k_a + k_1 + k_2[OH]}\right)k_a[OH][F_{HA}]$$

$$\frac{dF_{HA}}{dt} = -\left(\frac{k_1 + k_2[OH]}{k_a + k_1 + k_2[OH]}\right)k_a[OH][F_{HA}]$$

Calculating the concentration of the ionized formanilide in terms of the concentration of the total substrate

$$\frac{dC}{dt} = -\left(\frac{k_1 + k_2[OH]}{k_a + k_1 + k_2[OH]}\right)k_a[OH]f_{HA}C$$

$$\frac{dC}{dt} = -\left(\frac{k_1 + k_2[OH]}{k_a + k_1 + k_2[OH]}\right)k_a[OH]\frac{K_w}{[OH]K_a + K_w}C$$

Where

$$k_1 = k_1'\frac{k_a}{k_{-a}}$$

$$k_2 = k_2'\frac{k_a}{k_{-a}}$$

$$k_{obs} = \frac{k_1 + k_2[OH]}{k_a + k_1 + k_2[OH]}k_a[OH](\frac{K_w}{[OH]K_a + K_w})$$

APPENDIX C

STATISTICAL INFORMATION

Data used for the multiple linear regression analysis of the ortho effect in the acidic hydrolysis of formanilide

Table C- 1: Data used in the analysis of the Fujita Nishioka Equation.

Substituent		**σ selected**	**F**	**E_s**	**Log_{10} k**
H	σ	0	0	0	0.8687
m-Br	σ_m^+	0.41	0	0	1.0329
m-C_2H_5	σ_m^+	-0.06	0	0	0.7815
m-CH_3	σ_m^+	-0.07	0	0	0.818
m-COOH	σ_m^+	0.32	0	0	0.9142
m-Cl	σ_m^+	0.4	0	0	0.9846
m-NO_2	σ_m^+	0.67	0	0	1.0547
m-OCH_3	σ_m^+	0.05	0	0	0.9339
m-OH	σ_m	0.12	0	0	0.8922
m-isoC_3H_7	σ_m	-0.07	0	0	0.7815
o-Br	σ_p	0.23	0.44	-1.16	0.845
o-C_2H_5	σ_p	-0.15	-0.05	-1.31	0.316
o-C_6H_5	σ_p	-0.01	0.08	-1.01	0.5007
o-CH_3	σ_p	-0.17	-0.04	-1.24	0.4095
o-COOH	σ_p	0.45	.	.	1.3914
o-Cl	σ_p	0.23	0.41	-0.97	0.86
o-NO_2	σ_p	0.78	0.67	-1.01	1.3966
o-OCH_3	σ_p	-0.27	0.26	-0.55	0.7186

Table C- 1-Continued

o-OH	σ_p	-0.45	0.29	.	0.5806
o-isoC$_3$H$_7$	σ_p	-0.15	-0.05	-1.71	0.1434
p-Br	σ_p^+	0.15	0	0	0.9202
p-C$_2$H$_5$	σ_p^+	-0.3	0	0	0.6623
p-C$_6$H$_5$	σ_p^+	-0.01	0	0	0.8768
p-CH$_3$	σ_p^+	-0.31	0	0	0.704
p-COOH	σ_p^-	0.73	0	0	1.2596
p-Cl	σ_p^+	0.11	0	0	0.8473
p-IsoC$_3$H$_7$	σ_p^+	-0.28	0	0	0.7337
p-NO$_2$	σ_p^-	1.24	0	0	1.4358
p-OCH$_3$	σ_p^+	-0.79	0	0	0.4704
p-OH	σ_p^+	-0.92	0	0	0.3941

Output Information after Multiple Regression Analysis

From JMP®

Figure C- 1: Actual versus fitted values for log of the rate constants for acidic hydrolysis of formanilides

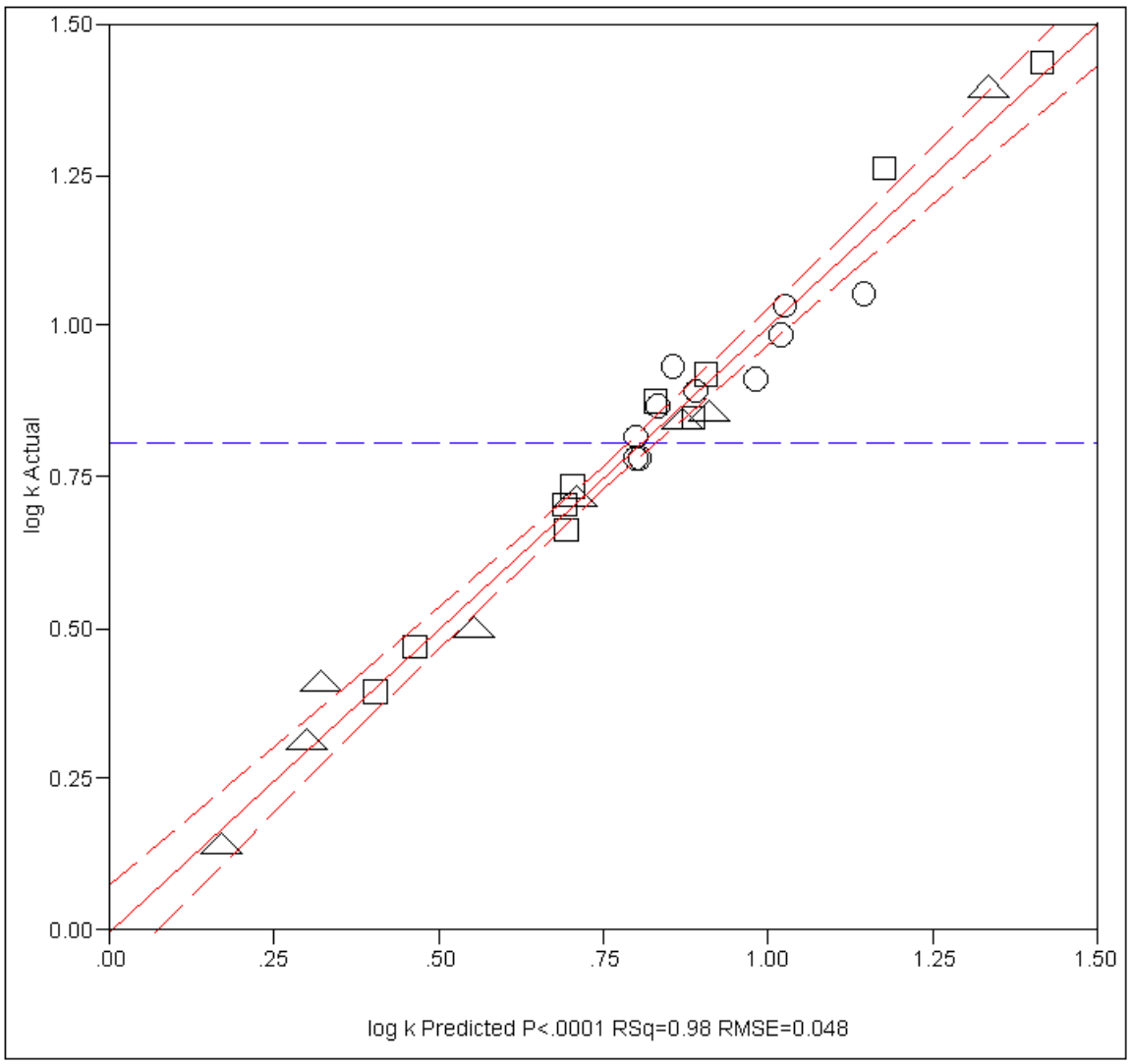

Table C- 2 Summary of Fit

RSquare	0.977092
RSquare Adj	0.974229
Root Mean Square Error	0.048034
Mean of Response	0.805571
Observations (or Sum Wgts)	28

Table C- 3 Analysis of Variance

Source	Degrees of Freedom	Sum of Squares	Mean Square	F Ratio
Model	3	2.3618546	0.787285	341.2249
Error	24	0.0553736	0.002307	Prob > F
C. Total	27	2.4172282		<.0001

Table C- 4 Parameter Estimates

Term	Estimate	Std Error	t Ratio	Prob>|t|
Intercept	0.8357806	0.010719	77.97	<.0001
Sigma or sigma +	0.4690681	0.02154	21.78	<.0001
F	0.6977465	0.062812	11.11	<.0001
E_s	0.3267682	0.019047	17.16	<.0001

Table C- 5 Effect Tests

Source	No. of Parameters	Degrees of Freedom	Sum of Squares	F Ratio	Prob > F
Sigma or sigma +	1	1	1.0941731	474.2364	<.0001
F	1	1	0.2847086	123.3984	<.0001
E_s	1	1	0.6791016	294.3361	<.0001

Figure C- 2: Residual by Predicted Plot

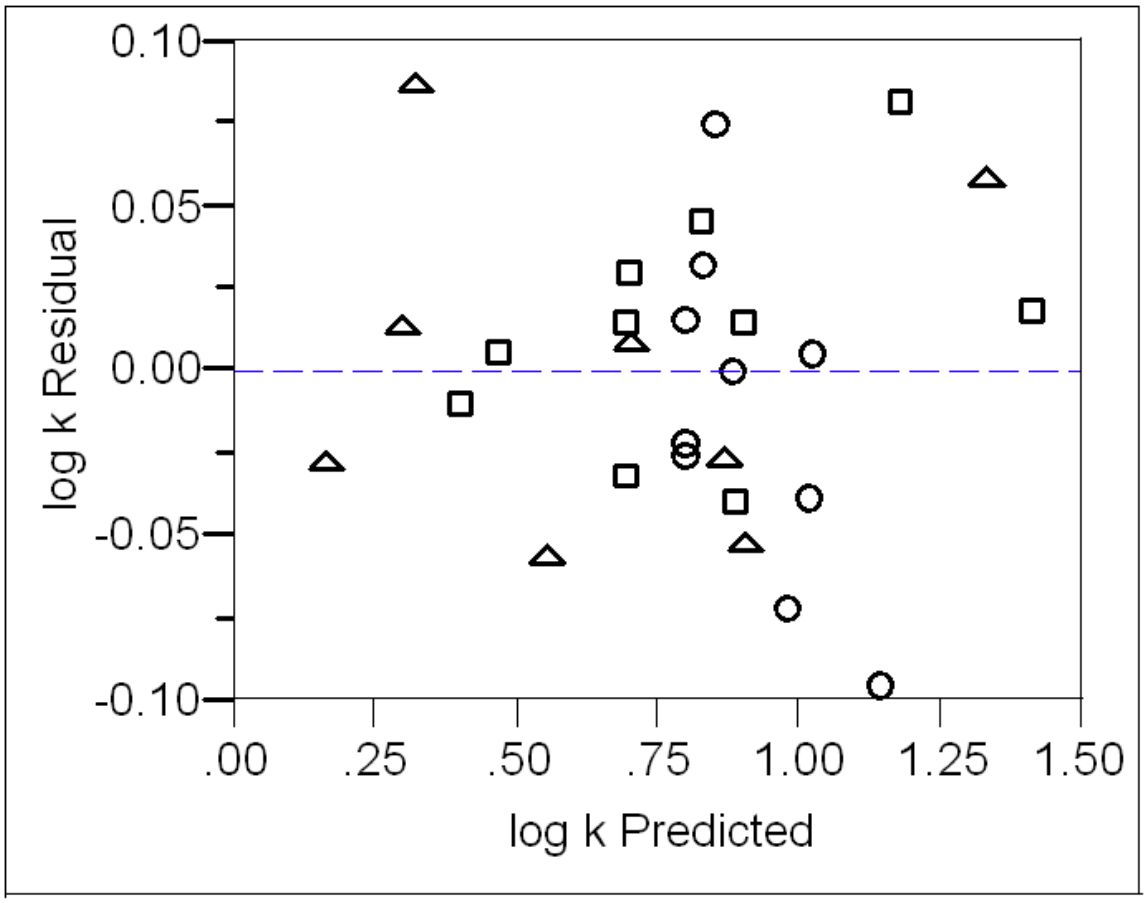

REFERENCES

1. Yoshioka, S. and V.J. Stella, *Stability of Drugs and Dosage Forms*, ed. S. Yoshioka and V.J. Stella. 2000, New York: Kluwer Academic Publishers. 272.

2. Wang, W., *Instability, Stabilization, and Formulation of Liquid Protein Pharmaceuticals.* International Journal of Pharmaceutics, 1999. **185**: p. 129-188.

3. Ma, M. and G. Sun, *Antimicrobial Cationic Dyes: Part 2 - Thermal and Hydrolytic stability.* Dyes and Pigments, 2004. **63**(1): p. 39-49.

4. Brown, R.S., *Studies in Amide Hydrolysis: The Acid, Base and Water Reactions*, in *The Amide Linkage: Selected Structural Aspects in Chemistry, Biochemistry and Material Science*, A. Greenberg, C.M. Breneman, and J.F. Liebman, Editors. 2000, John Wiley & Sons, Inc.: New York. p. 85-114.

5. Challis, B.C. and J. Challis, *Reactions of the Carboxamide Group*, in *The chemistry of amides*, J. Zabicky, Editor. 1970, Interscience Publishers: New York. p. 731-858.

6. Slebocka-Tilk, H., R.S. Brown, and J. Olekszyk, *Reversible Formation of Intermediates During H3o+-Catalyzed Hydrolysis of Amides - Observation of Substantial O-18 Exchange Accompanying the Hydrolysis of Acetanilide and N-Cyclohexylacetamide.* Journal of the American Chemical Society, 1987. **109**(15): p. 4620-4622.

7. Cheshmedzhieva, D., S. Ilieva, and B. Galabov, *Computational Study of the Alkaline Hydrolysis of Acetanilide.* Journal of Molecular Structure-Theochem, 2004. **681**(1-3): p. 105-112.

8. Hori, K., et al., *Ab initio Molecular Orbital Study on the Mechanism of Amide Hydrolysis Dependent on Leaving Groups.* Tetrahedron, 1997. **53**(12): p. 4317-4330.

9. Giffney, C.J. and C.J. O'Connor, *Acid-catalyzed Hydrolysis of Substituted Acetanilides. II.* Journal of the Chemical Society, Perkin Transactions 2: Physical Organic Chemistry, 1975(12): p. 1357-60.

10. Barnett, J.W. and C. O'Connor, *Acid-Catalysed Hydrolysis of Substituted Acetanilides.* Journal of the Chemical Society, Perkin Transactions 2: Physical Organic Chemistry, 1972(15): p. 2378 - 2381.

11. Slebocka-Tilk, H., et al., *Water Catalyzed Hydrolysis of p-Nitrotrifluoroacetanilide and Trifluoroacetanilide. Carbonyl ^{18}O-exchange Does Not Accompany the Water Reaction.* Journal of the American Chemical Society, 1997. **119**(45): p. 10969-10975.

12. Bender, M.L. and R.J. Thomas, *The Concurrent Alkaline Hydrolysis and Isotopic Oxygen Exchange of a Series of p-Substituted Acetanilides.* Journal of the American Chemical Society, 1961. **83**(20): p. 4183-4189.

13. Eriksson, S.O., *Hydrolysis of Anilides .VII. Alkaline Hydrolysis Aminolysis and General Acid Catalyzed Alkaline Hydrolysis of Acetanilide . Kinetic Evidence for Existence of More Than One Intermediate in Hydrogen Carbonate Ion Catalyzed Alkaline Hydrolysis.* Acta Pharmaceutica Suecica, 1969. **6**(2): p. 121-138.

14. Kavalek, J. and V. Sterba, *Kinetics of Base-Catalyzed-Hydrolysis of Substituted Formanilides.* Collection of Czechoslovak Chemical Communications, 1975. **40**(4): p. 1176-1182.

15. Biechler, S.S. and R.W. Taft, *The Effect of Structure on Kinetics and Mechanism of the Alkaline Hydrolysis of Anilides.* Journal of the American Chemical Society, 1957. **79**(18): p. 4927-4935.

16. DeWolfe, R.H. and R.C. Newcomb, *Hydrolysis of formanilides in alkaline solutions.* Journal of Organic Chemistry, 1971. **36**(25): p. 3870-8.

17. Kershner, L.D. and R.L. Schowen, *Amide Hydrolysis. IV. Proton Transfer and Heavy-atom Reorganization in Amide Hydrolysis. Valence-Isomeric Transition States.* Journal of the American Chemical Society, 1971. **93**(8): p. 2014-2024.

18. Young, J.K., S. Pazhanisamy, and R.L. Schowen, *Energetics of Carbonyl Addition and Elimination - Kinetic Manifestations of Acyl Substituent Effects in Anilide Hydrolysis.* Journal of Organic Chemistry, 1984. **49**(22): p. 4148-4152.

19. Kirsch, L., et al., *Development of a lyophilized formulation for (R,R)-formoterol (L)-tartrate.* Drug Development and Industrial Pharmacy, 2001. **27**(1): p. 89-96.

20. Kalvakota, B.P., *Personal Communication*.

21. Agbo, J.K., et al., *Quantum energy flow and the kinetics of water shuttling between hydrogen bonding sites on trans-formanilide.* Journal of Chemical Physics, 2007. **127**(6): p. 064315/1-064315/10.

22. Aviles Moreno, J.R., T.R. Huet, and D. Petitprez, *The trans-isomer of formanilide studied by microwave Fourier transform spectroscopy.* Journal of Molecular Structure, 2006. **780-781**: p. 234-237.

23. Fedorov, A.V. and J.R. Cable, *Spectroscopy of Hydrogen-Bonded Formanilide Clusters in a Supersonic Jet: Solvation of a Model Trans Amide.* Journal of Physical Chemistry A, 2000. **104**(21): p. 4943-4952.

24. Ilieva, S., B. Hadjieva, and B. Galabov, *Ab initio molecular orbital and infrared spectroscopic study of the conformation of secondary amides: derivatives of formanilide, acetanilide and benzylamides.* Journal of Molecular Structure, 1999. **508**(1-3): p. 73-80.

25. Mons, M., et al., *Energetics of the Gas Phase Hydrates of trans-Formanilide: A Microscopic Approach to the Hydration Sites of the Peptide Bond.* Journal of Physical Chemistry A, 2001. **105**(6): p. 969-973.

26. Ottaviani, P., et al., *Free-Jet Rotational Spectrum and ab Initio Calculations of Formanilide.* Journal of Molecular Spectroscopy, 2001. **205**(1): p. 173-176.

27. Ullrich, S., et al., *A ZEKE photoelectron spectroscopy and ab initio study of the cis- and trans-isomers of formanilide: Characterizing the cationic amide bond.* Physical Chemistry Chemical Physics, 2001. **3**(24): p. 5450-5458.

28. Ulrich, S., et al., *Communications: ZEKE photoelectron spectroscopy of the cis and trans isomers of formanilide.* Angewandte Chemie, International Edition, 2002. **41**(1): p. 166-168.

29. Koshy, K.T. and J.L. Lach, *Stability of Aqueous Solutions of N-acetyl-p-aminophenol.* Journal of Pharmaceutical Sciences, 1961. **50**(2): p. 113-118.

30. Kavalek, J. and V. Sterba, *Kinetics of Acid-catalyzed Hydrolysis of Substituted Formanilides.* Collection of Czechoslovak Chemical Communications, 1975. **40**(6): p. 1924-31.

31. Bergstrand, B., *Aminolysis and Hydrolysis of Formanilide in Water Solutions: Influence of pH and of the structure of the catalyzing imidazole derivative.* Acta Pharmaceutica Suecica, 1983. **20**(2): p. 81-98.

32. Bergstrand, B., *Aminolysis and Hydrolysis of Formanilide in Water Solutions. III. Influence of Ionic Strength.* Acta Pharmaceutica Suecica, 1984. **21**: p. 43-54.

33. Bergstrand, B., *Aminolysis and Hydrolysis of Formanilide in Water Solutions: IV Influence of a Surface Active Agent - Hexadecylpyridinium Chloride on Reaction Rate.* Acta Pharmaceutica Suecica, 1984. **21**: p. 55-66.

34. Bergstrand, B., *Aminolysis and Hydrolysis of Formanilide in Water Solutions .V. Influence of the Substituent in Para-Position.* Acta Pharmaceutica Suecica, 1985. **22**(1): p. 1-16.

35. Bergstrand, B. and L.O. Sundelof, *Kinetic Features of the Aminolysis of Formanilide and Para-Chloroformanilide in Water Solutions in the Presence of Imidazole.* Acta Pharmaceutica Suecica, 1981. **18**(5): p. 283-298.

36. Connors, K.A., *Reaction Rates*, in *Reaction Mechanisms in Organic Analytical Chemistry*, K.A. Connors, Editor. 1973, John Wiley & Sons: New York. p. 41-110.

37. Loudon, G.M., *Mechanistic Interpretation of pH-rate Profiles.* Journal of Chemical Education, 1991. **68**(12): p. 973-984.

38. Higuchi, T. and A.D. Marcus, *The kinetics of degradation of chloramphenicol in solution. III. The nature, specific hydrogen-ion catalysis, and temperature dependencies of the degradative reactions.* Journal of the American Pharmaceutical Association (1912-1977), 1954. **43**: p. 530-5.

39. Khalil, S.A. and S. El-Masry, *Instability of digoxin in acid medium using a nonisotopic method.* Journal of pharmaceutical sciences, 1978. **67**(10): p. 1358-60.

40. Powell, M.F., *Stability of Lidocaine in Aqueous Solution: Effect of Temperature , pH, Buffer, and Metal Ions on Amide Hydrolysis.* Pharmaceutical Research, 1987. **4**(1): p. 42-45.

41. H. Fabre, N.H.E.G.B., *Degradation kinetics in aqueous solution of cefotaxime sodium, a third-generation cephalosporin*. 1984. p. 611-618.

42. Sunderland, V.B. and D.W. Watts, *Kinetics of the Degradation of Methyl, Ethyl and n-Propyl 4-Hydroxybenzoate Esters in Aqueous Solution.* International Journal of Pharmaceutics, 1984. **19**(1): p. 1-15.

43. Gokhale, M.Y., *Kinetic and Mechanistic Studies of the Reactions of Weakly Basic Aromatic Amines and Reducing Monosaccharides in Aqueous solutions*, in *Division of Pharmaceutics*. 2006, University of Iowa: Iowa City. p. 289

44. Anderson, B.M. and W.P. Jencks, *The Effect of Structure on Reactivity in Semicarbazone Formation.* Journal of the American Chemical Society, 1960. **82**: p. 1773-1777.

45. Connors, K.A., *Phenomenon for Study*, in *Chemical Kinetics: The Study of Reaction Rates in Solution*, K.A. Connors, Editor. 1990, VCH Publishers, Inc.: New York. p. 245-310.

46. Sykes, P., *Nucleophilic addition to CO*, in *A Guidebook to Mechanism in Organic Chemistry*, P. Sykes, Editor. 1985, John Wiley & Sons, Inc.: New York. p. 241.

47. Patel, J.M. and D.E. Wurster, *Catalysis of Carbaryl Hydrolysis in Micellar Solutions of Cetyltrimethylammonium Bromide.* Pharmaceutical Research, 1991. **8**(9): p. 1155-1158.

48. Carstensen, J.T., *Kinetic Salt Effect in Pharmaceutical Investigations.* Journal of Pharmaceutical Sciences, 1970. **59**(8): p. 1140-1143.

49. Kirsch, L.E. and R.E. Notari, *Aqueous Conversion Kinetics and Mechanisms of Ancitabine, a Prodrug of the Antileukemic Agent Cytarabine.* Journal of Pharmaceutical Sciences, 1984. **73**(7): p. 896-902.

50. Connors, K.A., *Medium Effects*, in *Chemical Kinetics: The Study of Reaction Rates in Solution*, K.A. Connors, Editor. 1990, VCH Publishers, Inc.: New York. p. 385-462.

51. Reichart, C., *Solvent Effects on the rates of Homogenous Chemical Reactions*, in *Solvents and Solvent Effects in Organic Chemistry*, C. Reichart, Editor. 2003, Wiley-VCH: Weinheim. p. 147-328.

52. Gani, V. and P. Viout, *Study on Mechanism of Alkaline-Hydrolysis of N-Methylacetanilides Using Solvent Effects.* Tetrahedron, 1976. **32**(14): p. 1669-1673.

53. Linda, P., et al., *Hydrolysis of Amides - Kinetics and Mechanism of the Basic Hydrolysis of N-Acylpyrroles, N-Acylindoles and N-Acylcarbazoles.* Journal of Heterocyclic Chemistry, 1983. **20**(1): p. 247-248.

54. Sykes, P., *Structure/reactivity correlations*, in *The Search for Organic Reaction Pathways*, P. Sykes, Editor. 1974, John Wiley & Sons: New York. p. 169-197.

55. Hammett, L.P., *Some Relations Between Reaction Rates and Equilibrium Constants.* Chemical Reviews, 1935. **17**(1): p. 125-136.

56. Brown, H.C. and Y. Okamoto, *Directive Effects in Aromatic Substitution. XXX. Electrophilic Substituent Constants.* Journal of the American Chemical Society, 1958. **80**: p. 4979-4987.

57. Taft, R.W., Jr., *Sigma Values from Reactivities.* Journal of Physical Chemistry, 1960. **64**: p. 1805-15.

58. van Bekkum, H., P.E. Verkade, and B.M. Wepster, *Simple re.ovrddot. Evaluation of the Hammett ρ-σ Relation.* Recueil des Travaux Chimiques des Pays-Bas et de la Belgique, 1959. **78**: p. 815-50.

59. Briggs, L.H. and J.W. Lyttleton, *Reactions of Hydrazoic Acid. II. Quantitative Study of the Action with Substituted Benzoic Acids.* Journal of the Chemical Society, 1943: p. 421-5.

60. Sotomatsu, T. and T. Fujita, *The Steric Effect of Ortho Substituents on the Acidic Hydrolysis of Benzamides.* Journal of Organic Chemistry, 1989. **54**: p. 4443-4448.

61. Connors, K.A., *Structure-reactivity Relationships*, in *Chemical Kinetics: The Study of Reaction Rates in Solution*, K.A. Connors, Editor. 1990, VCH Publishers: New York. p. 311-384.

62. Isaacs, N., *Correlation of Structure with Reactivity*, in *Physical Organic Chemistry*, N. Isaacs, Editor. 1995, Prentice Hall: New York. p. 146-192.

63. Gassman, P.G. and A.F. Fenitman, Jr, *Characteristics of the abrupt change from participation to the non-participation of a neighbouring group.* Journal of the American Chemical Society, 1972. **92**: p. 2549.

64. Isaacs, N., *Steric and Conformational properties*, in *Physical Organic Chemistry*, N. Isaacs, Editor. 1995, Prentice Hall: New York. p. 319-368.

65. Taft, R.W., *Polar and Steric Substituent Constants for Aliphatic and o-Benzoate Groups from Rates of Esterification and Hydrolysis of Esters.* Journal of the American Chemical Society, 1952. **74**: p. 3120-3128.

66. Bruice, T.C. and D.W. Tanner, *Neighboring Hydroxyl Group Assistance .6. in Amide Hydrolysis.* Journal of Organic Chemistry, 1965. **30**(5): p. 1668-1669.

67. Leffler, J.E. and E. Grunwald, *Extrathermodynamic Analysis of Enthalpy and Entropy Changes*, in *Rates and Equilibria of Organic Reactions*, J.E. Leffler and E. Grunwald, Editors. 1989, Dover Publications, Inc: New York. p. 315-402.

68. Liu, L. and Q.-X. Guo, *Isokinetic Relationship, Isoequilibrium Relationship, and Enthalpy-Entropy Compensation.* Chemical Reviews, 2001. **101**: p. 673-695.

69. Krug, R.R., W.G. Hunter, and R.A. Grieger, *Enthalpy-entropy Compensation. 2. Separation of the Chemical from the Statistical Effect.* Journal of Physical Chemistry, 1976. **80**(21): p. 2341-51.

70. Krug, R.R., W.G. Hunter, and R.A. Grieger, *Enthalpy-entropy Compensation. 1. Some Fundamental Statistical Problems Associated with the Analysis of van't Hoff and Arrhenius Data.* Journal of Physical Chemistry, 1976. **80**(21): p. 2335-41.

71. Krug, R.R., W.G. Hunter, and R.A. Grieger, *Statistical Interpretation of Enthalpy-Entropy Compensation.* Nature (London), 1976. **261**: p. 566-567.

72. Exner, O., *The Enthalpy-Enthropy Relationship.* Progress in Physical Organic Chemistry, 1973. **10**: p. 411-482.

73. Exner, O., *A Critical Compilation of Substituent Constants*, in *Correlation Analysis in Chemistry: Recent Advances*, N.B. Chapman and J. Shorter, Editors. 1978, Plenum Press: New York. p. 439-540.

74. Atkins, P., *Physical Chemistry*. Sixth ed. 1998, New York: W. H. Freeman and Company. 200.

75. Werner, W., *Reactions with Formic-Acid .Part 3. Azeotropic Synthesis of Formanilides.* Journal of Chemical Research, Synopses, 1981(4): p. 120-120.

76. Huffman, C.W., *Formylation of Amines.* Journal of Organic Chemistry, 1958. **23**: p. 727-9.

77. Harris, D.C., *Introduction to Analytical Separations*, in *Quantitative Chemical Analysis*, D.C. Harris, Editor. 1995, W. H. Freeman and Company: New York. p. 621-654.

78. Sichina, W.J., *Purity Measurements of Pharmaceuticals and Organics by DSC*. 2000, Perkin Elmer Instruments. p. 1-4.

79. Plato, C. and A.R. Glasgow, Jr, *Differential Scanning Calorimetry as a General Method for Determining the Purity and Heat of fFsion of High-Purity Organic Chemicals: Application to 95 Compounds.* Analytical Chemistry, 1969. **41**(2): p. 330-336.

80. Gran, G., *Determination of Equivalence Point in Potentiometric Titrations. Part II.* Analyst, 1952. **77**: p. 661-671.

81. Albert, A. and E.P. Serjeant, *The Determination of Ionization Constants: A Laboratory Manual*. 1984, Chapman and Hall: New York. p. 70-73.

82. Niwa, J., *Proton NMR Studies of Substituent Effects. The Hammett-type Relationship in meta- and para-Substituted Formanilides.* Bulletin of the Chemical Society of Japan, 1969. **42**(7): p. 1926-1934.

83. Hosseini-Sarvari, M. and H. Sharghi, *ZnO as a New Catalyst for N-Formylation of Amines under Solvent-free Conditions.* Journal of Organic Chemistry, 2006. **71**(17): p. 6652-6654.

84. Yale, H.L., *Formulation of Amines with Phenyl Formate.* Journal of Organic Chemistry, 1971. **36**(21): p. 3238-40.

85. Hill, D.R., et al., *2,2,2-Trifluoroethyl Formate: A Versatile and Selective Reagent for the Formylation of Alcohols, Amines, and N-Hydroxylamines.* Organic Letters, 2002. **4**(1): p. 111-113.

86. Di Nunno, L. and A. Scilimati, *Decomposition of Arylazides by thf/-butyllithium-II-isolation of 1-aryl-4,5-dihydro-5-hydroxy-1h-1,2,3-triazoles.* Tetrahedron, 1986. **42**(14): p. 3913-3920.

87. Pettit, G.R., et al., *Potential Cancerocidal Agents. III. Formanilides.* Journal of Organic Chemistry, 1961. **26**: p. 2563-6.

88. Berrier, C., et al., *Direct Hydroxylation of Phenyl Esters and Anilides with Hydrogen Peroxide in Superacid Media.* Bulletin de la Societe Chimique de France, 1987(1): p. 158-64.

89. Farley, T.M., F.M. Strong, and T.J. Bydalek, *Chemistry of Antimycin A. XII. Dissociation Constants and Iron(III) Chelates of Antimycin A3 and Some Analogs.* Journal of the American Chemical Society, 1965. **87**(15): p. 3501-3504.

90. Pettit, G.R. and E.G. Thomas, *Formylation of Aromatic Amines with Dimethylformamide.* Journal of Organic Chemistry, 1959. **24**: p. 895-896.

91. Exner, O. and J. Lakomy, *Inductive Effect. VII. Inductive and Mesomeric Effects of Nitrogen and Oxygen Substituents.* Collection of Czechoslovak Chemical Communications, 1970. **35**(5): p. 1371-86.

92. Buss, C.E. and K.R. Mann, *Synthesis and Characterization of Pt(CN-p-(C2H5)C6H4)2(CN)2, a Crystalline Vapoluminescent Compound That Detects Vapor-Phase Aromatic Hydrocarbons.* Journal of the American Chemical Society, 2002. **124**(6): p. 1031-1039.

93. Wiberg, K.B., T.M. Shryne, and R.R. Kintner, *1,3-Shifts. V. The Intramolecular Nature of Some 1,3-shifts.* Journal of the American Chemical Society, 1957. **79**: p. 3160-3164.

94. Lesiak, T., *Utilization of o-nitroethylbenzene. VI. Condensation of o-ethyl-N-formylaniline to Skatole in Carbon Monoxide Atmosphere at Elevated Temperatures.* Chem. Stosowana Ser. A, 1963. **7**(4): p. 593-601.

95. Gim, H.J., B.M. Kang, and R. Jeon, *Synthesis and Biological Activity of 5-{4-[2-(methyl-p-substituted phenylamino)ethoxy]benzyl}thiazolidine-2,4-diones.* Archives of Pharmacal Research, 2007. **30**(9): p. 1055-1061.

96. Arient, J. and J. Dovorak, *N-Methyl-o-cumidine.* Chemicke Listy pro Vedu a Prumysl, 1956. **50**: p. 1636-8.

97. Zimmermann, J., *Derivate des Paraamidodiphenyls (Xenylamins).* Berichte der deutschen chemischen Gesellschaft, 1880. **13**(2): p. 1963-1969.

98. Kamer, P.C.J., R.J.M. Nolte, and W. Drenth, *Screw-sense selective polymerization of achiral isocyanides catalyzed by optically active nickel(II) complexes.* Journal of the American Chemical Society, 1988. **110**(20): p. 6818-6825.

99. Kisfaludy, L. and L. Otvos, Jr., *Rapid and Selective Formylation with Pentafluorophenyl Formate.* Synthesis, 1987(5): p. 510.

100. Yates, K. and J.C. Riordan, *The H_A acidity Function and the Mechanism of Amide Hydrolysis in Hydrochloric Acid.* Canadian Journal of Chemistry, 1965. **43**(8): p. 2328-35.

101. Bruice, T.C. and S. Benkovic, *Acyl Transfer Reactions Involving Carboxylic Acid Esters and Amides*, in *Bioorganic Mechansims* T.C. Bruice and S. Benkovic, Editors. 1966, W. A. Benjamin, Inc.: New York. p. 1-211.

102. Reichardt, C., *Solvents and Solvent Effects in Organic Chemistry*. 1988, VCH: New York. p. 408-411.

103. Fujita, T. and T. Nishioka, *The Analysis of the Ortho Effect*, in *Progress in Physical Organic Chemistry*, R.W. Taft, Editor. 1976, John Wiley & Sons: New York. p. 49-89.

104. Bowden, K., *Acidity Functions For Strongly Basic Solutions.* Chemical Reviews, 1966. **66**(2): p. 119-131.

105. Edward, J.T. and I.C. Wang, *Ionization of Organic Compounds II. Thioacetamide in Aqueous Sodium Hydroxide. the H- Acidity Function.* Canadian Journal of Chemistry, 1962. **40**: p. 399-408.

106. Bowden, K. and K. Bromley, *Reactions of Carbonyl-Compounds in Basic Solutions .14. the Alkaline-Hydrolysis of Substituted N-Methylformanilides, N-Methylacetanilides, 1-Phenylazetidin-2-Ones, 1-Phenyl-2-Pyrrolidones, and 1-Phenyl-2-Piperidones.* Journal of the Chemical Society, Perkin Transactions 2: Physical Organic Chemistry 1990(12): p. 2103-2109.

107. Harned, H.S. and J.C. Hecker, *The Thermodyanmics of Aqueous Sodium Hydroxide Solutions from Electromotive Force Measurements.* Journal of the American Chemical Society, 1933. **55**: p. 4838-4849.

108. Anbar, M., et al., *The Effect of Ionic Hydration on Rate and Equilibrium in Concentrated Alkaline Solutions. II The Kinetics of Base Catalyzed Reactions in Concentrated Hydroxide Solutions.* Journal of the American Chemical Society, 1963. **85**(16): p. 2380-2384.

109. Stokes, R.H. and H.A. Robinson, *Standard Solutions for Humidity Control at 25 °C.* Journal of Industrial and Engineering Chemsitry, 1949. **41**: p. 2013.

110. Yukawa, Y., Y. Tsuno, and M. Sawada, *The Substituent Effect. I. Normal Substituent Constants from the Hydrolysis of Substituted-benzyl Benzoates.* Bulletin of the Chemical Society of Japan, 1972. **45**(4): p. 1198-1205.

111. Motulsky, H. and A. Christopoulos, *Unequal Weighting of Data Points*, in *Fitting Models to Biological Data using Linear and NonLinear Regression. A Practical Guide to Curve Fitting*, H. Motulsky and A. Christopoulos, Editors. 2003, GraphPad Software, Inc: San Diego CA. p. 84-89.

112. Gani, V. and P. Viout, *Effects of Methyl Sulfoxide and Base Hydrolysis Mechanism of Acetanilides.* Tetrahedron Letters, 1972. **13**(51): p. 5241-5244.

113. Reichart, C., *Solvents and Solvent Effects in Organic Chemistry*. 1988, VCH: New York. p. 408-411.

114. Pollack, R.M. and T.C. Dumsha, *Specific Base-General Acid Catalysis of Alkaline-Hydrolysis of para-nitrotrifluoroacetanilide.* Journal of the American Chemical Society, 1973. **95**(13): p. 4463-4465.

115. Pollack, R.M. and M.L. Bender, *The Alkaline Hydrolysis of para-nitroacetanilide and para-formylacetanilide.* Journal of the American Chemical Society, 1970. **92**(24): p. 7190-&.

116. Drake, D., R.L. Schowen, and H. Jayaraman, *Amide Hydrolysis. VI. Diffusion-controlled Proton Transfer and Heavy-atom Reorganization in the General acid, Specific Base Catalyzed Hydrolysis of Amides.* Journal of the American Chemical Society, 1973. **95**(2): p. 454-458.

117. Schowen, R.L. and G.W. Zuorick, *Amide Hydrolysis. Superimposed General Base Catalysis in the Cleavage of Anilides.* Journal of the American Chemical Society, 1966. **88**(6): p. 1223-5.

118. Jaffe, H.H., *A Reexamination of the Hammett equation.* Chemical Reviews, 1953. **53**: p. 191-261.

119. Sorci, J.J. and D.L. Macalady, *Quantitative Structure-Activity-Relationships in Bacterial and Abiotic Alkaline Hydrolyzes of Parasubstituted Acetanilides.* Journal of Agricultural and Food Chemistry, 1993. **41**(10): p. 1760-1766.

120. Skarzewski, J., M. Aoki, and S. Sekiguchi, *Alkaline-Hydrolysis of N-Ethyl-2,4-Dinitroacetanilide.* Journal of Organic Chemistry, 1982. **47**(9): p. 1764-1766.

121. Broxton, T.J. and L.W. Deady, *Basic Methanolysis of Anilides - Evidence for Mechanism Applying to Special Case of N-Methyl-4'-Nitroanilides.* Journal of Organic Chemistry, 1975. **40**(20): p. 2906-2910.